ASSESSMENT OF CONFINEMENT MODELS FOR REINFORCED CONCRETE COLUMNS SUBJECTED TO SEISMIC LOADING

by

Kevin Allen Riederer
B.Sc., University of Alberta, 2003

A THESIS SUBMITTED IN PARTIAL FULFILLMENT OF
THE REQUIREMENTS FOR THE DEGREE OF

MASTER OF APPLIED SCIENCE

in

The Faculty of Graduate Studies
(Civil Engineering)

THE UNIVERSITY OF BRITISH COLUMBIA
December 2006

ABSTRACT

Research conducted over the past several years has shown that factors such as axial load level and the amount and spacing of confinement steel influence the performance of reinforced concrete columns subjected to seismic loading. The aim of this research project was to investigate the performance of the current ACI 318 confining steel requirements and compare them to other codes and proposed models to determine their suitability for a performance based design equation for implementation in Chapter 21 of ACI 318.

The investigation was performed by analyzing the results of multiple reverse-cyclic column tests presented in the UW/PEER Structural Performance Database. The condensed database used in this investigation consisted solely of columns which exhibited flexural failure and contained 145 rectangular and 50 circular columns.

First, a scatter plot was used to compare the confining requirements of each model with the lateral drift observed for each column within the database. The plot showed the drift ratio achieved by the column test versus a ratio of lateral steel A_{sh} provided over that which is required by ACI ($A_{sh\ Provided} / A_{sh\ ACI}$). A drift ratio of 2.5% was selected as the performance target for the evaluation. Columns were identified as those which satisfied the requirements of the model but failed the performance target ('unconservative') or those which failed the requirements of the model but satisfied the performance target ('conservative'). For each model, the percentage of columns falling into these classifications was calculated and compared.

Two fragility curves were generated for each model which provided the probability of a column being classified as 'unconservative' or 'conservative' as a function of drift ratio. A third curve was a combination of the first two and provided insight as to the overall performance of the model.

For both the rectangular and circular column evaluations, the ACI model was determined to be the least desirable of all models investigated. Based on the evaluation techniques developed, specific models were selected as recommended alternatives to the current ACI requirements. The recommended models minimize the potential of a column experiencing lateral strength degradation before reaching the prescribed lateral drift limit.

TABLE OF CONTENTS

LIST OF TABLES

LIST OF FIGURES

LIST OF NOTATIONS

A_{ch}	=	cross-sectional area of a structural member measured out-to-out of transverse reinforcement
A_g	=	gross area of column
A_{sh}	=	total cross-sectional area of transverse reinforcement (including crossties) within spacing s and perpendicular to dimension h_c
A_{sp}	=	cross-sectional area of spiral or circular hoop reinforcement
b_c	=	cross-sectional dimension of column core measured centre-to-centre of confining reinforcement
f'_c	=	specified concrete strength of concrete
f_y	=	specified yield strength of nonprestressed reinforcement
f_{yt}	=	specified yield strength of transverse reinforcement
P	=	Axial compressive force on column
P_0	=	nominal axial load strength at zero eccentricity
s	=	spacing of transverse reinforcement measured along the longitudinal axis of the member
s_l	=	centre-to-centre spacing of longitudinal reinforcement, laterally supported by corner of hoop or hook of crosstie
ϕ	=	capacity reduction factor
ρ_{area}	=	area ratio of transverse confinement reinforcement ($A_{sh} / s \cdot h_c$)
ρ_s	=	ratio of volume of spiral reinforcement to the core volume confined by the spiral reinforcement (measured out-to-out)
ρ_t	=	area of longitudinal reinforcement divided by gross area of column section
$\rho_l m$	=	mechanical reinforcing ratio ($m = f_y / 0.85f'_c$)
ρ_{vol}	=	volume ratio of transverse confinement reinforcement

ACKNOWLEDGEMENTS

First, I would like to express my sincere gratitude to my supervisor Dr. Kenneth Elwood for his guidance, encouragement, patience and friendship throughout my time at UBC. It was a privilege to work with him. I would also like to thank Dr. Terje Haukaas for his support throughout my graduate studies.

This research project would not have been possible if it were not for the financial assistance provided by the Portland Cement Association through the Education Foundation Research Fellowship. Their support is greatly appreciated.

I owe a great deal to my colleagues at UBC. In particular I want to thank Dominic Mattman, Chris Meisl, Aaron Korchinski, Tim Mathews, Arnoud Charlet, and Soheil Yavari for their support and friendship. I also want to thank my close friends outside of UBC for their encouragement, support and for their belief in me.

I would like to like to express my sincere appreciation to my family, especially Michael, Andrea, Jim and Margaret Hoffman. Their support over the years was instrumental in helping me reach all of my educational goals and this work would not have been possible without them.

Finally, I want to thank my parents, Allen and Ann Riederer, who have taught me everything in life which is truly important to learn. Their unconditional love and support will be remembered always. My work is dedicated to them. Thank you.

1 INTRODUCTION

1.1 Motivation

Reinforced concrete columns subjected to seismic loading must be able to withstand several inelastic deformation reversals to maintain the integrity of the structure which they are supporting. Previous earthquakes and laboratory test results have shown that the ability of columns to undergo these deformations without a significant loss in strength can be linked to the level of confinement applied to the concrete within the core of the column. In reinforced concrete columns, confinement is provided by the amount, arrangement and spacing of transverse steel.

To ensure columns are able to reach acceptable levels of deformation during an earthquake, concrete design codes must appropriately incorporate all the variables which contribute to their seismic performance. This work will investigate current design codes and proposed models found in the literature with the aim of determining the optimum requirement for confining steel.

To form the basis of this investigation, the following section will present the mechanics by which transverse steel confines the core concrete within a column and how the level of confinement affects the columns seismic performance.

1.2 Ductility and Lateral Steel

It is well known throughout the structural and earthquake engineering community that the lateral steel in reinforced concrete columns serves three primary functions, it provides shear reinforcement, it acts to restrain the buckling of longitudinal compression steel, and it confines the concrete within the core of the column.

For members subjected to shear forces, engineers commonly use the widely accepted truss model for the shear resistance mechanism. The transverse steel bars in these members behave as tension components within these idealized truss models. Depending on weather or not the concrete contribution to shear resistance is accounted for, the transverse steel will be needed to resist some or all of the design shear force. The amount and orientation of transverse steel required for shear resistance is not the focus of this study.

Buckling of longitudinal compression reinforcement can limit the performance of columns subjected to seismic loading. For this reason, the lateral support of the longitudinal reinforcement provided by the transverse reinforcement is an important parameter in the design of reinforced concrete columns. Therefore, the lateral steel spacing in the end regions where hinges are likely to form is crucial to reducing buckling of the compression bars. However, the design of lateral steel for support of longitudinal bars is not the focus of this study.

The area, spacing and orientation of lateral bars also play a key role in the effectiveness of the transverse reinforcement to confine the core concrete of a column. The relationship between the ductility of reinforced concrete columns, a crucial component within seismic design of buildings, and transverse steel in the column falls primarily out of the confining action of the steel. It is this confining action of transverse steel that is the focus of this work.

1.3 Confinement Action of Transverse Steel

It is important first to understand the mechanism by which the transverse reinforcement confines the concrete core of a column. The definitive work in this area was done by Sheikh and Uzumeri (1980) and (1982) and was presented again in Mander et. al. (1988). Based on a series of column tests, the authors concluded that the area of the effectively confined concrete is less than the area bounded by the perimeter tie. In other words, $A_e < A_{ch}$ where A_e is the effectively confined area of concrete and A_{ch} is the area of concrete enclosed by the perimeter tie. They also concluded that the effectively confined concrete

is determined by the distribution of the longitudinal steel and the resulting tie configuration and spacing. To account for this, the authors propose the following for the effective lateral confining pressure, f_l'

$$f'_l = f_l k_e \qquad (1.1)$$

where k_e is a confinement effectiveness coefficient expressed as:

$$k_e = \frac{A_e}{A_{cc}} \qquad (1.2)$$

where A_{cc}, the area of core within centre lines of the perimeter spiral or hoops excluding area of longitudinal steel, expressed as:

$$A_{cc} = A_c(1 - \rho_{cc}) \qquad (1.3)$$

where ρ_{cc} is the ratio of longitudinal reinforcement to area of core of section.

The parameter f_l is the lateral pressure from the transverse reinforcement. For various configurations of transverse reinforcement, f_l can be calculated as shown in Figure 1.1

Figure 1.2 and Figure 1.3 show the relationship between the effectively confined core and the lateral steel configuration and spacing. The confinement effectiveness coefficient for sections confined by circular hoops is expressed as:

$$k_e = \frac{\left(1 - \frac{s'}{2d_s}\right)^2}{1 - \rho_{cc}} \qquad (1.4)$$

and for circular spirals as:

$$k_e = \frac{1 - \frac{s'}{2d_s}}{1 - \rho_{cc}} \qquad (1.5)$$

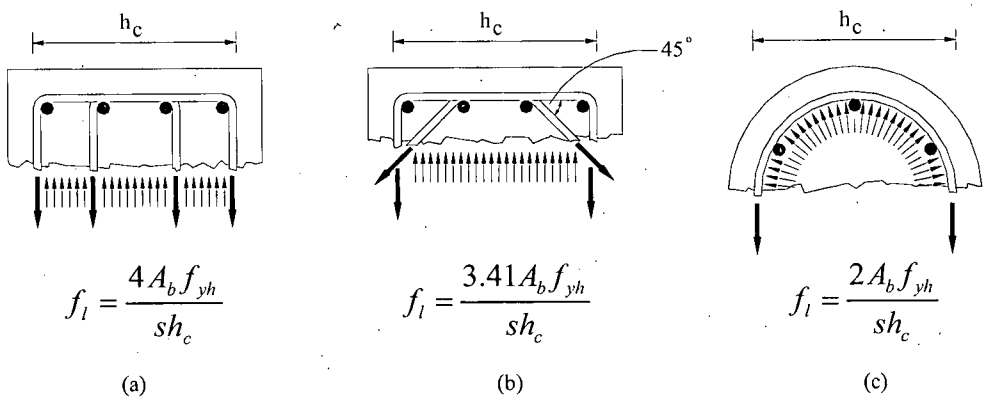

Figure 1.1 Confining stresses provided by different arrangements of transverse reinforcement (Watson et. al 1994)

The lateral confining pressure is found by considering the half body confined by the lateral steel. Equilibrium of forces requires that for circular columns:

$$f_l = \frac{2A_b f_{yh}}{sh_c} \qquad (1.6)$$

From Equation 1.1 the effective lateral confining stress imposed on a circular column can be expressed as:

$$f'_l = \frac{1}{2} k_e \rho_s f_{yh} \qquad (1.7)$$

where ρ_s is the volumetric transverse reinforcement ratio and k_e is given in Equations 1.4 and 1.5.

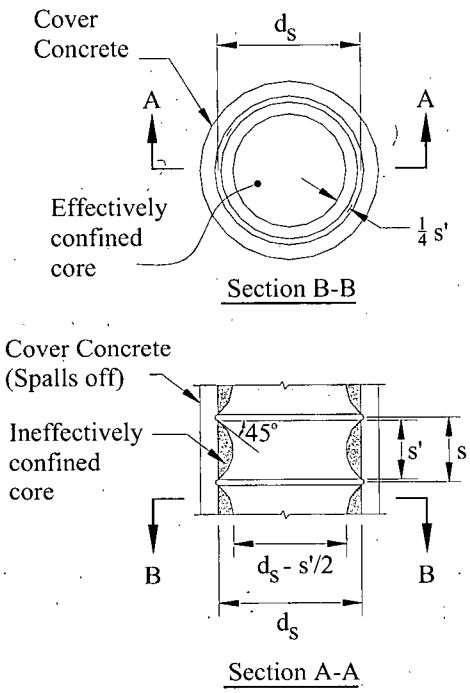

Figure 1.2 Effectively confined core for circular hoop reinforcement (Mander et. al 1988)

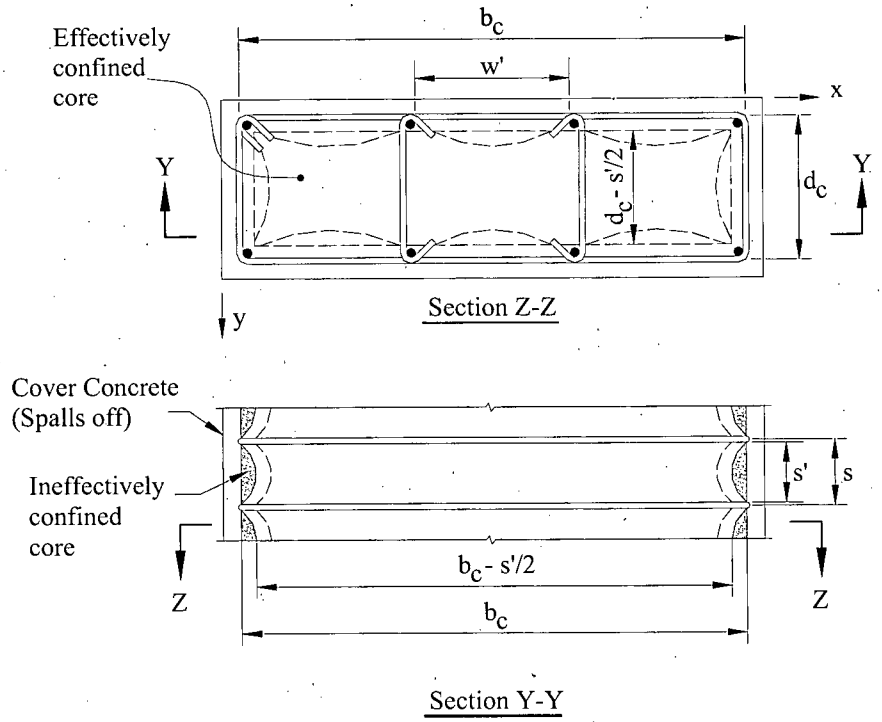

Figure 1.3 Effectively confined core for rectangular hoop reinforcement (Mander et. al 1998)

Similar expressions for rectangular columns are also presented. From Equation 1.2 it can be found that for rectangular sections:

$$k_e = \frac{\left(1 - \sum_{i=1}^{n} \frac{(w'_i)^2}{6b_c d_c}\right)\left(1 - \frac{s'}{2b_c}\right)\left(1 - \frac{s'}{2d_c}\right)}{(1 - \rho_{cc})} \qquad (1.8)$$

where w'_i, the ith clear distance between adjacent longitudinal bars, along with the dimensions s', b_c and d_c are shown in Figure 1.2 and Figure 1.3. Since many rectangular columns have different quantities of lateral steel in the x and y directions, separate transverse reinforcement ratios are defined as:

$$\rho_x = \frac{A_{sx}}{sd_c} \qquad (1.9)$$

$$\rho_y = \frac{A_{sy}}{sd_c} \qquad (1.10)$$

Again recognizing the relationship given in Equation 1.1, the effective lateral confining stresses for a rectangular column in the x and y directions are:

$$f'_{lx} = k_e \rho_x f_{yh} \qquad (1.11)$$

and

$$f'_{ly} = k_e \rho_y f_{yh} \qquad (1.12)$$

where k_e is given in Equation 1.8.

Figures 1.1, 1.2 and 1.3 as well as Equations 1.1, 1.4, 1.5 and 1.8 provide valuable insight as to which lateral steel parameters ought to be considered in confinement steel provisions. They include: area of transverse bar, spacing of transverse bars and dimension of concrete core, yield strength of steel, density of longitudinal reinforcement and in the case of rectangular columns, spacing of longitudinal reinforcing bars.

1.4 Properties of Confined Concrete

Now that the relationship between the transverse steel and concrete confinement has been illustrated, the effect of confinement on the expected behaviour of concrete can be addressed. For nearly a century, investigators have known the effects on confining

pressures on the stress-strain behaviour of concrete. Richart et al. (1928) studied the strength and corresponding longitudinal strain of concrete confined by an active hydrostatic fluid pressure. Since that time, many mathematical relationships predicting the stress-strain response of confined concrete have been proposed.

1.4.1 Mander Model for Confined Concrete

Mander et al. (1988) proposed a unified stress-strain approach based on the work done previously by researchers including Richart et. al. The approach was developed to be applicable to columns confined by either circular or rectangular transverse reinforcement. The model, illustrated in Figure 1.4, was developed for concrete tested with a slow, or quasi-static, strain rate and monotonic loading. The authors proposed that the longitudinal compressive concrete stress, f_c is given by:

$$f_c = \frac{f'_{cc}\, xr}{r - 1 + x^r} \qquad (1.13)$$

where f'_{cc} = compressive strength of confined concrete,

$$x = \frac{\varepsilon_c}{\varepsilon_{cc}} \qquad (1.14)$$

where ε_c = longitudinal compressive concrete strain,

$$\varepsilon_{cc} = \varepsilon_{co}\left[1 + 5\left(\frac{f'_{cc}}{f'_{co}} - 1\right)\right] \qquad (1.15)$$

where f'_{co} is the unconfined concrete strength and ε_{co} is the corresponding strain typically assumed to be 0.002,

$$r = \frac{E_c}{E_c - E_{\sec}} \qquad (1.16)$$

where

$$E_c = 5000\sqrt{f'_{co}}\,(MPa) \qquad (1.17)$$

is the tangent modulus of elasticity of the concrete and

$$E_{\sec} = \frac{f'_{cc}}{\varepsilon_{cc}} \qquad (1.18)$$

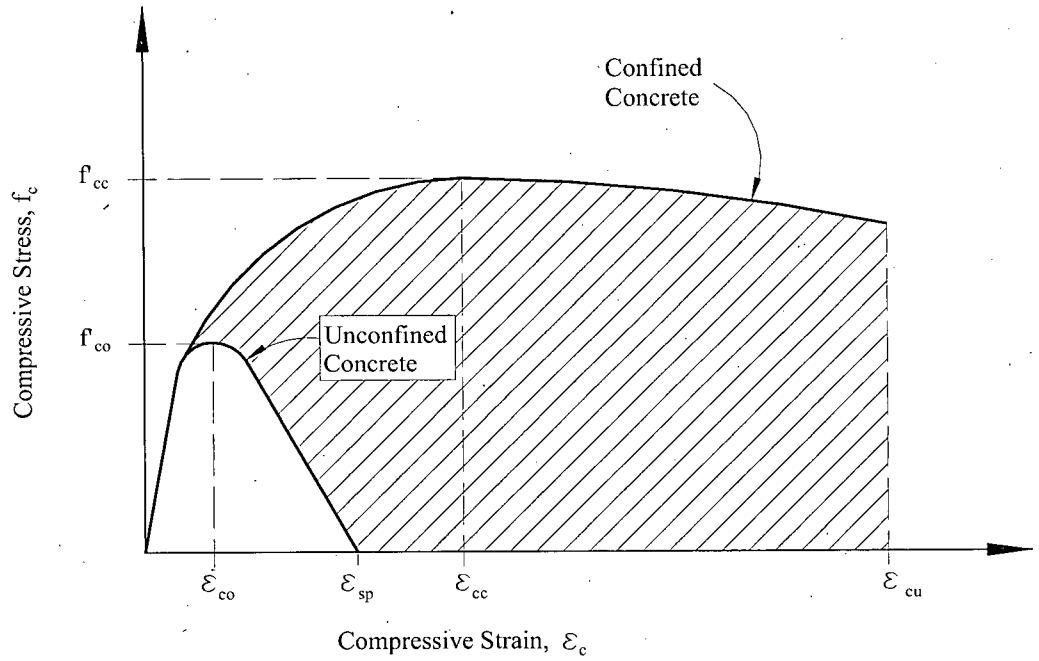

Figure 1.4 Proposed concrete compressive stress-strain model (Mander et. al. 1988)

To determine the confined concrete compressive strength f'_{cc}, the authors use a constitutive model based on tri-axial compression tests and described by William and Warnke (1975). As shown in Figure 1.5, the William and Warnke model relates the confined strength ratio f'_{cc}/f'_{co} to the two lateral confining stresses f'_{l1} and f'_{l2}.

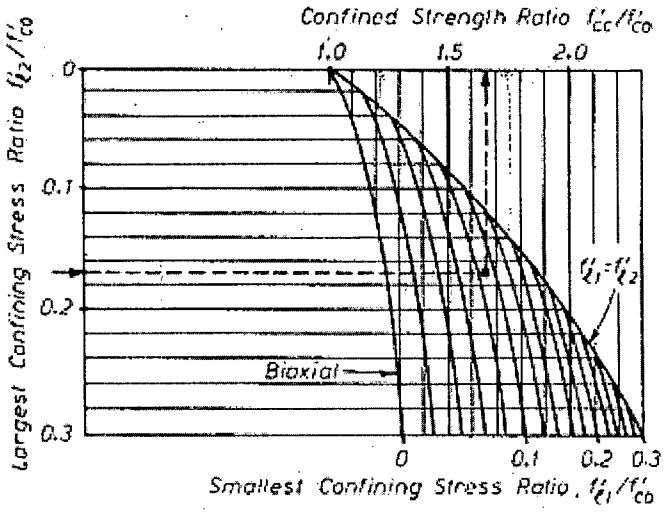

Figure 1.5 Confined strength determination from confining stresses for rectangular sections (Mander et. al. 1988)

When the concrete core is confined by equal lateral confining stresses (i.e. $f'_{l1} = f'_{l2}$), it can be shown that the compressive strength can be given as:

$$f'_{cc} = f'_{co}\left(-1.254 + 2.254\sqrt{1 + \frac{7.94 f'_l}{f'_{co}}} - 2\frac{f'_l}{f'_{co}}\right) \qquad (1.19)$$

1.4.2 Légeron and Paultre Model for Confined Concrete

More recently, Légeron and Paultre (2003) proposed a stress-strain model for confined concrete based on strain compatibility and transverse force equilibrium. The model is an expansion of a proposal by Cusson and Paultre (1995) which was developed for high strength concretes.

The curve shown in Figure 1.6 is defined by locating two distinct points labeled A and B on the figure. Point A is the confined compressive strength f'_{cc} corresponding to the strain ε'_{cc}, and point B is the post-peak axial strain ε_{cc50} in the concrete when the capacity drops to 50% of the confined strength. The stress in the confined concrete, f_{cc}, corresponding to a strain ε_{cc}, in the ascending portion (point 0 to point A) of the stress-strain curve is given as:

$$f_{cc} = f'_{cc}\left[\frac{k(\varepsilon_{cc}/\varepsilon'_{cc})}{k - 1 + (\varepsilon_{cc}/\varepsilon'_{cc})^k}\right], \quad \varepsilon_{cc} \le \varepsilon'_{cc} \qquad (1.20)$$

where the prime signifies that a term is being evaluated at the peak of the stress-strain curve and the slope controlling parameter k is given as:

$$k = \frac{E_{ct}}{E_{ct} - (f'_{cc}/\varepsilon'_{cc})} \qquad (1.21)$$

where E_{ct} is the tangent modulus of elasticity of the unconfined concrete.

The post-peak portion of the curve is described by the following equation:

$$f_{cc} = f'_{cc}\exp\left[k_1(\varepsilon_{cc} - \varepsilon'_{cc})^{k_2}\right], \quad \varepsilon_{cc} \ge \varepsilon'_{cc} \qquad (1.22)$$

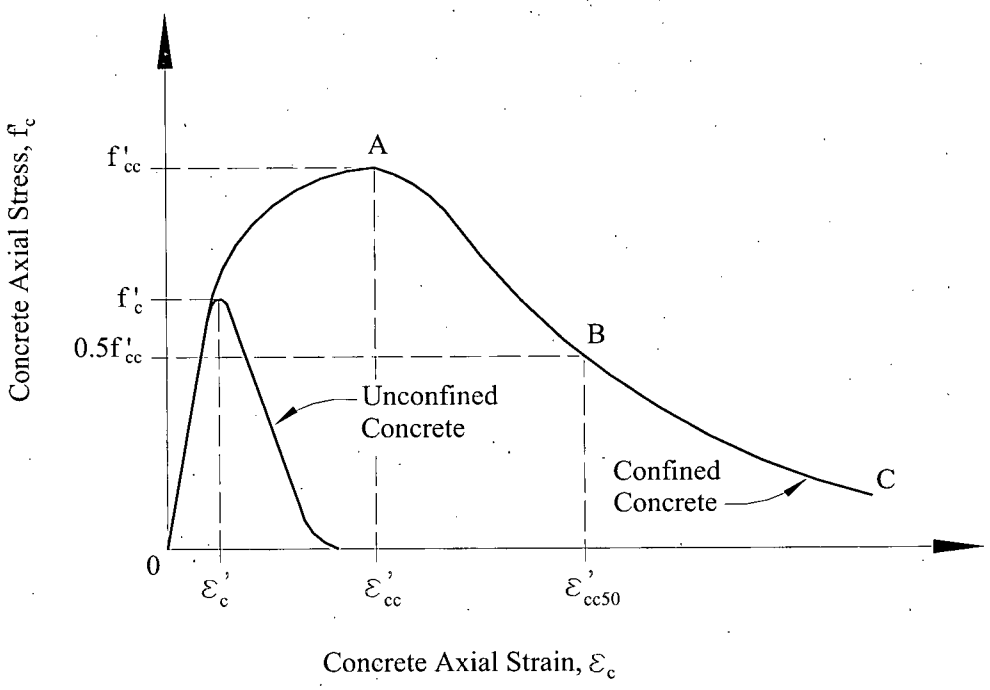

Figure 1.6 Stress-strain relationship of confined concrete (Cusson and Paultre 1995)

where the authors define the parameters k_1 and k_2 as:

$$k_1 = \frac{\ln 0.5}{(\varepsilon_{cc50} - \varepsilon'_{cc})^{k_2}} \qquad (1.23)$$

$$k_2 = 1 + 25(I_{e50})^2 \qquad (1.24)$$

where I_{e50} is the effective confinement index evaluated at the post-peak strain ε_{cc50} shown in Figure 1.6.

To develop expressions for f'_{cc} and ε'_{cc}, the authors use the effective confinement index at peak stress, a nondimensional parameter first introduced in Cusson and Paultre (1995).

$$I'_e = \frac{f'_{le}}{f'_c} \qquad (1.25)$$

where

$$f'_{le} = K_e \frac{A_{sh}}{sc} f'_h \qquad (1.26)$$

and the following relationships are provided:

$$f'_{cc} = f'_c \left[1 + 2.4(I'_e)^{0.7}\right] \qquad (1.27)$$

$$\varepsilon'_{cc} = \varepsilon'_c \left[1 + 35(I'_e)^{1.2}\right] \quad (1.28)$$

The authors note that recent research has concluded that the stress in the confining steel does not necessarily reach the yield limit. This is especially true in columns with low confinement or in which high-yield strength steel is used. To include this phenomenon, the authors introduce the following parameter:

$$\kappa = \frac{f'_c}{\rho_{sey} E_s \varepsilon'_c} \quad (1.29)$$

and define the stress in the confinement reinforcement at peak strength f'_h as:

$$f'_h = \begin{cases} f_{hy} & if \kappa \le 10 \\ \dfrac{0.25 f'_c}{\rho_{sey}(\kappa - 10)} \ge 0.43 \varepsilon'_c E_s & if \kappa > 10 \end{cases} \quad (1.30)$$

The post-peak strain ε_{cc50} is taken from the curve where the stress reaches 50% of the maximum value. In equation form, it can be expressed as:

$$\varepsilon_{cc50} = \varepsilon_{c50}(1 + 60 I_{e50}) \quad (1.31)$$

where ε_{c50} is the post-peak strain in the unconfined concrete taken from the curve at the point of $0.5f'_c$ and I_{e50} is the effective confinement index at ε_{cc50} and is expressed by the authors in the following form:

$$I_{e50} = \rho_{se} \frac{f_{hy}}{f'_c} \quad (1.32)$$

For the relationships shown above, f_{hy} is the yield strength of the transverse reinforcement and ρ_{se} is the effective volumetric ratio of confinement reinforcement

$$\rho_{se} = K_e \frac{A_{sh}}{sc} \quad (1.33)$$

where for a given column, A_{sh} is the total area of transverse reinforcement within spacing s, and c is the dimension of the confined core for a given direction.

1.5 Confinement and Lateral Deformation

For earthquake engineers, the most important trend observed by investigators who have researched the effect of confinement on concrete stress-strain behaviour has been the

significant increase in axial strain capacity. Paulay and Priestley (1992) suggest this increase can lead to ultimate compression strains on the order of 4 to 16 times the value of 0.003 traditionally assumed for unconfined concrete. This trend is clearly shown in the two models presented here, Figure 1.4 and Figure 1.6, and in the various other models found in the literature. To understand how an increase in axial strain capacity of concrete relates to improved lateral ductility in reinforced concrete columns, one must examine the strain gradient that exists in members subjected to axial load and bending forces.

Consider the reinforced concrete element of length L, subjected to axial compressive force P and bending moment M shown in Figure 1.7(a). The deformed shape is represented in Figure 1.7(b) which also shows the curvature resulting from the loading condition, and Figure 1.7(c) shows how the curvature is related to the sectional strain distribution as well as the location of the neutral (no strain) axis.

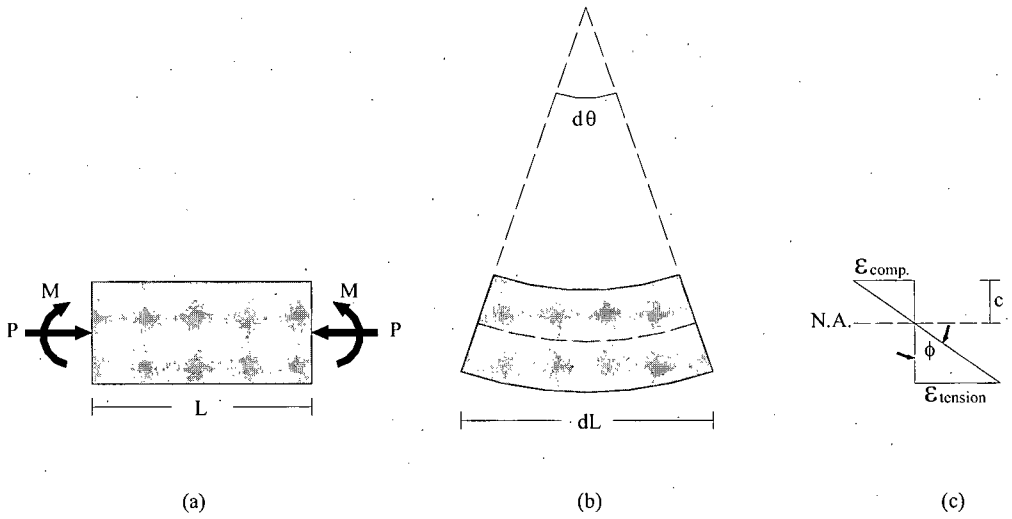

Figure 1.7 Curvature defined

Curvature, ϕ, can be defined as the change in angle over a given length or:

$$\phi = \frac{\partial \theta}{\partial L} = \frac{\varepsilon_{comp}}{c} \qquad (1.34)$$

The assumption in reinforced concrete design is that the formation of cracks in the tension region of the element results in the tension steel resisting all tension forces and being strained to a value of ε_{ten}, while the concrete in the compression region resists the compressive forces with the most extreme compression fibers reaching a strain of ε_{comp}. From the relationship given in Equation 1.34 it is clear that if a larger ultimate compression strain is reached, a larger resulting ultimate curvature will be achieved. Additionally, the increase in compressive stresses found in confined concrete requires that a smaller amount of concrete is required to balance the sectional tension forces, causing the neutral axis to shift closer to the compression face and further increasing the ultimate curvature of the member. A larger curvature capacity of a concrete section translates into larger lateral deformations for a concrete member such as a column.

1.6 Ductility and Axial Load

The impact of axial load on the deformability of reinforced concrete columns has been the focus of many recent investigations. The consistent conclusion is that the effect of axial compression is to reduce column deformability (Saatcioglu 1991). This is explained by considering the interaction diagrams which are commonly used by engineers in the design of reinforced concrete columns. A typical interaction diagram shows the moment capacity of a particular column cross section at various levels of axial load. Likewise, an axial load and curvature capacity interaction diagram can be produced for a particular column cross section. The effect of axial load and confinement on the curvature capacity is evidenced in the axial load curvature diagram shown below in Figure 1.8. The interaction diagram is given for an example column cross section with dimensions 400mm x 400mm, 12 16mm diameter longitudinal bars, and 7mm diameter transverse bars and represents the point at which maximum compressive strain of 0.004 is reached in the concrete. The interaction between axial load ratio and curvature is shown for three different spacings of transverse reinforcement. The maximum compression strain in the concrete was calculated using the Mander model. As the spacing decreases, the

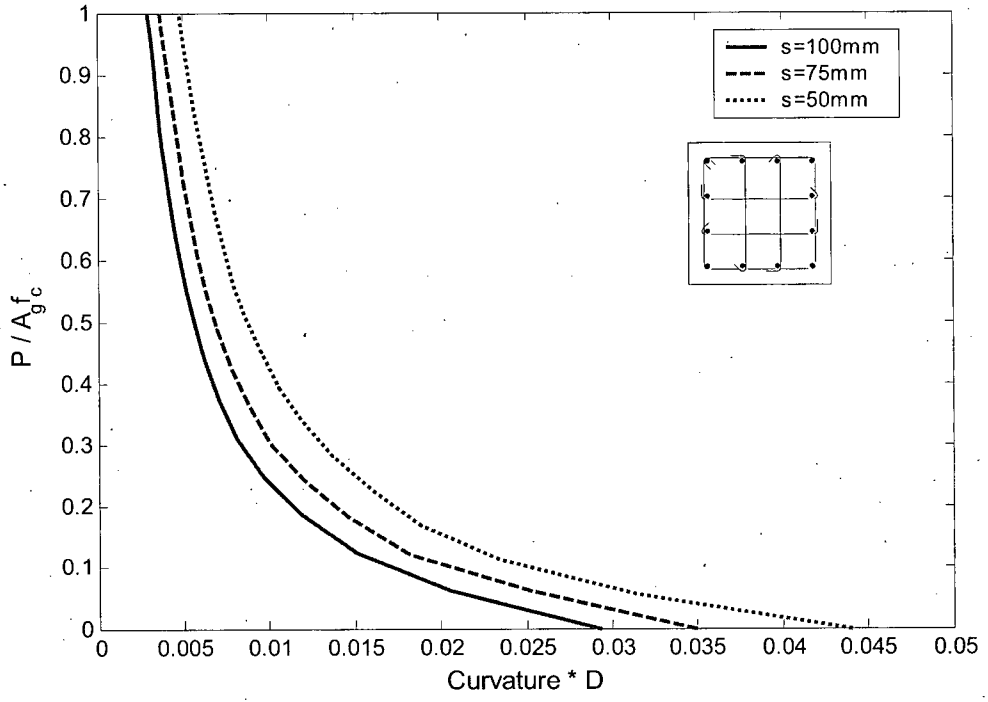

Figure 1.8 Axial load ratio vs. curvature

confinement effectiveness of the transverse steel increases, the maximum compression strain increases, and the curvature capacity increases. The figure shows that for an axial load ratio of 0.5, the column is able to achieve a 53% increase in curvature when the spacing is decreased from 100mm to 50mm. The figure clearly shows that for a given cross section, the axial load significantly impacts the curvature capacity.

Further evidence of the influence of axial load on the lateral drift performance of reinforced concrete columns was presented by Elwood and Eberhard (2006). The authors investigated the effect of axial load on the amount of lateral displacement experienced by a column due to bar slip. When a reinforced concrete column is subjected to a lateral load, elongation of the longitudinal reinforcing bars in tension occurs within the beam-column joint or footing. This bar slip results in lateral displacements in addition to those caused by flexural deformation of the column. Therefore, the displacement of a column can be considered as the sum of the displacements due to flexure, bar slip, and often negligible shear displacements. Elwood and Eberhard reported that for columns with low

levels of axial load, $P / A_g f_c' < 0.2$, slip deformations can account for up to approximately half of the total deformation at yield, and for columns with high values for axial load ratio, $P / A_g f_c' > 0.5$, the displacement due to bar slip is negligible. The conclusion that can be reached from this result is that for columns with high axial load the flexural displacements, which are significantly influenced by the level of confinement, dominate the total column displacement at yield. Also, this indicates that columns with low axial load have the added deformation component from bar slip which does not depend on the amount of confinement and have improved deformation capacity without the need for additional confining steel. This effect disappears as the axial load increases, thereby increasing the need for confinement for columns with high axial loads.

1.7 Research Objectives and Scope

The aim of this research project is to investigate the performance of the current ACI 318 confining steel requirements and compare them to other codes and proposed models to determine their suitability for a performance based design equation for implementation in Chapter 21 of ACI 318. This is done by addressing both the area requirement of section 21.4.4.1 and the spacing requirements of section 21.4.4.2. The performance of the ACI model will be evaluated in a relative manner to the current building codes in Canada and New Zealand, as well as proposed models found in the literature. For reasons discussed above, a key variable to be investigated is the axial load level which is currently not present in the confinement requirement within the ACI code. An important conclusion to be drawn is if confinement models incorporating axial load provide an improvement over the ACI model.

Rectangular and circular column test databases, made available by the University of Washington and the Pacific Earthquake Engineering Research (PEER) Center, will be used to compare the requirements of each model with the performance of the columns in the database subjected to simulated seismic loads.

Once the evaluation is complete, the results will be used to determine if the current ACI expressions are adequate to achieve acceptable levels of performance. If it is found that

the confinement requirements of ACI are not the most desired model, a recommended alternative will be proposed. The proposed model will ensure that a column will experience only modest lateral strength degradation before reaching the prescribed lateral drift limit. Also, the form of the confinement requirements and their phrasing within chapter 21 of ACI 318 will be investigated. The intent is to provide a clear and concise clause which explicitly states all confining steel requirements for reinforced concrete columns.

2 CODE EQUATIONS AND PROPOSED MODELS

2.1 Introduction

This chapter introduces the confinement models evaluated in this study. The goal of determining an appropriate confinement model will be reached through an evaluation of these models as apposed to developing a new one. The database of column tests used to perform the evaluation and subsequent results and conclusions are presented in the chapters which follow.

Three building code requirements as well as nine proposed models taken from the literature are presented. The building code requirements are from the current reinforced concrete codes in the United States, Canada and New Zealand. The proposed models evaluated in this study include: Wehbe, Saiidi, and Sanders 1999 , Saatcioglu and Razvi 2002 , Brachmann, Browning and Matamoros 2005 , Sheikh and Khoury 1997 , Bayrak and Sheikh 1998, Paulay and Priestly 1992, Watson, Zahn and Park 1994, Li and Park 2004. The model presented by Paultre and Légeron 2005 is included in the evaluation however, this model has since been adopted as the current Canadian building code requirement as is evaluated under that title. The paper by Li and Park (2004) also provides a short comparison of most the models listed above.

2.2 Current Code Requirements

The following sections outline the confinement requirement of the current reinforced concrete building codes in the United States, Canada and New Zealand.

2.2.1 American Concrete Institute 318-05 (ACI)

Since the early 1900's, the design requirements for lateral steel in reinforced concrete columns have consisted of an area requirement as well as a spacing requirement. Both of

these requirements have undergone modifications as the building code has progressed into the 2005 document. The following is a summary of the lateral steel requirements over the past 70 years.

The first equation for determining the area of lateral steel required for the design of reinforced concrete columns appeared in the 1936 Building Regulations for Reinforced Concrete (ACI 2006). The basic philosophy of the requirement was to ensure that the axial load carrying capacity of the column was maintained after spalling of the cover concrete. This was achieved by considering the material capacity enhancements due to confinement described in Chapter 1. The derivation for the amount of confining steel was first carried out for columns with circular or spiral transverse steel. The strength gain in confined concrete, assumed to be $(f'_{cc}-f'_{co}) = 4.1f_l$ (Richart 1929), was linked to the strength provided by cover concrete

$$0.85f'_c(A_g - A_c) = 4.1f_l(A_c - A_s) \qquad (2.1)$$

Recall from Figure 1.1, the lateral pressure due to the confining steel for a circular column at yield is

$$f_l = \frac{2A_{sp}f_{yt}}{sh_c} \qquad (2.2)$$

Substituting f_l into Equation 2.1 and dividing each side by $(2.05f_{yh}A_c)$, and rearranging the equation gives:

$$\frac{4A_{sp}}{sb_c} = 0.415\frac{f'_c}{f_{yt}}\left(\frac{A_g}{A_c} - 1\right) + \frac{4A_{sp}A_s}{sb_cA_c} \qquad (2.3)$$

Recognizing that the left hand side of the above equation is the volumetric transverse steel ratio for a column with circular or spiral lateral steel, increasing 0.415 to 0.45 and dropping the last term on the right hand side, Equation 2.3 became the ACI code equation for circular columns. The form of the equation shown below in Equation 2-4 has not changed since its original inclusion in the 1936 building code and remains as the current expression for determining the volumetric ratio of transverse steel required by ACI.

$$\rho_s = 0.45\left(\frac{A_g}{A_{ch}} - 1\right)\frac{f_c'}{f_{yt}} \qquad \text{[ACI318-05 Eq 10-5]} \qquad (2.4)$$

The 1936 code also required that the center to center spacing of the spirals was not to exceed one-sixth of the core dimension.

For tied columns, the 1936 code simply required that the lateral ties were at least ¼ in. in diameter and had a spacing of not more than 16 bar diameters, 48 tie diameters or the least dimension of the column.

The requirement of the 1936 code remained unchanged until the 1971 ACI 318 Building Code Requirements for Reinforced Concrete. This was the first ACI code with special provisions for seismic design where in addition to the non-seismic requirement of Equation 2-4, it was stated that the volumetric ratio of lateral steel in circular columns shall not be less than Equation 2-5. Equation 2-5 has remained unchanged and is included in ACI 318 2005.

$$\rho_s = 0.12\frac{f_c'}{ft} \qquad \text{[ACI318-05 Eq 21-2]} \qquad (2.5)$$

Equation 2.5 is a lower bound expression that imposes a limit on the (A_g/A_{ch}) ratio which can approach unity for large columns. The ratio is limited to a minimum of 1.27.

The first equation stipulating the amount of transverse steel in tied columns also was introduced in the 1971 version of the code. For rectangular hoop reinforcement the required area of the bar was determined by the following equation

$$A_{sh} = \frac{l_h \rho_s s_h}{2} \qquad (2.6)$$

where ρ_s is the volumetric ratio required by Equation 2.4 with A_{ch} substituted for A_c and l_h is the maximum unsupported length of rectangular hoop reinforcement. The commentary to the 1971 code states that the equation was intended to provide confinement to the

rectangular core of the column and was devised to provide the same average compressive stress in the core as would exist in the core of an equivalent circular spiral column having equal gross area, core area, center to center spacing of lateral reinforcement and strength of concrete and lateral reinforcement.

The spacing limit for spiral reinforcement in the 1971 version of ACI 318 was changed to a maximum center to center distance of 4 inches.

In the 1983 version of the code, it was recognized that the confining effectiveness of rectangular hoops was less than that of circular or spiral hoops and that this difference should be reflected in the requirements. The code stated that the total cross-sectional area of rectangular hoop reinforcement shall be the greater of

$$A_{sh} = 0.3sb_c \frac{f_c'}{f_{yt}}\left(\frac{A_g}{A_{ch}} - 1\right) \qquad \text{[ACI318-05 Eq 21-3]} \qquad (2.7)$$

and

$$A_{sh} = 0.12sb_c \frac{f'_c}{f_{yt}} \qquad (2.8)$$

Where similar to Equation 2.5 for circular columns, Equation 2.8 is a lower limit applicable to columns with large cross-sectional dimensions.

The 1983 code also implemented a second spacing limit, of one quarter of the minimum member dimension, in addition to the 4 inch maximum stated in the 1971 code.

The 1989 ACI 318 code changed Equation 2.8 to a slightly different lower limit for larger columns which limited the (A_g/A_{ch}) ratio to a minimum of 1.3. The expression, first given in the 1989 code, remains as the current minimum expression in the 2005 code

$$A_{sh} = 0.09sb_c \frac{f'_c}{f_{yt}} \qquad \text{[ACI318-05 Eq 21-4]} \qquad (2.9)$$

The 1999 version of the ACI code implemented changes to the spacing requirements for the seismic design of transverse steel in reinforced concrete columns. Three limits were given and still form the spacing requirements in the 2005 code. As was first given in the 1999 code, Section 21.4.4.2 of ACI 318-05 states that the transverse reinforcement shall be spaced at a distance not exceeding any of the three limits:

$$s \leq 0.25D \qquad (2.10)$$

where D is the minimum column dimension

or

$$s \leq 6d_b \qquad (2.11)$$

where d_b is the diameter of the longitudinal reinforcement

or

$$s_x \leq 4 + \left(\frac{14 - h_x}{3}\right) \qquad \text{[ACI318-05 Eq 21-5]} \qquad (2.12)$$

where h_x is the maximum horizontal spacing of hoop or crosstie legs on all faces of the column. The value of s_x shall not exceed 6 inches and need not be taken less than 4 inches.

According to the ACI-318 -05 commentary, Equation 2.9 is intended to obtain adequate concrete confinement. Equation 2.11 was introduced to recognize that the 4 inch maximum could be relaxed up to 6 inches depending on the arrangement of the longitudinal reinforcement and again the intent was to insure adequate concrete confinement. Equation 2.10, according to the commentary, is intended to restrain the longitudinal reinforcement bars against buckling after spalling of the cover concrete. It is important to state that the spacing limit intended to prevent buckling of the longitudinal reinforcement is not the focus of this study. Only the area and spacing limits which are specifically stated as confinement requirements are of interest here.

It is important to state that it is noted in the Commentary to ACI 318-05 that axial loads and deformation demands required during earthquake loading are not known with sufficient accuracy, hence, the above equations for required confinement are not a function of design earthquake demands.

Table 2.1 Circular column ACI confinement requirements timeline

Circular Columns		
Year	Area Req'mt	Spacing Req'mt
1936	$\rho_s = 0.45\left(\frac{A_g}{A_{ch}} - 1\right)\frac{f_c'}{f_{yt}}$	1/6 h_c
1971	$\rho_s = 0.45\left(\frac{A_g}{A_{ch}} - 1\right)\frac{f_c'}{f_{yt}}$ $\rho_s = 0.12\frac{f_c'}{ft}$	
1999 – Current		$s \le 0.25D$ $s \le 6d_b$

Table 2.2 Rectangular column ACI confinement requirements timeline

	Rectangular Columns	
Year	Area Req'mt	Spacing Req'mt
1936	-	16 diam. long. bar / 48 diam. trans. bar / column dimension
1971	$A_{sh} = \frac{l_h \rho_s s_h}{2}$	4 inches
1983	$A_{sh} = 0.3sb_c \frac{f_c'}{f_{yt}}\left(\frac{A_g}{A_{ch}} - 1\right)$ $A_{sh} = 0.12sb_c \frac{f'_c}{f_{yt}}$	4 inches / ¼ column dim.
1989	$A_{sh} = 0.3sb_c \frac{f_c'}{f_{yt}}\left(\frac{A_g}{A_{ch}} - 1\right)$ $A_{sh} = 0.09sb_c \frac{f'_c}{f_{yt}}$	
1999		$s \le 0.25D$ $s \le 6d_b$ $s_x \le 4 + \left(\frac{14 - h_x}{3}\right)$

2.2.2 Canadian Standards Association A23.3-04 (CSA)

Up until the 2004 version of the A23.3 standard of the Canadian Standards Association (2004), the confining steel requirements for reinforced concrete columns mirrored those of the ACI 318 code. The current requirements for the area of transverse steel in Chapter 21 are taken from a recent proposal by Paultre and Légeron (2005). The details of the proposal are presented in Section 2.3.11.

Based on the equations given in Paultre and Légeron (2005), A23.3 Chapter 21 stipulates that the volumetric ratio of circular hoop reinforcement shall not be less than the larger of

$$\rho_s = 0.4k_p \frac{f_c'}{ft} \qquad \text{[CSA A23.3-04 Eq 21-4]} \qquad (2.13)$$

and

$$\rho_s = 0.45\left(\frac{A_g}{A_{ch}} - 1\right)\frac{f_c'}{f_{yt}} \qquad \text{[CSA A23.3-04 Eq 10-7]} \qquad (2.14)$$

where the factor, k_p, is the ratio of factored axial load for earthquake loading cases to nominal axial resistance at zero eccentricity. Note that for $k_p = 0.3$, these requirements are the same as ACI 318-05.

For columns with rectilinear transverse steel, the code states that the total effective area in each of the principal directions of the cross-section shall not be less than the larger of the amounts required by the following equations:

$$A_{sh} = 0.2k_n k_p \frac{A_g}{A_{ch}}\frac{f_c'}{f_{yt}} sb_c \qquad \text{[CSA A23.3-04 Eq 21-5]} \qquad (2.15)$$

and

$$A_{sh} = 0.09\frac{f_c'}{f_{yt}} sb_c \qquad \text{[CSA A23.3-04 Eq 21-6]} \qquad (2.16)$$

where

$$k_n = n_l/(n_l - 2) \qquad (2.17)$$

and n_l is the total number of longitudinal bars in the column cross-section that are longitudinally supported by the corner of hoops or by hooks of seismic crossties.

Note that in all of the above A23.3 equations, the specified yield strength of hoop reinforcement, f_{yh}, shall not be taken as greater than 500 MPa.

In addition to the area requirements, the CSA code also imposes spacing limits. The same three spacing limits required by ACI (Equation 2.10, 2.11 and 2.12) are required by CSA.

Again, the spacing limit for longitudinal bar buckling is not the focus of this work and will not be considered in the evaluation of the CSA model.

2.2.3 NZS 3101:2006 (NZS)

Section 10.3.10.6 of the New Zealand Standard NZS 3101 (2006) requires that the transverse reinforcement within the plastic hinge region of reinforced concrete columns having rectangular hoops with or without crossties be not less than

$$A_{sh} = sb_c\left[\left(\frac{A_g}{A_{ch}}\frac{1.0-\rho_t m}{3.3}\frac{f_c'}{f_{yt}}\frac{P}{\phi f_c' A_g}\right)-0.0065\right] \quad \text{[NZS3101-06 Eq 10-22]} \qquad (2.18)$$

where

$$m = \frac{f_y}{0.85 f_c'} \qquad (2.19)$$

For columns with circular hoops or spirals, the volumetric ratio of must not be less than

$$\rho_s = \left(\frac{A_g}{A_{ch}}\frac{1.0-\rho_t m}{2.4}\frac{f_c'}{f_{yt}}\frac{P}{\phi f_c' A_g}\right)-0.0084 \qquad \text{[NZS3101-06 Eq 10-20]} \qquad (2.20)$$

where

$$m = \frac{f_y}{0.85 f_c'} \qquad (2.21)$$

The factor $\rho_t m$ shall not be taken greater than 0.4 and the ratio A_g/A_c shall not be greater than 1.5 unless it can be shown that the design strength of the core of the column can resist the design actions. It is also stated in the New Zealand code the f_{yh} shall not be taken as greater than 800 MPa.

In addition to the area requirements described above, the New Zealand code also has spacing limits applied to the lateral steel in reinforced concrete columns. The New Zealand code requires for circular columns that the center-to-center spacing of spirals or circular hoops along the member shall be less than or equal to the smaller of one-third of

the diameter of the cross-section of the member or ten longitudinal bar diameters. For rectangular columns, the center-to-center spacing of tie sets along the member shall be less than or equal to the smaller of one-third of the least lateral dimension of the cross-section or ten diameters of the longitudinal bar being restrained. According to the commentary to the New Zealand code, the spacing limits are considered necessary to restrain buckling of longitudinal steel as well as ensure adequate confinement of the concrete.

There are no minimum limits in NZS3101 analogous to ACI 318 Eq. 21-2 and 21-4 however, in the New Zealand code, the issue of bar buckling is dealt with via another area requirement. For circular columns the following equation is given in addition to Equation 2.17.

$$\rho_s = \frac{A_{st}}{155d''}\frac{f_y}{f_{yt}}\frac{1}{d_b} \qquad \text{[NZS3101-06 Eq 10-21]} \qquad (2.22)$$

In the 2006 version of the New Zealand code, the following condition was introduced for rectangular columns: No individual leg of a stirrup-tie shall be less than

$$A_{te} = \frac{\sum A_b f_y}{135 f_{yt}}\frac{s}{d_b} \qquad \text{[NZS3101-06 Eq 10-23]} \qquad (2.23)$$

where $\sum A_b$ is the sum of the areas of the longitudinal bars reliant on the tie.

The two limitations given in Equations 2.22 and 2.23 are not incorporated in the analysis of the NZS model as they are specifically stated as requirements to prevent longitudinal bar buckling and not for confinement.

The requirements of the current New Zealand code were derived from the work presented in Watson and Park (1989). The same work by Watson and Park was used to develop the Watson Zahn and Park 1994 model discussed below.

2.3 Proposed Models

The following section outlines the proposed confinement models currently found in the literature over the past 15 years. Only models that were developed based on a deformation measure were considered in this study. The first model presented was developed based on displacement ductility, followed by those developed based on drift ratio and then those developed based on curvature ductility.

2.3.1 Wehbe, Saiidi, and Sanders 1999 (WSS99)

Wehbe Saiidi and Sanders (1999) conducted tests on rectangular columns as part of a study to develop detailing guidelines for reinforced concrete bridge columns in areas of low to moderate seismicity. Their research was aimed at investigating the cyclic behavior of columns with moderate amounts of confining steel.

The columns tested in the experimental program contained 46% to 60% of the minimum lateral reinforcement required by the American Association of State Highway and Transportation Officials (AASHTO 1992) provisions. The applied axial loads were 10% to 20% of $A_g f'_c$. The specimens were tested under constant axial loads and reversed cyclic lateral loads. The column specimens exhibited displacement ductilities, μ_Δ, ranging from 5 to 7.

The investigation also aimed to determine the most appropriate equation for determining the quantity of confinement steel. The requirements of the current ACI and New Zealand codes, along with those of AASHTO, the California Department of Transportation (CALTRANS 1983), the Applied Technology Council (ATC 1996) and the proposed method by Paulay and Priestly (1992) (See Section 2.3.7) were evaluated. The ATC-32 method was selected as a benchmark for proportioning moderate ductility confinement. This decision was based on the fact that the ATC-32 equation included that axial load index, the ratio of concrete strength to lateral steel yield stress and incorporated the

longitudinal steel ratio as parameters in determining the confinement steel amount. The The ATC-32 expression is

$$\frac{A_{sh}}{s\ b_c} = 0.12\frac{f'_{ce}}{f_{ye}}\left(0.5+1.25\frac{P}{f'_{ce}\ A_g}\right)+0.13(\rho_t - 0.01) \qquad (2.24)$$

where f'_{ce} is the expected concrete strength and f_{ye} is the expected yield stress of the transverse reinforcement.

ATC-32 expression is identical to the CALTRANS equation with the exception of the additional term on the right hand side of the equation. The ATC expression uses the expected material strengths rather than the specified strengths used in the CALTRANS expression.

Based on the analytical and experimental results, the following equation, using the ATC-32 approach, was proposed to relate the amount of confining reinforcement to attainable displacement ductility, μ_Δ:

$$\frac{A_{sh}}{s\ b_c} = 0.1\mu_\Delta\sqrt{\frac{f_{c,n}}{f'_c}}\left[0.12\frac{f'_c}{f_{yt}}\left(0.5+1.25\frac{P}{f'_c\ A_g}\right)+0.13\left(\rho_t\frac{f_{yt}}{f_{s,n}}-0.01\right)\right] \qquad (2.25)$$

where,

$f_{c,n}$ = 27.6 MPa (or 4 ksi)

$f_{s,n}$ = 414 MPa (or 60 ksi)

A target displacement ductility of 10 is suggested to provide the minimum lateral steel required in areas of high seismicity. A value for μ_Δ of less than 10 could be selected for columns in which the seismic demand is moderate to low. Given the similarity of the proposed equation to both the ATC-31 and CALTRANS expressions and that the model proposed related the confinement to a target displacement ductility, only Equation 2.25 will be evaluated in this study.

The researchers note that the current ACI requirements for confining steel are generally for building design and the applicability of the provisions to bridge columns is not

addressed in the code. By the same rationale, one could suggest that the equation proposed here is intended for use in the design of bridge columns, and its applicability to building structures, the focus of this study, is in question. This is particularly a concern for columns with high axial loads, since the axial load ratio for bridge columns seldom exceeds 30%.

2.3.2 Saatcioglu and Razvi 2002 (SR02)

Saatcioglu and Razvi (2002) present a displacement-based design procedure for confinement of concrete columns subjected to earthquake loads. The design approach, in which lateral drift is the performance criterion, is based on computed drift capacities of columns with varying levels of axial load and confining steel. The authors note that the lateral drift was computed using a computer program for static inelastic loading that incorporates analytical models for confined concrete, steel strain hardening, bar buckling, formation and progression of plastic hinging, anchorage slip and also includes an option for second order deformations caused by P-Δ effects. The lateral drift capacity was computed either at 20% strength decay in moment resistance or at the same level of decay in lateral force resistance. The decay in the latter case included the portion caused by the P-Δ effect.

The authors made use of an extensive investigation of parameters which impacted the lateral drift of columns presented in Razvi and Saatcioglu (1999). The investigation concluded that columns which have a consistent 'parameter ratio' would exhibit approximately similar drift capacities when all other parameters remained constant, irrespective of the individual values of the parameters within the ratio. The parameter ratio, r, was expressed as:

$$r = \frac{\rho_{area} f_{yt}}{f_c' \left[\frac{A_g}{A_{ch}} - 1 \right]} \qquad (2.26)$$

A comparison of column drift capacity with coefficient r, was made for columns with different levels of axial load and efficiency of transverse reinforcement, k_2. The results suggested that the following approximation could be made between r and the lateral drift ratio δ:

$$r = 14 \frac{1}{\sqrt{k_2}} \frac{P}{P_0} \delta \qquad (2.27)$$

where

$$k_2 = 0.15 \sqrt{\frac{b_c}{s} \cdot \frac{b_c}{s_l}} \qquad (2.28)$$

Equating the two expressions for r, and solving for the reinforcement ratio, yields the proposed equation:

$$\rho_{area} = 14 \frac{f'_c}{f_{yt}} \left[\frac{A_g}{A_{ch}} - 1 \right] \frac{1}{\sqrt{k_2}} \frac{P}{P_0} \delta \qquad (2.29)$$

The authors also assume an average longitudinal reinforcement ratio of 2 %.
Equation 2.31 may be used for different drift ratios up to 4%. The proposed equation incorporates the effects of reinforcement arrangement and higher strengths of steel and concrete and also incorporates the effect of axial force for a displacement-based design.

When a 2.5% drift ratio is substituted into the expression and the axial force ratio P/P_0 is replaced with $P_u / \phi P_0$ the following design equation is presented:

$$\frac{A_{sh}}{s b_c} = 0.35 \frac{f'_c}{f_{yt}} \left[\frac{A_g}{A_{ch}} - 1 \right] \frac{1}{\sqrt{k_2}} \frac{P_u}{\phi P_0} \qquad (2.30)$$

The authors recommend that the following limitations are used to ensure a minimum amount of transverse reinforcement is required for columns with low axial loads or very large cross sections:

$$\frac{P}{P_0} \geq 0.2 \quad \text{and} \quad \frac{A_g}{A_c} - 1 \geq 0.3$$

The axial force P_u is maximum compressive load which a column will experience during a strong earthquake. The authors suggest that the capacity reduction factor, ϕ, can be increased to 0.90 from 0.7 and 0.75 currently recommended in ACI 318 due to the improved ductility of properly confined columns.

2.3.3 Brachmann, Browning and Matamoros 2005 (BBM05)

The original Brachmann, Browning and Matamoros model (BBM04) was based on the work by Brachmann et. al. 2004(b). The nature of the equations proposed was such that only a small range of axial loads, with a maximum value of 33%, would provide a meaningful value for required transverse reinforcement. This limitation alone would render the proposed equation as highly impractical given that axial load ratios commonly exceed 33%. With this fact in mind, and considering that the same authors proposed new transverse reinforcement equations a year later (Brachmann et. al. 2004(a)), only the later proposal (given the name BBM05 for simplicity) is included in this study.

The primary objective in the work by Brachmann, Browning and Matamoros (2004(a)) was to define a relationship between the limiting drift ratio of reinforced concrete columns and their material and structural properties. To do this, the authors utilized data from 184 rectangular column specimens. Shear span-to-depth ratios of at least 2.5 were used to ensure that the selected specimens exhibit predominantly flexural response. The parameters considered in the study included concrete compressive strength, transverse reinforcement ratio, yield strength of transverse steel and axial load.

The authors presented a nonlinear relationship which relates the estimated limiting drift ratio of a column with the transverse reinforcement ratio, steel and concrete strengths, and axial load. A design procedure to determine the proper amount of confinement reinforcement was proposed based on this nonlinear expression. The expression can be used to prescribe confinement requirements for regions of moderate and high seismicity. This is done by assuming limiting drift ratios of 1.5% and 2.5% for each of these regions,

respectively. Consequently, the resulting design expression proposed by the authors, expressed in terms of area or volume transverse reinforcement ratio, is as follows:

$$\rho = \left(\frac{\gamma}{1 - 0.8 f_{pc}} \right)^2 \frac{f'_c}{f_{yt}} \qquad (2.31)$$

where f_{pc} is the axial load ratio (to confined core) given as $P / A_{ch} f'_c$ and the coefficient γ is taken from the following table: (note that this study considers only high seismic demand)

Table 2.3 Value of Coefficient γ for Equation 2.33 (adapted from Brachmann et. al 2004(a))

Type of Seismic Demand	Transverse Reinforcement Ratio, ρ	Coefficient γ, Circular Columns	Coefficient γ, Rectangular Columns
Moderate Seismicity	ρ_{vol}	0.15	0.18
	ρ_{area}	0.09	0.12
High Seismicity	ρ_{vol}	0.25	0.30
	ρ_{area}	0.15	0.20

The proposed equation provided safe estimates of the limiting drift of columns with compressive strengths up to 116 MPa and it is recommended that these equations not be used when the yield strength of the reinforcement exceeds 830 MPa.

2.3.4 Sheikh and Khoury 1997 (SK97)

Sheikh and Khoury (1997) used the details from previous column tests to propose a performance-based confining reinforcement design procedure. The researchers aimed at developing a procedure which related the confinement requirements to the desired column performance. Additionally, they included in their proposal two parameters, steel

configuration and axial load level, to account for the vast amount of research which identified them as key contributors to confinement effectiveness.

The following equation provides the relationship between the amount of lateral steel as recommended by the current ACI Code ($A_{sh,\ ACI}$) and the requirement proposed by the authors (A_{sh}):

$$A_{sh} = (A_{sh,ACI}) \cdot \alpha \cdot Y_p \cdot Y_\phi \qquad (2.32)$$

where,

α = steel configuration factor

Y_p = axial load level factor

Y_φ = section performance factor

The α parameter is dependent upon the steel configuration category. Sheikh and Khoury identified three lateral steel configuration categories and defined as follows:

Category I: where only single-perimeter hoops are used as confining steel.

Category II: in addition to the perimeter hoops supporting four corner bars, at least one middle longitudinal bar at each face is supported at alternate points by hooks that are not anchored in the core.

Category III: in which a minimum of three longitudinal bars are effectively supported by tie corners on each face and hooks are anchored into the core concrete.

The α parameter is assumed to be unity for category III configurations, and greater than unity for category I. An average value of 2.5 is assumed for all configuration types in this category. The authors note that using a value of α equal to unity for category II configurations is reasonable in situations where the opening of hooks which are not anchored in the core concrete does not happen until after the column has reached a sufficient level of ductility.

The authors also developed two empirically determined equations for the two adjustment factors Y_p and Y_φ. Y_p is a factor developed to adjust the confining steel requirement according to the axial load level and Y_φ takes into account the section ductility demand. The equations are expressed as follows:

$$Y_p = \left\{1+13\left(\frac{P}{P_0}\right)^5\right\} \qquad (2.33)$$

$$Y_\phi = \frac{(\mu_\phi)^{1.15}}{29} \qquad (2.34)$$

where μ_φ is the target curvature ductility.

To select the target curvature ductility, the seismic performance of a column was classified into three categories: 1) high ductility ($\mu_\varphi \geq 16$), 2) moderate ductility ($16 \geq \mu_\varphi \geq 8$) and 3) low ductility ($\mu_\varphi < 8$). Once the desired performance is identified, the appropriate value for μ_φ is inserted into Equation 2.23. A curvature ductility of 16 is used in this study to evaluate the SK97 model.

The equations presented by Sheikh and Khoury were proposed for tied columns only. However, the model will also be considered in the analysis of circular columns, assuming an α value of 1.

2.3.5 Bayrak and Sheikh 1998 (BS98)

Bayrak and Sheikh (1998) presented results of four column tests and combined the results with previous tests to evaluate the suitability of the design equations presented earlier by Sheikh and Khoury (1997) to columns made with high strength concrete (HSC) and ultra high strength concrete (UHSC). Using the same procedure as Sheikh and Khoury, the authors developed a new design procedure for confinement of HSC columns with f'_c greater than 55 MPa.

The authors again took the approach of multiplying the total cross-sectional area of rectilinear ties required by the current ACI ($A_{sh,\ ACI}$) code by factors which account for steel configuration, the effect of axial load, and the section ductility demand. The researchers concluded that the effect of axial load on the lateral reinforcement demand is independent of concrete strength, while the section ductility demand is significantly

influenced by concrete strength. Consequently, the researchers proposed equations in similar form to those presented by Sheikh and Khoury with a modification to Equation 2.23 to accommodate for higher concrete strengths:

$$Ash = (A_{sh,ACI}) \cdot \alpha \cdot Y_p \cdot Y_\phi \quad (2.35)$$

$$Y_p = \left\{ 1 + 13 \left(\frac{P}{P_0} \right)^5 \right\} \quad (2.36)$$

$$Y_\phi = \frac{(\mu_\phi)^{0.82}}{8.12} \quad (2.37)$$

The researchers again suggest that a curvature ductility factor of 16 can be used to define a highly ductile column therefore this value is used here to evaluate the BS98 model. Again, the BS98 model was specifically proposed for tied columns but will be evaluated for circular columns as well using an α value of 1.

2.3.6 Bayrak and Sheikh & Sheikh and Khoury

Given that the equations for high strength concrete in Bayrak and Sheihk (1998) are extensions of the Sheikh and Khoury (1997) equations, a true transverse reinforcement model, representing the intent in which they are proposed, should be a combination of the two. The model, termed here SKBS, utilizes the SK97 model for columns with concrete compressive strengths less than 55 MPa, and the BS98 model for any column with compressive strength of 55 MPa or greater. A curvature ductility of 16 is used to evaluate the SKBS model.

2.3.7 Paulay and Priestly 1992 (PP92)

Paulay and Priestley (1992) wrote one the most widely used seismic design text books in the world. In it, the authors proposed a design equation which relates the transverse reinforcement cross-sectional area, A_{sh}, to required curvature ductility, μ_φ. The required

confining reinforcement area is given for rectangular sections by the following relationship:

$$A_{sh} = sb_c(0.15 + 0.01\mu_\phi) \cdot \frac{f_c'}{f_{yt}} \cdot \frac{A_g}{A_{ch}} \cdot \left(\frac{P}{A_g f_c'} - 0.08 \right) \qquad (2.38)$$

The equation can also be expressed as:

$$\frac{A_{sh}}{sb_c} = k \frac{f_c'}{f_{yt}} \frac{A_g}{A_{ch}} \left(\frac{P}{A_g f_c'} - 0.08 \right) \qquad (2.39)$$

Where k = 0.35 for a required curvature ductility of 20 (high ductility demand), and k=0.25 for curvature ductility of 10 (low ductility demand). Since this study is considering only high seismic demands, a curvature ductility of 20 is assumed.

The right hand side of equation 2.35 may also be used to estimate the required volumetric ratio of confinement for circular columns. Recall, for circular columns the volumetric transverse reinforcement ratio is:

$$\rho_s = \frac{4A_{sp}}{s_h \cdot b_c} \qquad (2.40)$$

where A_{sp} is the cross-sectional area of the spiral or circular hoop reinforcement, and h_c is the diameter of the confined core. For circular columns, k = 0.5 and 0.35 for curvature ductilities of 20 and 10 respectively.

2.3.8 Watson, Zahn and Park 1994 (WZP94)

Zahn, Park and Priestley (1986) used a computer program for cyclic moment-curvature analysis to derive design charts for the flexural strength and ductility of reinforced concrete columns. The curvature ductility charts, developed for circular reinforced concrete columns, related the available curvature ductility at the critical section of the plastic hinge to the magnitude of the effective lateral confining stress acting on the core concrete and the axial load level. Zahn et al. also developed charts to determine the ideal flexural strength of a circular column with a specified mechanical reinforcing ratio, $\rho_t m$.

Based on their design charts, Zahn et al. developed a design procedure for the flexural strength and ductility of reinforced concrete bridge columns. A designer chooses the level of displacement ductility and obtains the associated code recommended design seismic lateral loading for the bridge substructure. From the substructure geometry and the imposed displacement ductility factor, the required curvature ductility could be obtained. Then, using the design charts for the curvature ductility factor, the appropriate amount of confining steel could be determined.

These design charts were used by Watson and Park (1989) to obtain refined design equations for confining steel. Watson and Park developed plots which gave the quantities of confining steel required within the plastic hinge region, obtained from the Zahn et. al. charts, to achieve a specific curvature ductility factor for a given mechanical ratio. From these plots, an equation was derived for square and rectangular columns. These equations have since been further simplified by Watson et. al. (1994) and extended to circular columns. According to Watson et. al. the design equations can be expressed in the equations given below.

For square or rectangular columns:

$$\frac{A_{sh}}{sb_c} = \left(\frac{A_g}{A_{ch}} \frac{(\phi_u / \phi_y) - 33\rho_t m + 22}{111} \frac{f_c'}{f_{yt}} \frac{P}{\phi f_c' A_g} \right) - 0.006 \qquad (2.41)$$

For columns with circular hoop or spiral transverse reinforcement:

$$\frac{4A_{sp}}{sb_c} = 1.4 \left(\frac{A_g}{A_{ch}} \frac{(\phi_u / \phi_y) - 33\rho_t m + 22}{111} \frac{f_c'}{f_{yt}} \frac{P}{\phi f_c' A_g} \right) - 0.008 \qquad (2.42)$$

The authors note that equations 2.37 and 2.38 provide the required area of confining steel to achieve a specific level of curvature ductility. They also suggest that for the curvature ductility factor, ϕ_u / ϕ_y, a value of 20 be used for ductile design and a value of 10 be used for limited ductility or cases where a full calculation of the required curvature ductility factor is unwarranted.

2.3.9 Li and Park 2004 (LP04)

The work done by Li and Park (2004) was aimed at deriving confining requirements more appropriate for columns designed with high strength concrete (HSC) with normal and high yield strength steel.

The authors used the same analytical procedure described above in section 2.3.8 and Zahn, Park and Priestley (1986). Again, curvature ductility was the performance criterion selected. The analytical model made use of the cyclic stress-strain model for HSC proposed by Mander, Priestley, and Park (1988) and later modified by Dodd and Cooke (1992), and the cyclic stress-strain model for steel proposed by Dodd and Restrepo-Posada (1995).

The results of their parametric study suggested that the current ACI 318 and NZS 3101 requirements should be revised for columns making used of HSC. The authors presented equations which provide the required amount of confining reinforcement for square, rectangular and circular HSC columns with normal and high yield strength steel. The equations are a modification of those proposed by Watson, Park and Zahn (1994).

For HSC columns confined by rectilinear normal yield strength steel:

$$\frac{A_{sh}}{sb_c} = \left(\frac{A_g}{A_{ch}} \frac{(\phi_u / \phi_y) - 33\rho_t m + 22}{\lambda} \frac{f_c'}{f_{yh}} \frac{P}{\phi f_c' A_g} \right) - 0.006 \qquad (2.43)$$

Where $\lambda = 117$ when $f_c < 70$ MPa, and $\lambda = 0.05(f_c')2\text{-}9.54f_c'+539.4$ when $f_c \geq 70$ MPa.

For HSC columns confined by circular normal yield strength steel:

$$\frac{A_{sh}}{s\ b_c} = \left(\left(\frac{A_g}{A_{ch}} \frac{(\phi_u / \phi_y) - 33\rho_t m + 22}{111} \frac{f_c'}{f_{yh}} \frac{P}{\phi f_c' A_g} \right) - 0.006 \right) \cdot \alpha \qquad (2.44)$$

where $\alpha = 1.1$ when $f_c < 80$ MPa and $\alpha = 1.0$ when $f_c \geq 80$ MPa.

For HSC columns confined by rectilinear high-yield-strength steel ($f_{yh} > 1150$ MPa):

$$\frac{A_{sh}}{sb_c} = \left(\frac{A_g}{A_{ch}} \frac{(\phi_u / \phi_y) - 30\rho_t m + 22}{\lambda} \frac{f_c'}{f_{yt}} \frac{P}{\phi f_c' A_g} \right) \quad (2.45)$$

where $\lambda = 91\text{-}0.1f_c'$

For HSC columns confined by circular high-yield-strength steel:

$$\frac{A_{sh}}{sb_c} = \left(\frac{A_g}{A_c} \frac{(\phi_u / \phi_y) - 55\rho_t m + 25}{79} \frac{f_c'}{f_{yt}} \frac{P_e}{\phi f_c' A_g} \right) \quad (2.46)$$

Note: $\rho_t m$ = mechanical reinforcing ratio

The authors also place the following limitations on their proposed equations:
The maximum value of $\rho_t m$ that can be substituted into any of the equations is 0.4.
A_c/A_g is not permitted to exceed 1.5 unless it can be shown that the design strength of the core of the column can resist the design axial load applied concentrically.

2.3.10 Watson Zahn and Park & Li and Park

Given that the Li and Park (1994) equations for use in the design of HSC columns are extensions of the Watson, Zahn and Park (1994), a true transverse reinforcement model, representing the intent in which they are proposed, should be a combination of the two. In this study, the model WZPLP uses the WZP94 mdoel for columns with concrete compressive strength less than 60 MPa, and LP04 for any column with compressive strength of 60 MPa or greater.

2.3.11 Paultre and Légeron 2005 (PL05)

Paultre and Légeron (2005) developed a new set of equations for confinement of concrete columns using a wide range of concrete strengths up to 120 MPa and confinement steel strength up to 1400 MPa. The authors proposed two sets of equations, depending on the curvature requirements. One set of equations given for columns with high ductility

demand assumes a target curvature of μ_ϕ= 16, while another set of equations given for columns with limited ductility assumes a target curvature of μ_ϕ=10. The equations were developed from a comprehensive study on the influence of the various parameters of importance on ductility of columns. The authors performed numerical simulation tests similar to actual lab tests to develop their equations.

To complete their numerical simulations, the authors had to select models which reflected, as accurately as possible, the behaviour of the materials. They used the Légeron and Paultre (2003) uniaxial model for the behaviour of confined concrete. The model, described earlier in Section 1.1, relates the materials increase in strength and ductility to the effective confinement Index I'_e

$$I'_e = \frac{f'_{le}}{f'_c} \qquad (2.47)$$

where f'_{le} is the peak effective confinement pressure. For rectangular columns in the y direction it is given by

$$f'_{le} = K_e \frac{A_{shy} f'_h}{c_y s} \qquad (2.48)$$

Recall K_e is the geometric coefficient of effectiveness and c_y is the cross section dimension in the y direction and f'_h is the stress in the confinement steel at peak stress. For circular columns f'_{le} is given by

$$f'_{le} = \frac{1}{2} K_e \rho_s f'_h \qquad (2.49)$$

The authors used the sectional behaviour of more than 200 column sections predicted with a simulation software program. The results were used to determine the relationship between the column ductility and the ratio of I'_e/k_p, where $k_p = P/P_0$ and P_0 is the nominal axial load capacity of the column. The authors found this relationship to be

$$I'_e = 0.0111 k_p \mu_\phi \qquad (2.50)$$

The authors then derive simplifications for the Geometric Coefficient of Effectiveness K_e for both rectangular and circular columns. The coefficient is broken down into vertical and horizontal components K_h and K_v where

$$K_e = K_h K_v \tag{2.51}$$

The expressions for K_v included the spacing of the lateral steel bars. To simplify the equations, the authors determined the K_v values for over 500 columns considering the minimum spacing requirements of ACI. They concluded that a conservative value for K_v could be expressed as a function of the ration A_{ch}/A_g. For members with rectangular hoops

$$K_h = 1 - \frac{2.0}{n_l} \tag{2.52}$$

$$K_v = 1.05\frac{A_{ch}}{A_g} \text{ (for } \mu_\phi = 16) \tag{2.53}$$

or

$$K_v = 0.95\frac{A_{ch}}{A_g} \text{ (for } \mu_\phi = 10) \tag{2.54}$$

For members with circular or spiral hoops, K_h is unity and K_v is 0.90.

The authors highlight that ties are not always effective with their full yield strength, therefore an effective stress f'_h, apposed to the yield stress f_{hy}, is used. The authors make the following conservative recommendations: for circular columns, $f'_h = 0.95 f_{hy}$, and for rectangular columns, $f'_h = 0.65 f_{hy}$.

To develop their proposed equations, the authers combined Equations 2.47 with Equation 2.48 for rectangular columns and Equation 2.49 for circular columns. Then they incorporated their K_v and K_h simplifications and fitting parameters to develop expressions for the different target curvature ductilites. The authors proposed the following equations: For rectangular columns, the required area of transverse steel in the y direction is given by:

$$A_{shy} = \Phi k_p k_n c_y s \frac{f'_c}{f_{yt}} \frac{A_g}{A_{ch}} \quad (2.55)$$

where Φ = 0.2 for columns with high ductility demand (μ_ϕ=**16**), 0.15 for columns with limited ductility demand (μ_ϕ=**10**) and where

$$k_n = n_l / (n_l - 2) \quad (2.56)$$

For circular columns, the required volumetric reinforcement ratio is given by

$$\rho_s = \Phi k_p \frac{f'_c}{f_{yt}} \quad (2.57)$$

where Φ = 0.4 for fully ductile columns and 0.25 for limited ductility. Note, the ratio A_g/A_{ch} does not appear in the epression for circular columns as the Kv value is independent of this ratio.

The equations proposed by Paultre and Légeron have been adopted into the Canadian concrete design code (CSA, 2004). Therefore, the model will be evaluated under that title (CSA) and not as alternate proposed model as is the case for the rest of the models described in this section.

2.4 Range of Properties Investigated

The table below is given to provide some insight to the range of values for the various parameters which were considered by the authors of each model. The table shows that some models considered a wider range of variables compared to others. It is expected that a model which was developed using a smaller range of parameter values will perform poorly in the evaluation conducted here compared to those developed with a wide range of parameter values.

Table 2.4 Range for parameters used in development of the proposed models

Model	f_c' (MPa)		$P/A_g f_c'$		f_{yt} (MPa)		ρ_{arca} (%)	
	Min	Max	Min	Max	Min	Max	Min	Max
SK97	25.9	58.3	0.46	0.777	461.9	558.5	0.77	4.3
BS98	71.7	102.2	0.36	0.5	463	542	2.72	6.74
WSS99	27.2	31.7	0.09	0.24	282.8	321.1	0.369	0.482
SR02	-	-	-	-	-	-	-	-
BBM05	22	116	0	0.7	255	1262	0.07	3.05
PP92	-	-	-	-	-	-	-	-
WZP94	20	40	0.2	0.7	275	275	-	-
LP04	50	100	0.2	0.7	430	1318	-	-
PL05	30	100	0.1	0.6	400	800	-	-

Note: values shown in the table above with a dash (-) were not given.

3 EVALUATION DATABASE

3.1 Experimental Database

The UW/PEER column database (http://maximus.ce.washington.edu/~peera1/) was used to compare the performance of the various proposed models and code equations. The column database is a result of the efforts of many researchers and is a comprehensive record of numerous column tests. The record for each column in the database contains column geometry, material properties, reinforcing details, test configuration (including P-Delta configurations), axial load, classification of failure type, and force-displacement history at the top of the column.

The complete database has 301 rectangular columns, and 168 circular columns, however the complete list was not used here. This study made use of the 230 rectangular column and 166 spiral column database tables established in Camarillo (2003), who used the force-displacement data for each column test to determine a displacement at failure. The procedure used by Camarillo is described in more detail in Section 3.2.

The Camarillo database removed 28 circular columns and 18 rectangular columns from the UW/PEER database due to unusual properties such as the use of lightweight concrete or spliced longitudinal reinforcement, and unknown properties such as unknown P-Δ configuration or missing steel properties. Also, 23 circular and 53 rectangular columns were removed because they did not fail according to the definition of failure established in Camarillo 2003, and presented again here in Section 3.2.2.

For this study, an additional 60 circular and 64 rectangular columns were removed from the Camarillo database because they did not exhibit flexural failure. As discussed in Chapter 1, the aim of this investigation is to establish the most appropriate model for confining steel requirements in columns to resist the flexural demands imposed by seismic excitation. Therefore, including data from column tests which produced shear or

flexure-shear failures would be inappropriate as the performance of the column was not governed by confinement. Taking this approach ensures that all of the columns satisfy the intent of the code which is to ensure that the column will not experience a shear failure. A detailed description of the failure classification procedure is presented in below.

Also, as discussed in Chapter 2, the particular code specifications in ACI, CSA and NZS which intended to prevent buckling of longitudinal reinforcement were not the focus of this work. Therefore, to eliminate the effects of these limits on the evaluation of the current column confinement requirements in ACI, test specimens which did not satisfy the ACI spacing requirement pertaining to bar buckling were removed from the database. This totaled 21 rectangular columns and three circular columns. For this study, the rectangular column "Flexural Failure" database contained 145 columns while its circular column counterpart contained 50 columns. A complete list of the columns in both databases, along with selected properties, can found in Appendix A.

While the lateral steel for all circular columns consists of circular hoops or spiral reinforcement, the lateral reinforcement for the rectangular columns are categorized into seven classifications. The definition and number of columns found within the database for each classification are given in Table 3.1.

Table 3.1 Confinement classification details

Notation	Description	No. of Columns
R	Rectangular ties (around perimeter)	51
RI	Rectangular and Interlocking ties	29
RU	Rectangular ties and U-bars	3
RJ	Rectangular ties and J-hooks	17
RD	Rectangular and Diagonal ties	35
RO	Rectangular and Octagonal ties	9
UJ	U-bars and J-hooks	1

All rectangular columns had rectangular (or square) cross-sections, but the circular columns had two cross-sectional shapes, circular and octagonal. These shapes were assigned codes which, along with the number of each found in the database used here, are given in Table 3.2.

Table 3.2 Cross-Section Classifications

Cross-Section Shape	Code	No. of Columns
Circular	0	40
Octagonal	2	10

3.2 Determination of Failure

The following is a summary of the procedure used in Camarillo (2003) to determine the failure displacement for columns in the database.

Since the database included column tests performed in a wide range of configurations, the lateral force-displacement data provided for each test was converted to represent the lateral forces and displacements which would be imposed on an equivalent cantilever column. This allowed for a consistent evaluation of the performance of each column within the database, regardless of test configuration.

3.2.1 Effective Force and P-Delta correction

Lateral force-displacement data had to be adjusted to take into account the secondary or P-Δ effects. This is of particular importance for columns with large axial loads and large lateral drifts. The following is taken from Parrish (2001) and Berry et. al. (2004), which explains the process used to implement the P-Δ correction.

The loads applied to each column by the vertical actuator were resolved into their vertical and horizontal components. The horizontal component could then be added or subtracted

to the force from the horizontal actuator to find the resulting net horizontal force. To incorporate a P-Δ correction, the database is organized into four types of lateral force-displacement histories, shown in Figure 3.1, each with a specific form of correction. Berry et. al. define the categories as follows:

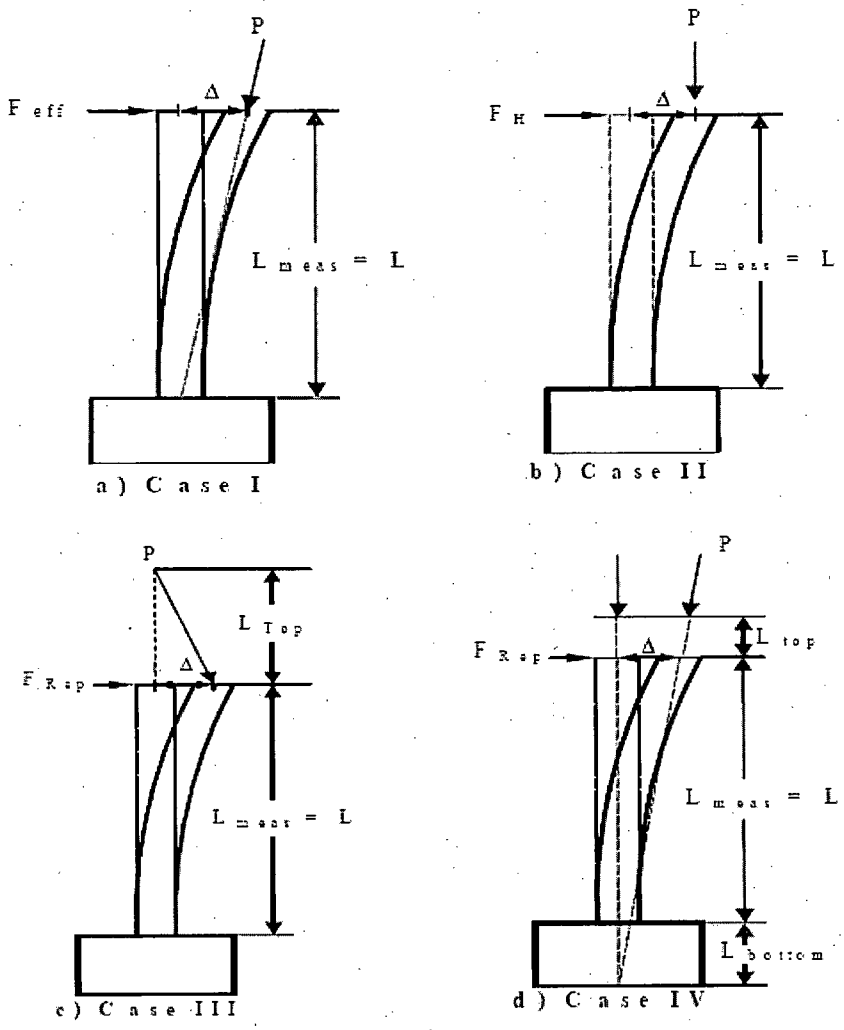

Figure 3.1 P-Δ correction cases (Berry et. al. (2004))

Case I: Force-deflection data provided by the researcher was in the form of effective force (F_{eff}) versus deflection (Δ) at L_{meas}. In this case, the net horizontal force (F_H) can be determined according to the following equation:

$$F_H = F_{eff} - P\Delta / L_{meas} \qquad (3.1)$$

Case II: Force-deflection data was provided by the researcher in the form of net horizontal force (F_H) versus deflection (Δ) at L_{meas}.

$$F_{rep} = F_H \tag{3.2}$$

Case III: Force data provided by the researcher represents the lateral load applied by the horizontal actuator, but the top of the vertical actuator does not translate. In this case, the horizontal component of the vertical load actuator needs to be added to the reported force, F_{rep}, to get the net horizontal force (F_H).

$$F_H = F_{rep} + PL_{Top} / \Delta \tag{3.3}$$

Case IV: Force data provided by the researcher represents the lateral load applied by the horizontal actuator. However, the axial load is not applied at the same elevation as the lateral force, or the line of action of the axial load does not pass through the column base. In this case, the horizontal component (P_H) of the vertical load actuator was subtracted from the reported force, F_{rep}, to get the net horizontal force (F_H).

$$\alpha = \tan^{-1}\left[\frac{\Delta\left(\frac{L + L_{top}}{L}\right)}{L + L_{bot} + L_{top}}\right] \tag{3.4}$$

$$P_H = P \sin\alpha \tag{3.5}$$

$$F_H = F_{rep} - P_H \tag{3.6}$$

The contributions of the net horizontal force and the gravity (vertical) load to the total base moment can then be determined as follows:

$$M_{base} = F_H L + P\Delta\left(\frac{L_{top} + L}{L_{meas}}\right) \tag{3.7}$$

where:

F_H - net horizontal force (Column Shear)

L - shear span length

P - gravity (vertical) load

Δ - measured displacement at cantilever elevation L_{meas}

L_{top} - distance from elevation at which lateral force was applied to elevation at which gravity (vertical) load is applied.

L_{meas} - elevation at which lateral column displacement was measured

The effective force can then be defined as:

$$F_{eff} = M_{base} / L \qquad (3.8)$$

3.2.2 Displacement at Failure

One possible definition of failure displacement is the maximum recorded drift during the test (Δ_{max}). However, the most commonly accepted definition of failure is the point at which a specimen reaches a 20% loss of lateral load capacity. Once the lateral force-displacement data had been corrected for P-Δ effects, the failure displacement, at 80% effective force, could be determined according to the following procedure. Camarillo (2003) describes the process for determining the failure displacement as follows:

From the force-displacement history, the displacement (Δ_{80}) and the data point (i_{80}) corresponding to the last time the column resisted 80% of the absolute maximum effective force were identified. Failure of the column was assumed to occur if:

- *the absolute maximum displacement after the identified 80% force ($\Delta_{post\text{-}80}$) exceeds Δ_{80}.*
  i.e., ($\Delta_{post\text{-}80} \geq \Delta_{80}$)
- *the maximum displacement following another zero crossing ($\Delta_{post\text{-}zero}$) exceeds 95% of Δ_{80}*
  i.e., ($\Delta_{post\text{-}zero} \geq 0.95\ \Delta_{80}$)
- *the force corresponding to the maximum displacement after the zero crossing*

($F_{post\text{-}zero}$), is less than or equal to the proportional force set by the force and displacement at the 80% location

i.e., ($F_{post\text{-}zero} \leq F_{80}$ ($\Delta_{post\text{-}zero}$ / Δ_{80}))

- *Otherwise the column has not failed.*

For columns that fail, the failure displacement (Δ_{fail}) was determined as the maximum displacement that the column was subjected to prior to the data point i_{80}.

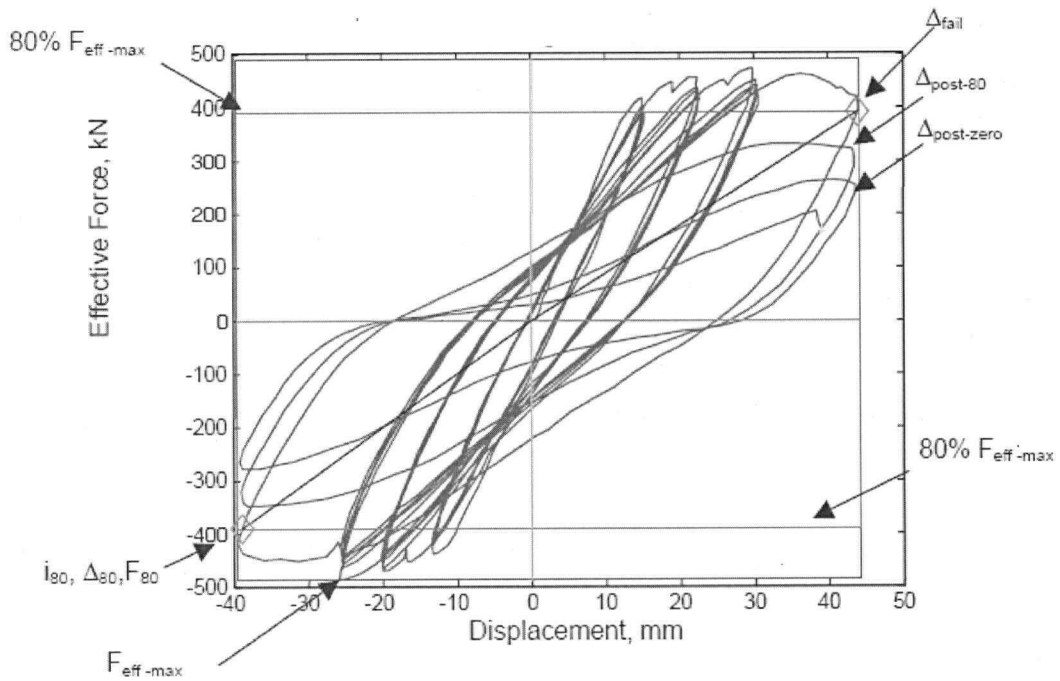

Figure 3.2 Example for confirming failure (Camarillo (2003))

3.3 Failure Classification

The failure behaviour of the columns within the database is categorized into three failure modes; flexural failure, shear failure and flexure-shear failure. For columns which exhibited flexural failure (the focus of the current study), the degradation in the lateral load capacity occurs after yielding of the longitudinal reinforcement and the observable damage includes flexural cracking, spalling of cover concrete, concrete crushing and longitudinal bar buckling. For columns which exhibit shear failure, the degradation of the

lateral load capacity occurs prior to yielding of the longitudinal steel and the observable damage includes diagonal cracking and a sudden loss in strength. Columns classified as flexure-shear failures exhibited a certain level of displacement ductility developing hinging before the shear failure. The schematic diagram shown in Figure 3.3 illustrates the distinction between the three failure modes.

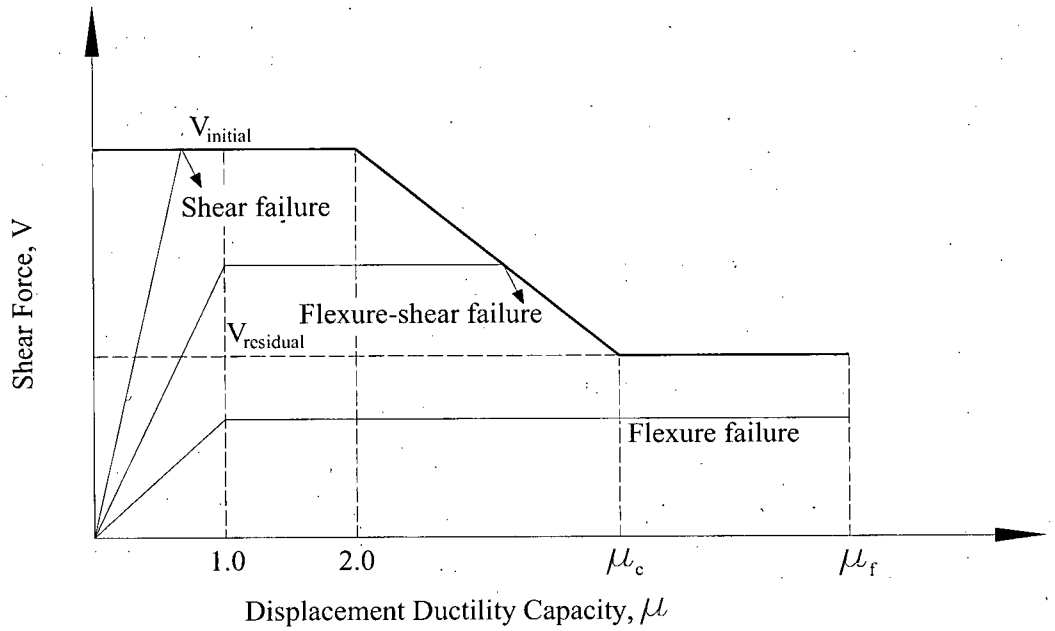

Figure 3.3 Conceptual definition of column failure modes

By combining these definitions, first presented by ATC (1981), with the column test observations, Berry et. al. (2004) classified each column within the UW/PEER database according the criteria shown in Figure 3.4. If no shear damage is reported, the column is classified as flexure-failure. If shear damage is reported, the absolute maximum effective force (F_{eff}), is compared with the calculated force corresponding to a maximum concrete compressive strain of 0.004 ($F_{0.004}$). The failure displacement ductility at the 80% effective force, μ_{fail}, is also considered. If the maximum effective force is less than 95 percent of the ideal force or if the failure displacement ductility was less than or equal to 2, the column was classified as shear-critical. Otherwise, the column is classified as flexure-shear-critical.

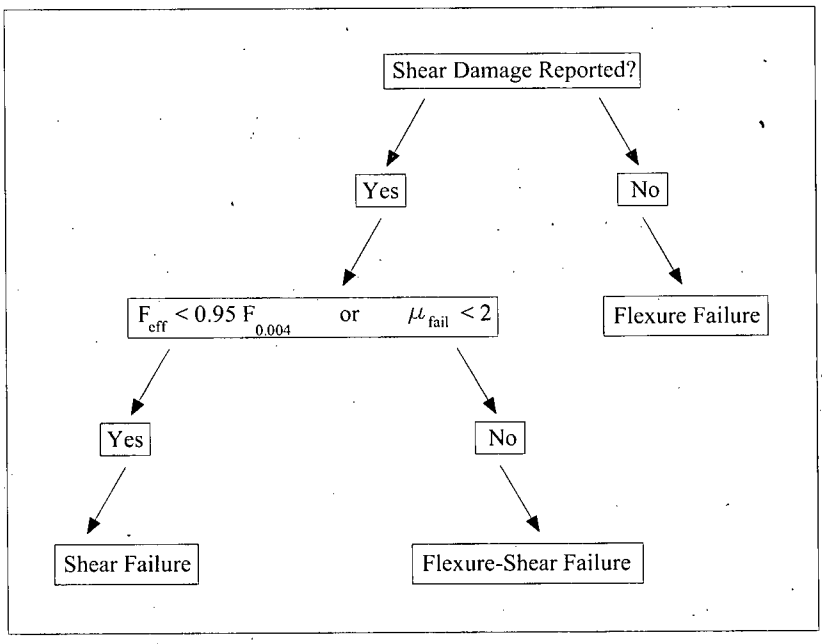

Figure 3.4 Failure Classification Flowchart (Berry et. al (2004))

3.4 Range and Verification of Database Parameter Values

Making use of the column test database, as apposed to conducting individual tests, is done to allow for a wider range of parameter values than is typically available within a particular experimental study. In order to use the database to evaluate the confinement models described in Chapter 2 with increased confidence, a comparative investigation was performed to verify that the parameter ranges in the database are comparable to typical designs carried out according to the most recent building codes. Typical column details from three buildings located in high seismic regions in western United States were provided by the Structural Engineer of Record. Table 3.3 and Table 3.4 present the ranges for the parameters which significantly influence the flexural behaviour of reinforced concrete columns, for both the typical column details and the experimental database. From these tables it can be seen that the range of most of the parameters covered by columns in the database is compatible with the range of values seen in these parameters for new construction. Detail drawings for the 8 rectangular and 12 circular typical columns are provided in Appendix B.

Table 3.3 Rectangular column parameter ranges (database and typical columns)

Parameter	Database			Typ. Details		
	Min.	Max.	Avg.	Min.	Max.	Avg.
f_{yt} (MPa)	255	1424	549.4	414	414	414
f_c (MPa)	20.2	118.0	60.4	28	72	57
s (mm)	25.4	228.6	77.5	76.2	114.3	94
ρ_{area} (A_{sh} / sh_c) (%)	0.11	3.43	1.14	0.90	1.94	1.46
ρ_{long} (%)	1.01	6.03	2.37	1.29	4.12	2.11
A_g (mm^2)	23226	360000	92451	209032	929030	588386
P/A_gf_c	0.0	0.80	0.28	0.33	0.71	0.48

Table 3.4 Circular column parameter ranges (database and typical columns)

Parameter	Database			Typ. Details		
	Min.	Max.	Avg.	Min.	Max.	Avg.
f_{yh} (MPa)	280	1000	473.0	414	414	414
f_c (MPa)	22.0	90.0	36.3	34	69	53
s (mm)	8.9	305.0	55.0	63.5	101.6	78.3
ρ_{vol} ($4A_{sp}$ / sh_c) (%)	0.10	3.13	1.00	1.15	2.76	2.01
ρ_{long} (%)	0.75	5.58	2.31	1.19	3.68	2.03
A_g (mm^2)	18146	1814600	211312	164173	585753	342196
P/A_gf_c	0.0	0.70	0.17	0.01	0.58	0.28

For the rectangular columns, the most glaring discrepancy is found in the gross area (A_g) where the average database value is well below the minimum value for the typical columns. This is to be expected since full scale column tests are often too difficult or expensive to conduct and are therefore not possible due to testing facility or budgetary limitations. The similarity in the values for area transverse reinforcement ratio demonstrates that the section dimensions of the columns in the database are proportionally scaled and the discrepancy in A_g is insignificant. For the circular column database, the same discrepancy is found for the gross area. Table 3.4 also shows that the volumetric ratio of transverse reinforcement is higher for the typical olumns than for the

database suggesting that more testing of columns with confinement levels typically found in building structures is needed.

One of the objectives of this work is to use the database to exemplify what is already known about the relationship between axial load and ductility for reinforced concrete columns. Figure 3.5 shows a plot of axial load ratio versus drift ratio for each test specimen in the rectangular and circular databases. An important observation to note is that the circular column database has significantly less data with high axial load ratios. The circular column database has only 10 columns with an axial load ratio higher than 0.30 as compared to the rectangular column database which has 59. This is because the majority of circular specimens are scaled versions of bridge piers which typically have smaller axial loads compared to columns found in building structures. Consequently, there are very few columns with low drift ratios in the circular column database. The disparity between the two databases will become more apparent in Chapter 4 when they

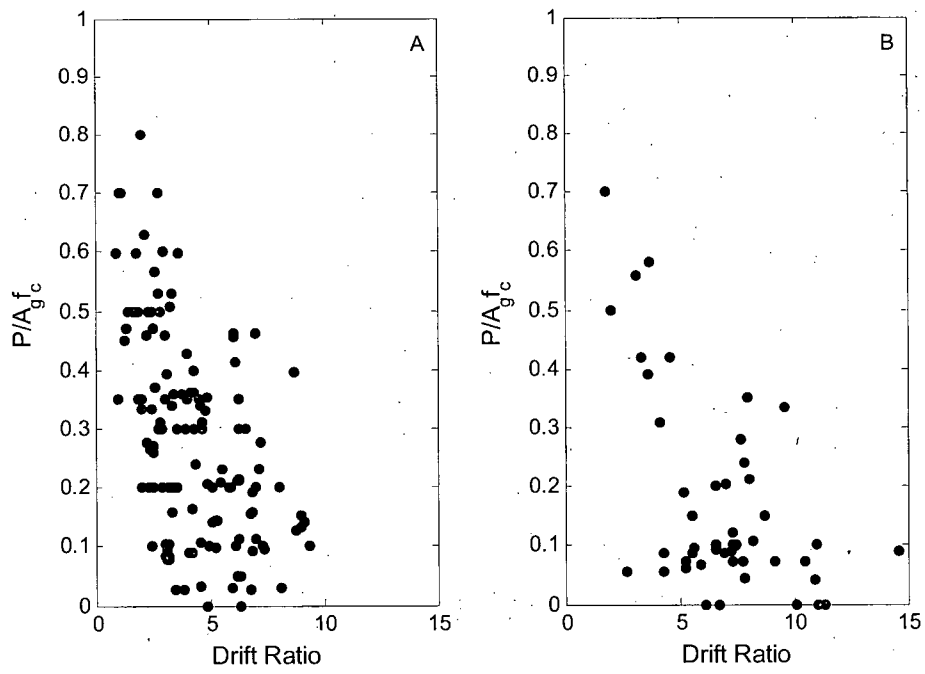

Figure 3.5 Axial Load ratio versus drift ratio

(A) rectangular database (B) circular database

are used to evaluate the performance of the models. It is also important to note that while even though there are fewer columns with a high axial load ratio, the drifts achieved by columns with lower axial loads was typically higher for circular columns than for rectangular columns.

Similar to Figure 3.5, Figure 3.6 to Figure 3.10 show plots for several parameters identified which influence the drift capacity of reinforced concrete columns, and are contained in most of the models described in Chapter 2. The figures show that while the parameters do seismic performance of columns, no single parameter appears to influence lateral drift with the same significance as axial load level. The trend observed in Figure 3.5 is not clear in any of the other plots.

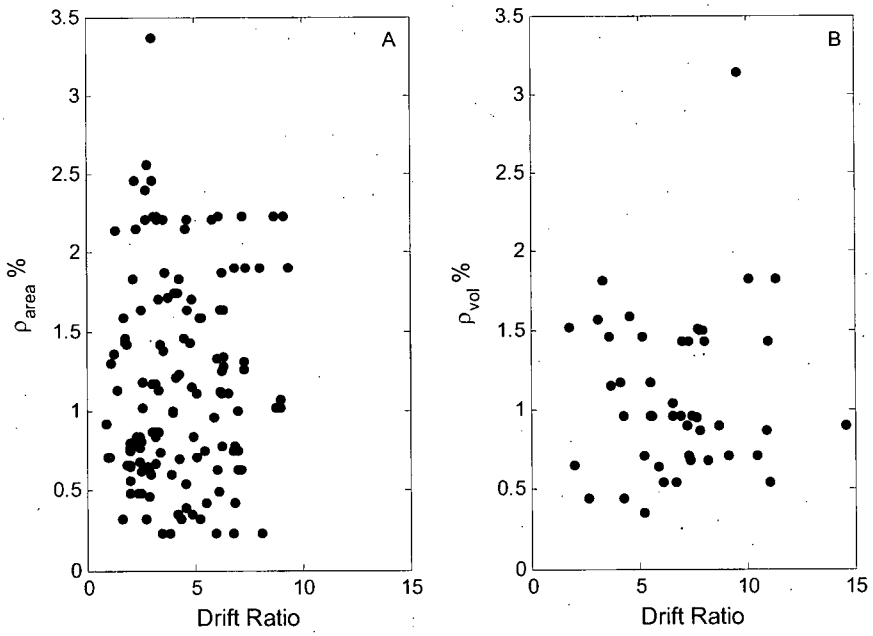

Figure 3.6 ρ_{area} and ρ_{vol} versus drift ratio

(A) rectangular database (B) circular database

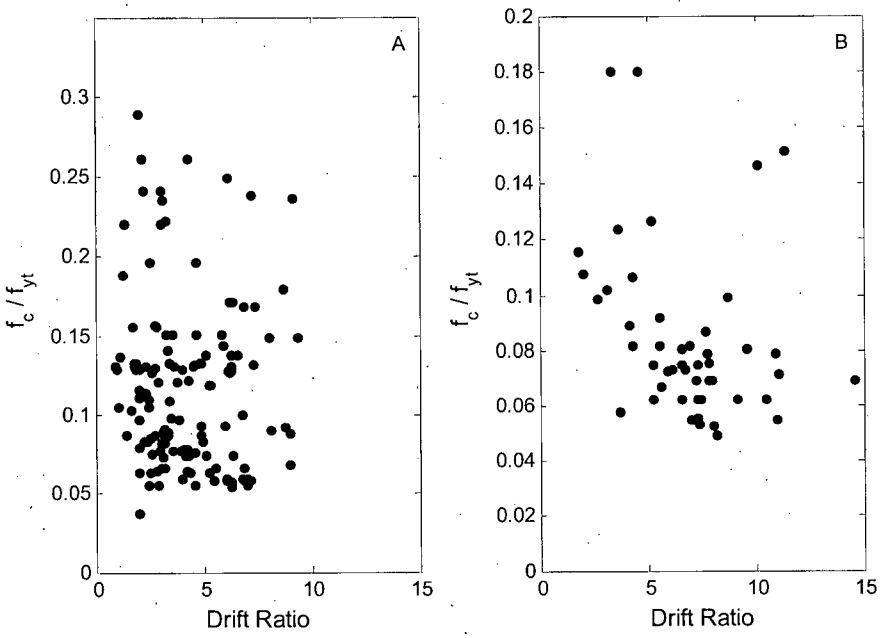

Figure 3.7 f_c' / f_{yt} versus drift ratio

(A) rectangular database (B) circular database

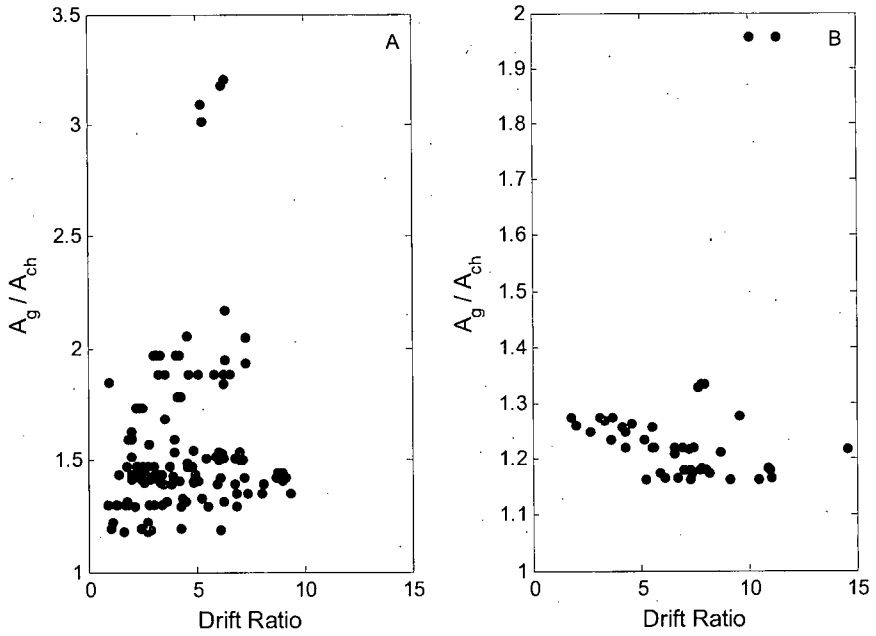

Figure 3.8 A_g / A_{ch} versus drift ratio

(A) rectangular database (B) circular database

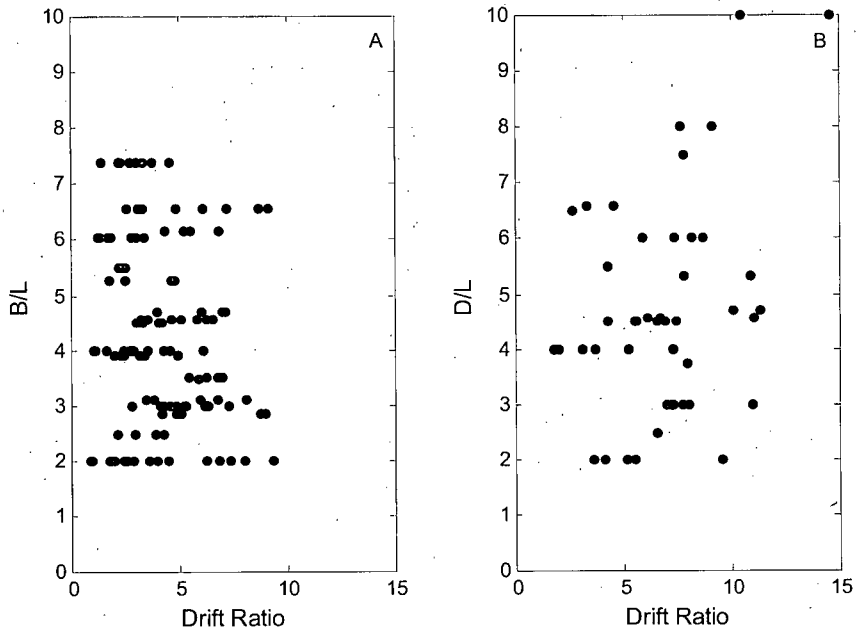

Figure 3.9 B/L and D/L versus drift ratio

(A) rectangular database (B) circular database

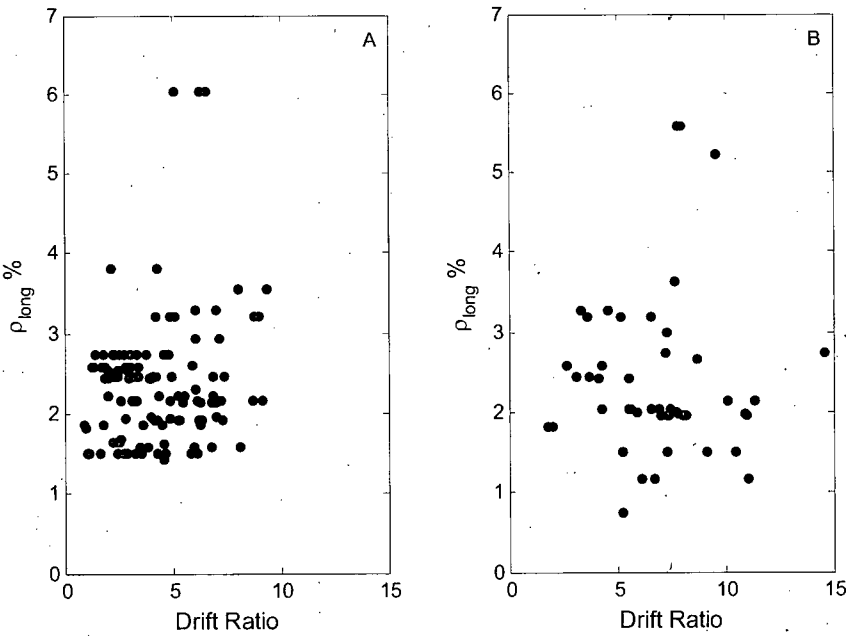

Figure 3.10 ρ_{long} versus drift ratio

(A) rectangular database (B) circular database

4 CONFINEMENT MODEL EVALUATIONS

This chapter presents the procedure and results of the evaluation techniques adopted to analyze the performance of each confinement model. In Chapter 1, it was shown that the amount and configuration of transverse reinforcement is the most important parameter in determining the drift capacity of a reinforced concrete column, and the evaluation approach taken here makes use of this conclusion. The interpretation of the results and the ensuing recommendations will follow in Chapter 5.

4.1 Rectangular Columns

4.1.1 Scatter Plot Evaluation

Each confining reinforcement model was evaluated using the properties and performance of the column specimens within the database discussed in Chapter 3. Two evaluation techniques were developed to investigate the performance of the models. The procedure and results for the first of these two techniques, a scatter plot evaluation, is outlined here and the second technique, a fragility curve evaluation, is outlined in the following section.

4.1.1.1 Evaluation Procedure

The amount of confining reinforcement required for each column in the database, based on the code and model equations from Chapter 2, was calculated and compared with the amount of transverse reinforcement provided. With these values known, it is possible to determine if each column in the database had sufficient transverse reinforcement to meet a particular model or code equation.

Once the amount of transverse steel was determined, a performance criterion had to be selected. As seen in the model descriptions, not all equations used the same performance parameter. One possible comparison technique would be to test each model against the

target performance for which it was designed. In other words, if an equation is developed by using a target curvature ductility of 20, the equation could be evaluated on how well it performs against the measured curvature ductilities of the columns in the database. Similar comparisons could be made for models which used other performance parameters such as displacement ductility or drift ratio. This technique however would not provide any information as to how the models or equations compare against each other, only how they compare with the targets they are designed to meet. Therefore, a consistent performance target had to be selected which could be applied to all models and equations and used as a universal criteria.

A drift ratio of 2.5% was selected as the performance target for this study. The interstory drift ratio is determined in the course of a standard design process and a value of 2% to 2.5% is commonly used as the performance target in many building codes. Ductility related targets are not as preferable for a performance criterion for two main reasons. Firstly, the test data generally does not provide measured curvatures and secondly, a ductility limit depends on the definition of yield for which different researchers take different approaches. A performance criterion which uses total drifts, such as drift ratio, avoids these issues. It should be noted that while choosing a drift ratio of 2.5% may appear to provide a minimal advantage to those models with drift ratio as the performance parameter, the results presented below do not suggest such a bias.

Figure 4.1 shows the layout of the scatter plots which will be used to conduct the first analysis of the confinement models. The figure shows a plot of the drift ratio at 20% loss in lateral strength (described in Chapter 3) versus the confining steel requirement ratio ($A_{sh\_provided}$ / A_{sh_model}). The figure is divided into quadrants with a vertical dashed line at $A_{sh\_provided}$ / A_{sh_model} = 1, and a horizontal dashed line at the performance target DR=2.5%. The introduction of theses two dashed lines divides the plotting area into four distinct quadrants, each with specific implications. Data points falling to the right of the vertical dashed line meet or exceed the confining requirements of a particular model, while those plotted to the left of the vertical dashed line do not meet the requirements. Data plotted above the horizontal dashed line achieved a drift ratio (at 20% loss in

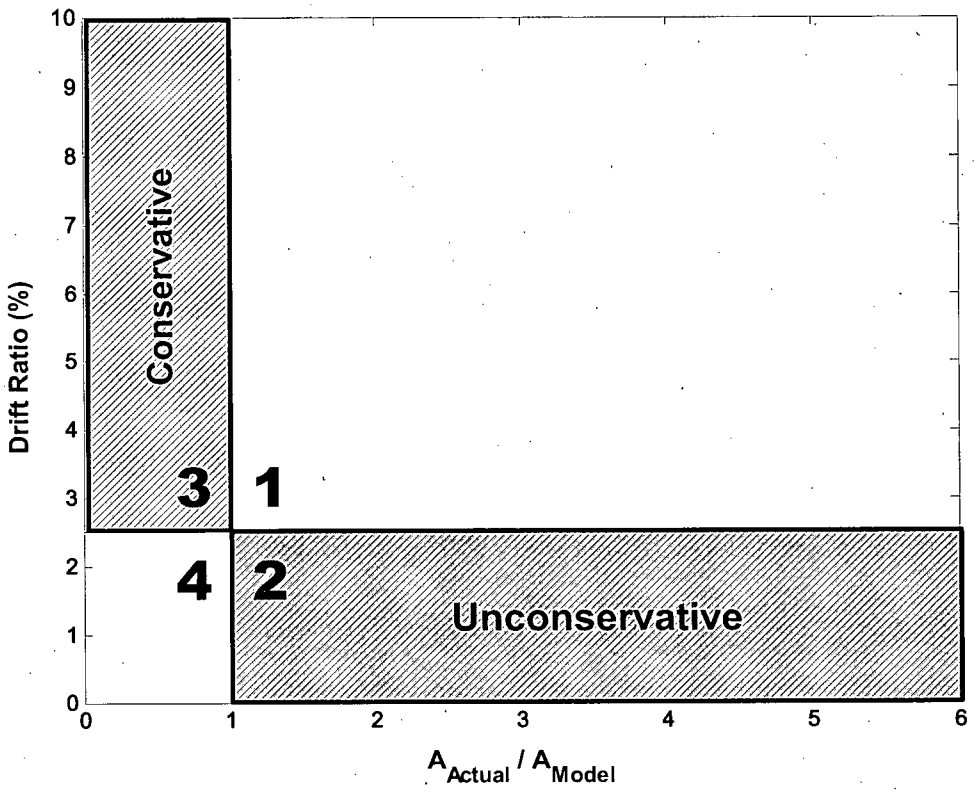

Figure 4.1 Scatter plot layout with identification of quadrant labels

strength) of greater than or equal to the performance target of 2.5%. Therefore, an ideal model would have all columns plotted in the quadrants labeled as "1" and "4", where all test columns which meet or exceed the confinement steel requirements, achieved acceptable levels of drift, and those which did not meet the confining steel requirement of the model did not reach acceptable levels of drift.

Therefore, for a favorable evaluation of a model the plot should have few data points fall in the remaining two quadrants. Data which plots in the upper left quadrant, quadrant 3, fails the confining steel requirements of the model, but meets or exceeds the performance target. This quadrant is termed the 'conservative' quadrant since for data points in this quadrant the model is requiring more steel than is necessary to reach acceptable levels of drift. Data which plots in the lower right quadrant, quadrant 2, meets the confining steel requirements of the model, but does not meet the performance target. This quadrant is

termed the 'unconservative' quadrant since for data points in this area the model requires an insufficient amount of confining steel to achieve acceptable levels of drift.

In order to make a quantitative comparison of the models using the scatter plots, two statistics were calculated for each model and code equation. The following statistic was selected to assess the ability of the model to provide sufficient drift capacity:

$$A(\%) = \frac{\#\text{ of columns that satisfy model AND achieve a drift ratio} \le 2.5\%}{\#\text{ of columns that satisfy model}} \qquad (4.1)$$

In terms of the quadrant numbers:

$$A(\%) = \frac{Q2}{Q1 + Q2} \qquad (4.2)$$

The second statistic was selected to indicate the degree of conservatism inherent in the model:

$$B(\%) = \frac{\#\text{ of columns that do not satisfy model AND achieve a drift ratio} \le 2.5\%}{\#\text{ of columns that do not satisfy model}} \qquad (4.3)$$

$$B(\%) = \frac{Q4}{Q3 + Q4} \qquad (4.4)$$

An ideal model would have an A value of 0% and, to avoid over-conservatism, the B value should be maximized. The difference between the two statistics above also provides an insight to the performance of the model, and is a good representation of the model's overall performance considering all columns.

$$C = B - A \qquad (4.5)$$

A large value for C indicates a model which is 'safe' yet not 'overconservative'.

4.1.1.2 Assessment of ACI 318-05 21.4.4.1

The rectangular column scatter plot for the ACI confining steel requirements is shown below in Figure 4.2. It should be noted that the plot represents only the evaluation of ACI Equations 21-3 and 21-4, and does not include the spacing requirements of ACI 318-05 clause 21.4.4.2. This issue is discussed in section 4.1.3

While properly observing the performance of the ACI model is done best in a relative sense with direct comparison to the other models investigated in this study (see Chapter 5), it is prudent to first fully understand the data presented in Figure 4.2. All columns which satisfy section 21.4.4.1 of ACI are plotted with a lightly shaded square marker, while those which fail the area of confining steel requirements are plotted with a dark shaded diamond marker. This is done such that in subsequent scatter plots for other models, the distinction can be made as to where the columns lie on the ACI scatter plot.

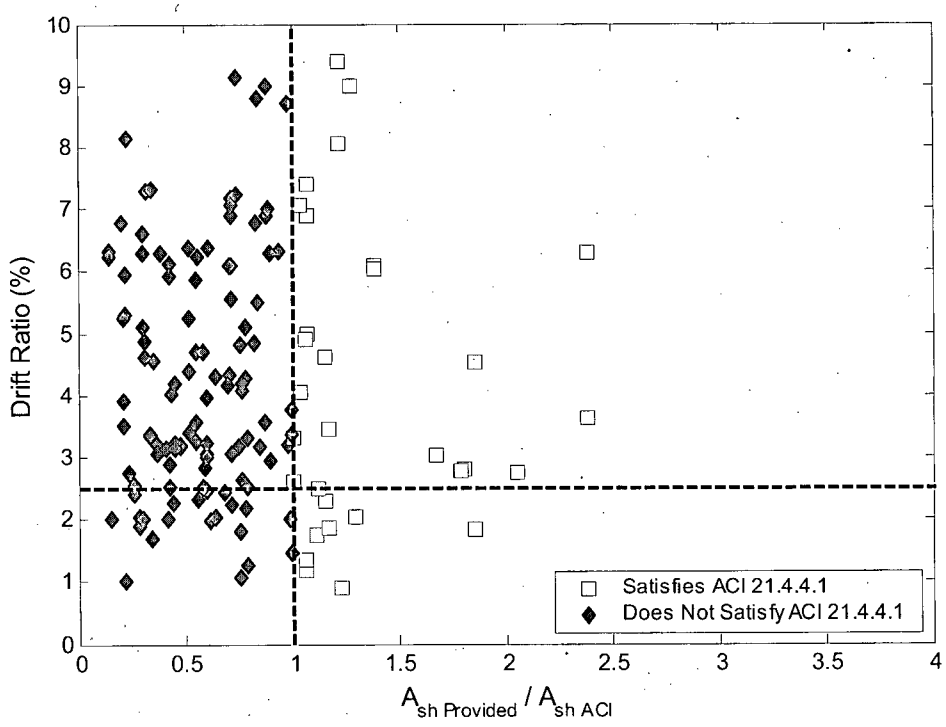

Figure 4.2 ACI scatter plot (rectangular columns)

The figure shows the following data distribution:

Table 4.1 Quadrant data distribution of Figure 4.2

Quadrant 1	Quadrant 2	Quadrant 3	Quadrant 4
23	9	92	21

From the numbers given in Table 4.1 the statistics A, B and C can be calculated as:

Table 4.2 Statistics for ACI rectangular scatter plot

A	B	C
28.1	18.6	-9.5

Earlier in this chapter, quadrants 2 and 3 were identified as the quadrants where it was desired to have as few data points as possible. Figure 4.2 and Table 4.1 show a number of data points in both of these quadrants. In an effort to determine common properties for these tests, Figure 4.3 shows a plot of concrete compressive strength (f_c') versus axial load ratio ($P/A_g f_c'$) for the columns found in quadrant 2 and 3 in Figure 4.2. As seen in Figure 4.3, all of the quadrant 2 columns for the ACI scatter plot have an axial load ratio of at least 0.33, with eight of the nine columns having a value of 0.47 or higher. In comparison, only six of the 92 quadrant 3 columns have an axial load ratio of 0.40 or greater. While the effect of concrete compressive strength on the ductility of a concrete member is well documented in the literature, the effect of axial load appears to be more dominant when assessing the performance of the ACI confining steel requirements. The observations of these figures are in agreement with the expectations based on the relationship between axial load and column ductility presented in Chapter 1.

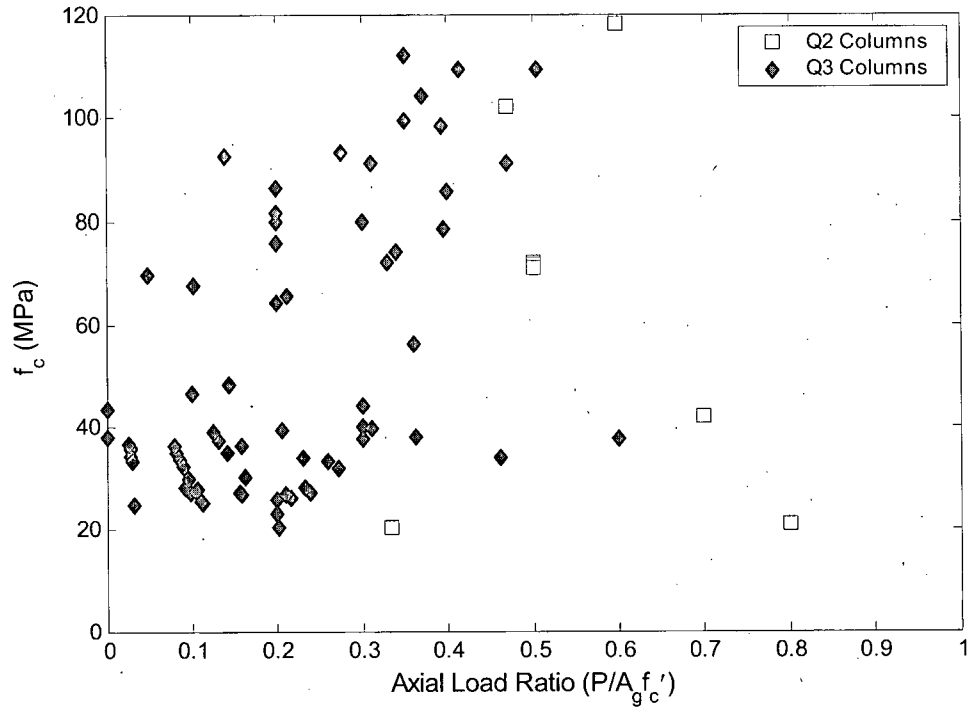

Figure 4.3 f_c' versus Axial Load Ratio for columns in quadrants 2 and 3 of ACI rectangular scatter plot

4.1.1.3 Assessment of Codes and Proposed Models

The scatter plot evaluation of the remaining models was done to compare their performances with that observed for the ACI requirements, and to determine which model is the most appropriate replacement for ACI. First, to perform an appropriate comparison, the ACI minimum requirement given in Equation 2.5 (ACI Equation 21-4) was included in the evaluation of the other models. This was done only to ensure that the effect of a minimum equation was not applied solely to the ACI model which would generate biased results. Once the initial comparison is made, the models will be evaluated strictly on their specific requirements and an appropriate minimum for the recommended model, which may or may not take the form of the current ACI equation, can be determined. Note, the current CSA code applies the same minimum but is not included in the evaluation of the CSA model as this minimum is not included in the PL05 model on which the CSA code is based.

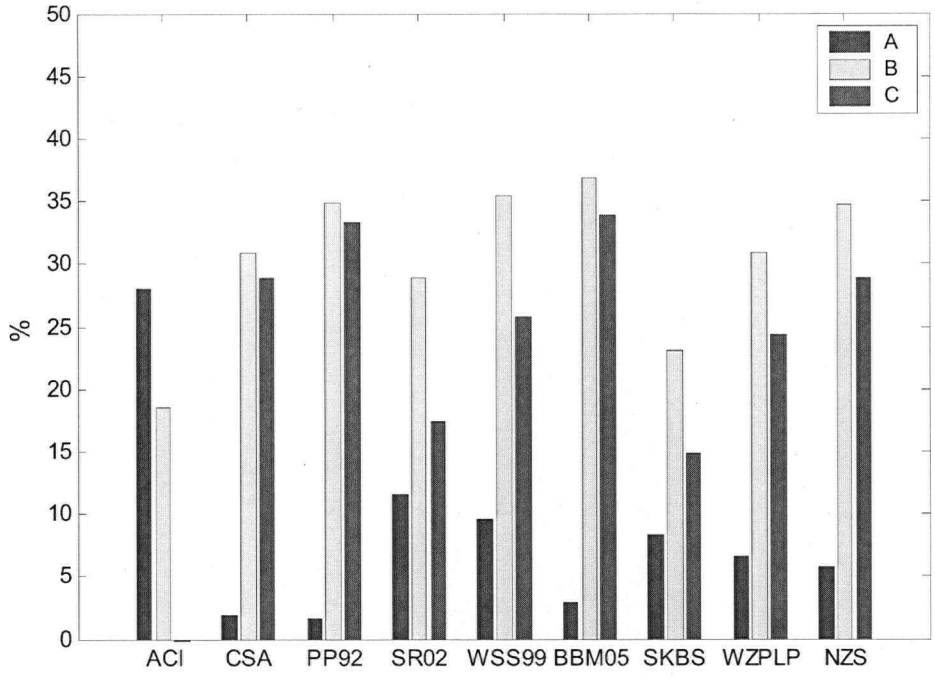

Figure 4.4 Rectangular scatter plot statistics all models (with ACI minimum)

Figure 4.4 shows the A, B and C statistics for all models, including ACI, where all models incorporate the current ACI minimum equation. Scatter plot statistics for SK97, BS98, WZP94, and LP04 are not shown. As noted in Chapter 2, these individual models are used in conjunction with each other to form the combination models SKBS and WZPLP. The individual scatter plots for all models can be found in Appendix D. The table shows that each model provides a significant statistical improvement over the ACI model. ACI had the highest A value, where a low value for A is desirable, and the lowest B value, where a high value for B is desirable. The ACI model was the only model to produce a negative C value, where a large positive value for C is desirable. The results shown in Figure 4.4 suggest that an alternate model to the current ACI equation should be recommended. To properly determine a replacement model, the models must be evaluated strictly on their specific requirements.

The scatter plots for the models not including the ACI minimum equation are presented in Figure 4.5 through Figure 4.12. Again, scatter plots for SK97, BS98, WZP94, and LP04 are not shown. All scatter plots, including those presented here, are included in Appendix D.

As shown in the figures, only the SR02 and WSS99 models had more column data points plotted in quadrant 2, and only SKBS had more data points plotted in quadrant 3, when compared to the ACI scatter plot (Figure 4.2). The most significant change in the number of data points in quadrant 2 is seen the plots for SKBS and CSA which had just two data points in the quadrant. The most significant change in the number of data points in quadrant 3 is seen in the plot for WSS99 which has just 41 data points and SR02 and PP92 which both have 59. The distribution of data points into the four quadrants for all the models is shown below in Table 4.3. The Table includes ACI for reference and it should be noted that the ACI minimum equation is included only for the ACI model. Further discussion of the scatter plots will be given in the presentation and justification of the final recommendations (See sections 5.2.1 and 5.3.1).

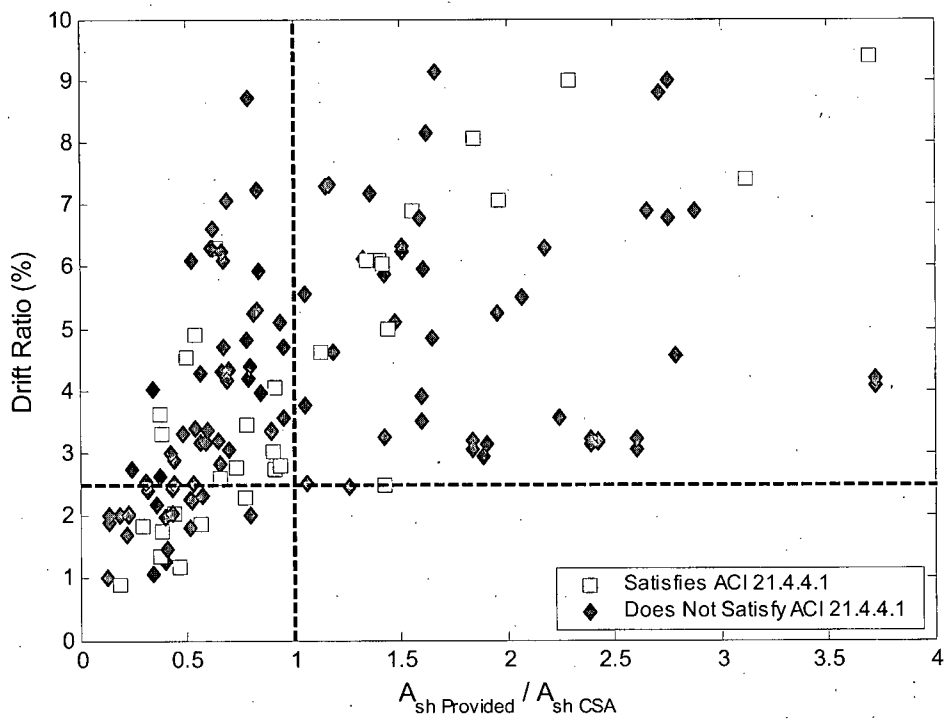

Figure 4.5 CSA scatter plot (rectangular columns)

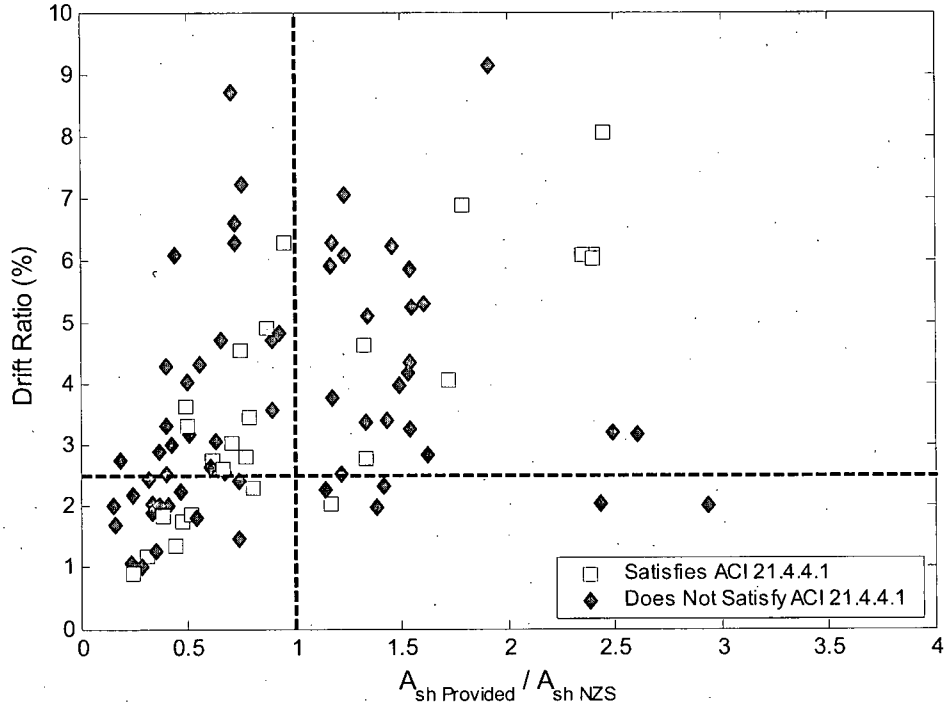

Figure 4.6 NZS scatter plot (rectangular columns)

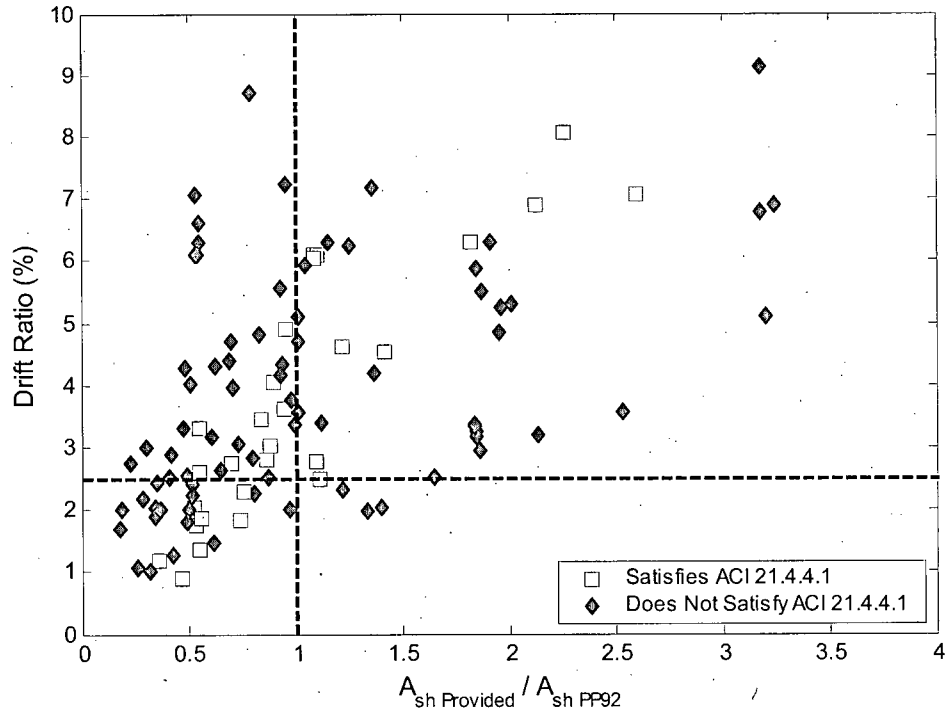

Figure 4.7 PP92 scatter plot (rectangular columns)

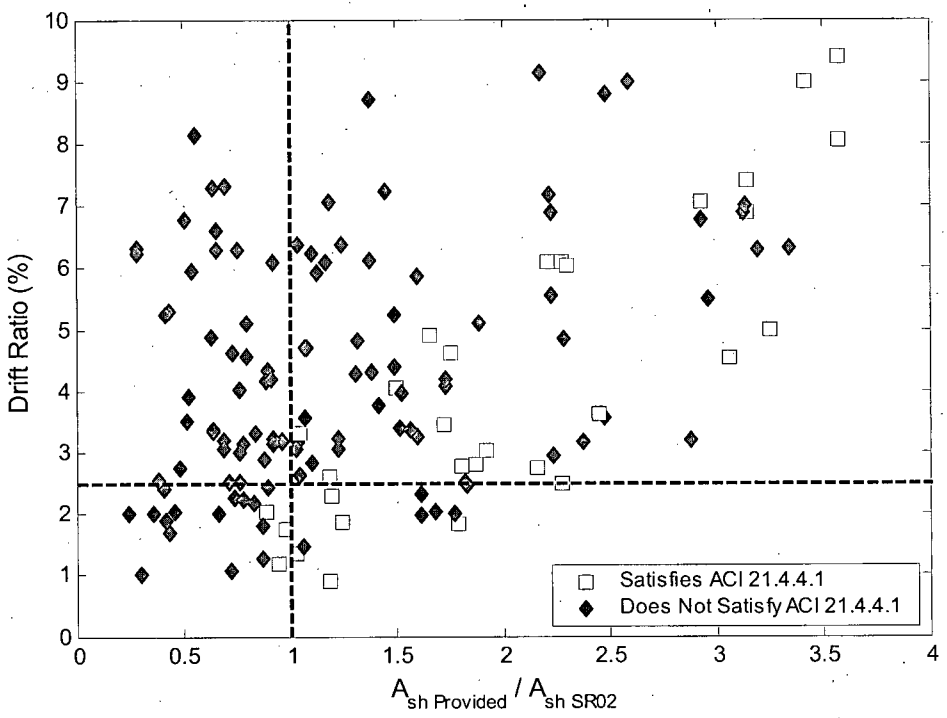

Figure 4.8 SR02 scatter plot (rectangular columns)

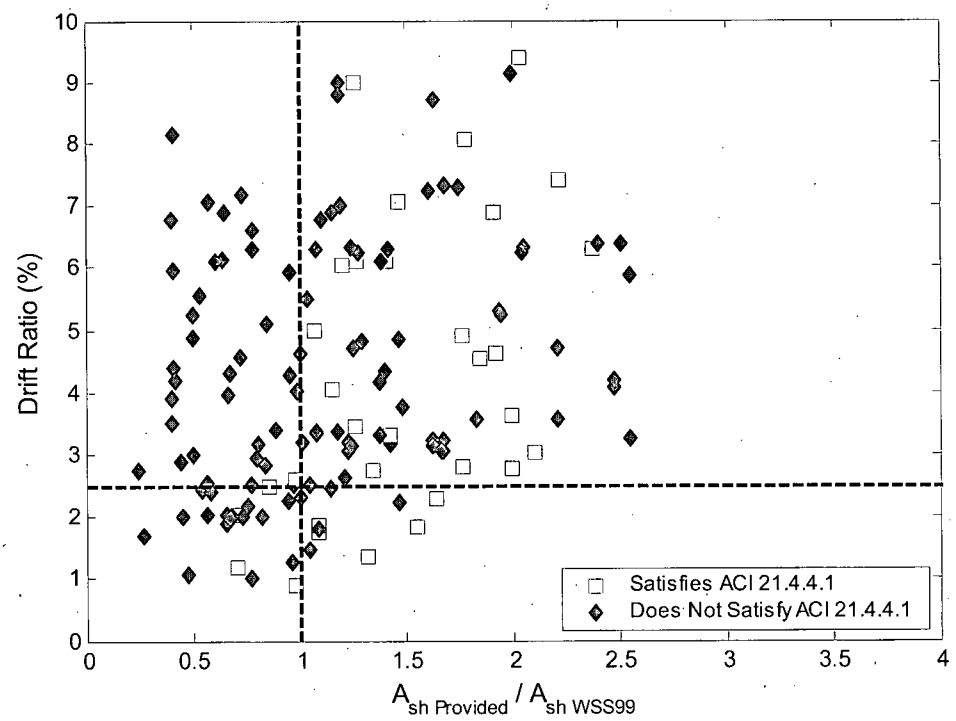

Figure 4.9 WSS99 scatter plot (rectangular columns)

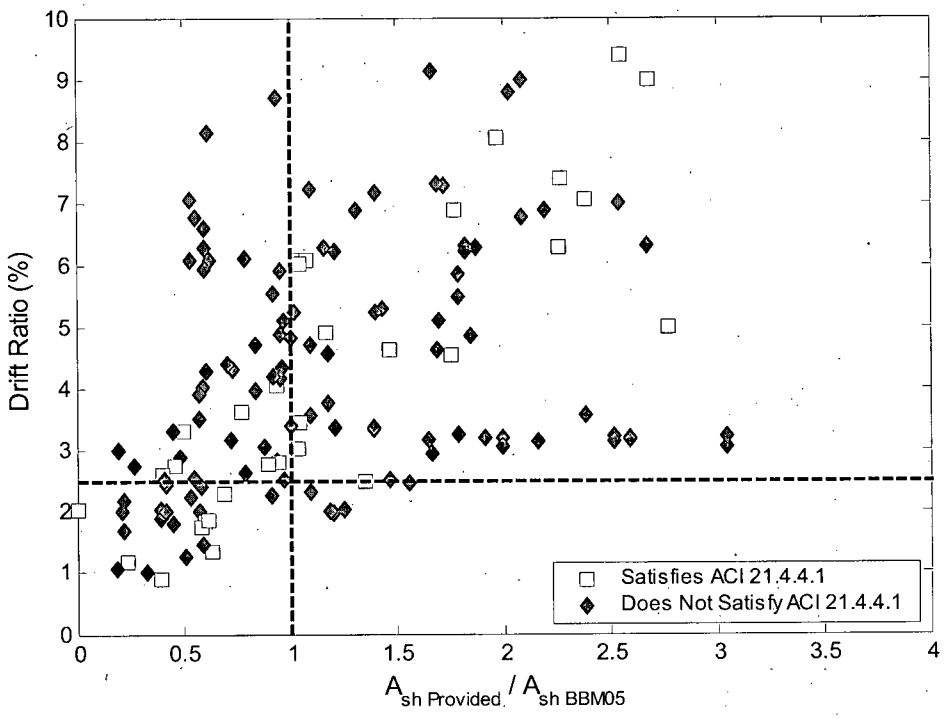

Figure 4.10 BBM05 scatter plot (rectangular columns)

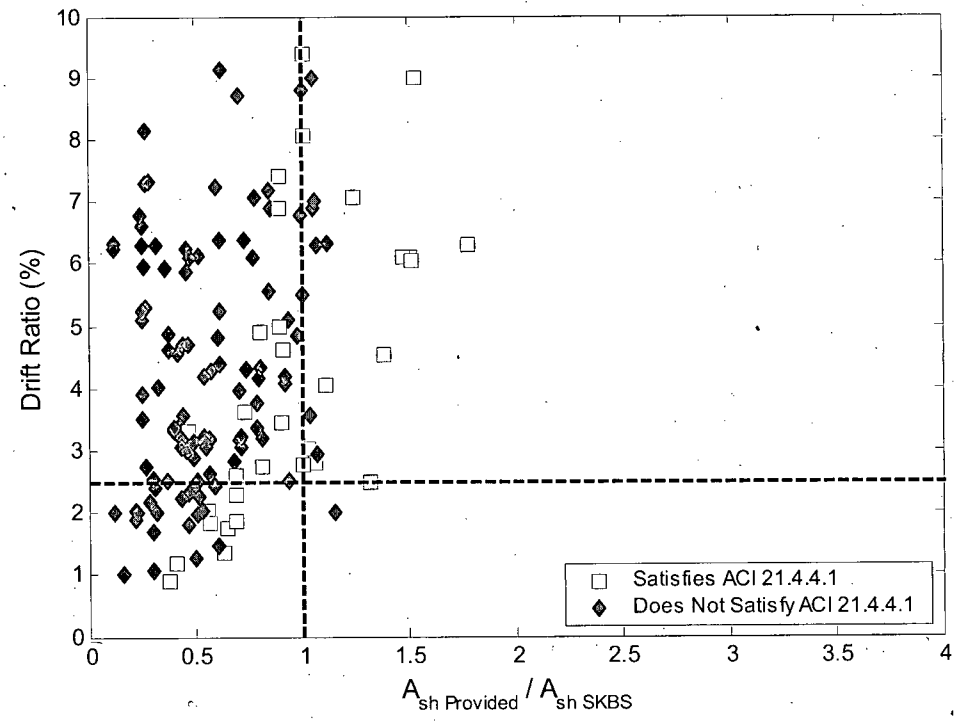

Figure 4.11 SKBS scatter plot (rectangular columns)

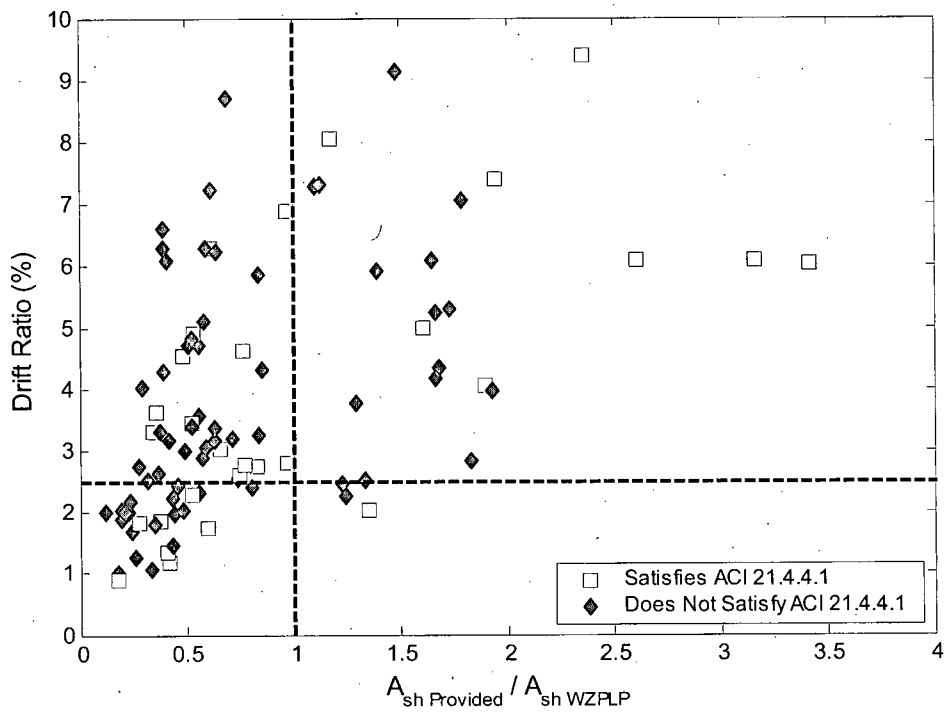

Figure 4.12 WZPLP scatter plot (rectangular columns)

Table 4.3 Quadrant data distribution for rectangular column scatter plots

Model	Q1	Q2	Q3	Q4
CSA	61	2	54	28
PP92	63	5	52	25
SR02	73	12	42	18
WSS99	79	10	36	20
BBM05	72	6	43	24
SKBS	22	2	93	28
WZPLP	28	4	87	26
NZS	42	7	73	23

Using Equations 4.1, 4.3, 4.5 and the data provided in Table 4.3, Figure 4.13 displays the A, B and C statistics for each model including the ACI values previously given in Table 4.2. The negative C value for ACI is not shown in the figure, and it is important to note

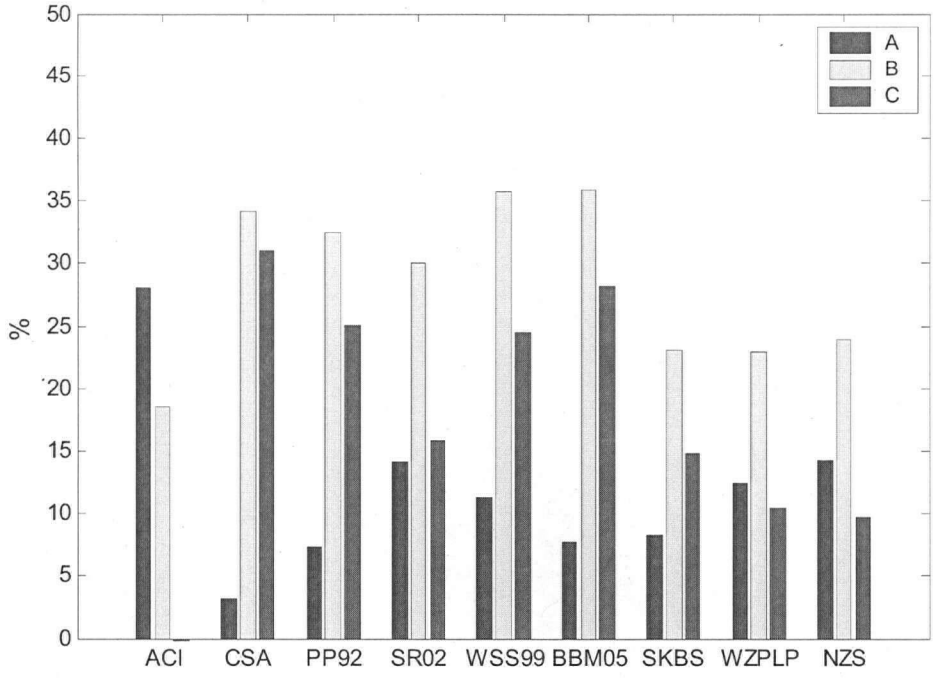

Figure 4.13 Rectangular scatter plot statistics bar graph

that, as was seen in Figure 4.4, ACI is the only model to generate a negative C value. As shown in Figure 4.13, CSA had the lowest A value with A = 3.2% followed by PP92, BBM05 and SKBS with A values of 7.4%, 7.7% and 8.3% respectively. BBM05 had the highest B value with B = 35.8% followed by WSS99, CSA and PP92 with B values of 35.7%, 34.1% and 32.5% respectively. The largest C value, the statistic which describes the overall performance of the model based on all the column data, belonged to CSA with a C value of 31.0% followed by BBM05, PP92 and WSS99 with C values of 28.1%, 25.1% and 24.5%, respectively. Recall that a large C value indicates a model that provides a safe design without significant overconservatism. Again, it is important to note that only the ACI values shown include the ACI minimum equation

4.1.2 Fragility Curve Evaluation

The data used to generate the scatter plots described above was used to generate another graphical presentation of the behaviour of each model. Rather than imposing a distinct

performance target as done above, fragility curves were generated to show the performance of the models at various levels of drift ratio.

4.1.2.1 Evaluation Procedure

To generate a fragility curve for a given model, all the columns that satisfied the confining steel requirements of that model were sorted and listed in increasing order according to their drift capacity. Progressing through the list it was possible to determine the percentage of columns that did not reach a given drift level. Using this procedure at a drift ratio of 2.5%, this method produces a value of A, where A is the scatter plot statistic described above. A lognormal cumulative distribution function was then used to generate a curve to fit the data. The curve is titled the *A fragility curve*. Based on the data used in this study, the curve describes the probability of a column not reaching a given drift limit if it satisfies the model. This fragility curve presents the general trend for columns that satisfy the model without having to select a particular drift level as the performance target. In equation form, the curve can be expressed as:

$$A = P(\delta < \delta_{target} \mid A_{provided} / A_{model} \geq 1) \qquad (4.6)$$

The process was repeated again for all the columns that did not satisfy the confining steel requirements of the model. For each model, a *B fragility curve* was generated to describe the probability of a column not reaching a given drift limit if it does not satisfy the model. Again, using this procedure at a drift ratio of 2.5%, this method produces a value which is analogous to B, where B is the scatter plot statistic described earlier. This fragility curve presents the general trend for columns that do not satisfy the model without having to select a particular drift level as the performance target. In equation form, the curve can be expressed as:

$$B = P(\delta < \delta_{target} \mid A_{provided} / A_{model} < 1) \qquad (4.7)$$

In the same manner that the C statistic was created to combine information provided by the A and B statistic, a third "fragility curve" was generated to combine the results of the two previous curves. The relationship is comparable to that given in Equation 4.5, or that the *C fragility curve* represents the *B fragility curve* minus the *A fragility curve*. Again,

for a given drift ratio an ideal model would have an *A* value of 0% and, to avoid over-conservatism, the *B* value should be maximized. The relationship between these two statistics will therefore change as the drift limit changes. A large value taken from the C statistic fragility curve indicates a model which is 'safe' yet not 'overconservative'.

4.1.2.2 Assessment of ACI 318-05 21.4.4.1

The A statistic fragility curve for ACI is shown below in Figure 4.14, along with the data which was used to generate the distribution. The B statistic fragility curve for ACI is shown below in Figure 4.15, also with the data which was used to generate the distribution. The C statistic fragility curve for ACI is shown below in Figure 4.16.

As the figures show, the lognormal CDF fits the data very well. Reading the curves at a drift ratio of 2.5% produces values very close to the A, B and C statistic given in section 4.1.1.2.

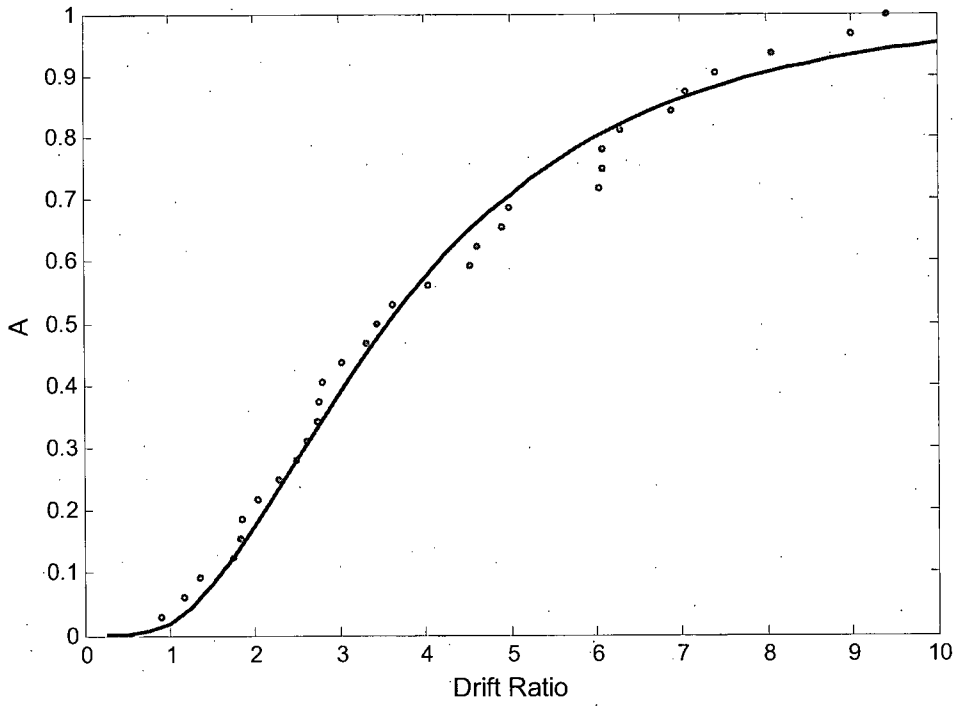

Figure 4.14 Rectangular A fragility curve for ACI

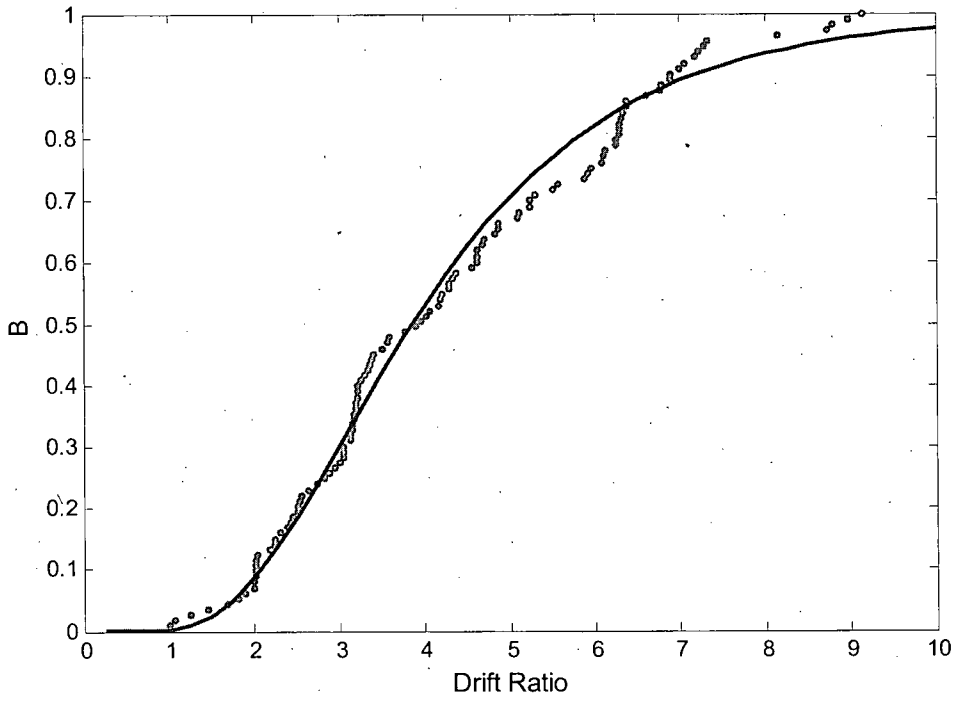

Figure 4.15 Rectangular B fragility curve for ACI

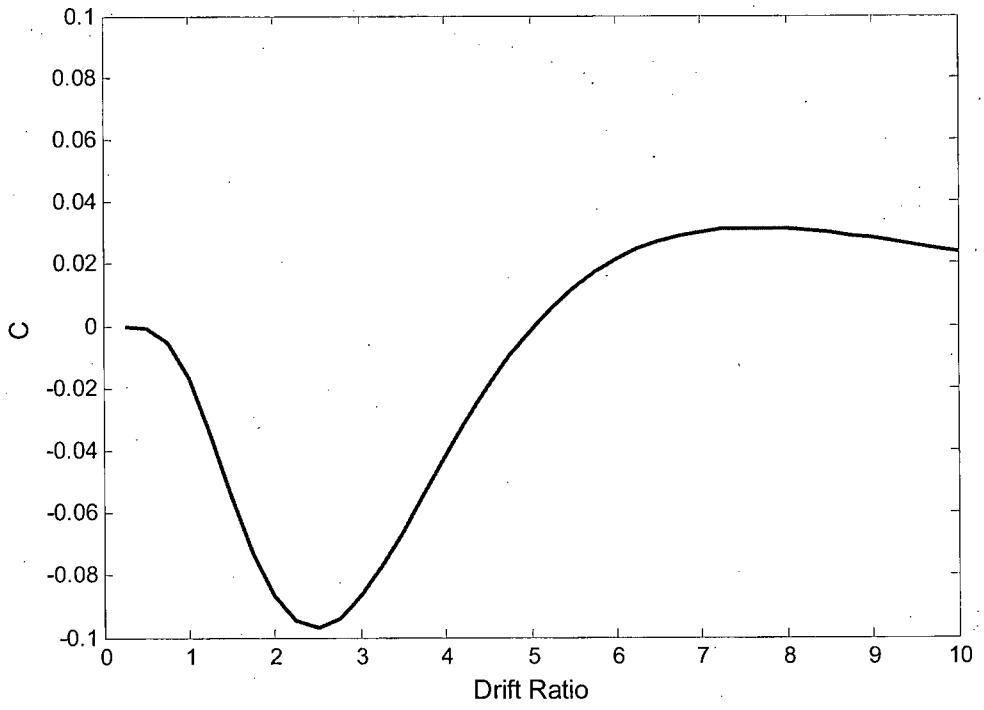

Figure 4.16 Rectangular C fragility curve for ACI

4.1.2.3 Assessment of Code and Proposed Models

As was done for the scatter plot evaluation, the ACI minimum equation is applied here to the remaining models for direct comparison with ACI. A fragility curve evaluation of each model without the minimum will follow.

Rather than presenting the A, B and C statistic fragility curves separately for each of the models, Figure 4.17, Figure 4.18 and Figure 4.19 show the A, B and C statistic fragility curves for all the models (including ACI) simultaneously, with the ACI minimum applied to all models. The fragility curves are shown here out to 10% drift only to be able to include all the data, but for all practical cases drifts are expected to be limited to less than 4% to 5%. Again, the SK97, BS98, WZP94 and LP04 models have been removed in favor of the combined models SKBS and WZPLP.

The curves show that the ACI model is statistically the worst performer with regard to all three statistical values (A, B and C) throughout the meaningful range of drift ratios. In particular, the discrepancy becomes abundantly clear in Figure 4.19 where all curves follow the general same shape with the exception of ACI.

The individual A, B and C fragility curves for all models (incorporating the ACI minimum) can be found in Appendix D.

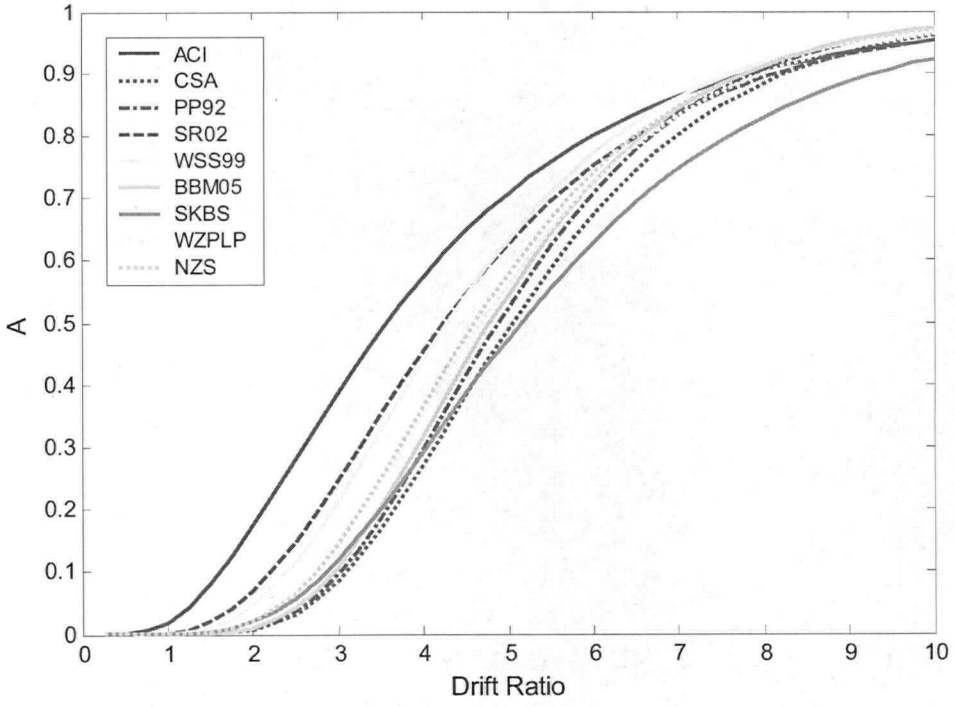

Figure 4.17 Rectangular A fragility curve all models (with ACI minimum)

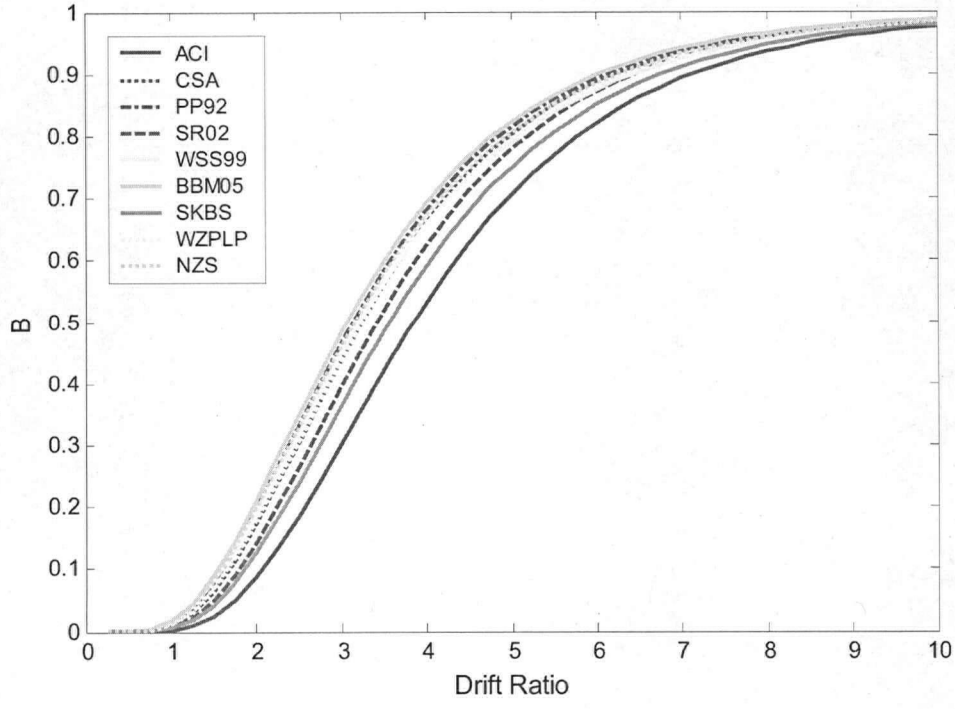

Figure 4.18 Rectangular B fragility curves all model (with ACI minimum)

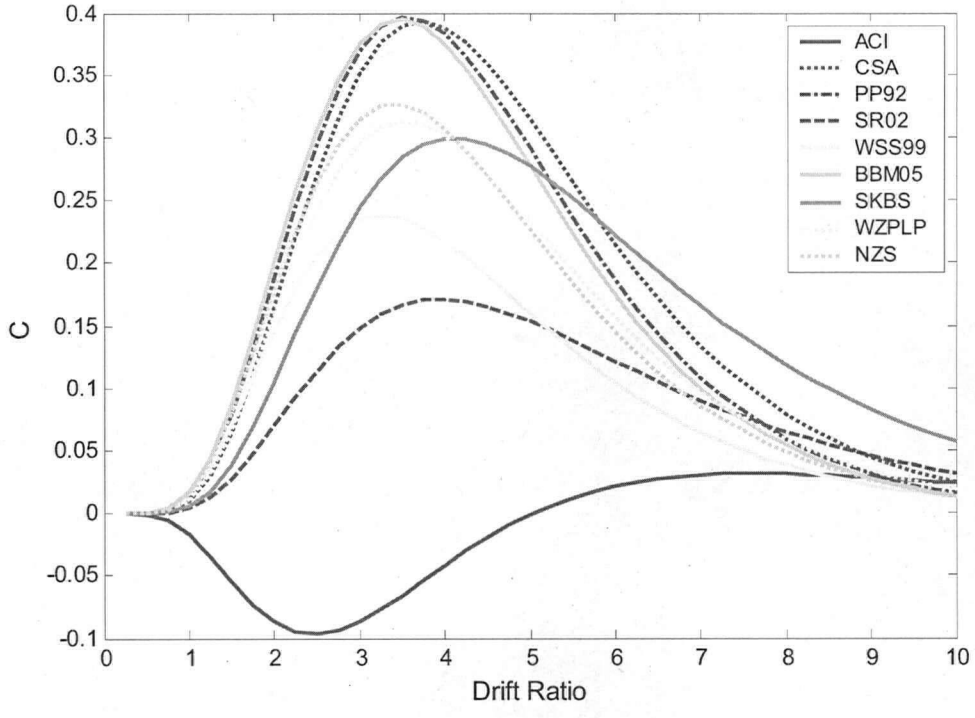

Figure 4.19 Rectangular C fragility curve all models (with ACI minimum)

The curves shown above confirm the results of the scatter plot evaluation and suggest that a replacement model be proposed and that the performance of the models consistent throughout the range of drift ratios. As was done in the scatter plot evaluation, to properly determine the most appropriate alternate model, a fragility curve evaluation for each model which does not include the ACI minimum equation was performed.

Figure 4.20 shows the rectangular column A fragility curves for all the models (including ACI) simultaneously. Likewise, Figure 4.21 shows the rectangular column B fragility curve for all the models and Figure 4.22 shows the rectangular column C fragility curve for all the models. The individual A, B and C statistic fragility curves for each model are presented in Appendix D. It should be noted that taking values from the curve at 2.5% or any other drift ratio, will produce close but not exact matches with the statistics for the corresponding scatter plot due to the need to fit the data with the lognormal cumulative distribution.

As seen in Figure 4.20, for drift ratios between 0 and 6%, the ACI model had the highest probability of a column not reaching the drift limit while satisfying the confining steel requirements. In other words, the A statistic is highest for ACI through this range. This trend is in agreement with the values shown in Figure 4.13. Conversely, the CSA model had the lowest probability of a column not reaching the drift limit while satisfying the confinement requirements in the drift ratio range of 0 to 4.5%, followed by SKBS, PP92 and BBM05. Again this is in agreement with the scatter plot statistics.

The tightly grouped curves shown in Figure 4.21 suggest that there is much more similarity in B statistic values for the various models than was seen in the A statistic figure. While the variation of B values for the models throughout the range drift ratios is smaller, similar trends to those of the scatter plot evaluation emerge. Again, the ACI model had the lowest B values, and the figure suggests that BBM05 and CSA have the highest B values throughout most of drift ratio range. This figure suggests that while the models behave in a much more similar manner with respect to the B statistic compared to the A statistic, variation between the models still exists such that investigating the rectangular column C statistic fragility curves is warranted.

The curves shown in Figure 4.22 are a graphical description of the overall performances of the models. It is here that the overall performance of the ACI model relative to the other models in this study clearly becomes evident. Not only is the C value lowest for the ACI model for all values of drift ratio, but it produces a negative value for drifts between approximately 0.5% and 5.0%. All other models behave similarly for small drift ratios but the performance differences become apparent for drift ratios between 1.5% and 5.0%. As was seen in the scatter plot evaluation, the CSA, BBM05 and PP92 models had the best overall performance. BBM05 has the highest values up to a drift ratio of approximately 2.0%, when CSA becomes higher. CSA has the highest overall C value of 43.7% at a drift ratio of 3.5%.

Again, the fragility curves are shown here out the 10% drift only to be able to include all the data. Chapter 5 shows these figures up to drifts of 4%.

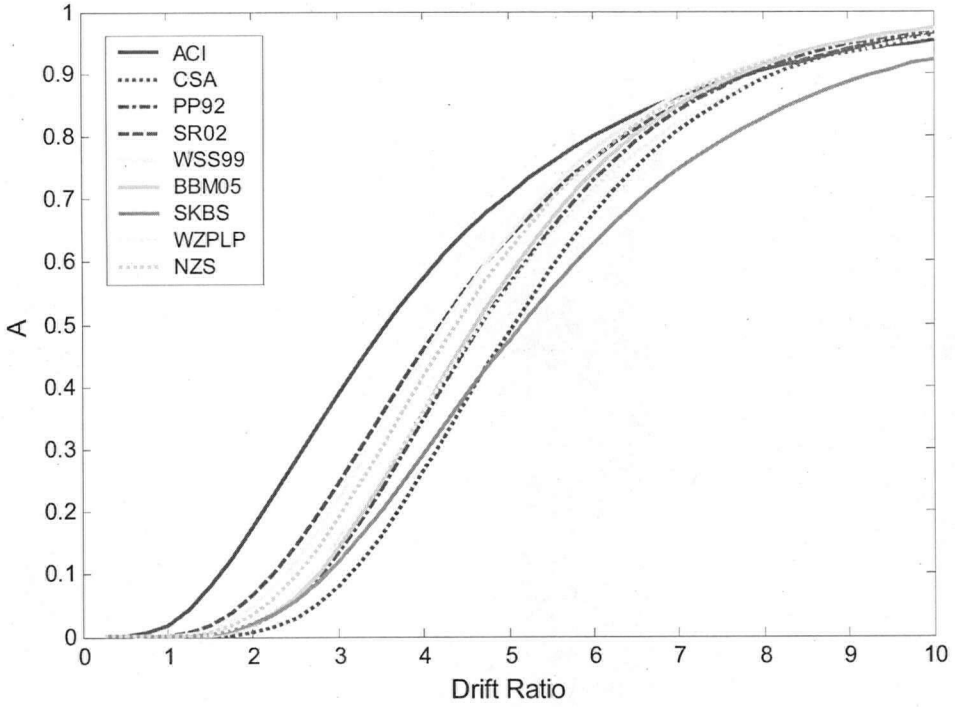

Figure 4.20 Rectangular A fragility curve for all models

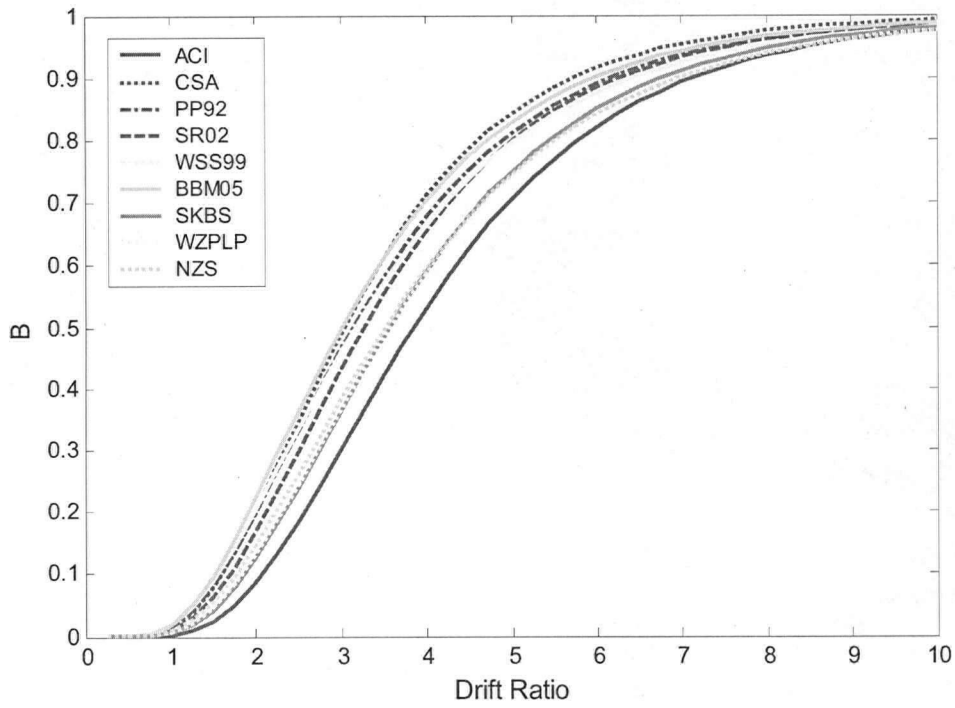

Figure 4.21 Rectangular B fragility curve for all models

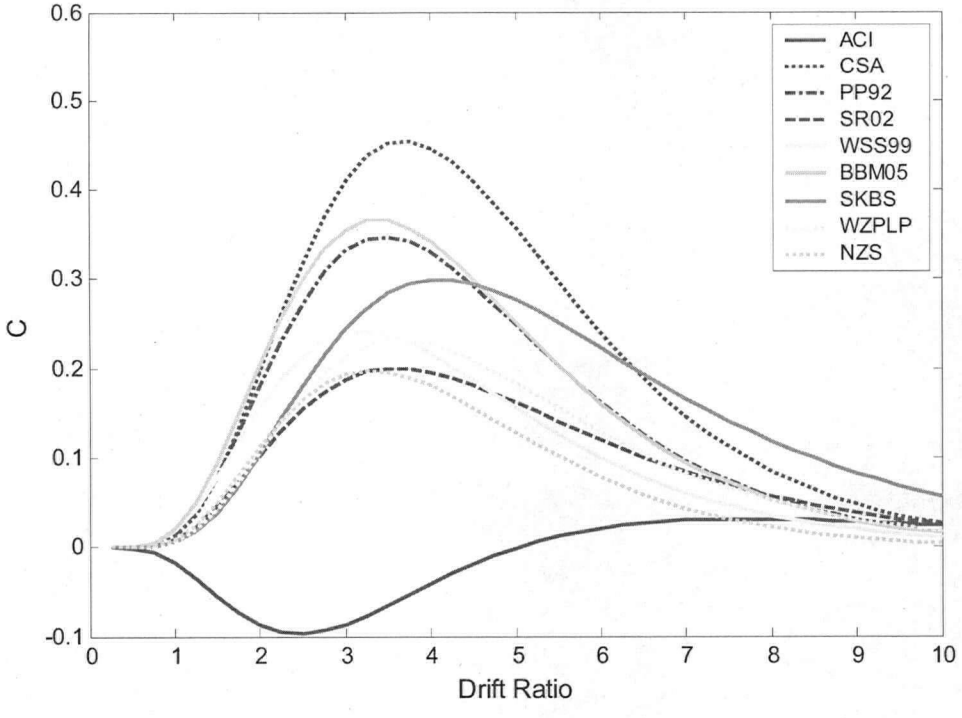

Figure 4.22 Rectangular C fragility curve for all models

4.1.2.4 Special Consideration for SR02

Only the BBM05 and SR02 models use drift ratio as the performance measure to derive the expression for the confining steel requirement. This parameter is not a direct input variable for determining the amount of confining steel for BBM05, however as stated in Chapter 2, the model was derived for limiting drifts of 1.5% and 2.5%, thus making it suitable for the above comparison. This is not the case for SR02 where the target drift ratio, δ, is a direct input variable. A value of 2.5% was selected to be consistent with scatter plot evaluation procedure; however this selection may be an unfair representation of the model for the fragility curve evaluation. Therefore, to account for this, the scatter plot A, B and C statistics were generated for target drift ratios from 2% to 5%, each using the appropriate drift ratio in Equation 2.31. The results are plotted in Figure 4.23 against the curves in Figure 4.20, Figure 4.21 and Figure 4.22 where $\delta = 2.5\%$. The figure shows a close agreement between the two approaches for drift ratios up to 3% at which point a slight variation is observed. The approach which holds the input drift ratio constant at

2.5% actually provides more favorable values for the A and C curves. Therefore, the results displayed in Figure 4.23 suggest that the fragility curves in Figures 4.16 through 4.18 are a valid representation of the SR02 model, and no further consideration for the model is needed. Note, the ACI minimum equation was not included in the evaluation.

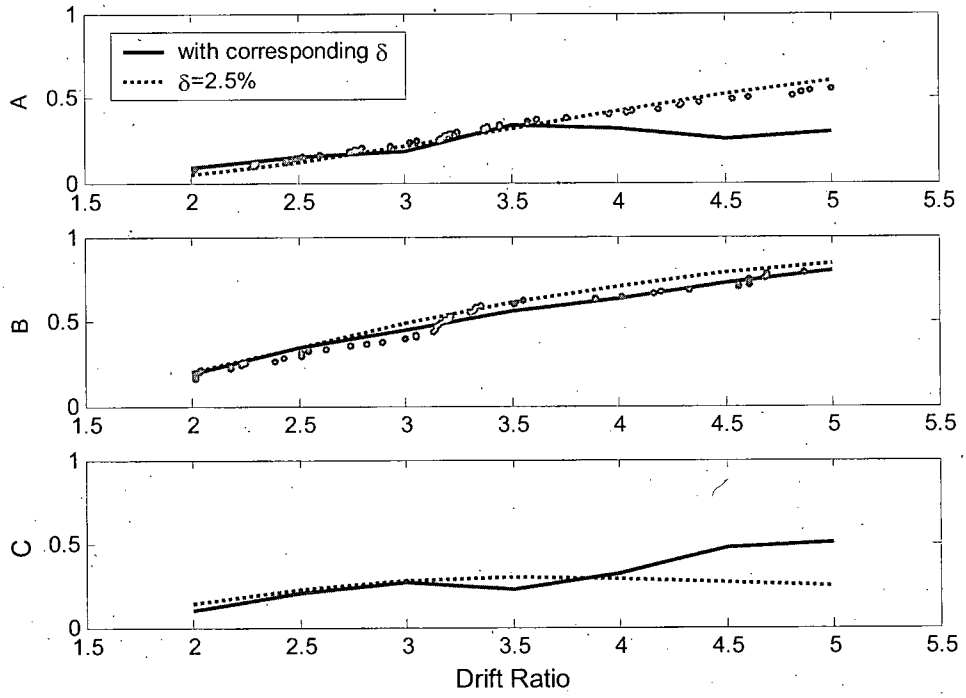

Figure 4.23 Rectangular SR02 fragility curve comparison

4.1.3 Spacing of Transverse Reinforcement

As was explained in Chapter 2, the spacing requirements of the three building codes investigated here are considered in addition to the confining steel area requirements.

4.1.3.1 Assessment of ACI 21.4.4.2

In ACI 318, the two spacing requirements related to confinement, Equation 2.10 and 2.12 are considered separately from the area requirements. Figure 4.1 shows the scatter plot for the spacing requirement of one quarter the minimum dimension. Figure 4.25 shows the corresponding C statistic fragility curve. Equation 2.12 was not evaluated due to the

fact that the database is composed of scaled tests. The range of acceptable spacing according to this expression (4 to 6 inches) is not suitable for these columns. Since the scaling factor is unknown for the majority of the columns, an accurate evaluation of this spacing limit is not possible. Further discussion of this issue is presented in Chapter 5.

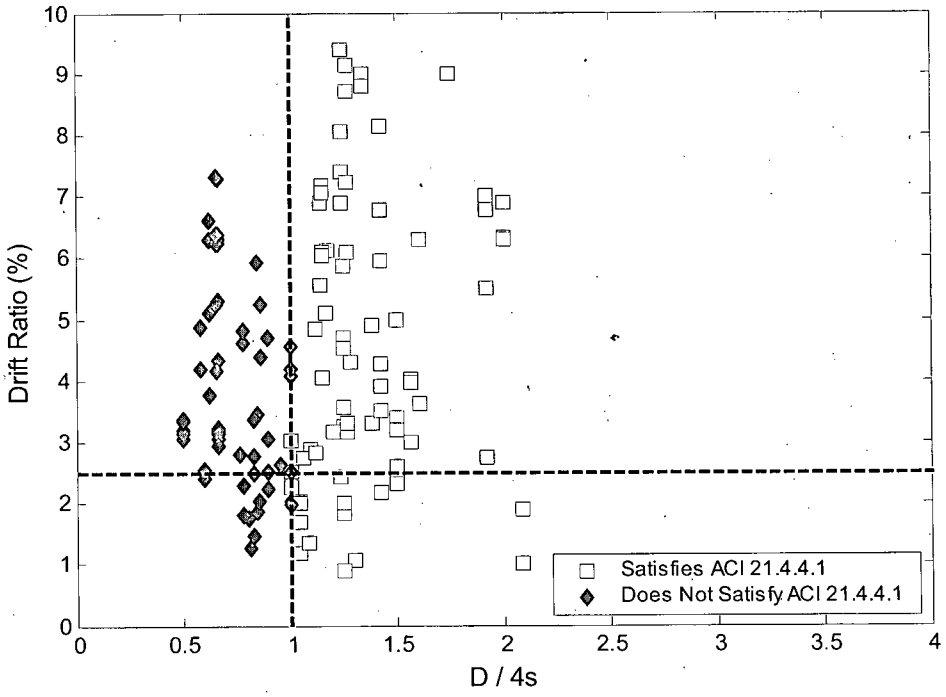

Figure 4.24 Rectangular scatter plot for spacing limit of H/4

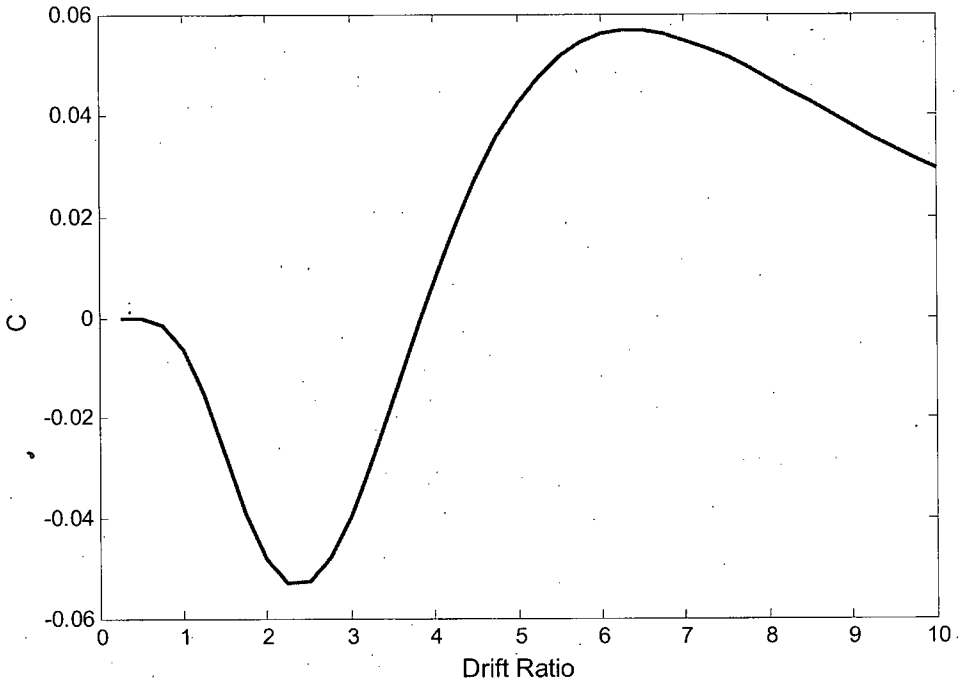

Figure 4.25 Rectangular C fragility curve for spacing limit H/4

The statistics for Figure 4.24 are provided in Table 4.4.

Table 4.4 Scatter plot statistics for ACI spacing limit shown in Figure 4.24.

A	B	C
22.2	18.2	-4.0

Figure 4.24 and Figure 4.25 show that the one quarter minimum dimension spacing limit when evaluated on its own performs at a similar level to the ACI area requirement. By comparison, the area requirements of the other models perform better than both ACI area and one quarter minimum dimension spacing requirements.

Figure 4.26 shows the properties of the data points which fall into quadrants 2 and 3 for Figure 4.24. Unlike the corresponding plot for the area requirements, a strong connection between the axial load and the performance of the requirement is lacking, although a modest connection is still observable on the figure.

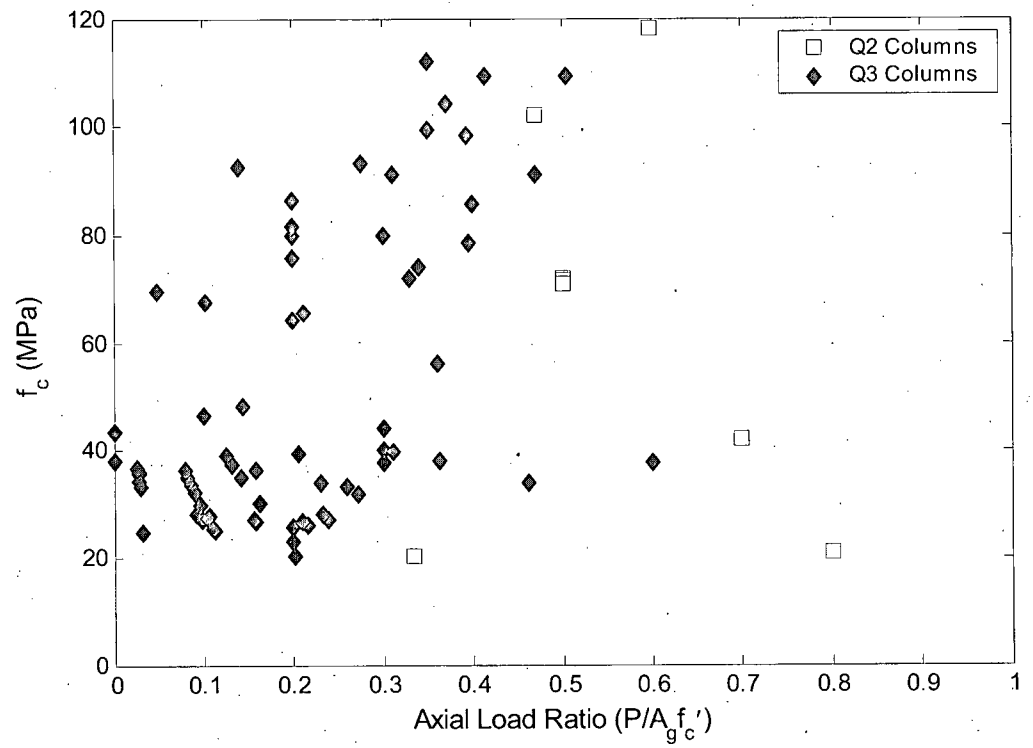

Figure 4.26 f_c' vs. axial load ratio for Q2 and Q3 columns for H/4 spacing limit

Finally, it is important to address how often each ACI confinement requirement governs the design of columns. Table 4.5 shows the number of instances where each requirement governs the spacing of the confinement reinforcement for the 145 rectangular columns.

The confinement area requirements of ACI 318 are rearranged and expressed as a spacing requirement (i.e. for a known area and arrangement of transverse bars).

$$s = \frac{A_{sh}}{0.3h_c \frac{f_c}{f_{yh}}\left(\frac{A_g}{A_{ch}} - 1\right)} \qquad (4.8)$$

This spacing requirement was then compared to the two spacing limits to determine which governed. Recall the other two spacing limits given in Chapter 2 and in ACI section 21.4.4.2 are $s \le 0.25D$ and $s \le 6d_b$. Again, the effect of scaling the test specimens renders the spacing limit given by Equation 2.12 (ACI Eq 21-5) inappropriate for application to the columns in the database.

Table 4.5 ACI 318-05 Governing spacing of rectangular transverse reinforcement

Spacing limit	# columns governed
Eq 2.10	19
Eq 2.11	3
Eq 4.8	124

The data in Table 4.5 shows that for the vast majority of reinforced concrete columns in the database, the area requirement dominates the spacing of the transverse steel. While not included in the table above, one would expect that for full scale columns the spacing limit given by Equation 2.12 would often govern for large columns with closely spaced longitudinal reinforcement, and the number of instances in which Equation 4.8 governs would be less than what is represented in Table 4.5. Of the 32 columns which satisfy the area requirements of section 21.4.4.1 of ACI 318-05, 8 do not satisfy the spacing requirement of section 21.4.4.2.

4.1.3.2 Assessment of CSA and NZS

A similar comparison was made for the CSA A23.3-04 and NZS 3101:2006 building codes. The confinement steel area requirements are rearranged and expressed as spacing requirements in Equation 4.9 for CSA and 4.10 for NZS.

$$s = \frac{A_{sh}}{0.2k_n k_p \frac{A_g}{A_{ch}} \frac{f_c'}{f_{yh}} h_c} \tag{4.9}$$

$$s = \frac{A_{sh}}{h_c \left[\left(\frac{A_g}{A_{ch}} \frac{1.0 - \rho_t m}{3.3} \frac{f_c'}{f_{yh}} \frac{P}{\phi f_c' A_g} \right) - 0.0065 \right]} \tag{4.10}$$

The spacing limits for CSA are the same as those for ACI (Eq 2.10 and Eq 2.11), and for NZS the spacing limits are given as

$$s \leq \frac{1}{3}D \qquad (4.11)$$

$$s \leq 10d_b \qquad (4.12)$$

The results are displayed below in Table 4.6. The table shows a lower number of instances in which the spacing is governed by the area requirement. Again it is important to determine how many columns which satisfy the area requirement, but fail the spacing limits. For the 63 columns which satisfy the area requirement of CSA, 22 do not meet the spacing requirements. For the 49 columns which satisfy the area requirement of NZS, 14 do not satisfy the spacing requirements.

Table 4.6 Governance breakdown for spacing of transverse reinforcement for CSA A23.3-04 and NZS 3101:2006

Spacing limit	# columns governed CSA	# columns governed NZS
Eq 2.10 / 4.11	44	70
Eq 2.11 / 4.12	2	5
Eq 4.9 / 4.10	99	70

4.1.4 Maximum Recorded Drifts

As discussed in Chapter 3, the failure drift of the columns was assumed to occur once the column demonstrated a 20% loss in lateral strength. However, while this assumption is valid for new construction and columns within the lateral force resisting system, in some instances it may be of interest to investigate the performance of the columns at their maximum recorded drifts. Such instances may include those in which the column is not incorporated into the structures lateral force resisting system, and thus gravity load carrying capacity, rather than lateral load capacity, is of importance. Figure 4.27 shows the scatter plot statistics for the models using drift ratios calculated using the maximum recorded drift for each test. Figure 4.28 shows the C statistic fragility curves. All scatter plots and fragility curves are given in Appendix D. Note, the ACI minimum equation was not included in any of the other models.

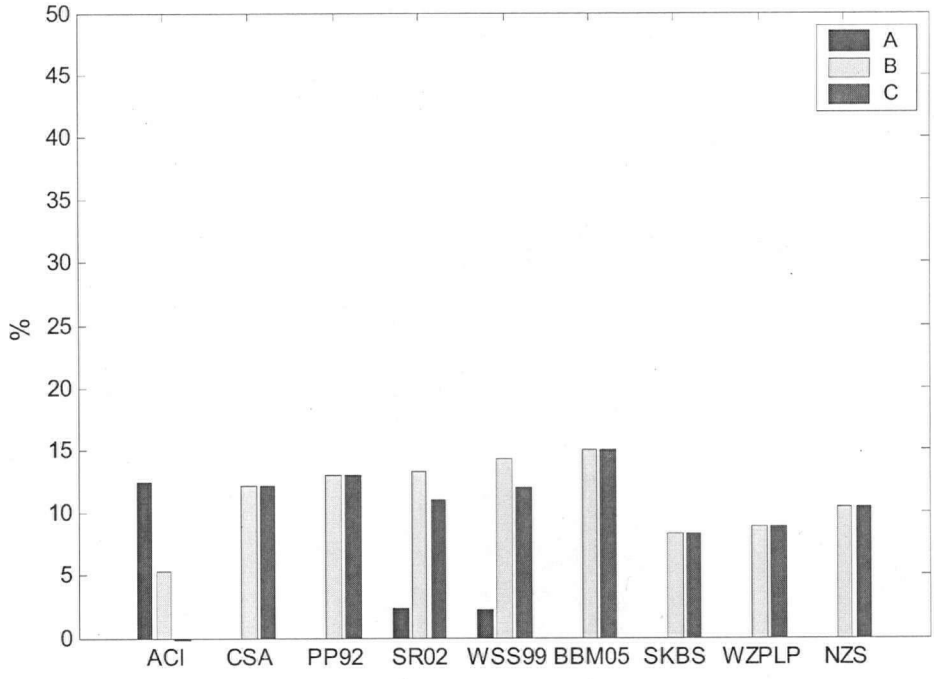

Figure 4.27 Rectangular Scatter plot statistics using maximum recorded drifts

The statistics found with maximum recorded drifts are similar to those which were observed for drifts at 20% loss in strength. The higher drifts resulted in fewer data points in quadrants 2 and 4, therefore reducing the A and B values. Also the emergence of CSA, BBM05 and PP92 as the superior models is shown in Figure 4.28. The important observation to gain from the two figures is that the ACI model is once again the statistically least desirable, it is the only model to produce a negative C value, and that a replacement model is desirable. The results of the evaluation at maximum recorded drifts support the validity of a proposal for a replacement model done through further interpretation of the results for drifts recorded at 20% loss in strength only. The drifts at 20% loss in strengths and the maximum recorded drifts can be found in Appendix A.

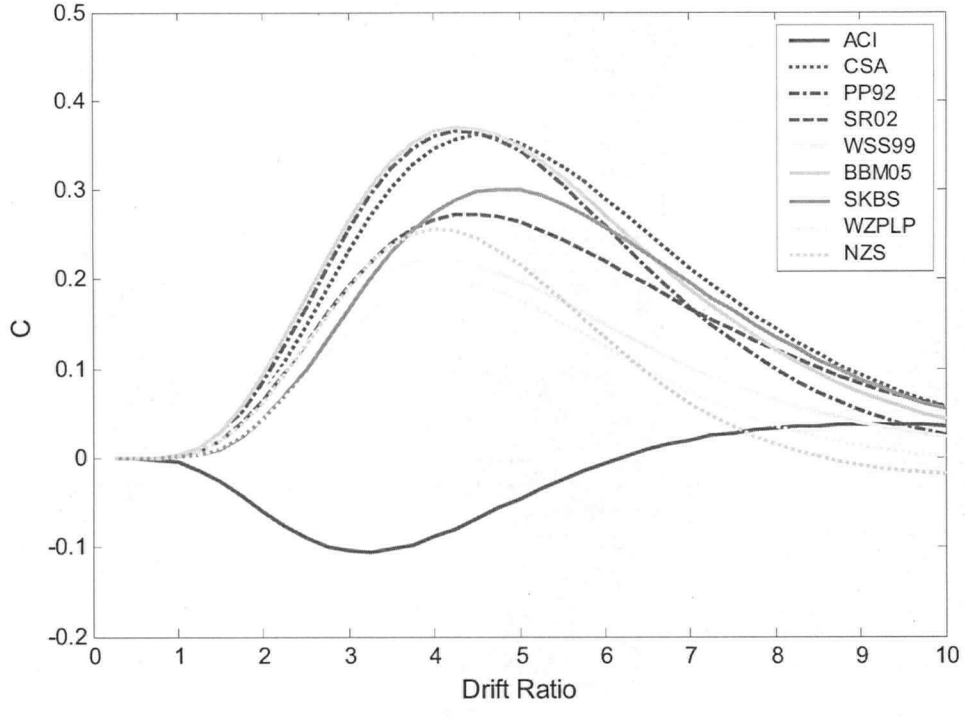

Figure 4.28 Rectangular C fragility curves using maximum recorded drifts.

4.2 Circular Columns

As was done for the rectangular column evaluation, each confining reinforcement model, including the code equations, was evaluated based on the properties and performance of the column specimens within the database. Again, the aim is to determine how the current ACI code equation compared with both the other code equations as well as the proposed models, and propose a replacement model should it be necessary. The same two evaluation techniques are used to make this comparison. The recommendations presented in Chapter 5 will consider the effects of the smaller database.

4.2.1 Scatter plot evaluation

4.2.1.1 Evaluation procedure

The circular column scatter plot evaluation procedure is identical to that of the rectangular column evaluation. The only difference here is that the x axis values are given

in terms of volumetric transverse reinforcement ratios rather than in terms of area of transverse steel. This is done in keeping with the manner in which the current ACI code states the confining steel requirements for circular columns.

4.2.1.2 Assessment of ACI 318-05 21.4.4.1

The circular column scatter plot for the ACI confining steel requirement is shown below in Figure 4.29. Again, all columns which satisfy the density of confining steel requirements of ACI are plotted with a lightly shaded square marker, while those which fail the density of confining steel requirements are plotted with a dark shaded diamond marker.

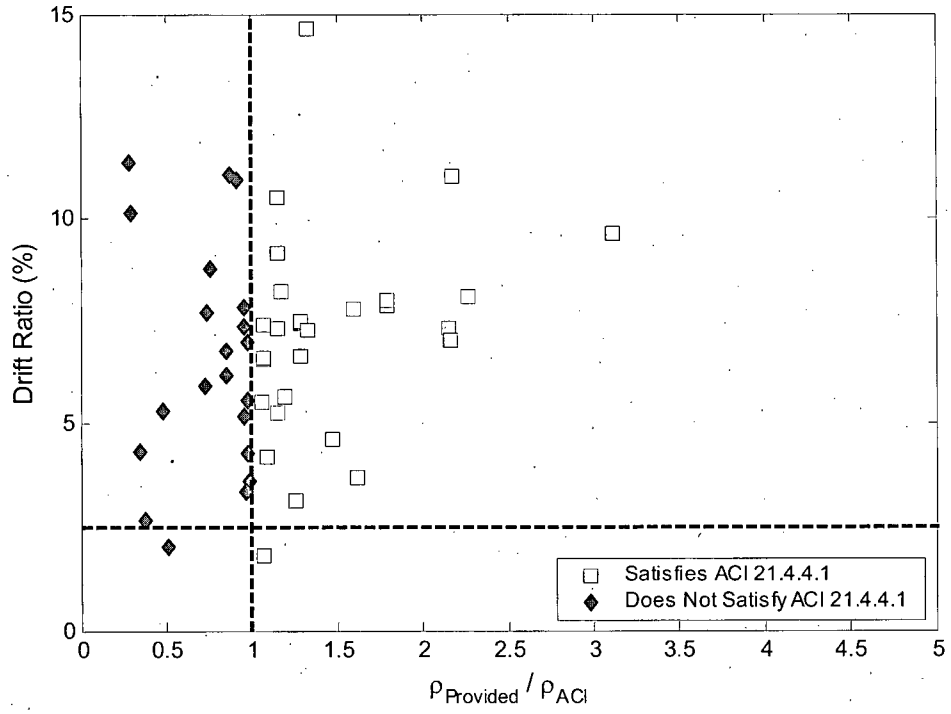

Figure 4.29 ACI scatter plot (circular columns)

The figure shows the following data distribution:

Table 4.7 Quadrant data distribution of ACI circular scatter plot

Quadrant 1	Quadrant 2	Quadrant 3	Quadrant 4
28	1	20	1

From the numbers given in Table 4.7 the A, B and C statistics can be calculated as:

Table 4.8 Statistics for ACI circular scatter plot

A	B	C
3.4	4.8	1.4

The first observation that can be made when comparing Figure 4.29 with Figure 4.2 is the significant difference in the number of data points which lie below the performance target drift ratio of 2.5%. Only two of the 53 columns within the circular column database fall below this limit. The axial load ratios for these two columns are 0.5 and 0.7, and are two of the four highest axially loaded columns in the circular column database. The shortage of data in the bottom two quadrants is likely due to the difference in the typical axial load ratios found in the two databases. As was shown in Table 3.3 and Table 3.4, the average axial load ratio for the rectangular column database was 0.28, while for the circular columns it was only 0.17. In fact, the circular column database has just 10 columns with an axial load ratio higher than 0.3. As has been highlighted throughout this work, columns with lower axial load ratios are capable of achieving higher drifts, a fact illustrated further by the data in Figure 4.29.

With only one column falling in quadrant two, the A statistic for ACI is quite low at 3.4%. If the percentage of 'safe' columns were the only criterion for evaluating the performance of the model, the A statistic would suggest that ACI performs very well. However, as described earlier, the B and C statistics are also insightful for investigating the performance of the model. The B statistic for ACI is also quite low at 4.8%, suggesting that the ACI model is very conservative. The C value for the ACI circular scatter plot is very low at 1.4%, suggesting that the overall performance of the model could be improved.

Figure 4.30 presents a plot of f_c' versus $P/A_g f_c$' for the 23 columns in quadrant 3, and shows only that 3 columns have an axial load above 0.2. Similar to the observations of the corresponding rectangular columns, the expectation is that the remaining models will have fewer columns in quadrant 3 since each of the models incorporates axial load level into the confining steel requirement.

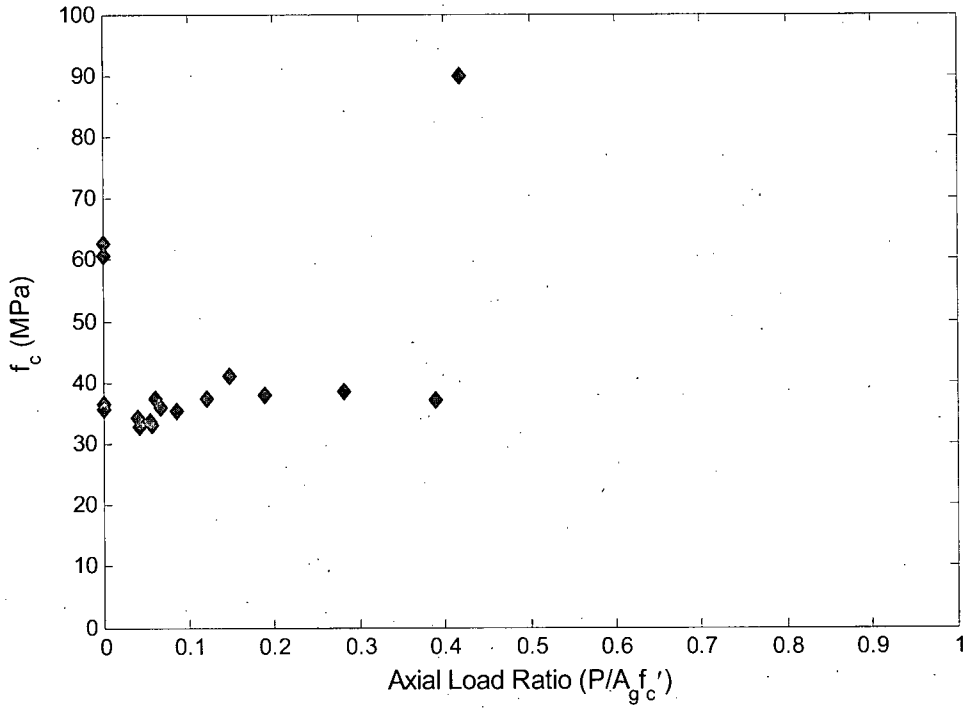

Figure 4.30 fc' vs. axial load ratio for Q3 columns of ACI scatter plot (circular columns)

4.2.1.3 Assessment of Codes and Proposed Models

The scatter plot evaluation for the remaining circular models follows the same procedure as was done for the rectangular evaluation. The ACI minimum given by Equation 2.5 (ACI Equation 21-2) is applied to all models to allow for an equal comparison with the ACI model. Figure 4.31 shows the scatter plot statistics with the ACI minimum applied to all models. There are two important observations to take from the figure. First, all the models provided a statistical improvement over the ACI model, although not as

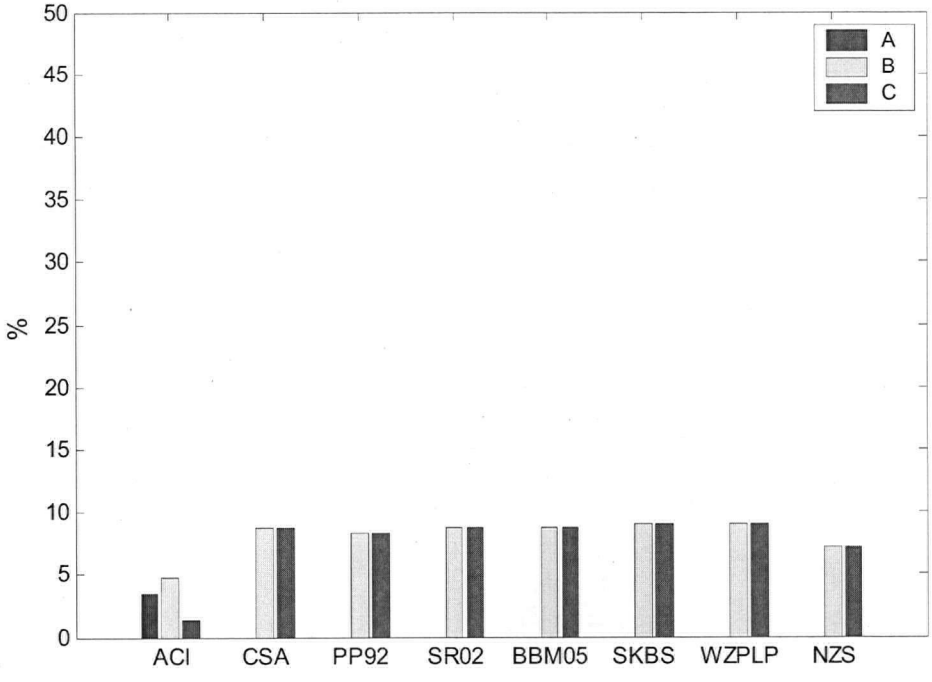

Figure 4.31 Circular scatter plot statistics all model (with ACI minimum)

significant as was seen in the rectangular evaluation. Secondly, the inclusion of the ACI minimum equation had a significant effect on the other models in that it governed the design for a large number of columns for each model, and therefore caused the performance of the models to become very similar. These two conclusions demonstrate that an evaluation of the models without the ACI minimum equation included is needed to determine an appropriate replacement for the ACI requirement. Once again, the SK97, BS98, WZP94 and LP04 models were not included in the evaluation in favor of the combination models SKBS and WZPLP. The scatter plots for all models incorporating the ACI minimum equation are given in Appendix D.

The scatter plots for the remaining models are presented in Figure 4.32 through Figure 4.38. All circular scatter plots including those presented here are included in Appendix D.

For the PP92, WZP94, LP04 and WZPLP models, columns with very low axial load required very small amounts of transverse steel, and in some cases the expression yielded

a negative density requirement. For these models, the ACI minimum limit was used in conjunction with model's expression, exactly as was done to determine the statistics given in Figure 4.31. Including this limit in the evaluation is not a true representation of the model alone, but the nature of the database used to perform the evaluation was such that a minimum value was needed for these models to provide meaningful scatter plot statistics. If any of these models are determined to be the most appropriate model, the appropriateness of this minimum will be re-evaluated before final conclusions are made.

As expected, each model had zero columns in quadrant 2 and most had fewer columns in quadrant 3, the most significant change belonging to SR02 which had 4 columns in quadrant 3. Further discussion of the scatter plots will be given where relevant in the presentation and justification of the final recommendations (Chapter 5).

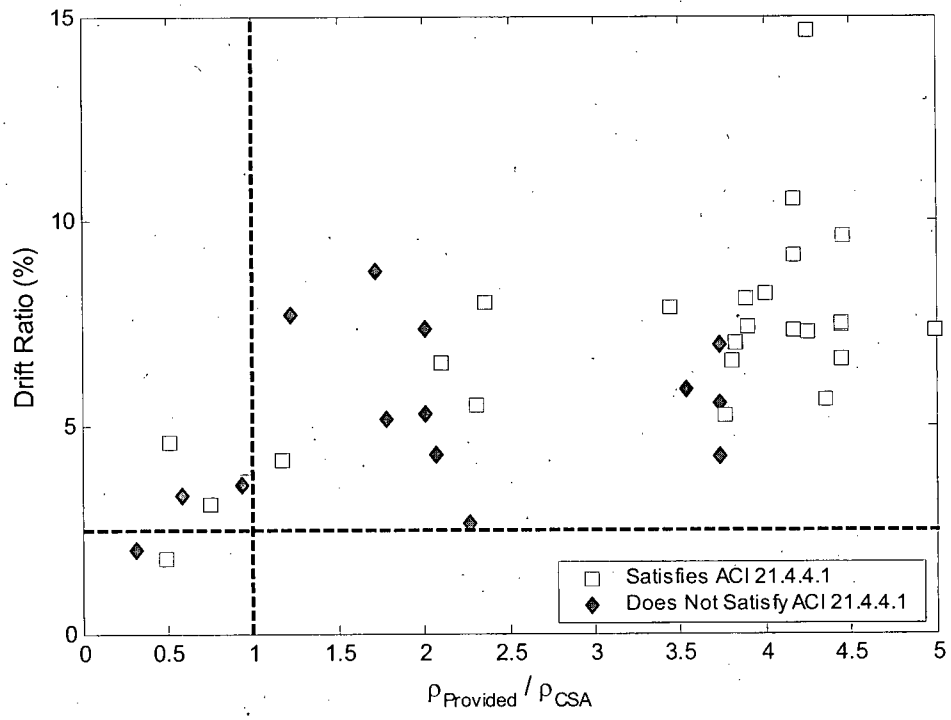

Figure 4.32 CSA scatter plot (circular columns)

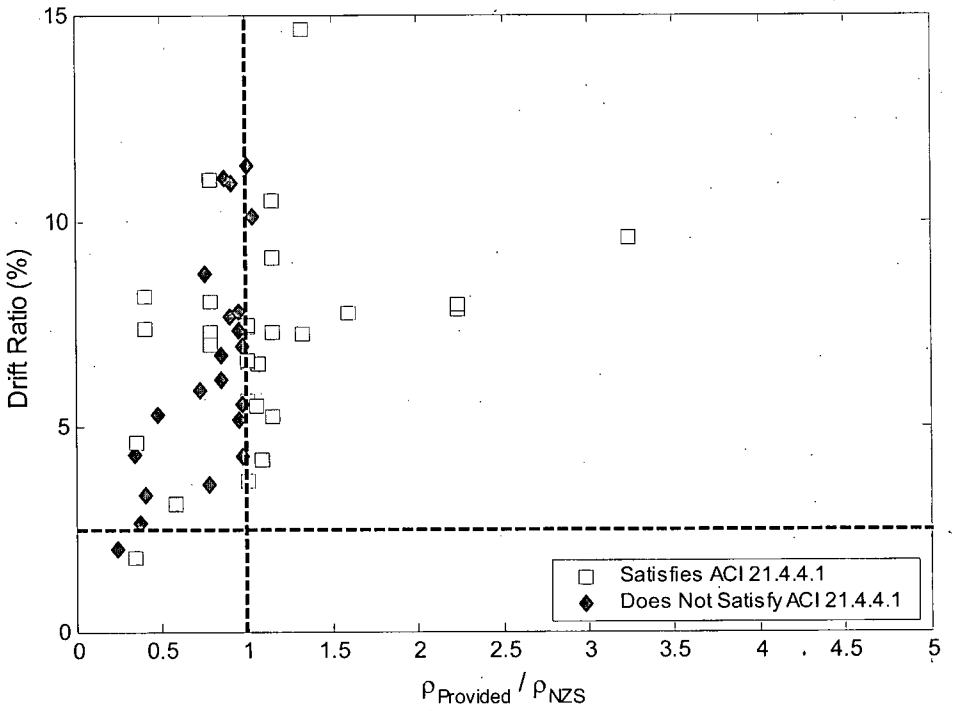

Figure 4.33 NZS scatter plot (circular columns)

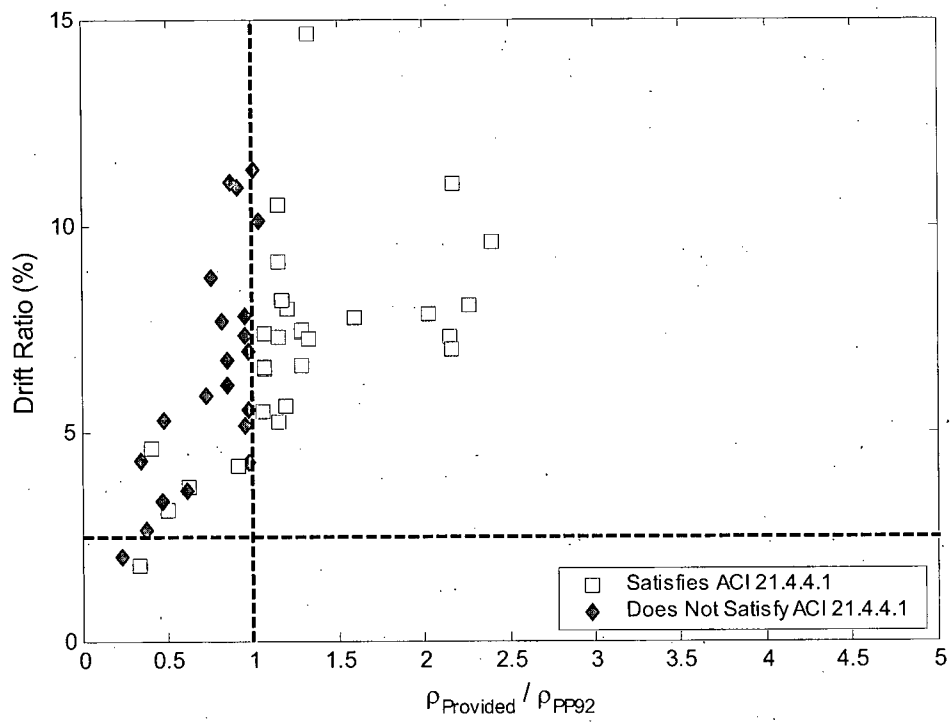

Figure 4.34 PP92 scatter plot (circular columns)

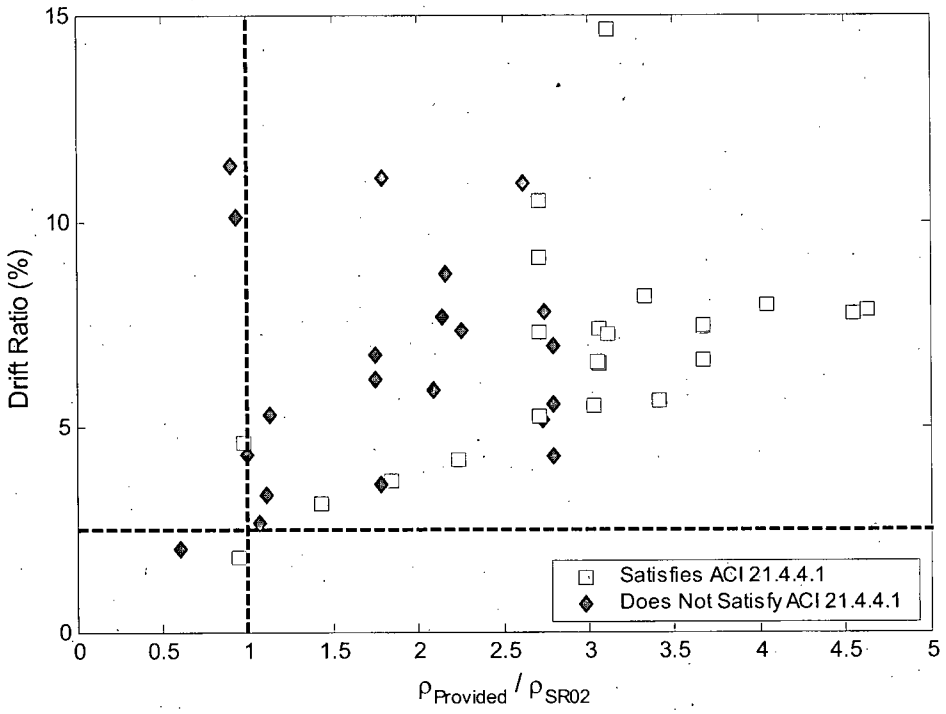

Figure 4.35 SR02 scatter plot (circular columns)

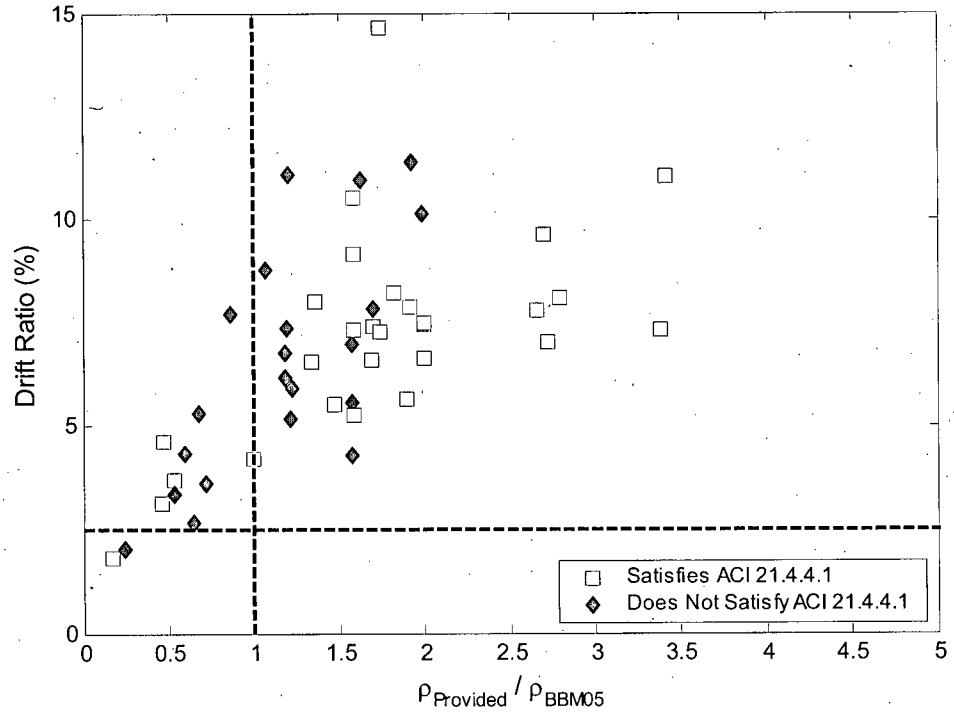

Figure 4.36 BBM05 scatter plot (circular columns)

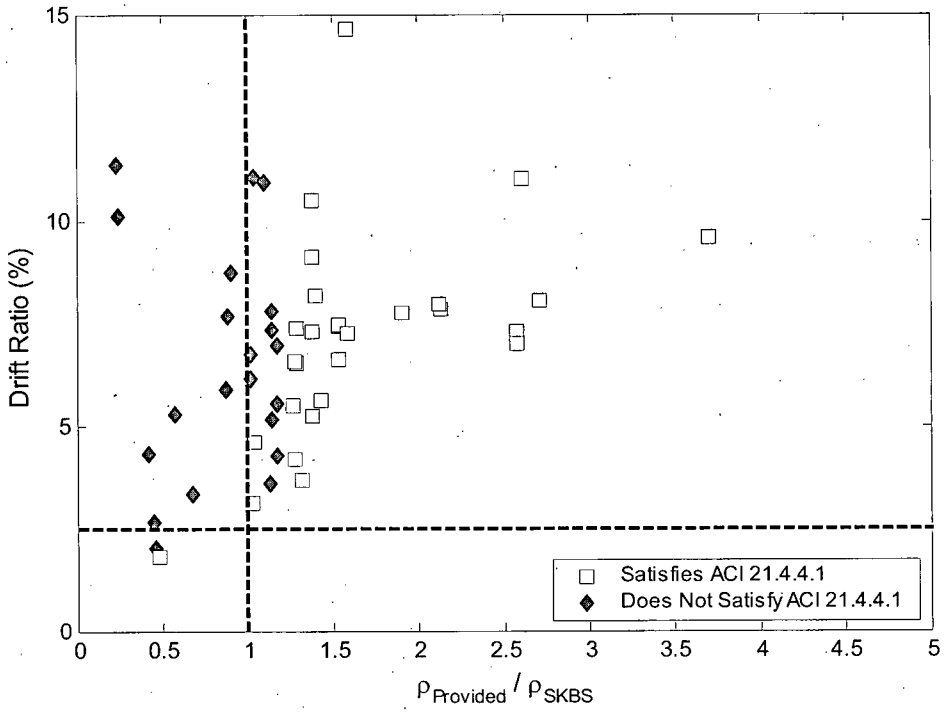

Figure 4.37 SKBS scatter plot (circular columns)

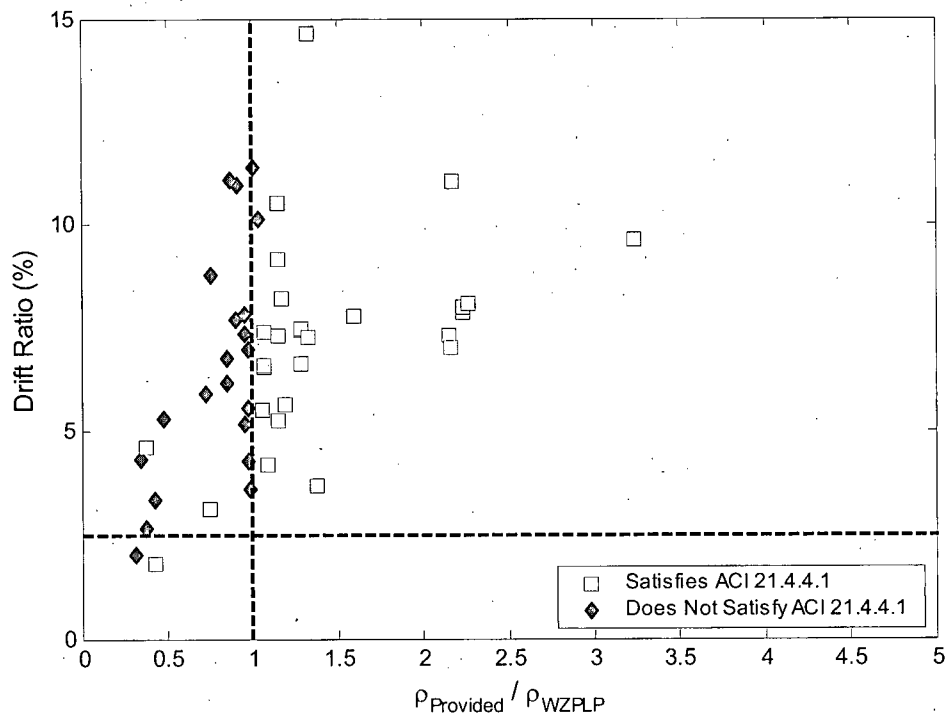

Figure 4.38 WZPLP scatter plot (circular columns)

The distribution of data points into the four quadrants for all the models shown below in Table 4.9.

Table 4.9 Quadrant data distribution for all models circular scatter plots

Model	Q1	Q2	Q3	Q4
CSA	43	0	5	2
PP92	26	0	22	2
SR02	44	0	4	2
BBM05	39	0	9	2
SKBS	39	0	9	2
WZPLP	28	0	20	2
NZS	38	0	10	2

The A, B and C statistics for each model including the previously given ACI values are displayed in Figure 4.39. As shown in the figure, only the ACI model does not have an A value of 0%. The highest B value (33.3%), and hence the largest C value (33.3%) belonged to SR02. CSA had the next best C value at 28.6%, followed by BBM05 and SKBS with 18.2%.

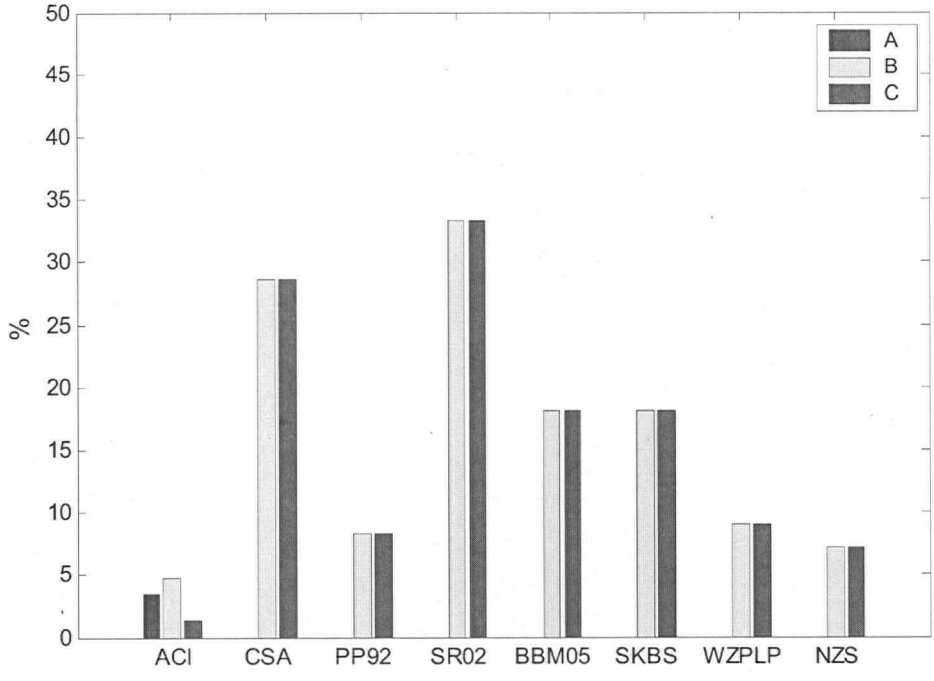

Figure 4.39 Circular scatter plot statistics bar graph

4.2.2 Fragility curve evaluation

4.2.2.1 Evaluation Procedure

The procedure for the circular fragility curve evaluation is identical to that for the rectangular evaluation. The curves are extended to a drift ratio of 15% as drifts of this magnitude were recorded in the database.

4.2.2.2 Assessment of ACI 318-05 21.4.4.1

Figure 4.40 and Figure 4.41 show the circular column A and B fragility curves for ACI along with the data which was used to generate the distributions. The circular column C circular statistic fragility curve for ACI is shown below in Figure 4.42.

As the figures show, the limited amount of data results in a lognormal CDF which does not fit the data as well as was seen for the rectangular columns (see Figure 4.14).

However, reading the curves at a drift ratio of 2.5% produces values very close to the A, B and C statistics given above.

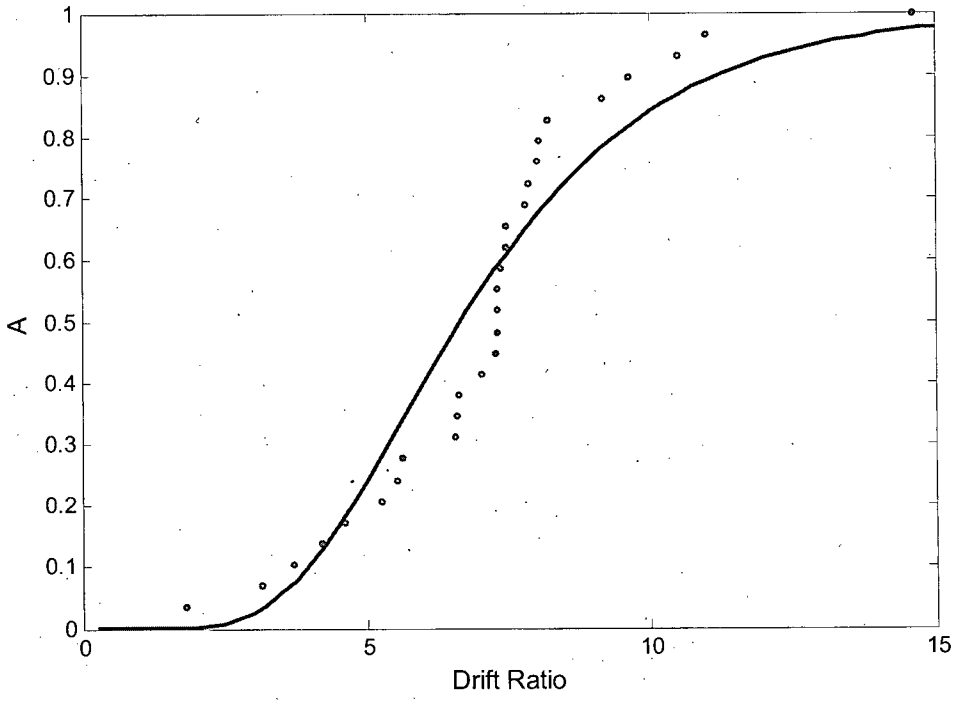

Figure 4.40 Circular A fragility curve for ACI

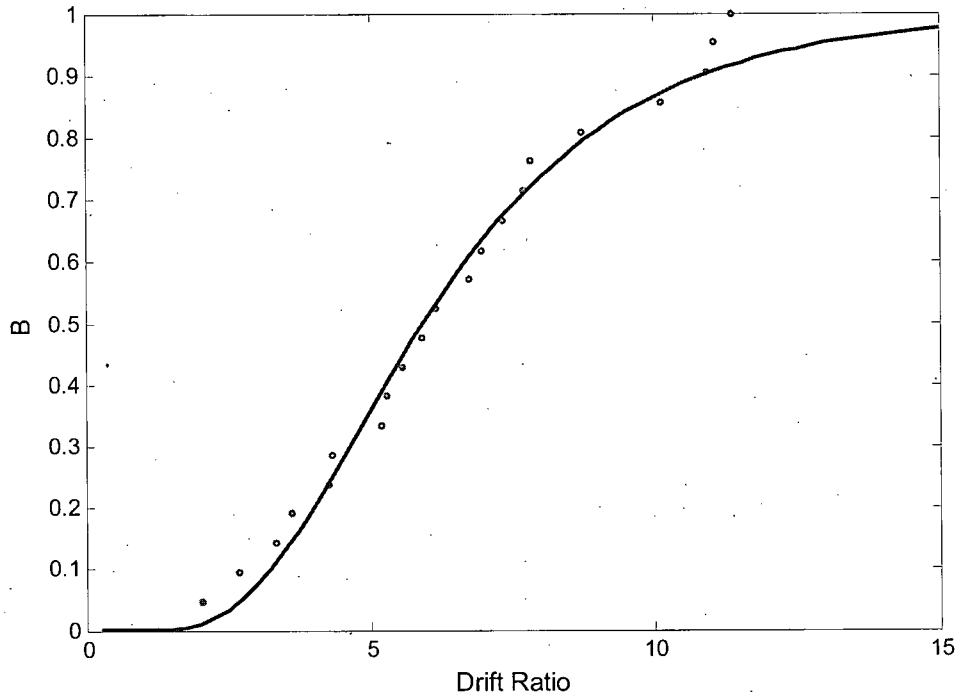

Figure 4.41 Circular B fragility curve for ACI

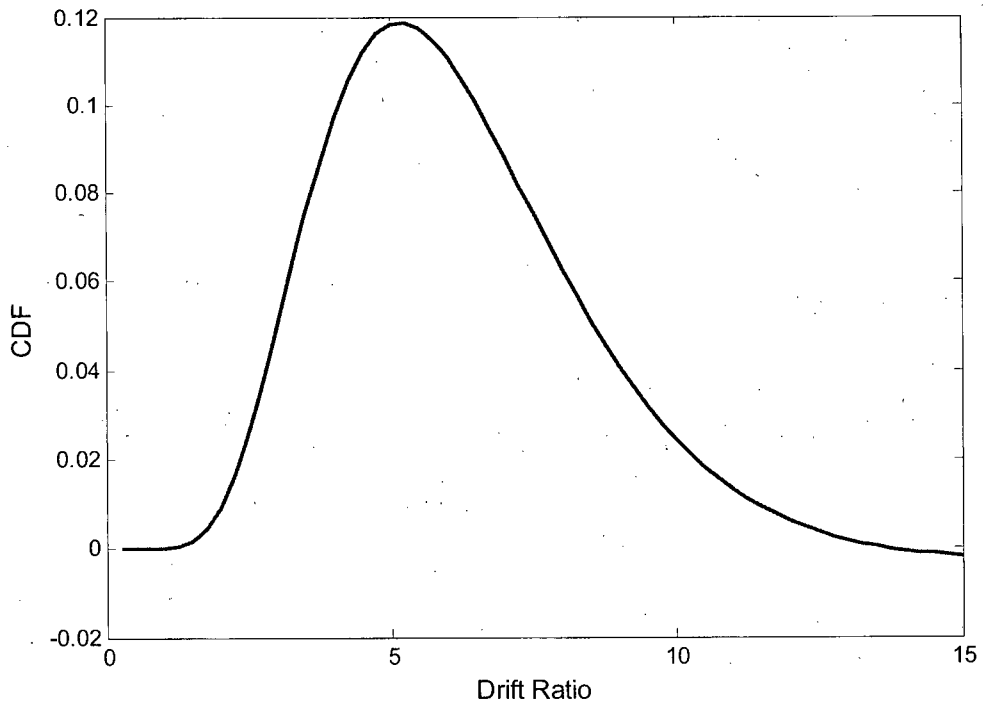

Figure 4.42 Circular C fragility curve for ACI

4.2.2.3 Assessment of Codes and Proposed Models

As was done for the scatter plot evaluation, the ACI minimum equation is applied here to the remaining models for direct comparison with ACI. A fragility curve evaluation of each model without the minimum will follow.

Figure 4.43, Figure 4.44 and Figure 4.45 show the A, B and C statistic fragility curves for ACI and all other models where the ACI minimum is applied to all models. As was stated earlier, the fragility curves are shown here up to very high drifts only to be able to include all the data. Again, the SK97, BS98, WZP94 and LP04 models have been removed in favor of the combined models SKBS and WZPLP.

The figures again confirm the conclusions reached in the initial scatter plot evaluation. For all three figures, the ACI model resulted in the least desirable curve. Again the

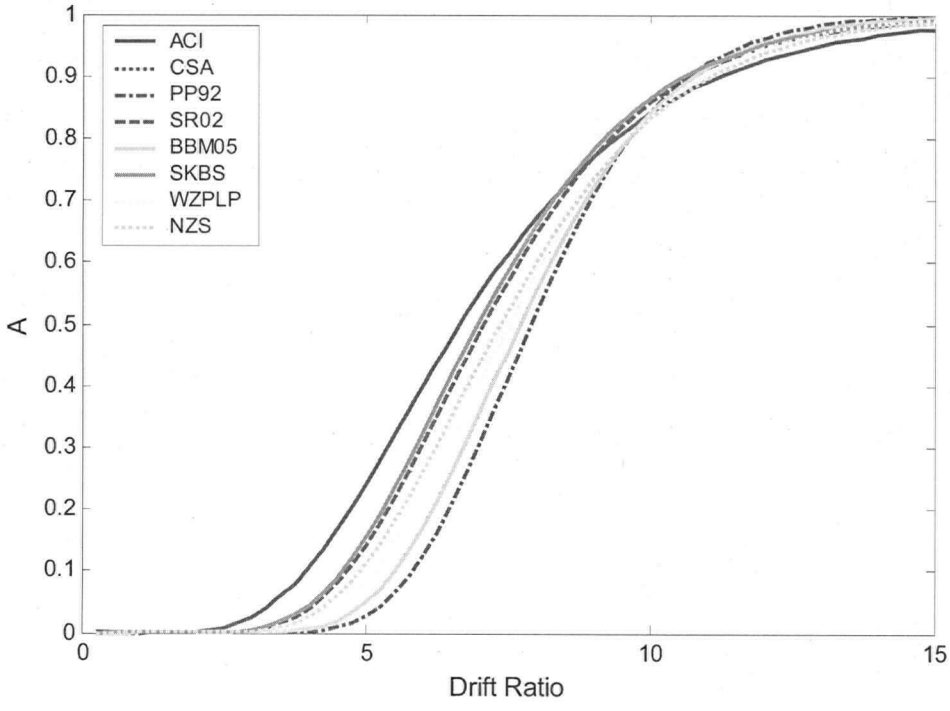

Figure 4.43 Circular A fragility curve all models (with ACI minimum)

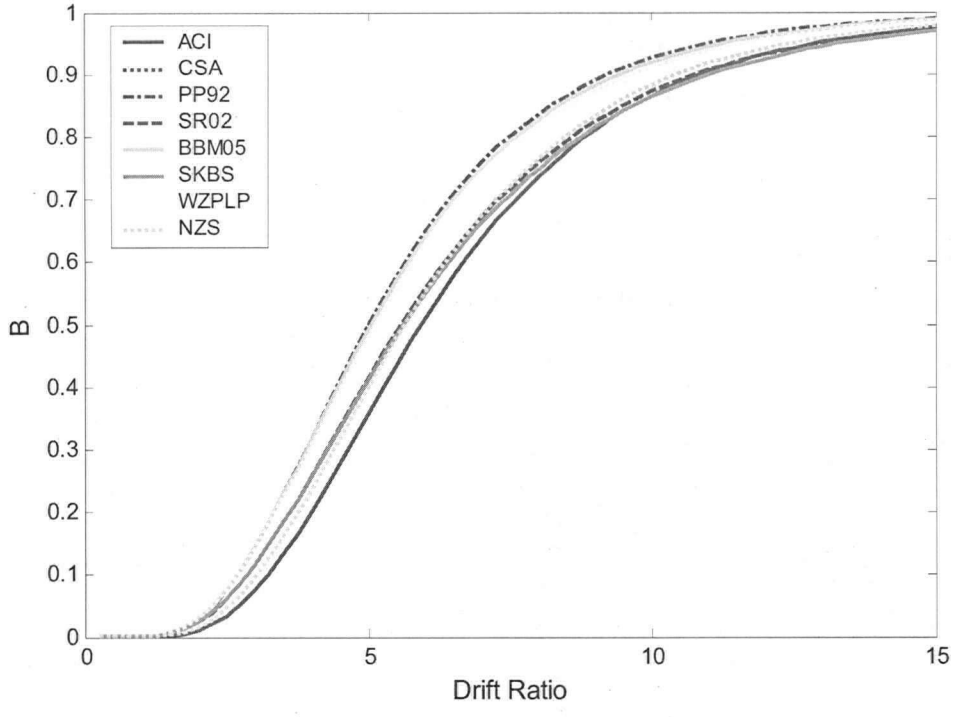

Figure 4.44 Circular B fragility curve all models (with ACI minimum)

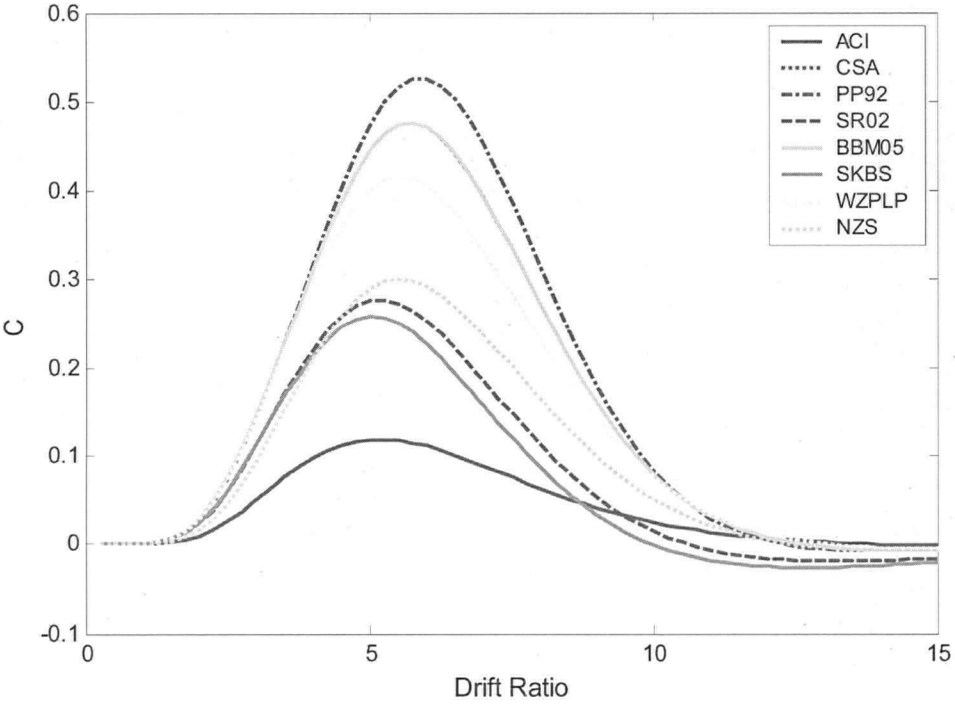

Figure 4.45 Circular C fragility curve all models (with ACI minimum)

inclusion of the ACI minimum had a significant effect on the performance of the models particularly at low drift ratios. The inclusion of the ACI minimum resulted in the CSA and BBM05 models demonstrating the exact same performance and their curves in all three figures lie on top of each other. Despite this fact and limitations of the database, the curves clearly indicate that the ACI model provides the least desirable performance and that a replacement model is warranted. To determine which model should act as the suggested replacement, a fragility curve evaluation of the models without the ACI minimum is needed.

Figure 4.46 shows the circular column A fragility curve for all the models including ACI. Likewise, Figure 4.47 shows the circular column B fragility curve for all the models and Figure 4.48 shows the circular column C fragility curve for all the models. The ACI minimum is not applied to any other model. Also, the current minimum of the CSA code given in Equation 2.14 (CSA Equation 10-7) is not included in the evaluation. This again is because this minimum does not form part of the PL05 model being evaluated. Again, the SK97, BS98, WZP94 and LP04 models have been removed in favor of the combination models SKBS and WZPLP. The individual A, B and C statistic fragility curves for each model are presented in Appendix C.

As expected, the curves in Figure 4.46 show essentially no difference in the A values at a drift ratio of 2.5%. This matches perfectly with the results of the scatter plot evaluation. While the individual behavior of the models is distinguishable at higher drift ratios, significant variation does not become apparent until drift ratios of approximately 4% are reached.

With no significant differences in the models at lower drift levels with regard to the A statistic fragility curve, the B statistic fragility curves becomes even more significant. As expected, the curve with the highest B value in Figure 4.47 at a drift ratio of 2.5% is SR02 followed by BBMO5 and CSA. These results are again in agreement with those from the scatter plot evaluation. However, as is clearly shown in the figure, CSA and

BBM05 become the highest curves, by a significant margin, at drifts beyond 3.0%. The ACI model provides the lowest B values for drift ratios up to approximately 9%

The SR02 C value, shown in Figure 4.48, is the highest at a drift ratio of 2.5%, however, as witnessed in the B statistic fragility curve, CSA and BBM05 become the best performing model at drifts higher than 2.5%. The ACI model provides the lowest C values at drift ratios below approximately 8%, which could be considered beyond the range of meaningful drifts.

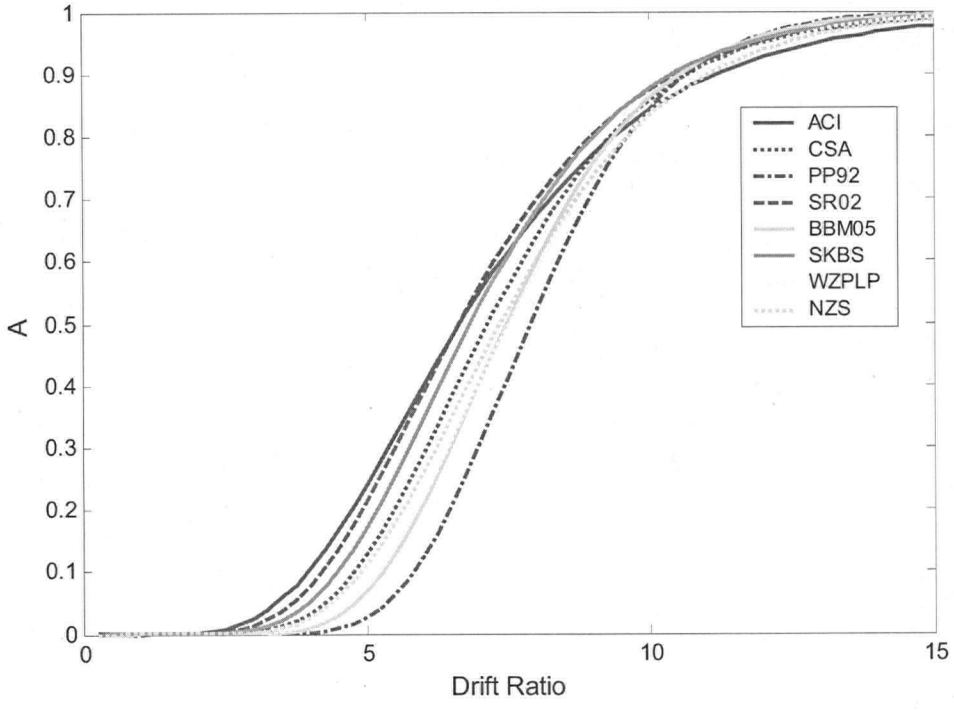

Figure 4.46 Circular A fragility curve for all models

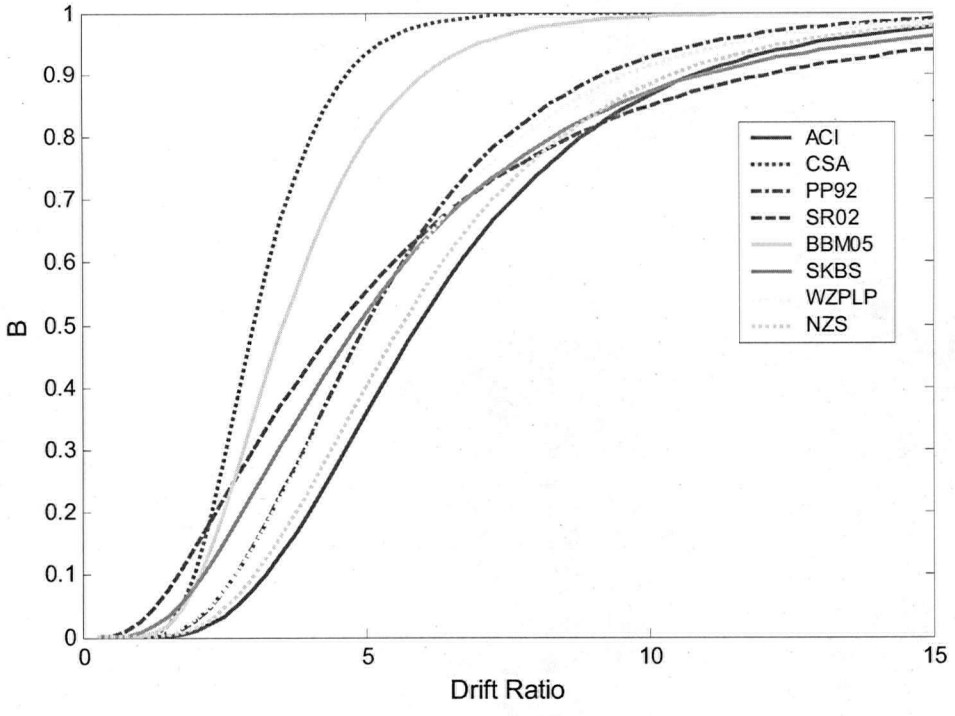

Figure 4.47 Circular B fragility curve for all models

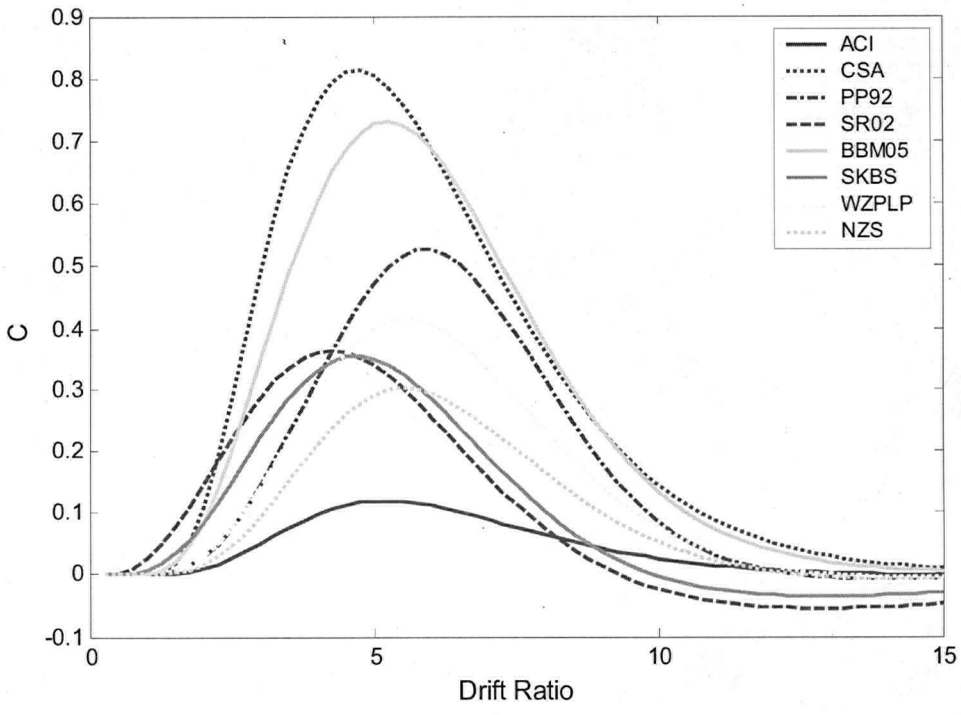

Figure 4.48 Circular C fragility curve for all models

4.2.2.4 Special Considerations for SR02

As was done in section 4.1.2.4, special consideration is given to the SR02 model due to the fact that the drift ratio is a direct input into the expression used to calculate the confinement requirement. Figure 4.49 shows a comparison of the A, B and C statistic curves generated using the appropriate drift ratios with those generated using a drift ratio of 2.5%. The figure suggests that for the circular column database used in this study, using a consistent drift ratio of 2.5% under-predicts the performance of the SR02 model at drifts greater that 2.25% and over-predicts the performance at drifts less than 2.25%. The conclusion is that the performance of the SR02 model is slightly better than shown in Figure 4.48.

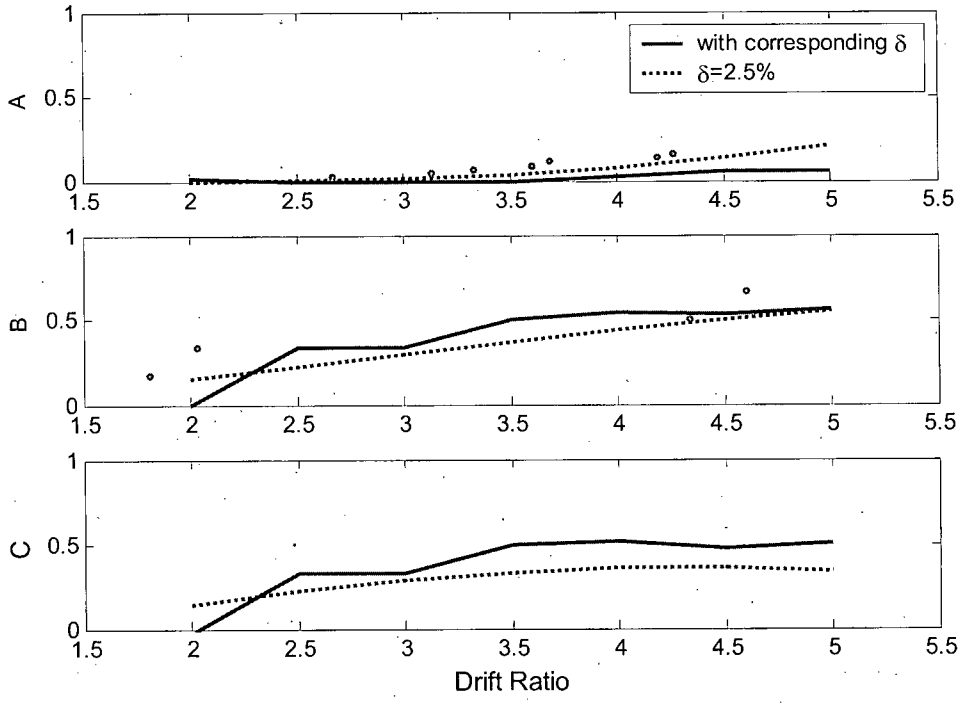

Figure 4.49 Circular SR02 fragility curve comparison

4.2.3 Spacing (Spiral Pitch) of Transverse Reinforcement

4.2.3.1 Assessment of ACI 21.4.4.2

As explained in Section 2.1.1, the spacing requirements for circular columns are the same as those provided for rectangular columns and are given in Equations 2.10 and 2.11. The exception that the third limit (Equation 2.12) does not apply to circular columns.

The scatter plot for the one quarter minimum dimension spacing limit is shown below in Figure 4.50. The figure shows every column in the database, including two columns which have drifts below 2.5%, meets the spacing requirement.

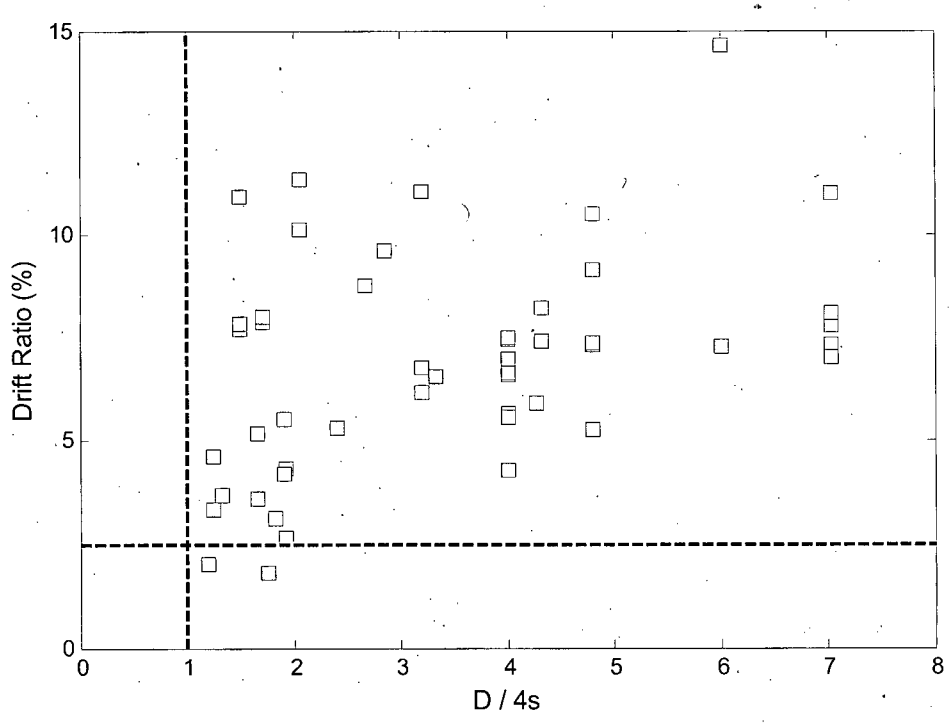

Figure 4.50 Circular scatter plot for one quarter minimum dimension spacing limit

The confinement area requirements of ACI 318 are rearranged and expressed as a spacing requirement (i.e. for a known area and arrangement of transverse bars).

$$s = \frac{4A_b}{0.45\frac{f_c'}{f_{yh}}h_c\left(\frac{A_g}{A_{ch}}-1\right)} \qquad (4.13)$$

This spacing requirement was then compared to the two spacing limits giving in Equations 2.10 and 2.11, to determine which governed. Table 4.10 shows how often each confinement requirement governs the spacing of transverse reinforcement for the 50 circular columns used in this study.

Table 4.10 ACI 318-05 Governing spacing of circular transverse reinforcement

Spacing limit	# columns governed
Eq 2.10	1
Eq 2.11	1
Eq 4.13	48

As was the case for the rectangular columns, the area requirement predominantly governs the spacing of the confining steel. This result is not surprising when considering that the ACI model was found to be the most overconservative in the scatter plot and fragility curve evaluations.

All of the 29 columns which satisfy the area requirements of ACI 318-05 section 21.4.4.1 also satisfy the spacing requirement of section 21.4.4.2. This statistic further indicates the conservative nature of the ACI confining steel area requirement for circular columns.

4.2.3.2 Assessment of CSA and NZS

The area requirement for the CSA and NZS models were rearranged and expressed as a spacing limit as follows:

$$s = \frac{4A_b}{0.4k_p\frac{f_c'}{f_{yh}}h_c} \qquad (4.14)$$

$$s = \frac{4A_b}{h_c\left(\frac{A_g}{A_{ch}}\frac{1.0-\rho_t m}{2.4}\frac{f_c'}{f_{yh}}\frac{P}{\phi f_c' A_g}\right) - 0.0084h_c} \qquad (4.15)$$

The results of the evaluation of the spacing limits for CSA and NZS are displayed below in Table 4.11. The table shows a similar number of instances in which the spacing is governed by the area requirement.

All of the 43 columns which satisfy the area requirement of CSA, and all of the 38 which satisfy the area requirement of NZS, also satisfied the spacing requirements.

The results shown in Table 4.10 and Table 4.11 show the potentially extraneous nature of the one quarter diameter spacing limit when used in conjunction with the area requirement for confining steel in circular columns. This issue is further discussed in the final recommendations (Chapter 5).

Table 4.11 Governance breakdown for spacing of transverse reinforcement for CSA A23.3-04 and NZS 3101:2006

Spacing limit	# columns governed CSA	# columns governed NZS
Eq 2.10 / 4.11	1	3
Eq 2.11 / 4.12	0	0
Eq 4.14 / 4.15	49	47

4.2.4 Maximum Recorded Drifts

As was done in the rectangular column analysis, the maximum recorded drifts were also analyzed. The effects of this adjustment were noticeable for the rectangular columns as many of them experienced drifts well beyond that recorded at 20% loss in lateral strength. For the circular column database this is not the case. In fact, the average increase between the two displacements for circular columns was a mere 9.1% versus 32.0% for the rectangular columns. The two columns in the original analysis which had drift ratios below 2.5% achieved higher drifts, but both still remained below 2.5%. Therefore, the

scatter plot evaluation produced the same statistical values for A, B and C as those obtained with drifts measured at 20% loss in strength, and the there was consequently no distinguishable difference in the fragility curves for the two analyses.

For some tests, the maximum recorded drift ratios where close to those measured at 20% loss in strength. This is simply because most tests are stopped shortly after this stage and does not suggest that circular columns have less reserve drift capacity than rectangular columns. The conclusion therefore is that the performance results of the models remains essentially unchanged for the analysis using the maximum recorded drifts for the circular columns, and the formulation of a final conclusion can be based on the results found in the analysis using drifts at 20% loss of lateral strength. The drifts at 20% loss in strengths as well as the maximum recorded drifts can be found in Appendix A.

5 SELECTION OF CONFINEMENT MODEL

5.1 Selection Procedure

The previous chapter presented the results of the performance evaluations for each model considered in this study. The results clearly indicated that the ACI criteria for confining steel in reinforced concrete columns should be improved. The following is a description of the procedure used to select the most appropriate confinement model for both rectangular and circular columns. The procedure uses the evaluation results presented in Chapter 4 to select (and eliminate) models based on their performance.

5.1.1 Objective

In the introduction, it was stated that the aim of this project is to evaluate the current requirements of ACI 318-05, and present a final recommendation for the design of confinement steel for both the rectangular and circular reinforced concrete columns. Part of the evaluation included considering the form of the requirements expressed in Chapter 21 of ACI318-05. The area of confining steel is stated in section 21.4.4.1, while the spacing requirements are given in section 21.4.4.2. The latter contains the two spacing limits which are confinement requirements and also the spacing limit which is intended to protect against longitudinal bar buckling. The recommendations given here are derived with the intent of presenting a requirement for both rectangular and circular columns which takes the following form:

i) *Minimum confinement level* (expressed as either a minimum area / density limit or a maximum spacing limit)

ii) *Appropriate varying confinement levels* (area / density or spacing requirements above the minimum value)

The minimum confinement level is intended to be a baseline for confinement for all columns. The need for a minimum level of confinement arises from a historical design practice that a minimum level be maintained for all columns, similar to Equations 21-2

and 21-4 in ACI318-05. The form of the minimum level will depend on the nature of the preferred model and therefore can be determined once the model has been selected. For confinement above the minimum level, the preferred model should consider all the variables which impact the performance of the columns and require confinement levels that are appropriate to achieve acceptable levels of drift.

5.1.2 Scatter Plot Evaluation

The data presented in the scatter plot evaluation is useful to understand how the performance of each model compares to the ACI model. Identifying data points with lightly shaded squares and dark shaded diamonds based on their location on the ACI scatter plot, allows for tracking the movement of data points on subsequent scatter plots. As was discussed in Chapter 4, the ideal model would have zero data points in quadrant 2 and the number of data points in quadrant 3 should be limited to an appropriate level of conservatism. The ACI rectangular model has 9 data points in quadrant 2 and 92 in quadrant 3, the ACI circular model has 1 data point in quadrant 2 and 20 in quadrant 3 (Table 4.3 and Table 4.9). Therefore, the scatter plot of a model which demonstrates an improved performance will display a movement of these data points from quadrant 2 to quadrant 4, and from quadrant 3 to quadrant 1. Figure 5.1 illustrates an example of this movement of for a few select data points. Figure 5.1(a) shows the location of the data points on the ACI scatter plot and the desired movement of the data in quadrants 2 and 3. Figure 5.1(b) shows the location of the data on the CSA scatter plot showing the improved performance. The figure also demonstrates a desired trend for improved models, one in which data points are aligned in a matter that demonstrates a proportionally increased drift with increased confinement (i.e. along the diagonally dashed line). This relationship is particularly meaningful at lower confinement levels; as the confinement approaches the model requirement, the drift should approach the performance target. As seen in Figure 4.2, this is not the case for the ACI model where test columns with only slightly less confinement than required had failure drift ratios well below the 2.5% target.

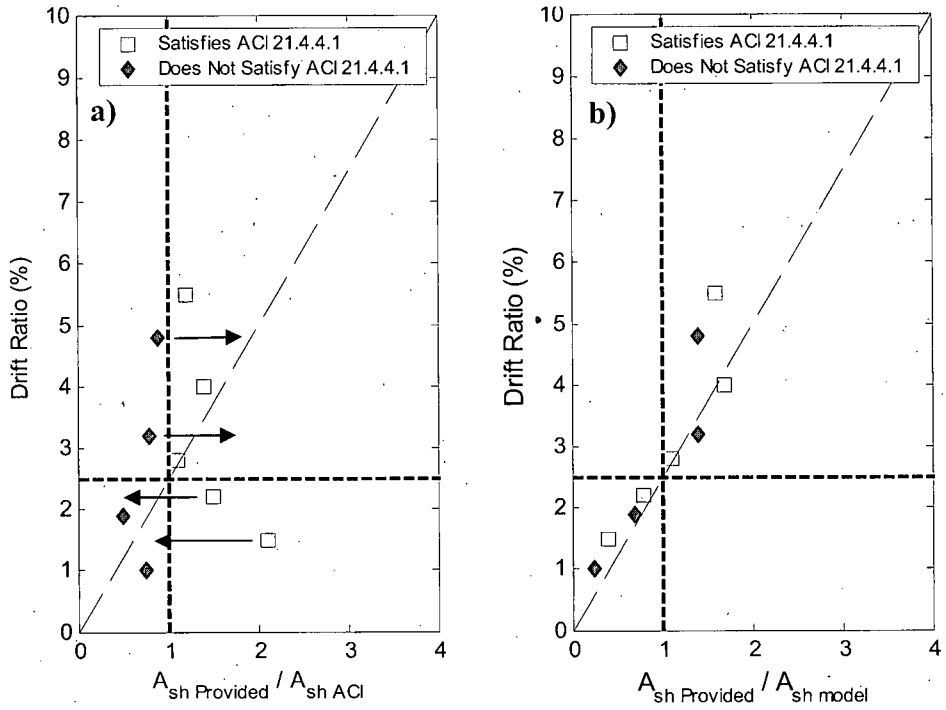

Figure 5.1 Desired movement of data points

To further illustrate this desired model improvement, two specific columns taken from the rectangular column database are shown below. The two tests have a similar transverse reinforcement ratios and the major difference between the two column tests is the level of axial load. Column 15 was subjected to an axial load ratio of $P/P_0 = 0.7$ and had a measured drift ratio of 1.2% at 20% loss in lateral strength. Column 106 was subjected to an axial load ratio of just $P/P_0 = 0.15$ and had a measured drift ratio of 9.0. Figure 5.2 shows that for the two columns, the CSA model which includes axial load in the design expression demonstrates more appropriate confinement levels.

The evaluation of the data movement and the values presented in Table 4.3 and Table 4.9 will be used to eliminate models which are not a significant improvement over the ACI model.

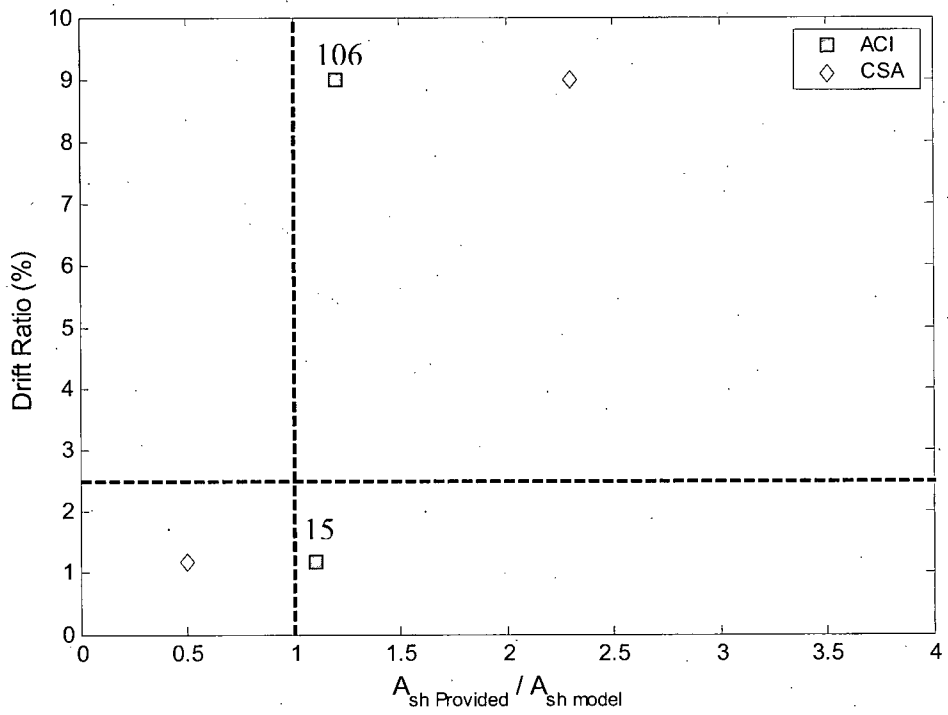

Figure 5.2 Location of specific column examples for ACI and CSA scatter plot

Table 5.1 Details for rectangular columns 15 and 106

Database No.	Specimen Name	f'c (MPa)	P/Agf'c	L(mm)	Gross Area (A_g) (mm^2)	ρ_{long} (%)	ρ_{area} (%)	Drift Ratio (%)
15	Watson and Park 1989, No. 7	42	0.7	1600	160000	1.51	1.30173	1.17
106	Saatcioglu and Ozcebe 1989, U4	32	0.15	1000	122500	3.21	1.0908	8.99

5.1.3 Fragility Curve Evaluation

The fragility curves presented in Chapter 4 will be compared for the models which were not eliminated in the scatter plot evaluation. The fragility curves will be examined within the range of meaningful drifts. As discussed in Chapter 4, the curves provide probability data up to the maximum drift ratio observed in the database (i.e. a drift ratio of 10% for rectangular columns and 15% for circular columns). However, it is highly unlikely that a

target drift ratio for a building, particularly in new construction, would exceed 3% to 4%, therefore data beyond these drifts is not meaningful.

The fragility curves can then be used to select the models which demonstrate the best overall performance. If the level of safety provided by the model was the only matter of interest, the A fragility curve would be the appropriate curve to examine. However, the interest of this study is to identify which model provides the optimum level of safety without significant overconservatism. Therefore, all three fragility curves will be addressed in the evaluation. It should be noted that the models which do no offer an improved level of safety will be removed from the list of potential replacement models during the scatter plot evaluation.

5.1.4 Comparison of Expressions

The form of the expressions given in Chapter 2 will be evaluated again after the scatter plot and fragility curve evaluations are complete. To be considered an appropriate replacement model, the form of the expression should contain variables that practicing engineers are familiar with, and should appear as transparent as possible. Any model which is drastically different than current design practice will be removed from the list of potential replacement models unless that model displays exceptional performance and its removal can not be justified.

5.1.5 Model Requirements

A typical example column, for both rectangular and circular cross-sections, will be used to evaluate how the requirements of the final models compare with the current requirements in ACI. The example columns are taken from the typical column details provided in section 3.4 and Appendix D.

The confining steel area, or volumetric density, requirement by each model for the example columns can be shown throughout the range of axial load ratios. A similar figure will be generated to show the spacing requirements which result from the form of each

model. This figure will give more insight to how the models compare with the spacing limits of ACI.

5.2 Rectangular Columns

5.2.1 Scatter Plot Evaluation

A review of the scatter plots presented in Section 4.1.1.3, the statistics shown in Figure 4.13 and the data presented in Table 4.3 show that the ACI model exhibited the poorest performance of all the models in this investigation. Table 4.3 also shows the movement of data points for the rectangular column models. The results indicate that the WSS99 and SR02 models had more data points in quadrant 2 than the ACI model, and SKBS had more data points in quadrant 3 than the ACI model. For these three models, the change in number of data points in the quadrants is not large, but the desired movement of data points as presented in Figure 5.1 is not demonstrated. While the number of data points in quadrant 1 for both the WSS99 and SR02 models increased, the presence of a larger number of 'unsafe' columns renders these models undesirable. For SKBS, the greater number of data points in quadrant 3 combined with fewer data points in quadrant 2 suggests that the model simply requires a greater amount of confinement reinforcement for virtually all columns and is not strongly correlated to the drift performance of the columns. While this greater requirement does significantly reduce the instances of 'unsafe' columns, it restricts the desired movement of data points at higher drifts.

Based on the discussion above, the WSS99, SR02 and SKBS models are removed from the list of suitable replacements for the ACI model. The scatter plots for the remaining models (CSA, PP92, BBM05, WZPLP and NZS) suggest that as the amount of confinement approaches the requirement of the model, the drift capacity approaches the performance target, a trend not observed in the models removed here.

5.1.6 Fragility Curve Evaluation

The A, B and C fragility curves for the CSA, PP92, BBM05, WZPLP and NZS models are shown again in Figure 5.3 through Figure 5.5 for the meaningful range of drift ratios discussed earlier. The figures show that at drift ratios below 1.0% there is no real significant difference in the performance of the models, however, at drifts greater than 1.0%, the CSA, PP92 and BBM05 models clearly exhibit superior statistics. The curves demonstrate that over the practical range of drift ratios, these three models best capture the desired overall performance which included both a suitable level of conservatism and safety. Figure 5.4 further suggests that the BBM05 model performs best at drift ratios below 2.2%, while the CSA model performs the best at higher drift ratios; although the difference between the models is not statistically significant.

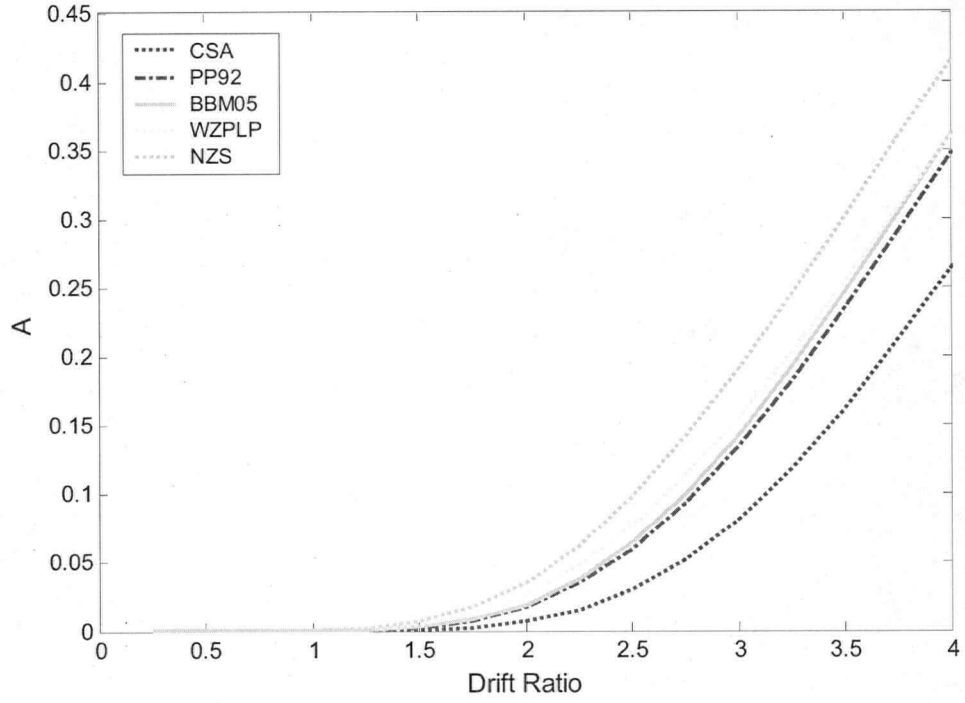

Figure 5.3 A fragility curves

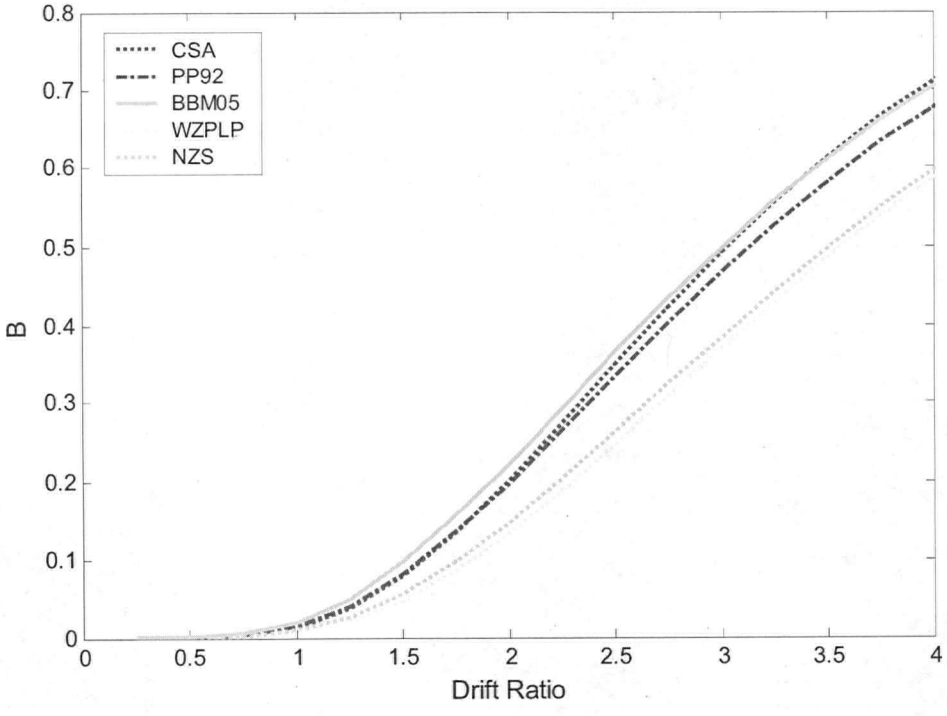

Figure 5.4 B fragility curves

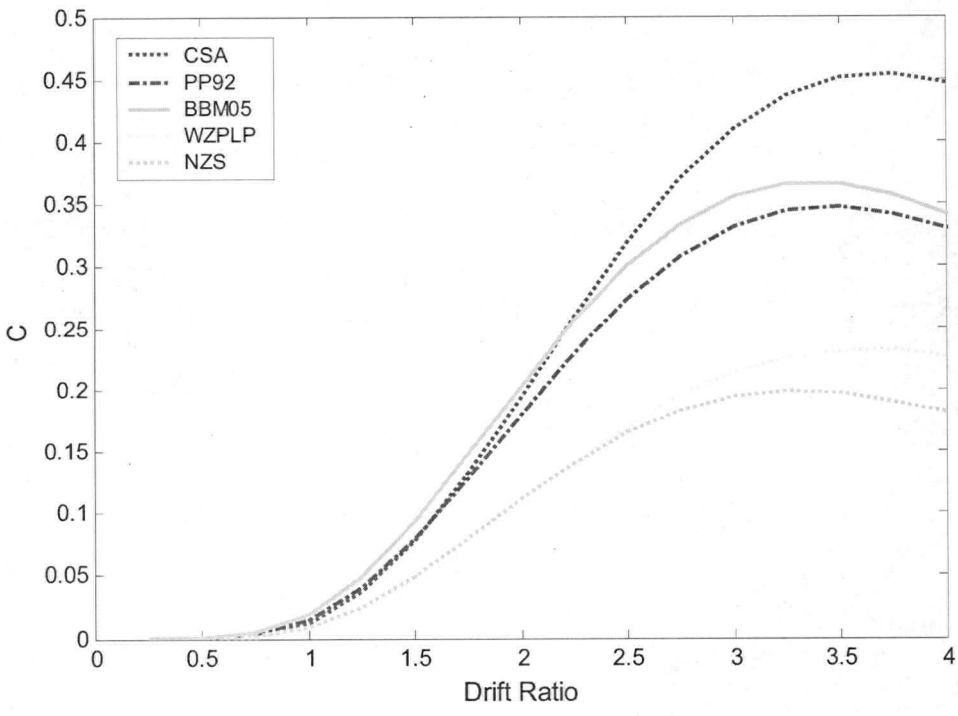

Figure 5.5 C fragility curves

These results clearly identify WZPLP and NZS as being the least desirable of the remaining models, and the conclusion therefore is to eliminate them from the list of suitable alternatives for the ACI model.

5.1.7 Comparison of Expressions

The form of the expression for each model is an important consideration in addition to its statistical performance. The expressions for the confinement requirements of each model were presented in Chapter 2. Review of the expressions for ACI, CSA, PP92 and BBM05 indicates a similarity amongst the models with the exception of BBM05. If BBM05 were adopted as a replacement for ACI, the form of the expression would be a drastic departure from its current form. Perhaps more importantly, the form of the BBM05 is much less intuitive and its derivation is hidden. Such a departure from the current form of the expression would undoubtedly be warranted if the performance of the model was vastly superior to all other models. However, as has been shown above, this is not the case. For this reason, the BBM05 model is removed from the list of potential replacement models.

5.1.8 Requirements of Models

The details of a typical rectangular column were used to examine the area requirements of the remaining models, CSA and PP92. Figure 5.6 shows the area of confining steel (A_{sh}) required for the example column for the CSA and PP92 models. For reference, the ACI model requirements are included in the figure. The area of confining steel is normalized to represent, as closely as possible, the trend that can be expected for columns with various material and geometric properties. The figure shows that the area requirement increases linearly with respect to axial load for the CSA and PP92 models, while ACI is independent of axial load. The figure shows that the two have similar requirements with a small difference in slopes and all three models require the same amount of confining steel at an axial load ratio of approximately 0.3. Above an axial

load ratio of 0.3, CSA and PP92 require more transverse reinforcement, while below this limit, CSA and PP92 require less transverse reinforcement.

Figure 5.7 shows the confinement spacing requirements for the typical column resulting from the requirements of the CSA and PP92 models. Again the spacing requirement is normalized to represent the trend that can be expected for columns with various material and geometric properties. The figure shows that unlike the area requirement, the spacing limit imposed by the CSA and PP92 models is not linear. The required maximum spacing increases dramatically as the axial load ratio approaches zero. This suggests that a minimum level of confinement will have to be applied in connection with the requirement imposed by either CSA or PP92.

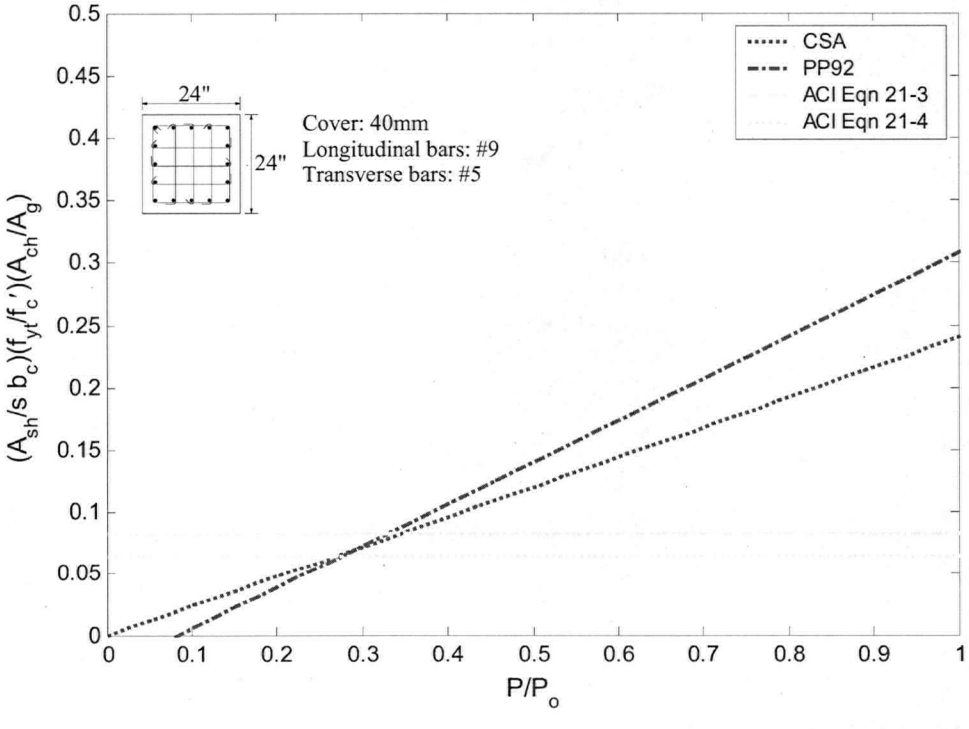

Figure 5.6 Confinement area requirements for range of axial load ratios

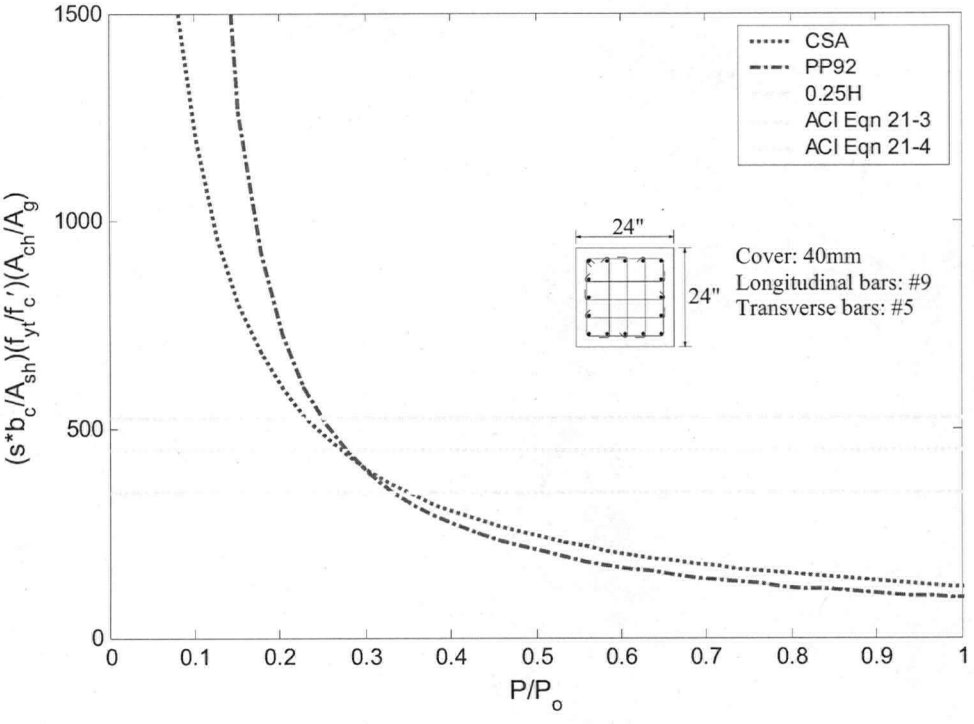

Figure 5.7 Confinement spacing requirements for range of axial load ratios

5.1.9 Conclusion and Recommendation

The curves shown above in Figure 5.6 and Figure 5.7 show comparable requirements for the CSA and PP92 models. Figure 5.3 showed that the CSA model out performed PP92 in the statistical analysis. Comparing the form of the CSA and PP92 models presented in Chapter 2 shows that the two are expressions are very similar. Both share the common term $(A_g/A_{ch})(f_c'/f_{yh})$ and both have a term which includes a linear variation with axial load. The main difference between the two expressions is that the CSA model includes the longitudinal reinforcement configuration and the PP92 model does not. Recall from Figure 1.3 the degree of confinement provided by an arrangement of transverse steel is dependant on the spacing of laterally supported vertical bars.

Considering both the statistically better performance and the more favourable form of the expression for the CSA model compared to the PP92 model, the final conclusion for the preferred model for rectangular concrete columns is the CSA model.

To present the final recommendation in the format discussed in section 5.1.1, the minimum and maximum confinement levels must also be addressed. The minimum confinement level is currently expressed in the ACI code by Equation 21-4, and by the spacing limits of section 21.4.4.2. The form the CSA expression dictates that as the level of axial load approaches zero, the area requirement approaches zero. Therefore, an alternative means of specifying a minimum level of confinement would be to introduce a minimum level of axial load that can be inserted into the CSA confinement expression. This technique is adopted by the SR02 model which suggests a limit of $P/P_0 = 0.2$. To evaluate the suitability of this limit the axial load ratio, P/P_0, was determined for each column in the database which produces an area requirement equal to that required by the current ACI minimum confinement expression. The values ranged from 0.07 to 0.32 and had a mean value of 0.21. This is in agreement with the curves shown in Figure 5.6 where the CSA curve and the curve for the ACI minimum equation intersect at a P/P_0 ratio slightly greater than 0.2. The results of this evaluation suggest that limiting the minimum P/P_0 value to 0.2 will provide a minimum level of confinement similar to that which is achieved by the current expression in ACI 318.

The data presented in section 4.1.3 suggested that the current area and spacing limits of ACI exhibited similar statistics when investigated individually. However, a closer look at the data shown in Figure 4.22 shows that the spacing limit impacts a number of columns with high axial loads. This suggests that when applied together, the two requirements provide an improved performance. Therefore, for an added level of safety and consistency with historical designs, the one-quarter of the minimum dimension spacing limit can be included in the minimum confinement level. The spacing limit of 4 to 6 inches given by Equation 2.12 (ACI Equation 21-5) is also included as there is no basis for its removal.

There is currently no maximum confinement level expressed in the ACI code. It is suggested that it should be noted in the commentary to the code that axial loads should be kept below a value that would result in unrealistically small transverse steel spacing.

This allows the engineer to use his or her judgement and leaves room for innovative designs.

The final recommendation for the design requirements for confinement steel in rectangular reinforced concrete columns is expressed as follows:

The total cross-sectional area of rectangular hoop reinforcement shall not be less than:

$$\frac{A_{sh}}{s_c b_c} = 0.2 k_n k_p \frac{A_g}{A_{ch}} \frac{f_c'}{f_{yh}}$$

where (a) $k_p = P/P_0$

(b) $k_n = n_l/(n_l-2)$

(c) k_p shall not be taken as less than 0.2

(d) s_c shall not exceed $6d_b$,one quarter of the minimum member dimension or s_x defined as:

$$s_x \leq 4 + \left(\frac{14 - h_x}{3} \right)$$

where s_x shall not exceed 6 inches and need not be taken less than 4 inches and h_x is the maximum horizontal spacing of hoop or crosstie legs on all faces of the column.

5.3 Circular Columns

In section 4.2 the performance of the models was evaluated for circular columns. From the statistical analysis, the ACI model determined to be the worst performer making a new equation desirable. The circular column database contains few column tests with high axial load and consequentially has few columns with low total drifts at 20% loss in lateral strength. A new equation is proposed here with the suggestion that more testing of high axially loaded circular columns is needed to further confirm the suitability of proposed model.

5.3.1 Scatter plot Evaluation

As stated in Chapter 4, the ACI model was the only model to have a data point in quadrant 2. The evaluation of the scatter plots then becomes an evaluation of the data with drift capacities higher than 2.5%. Only the PP92 and WZPLP models did not demonstrate an improvement over the ACI model with respect to these data points (i.e., the movement of the data points from quadrant 3 to quadrant 1 is not seen for these models). This conclusion is illustrated in Figure 4-34 which shows that these two models resulted with the worst overall behaviour as seen by their lower C statistic values.

Therefore, via the evaluation of the scatter plots, the PP92 and WZPLP models are removed from the list of suitable alternatives for the ACI model.

5.3.2 Fragility Curve Evaluation

The C statistic fragility curves for the CSA, SR02, BBM05, SKBS and NZS models are shown again in Figure 5.8 for the meaningful range of drift ratios discussed earlier. The figure shows a significant difference in the performance of the models throughout the range of drift ratios, and that different models perform better within certain ranges, making it difficult to eliminate models using these curves. However, the NZS model is consistently below the other four models throughout the drift range of interest. Therefore this model can justifiably be removed from the list of suitable alternatives for the ACI model.

5.3.3 Comparison of Expressions

A review of the expressions for the CSA, BBM05, SR02 and SKBS models shows a relative similarity amongst the models with the exception of BBM05, similar to the evaluation of rectangular column confinement models. If BBM05 were adopted as a replacement for ACI, the form of the expression would again be a drastic departure from

its current form. Once again, the form of the BBM05 is much less intuitive and its derivation is hidden. Figure 5.8 shows that the BBM05 model is not the preeminent model for any target drift ratio, and removing it will not impact the final decision. Therefore, the BBM05 model is removed from the list of potential replacement models.

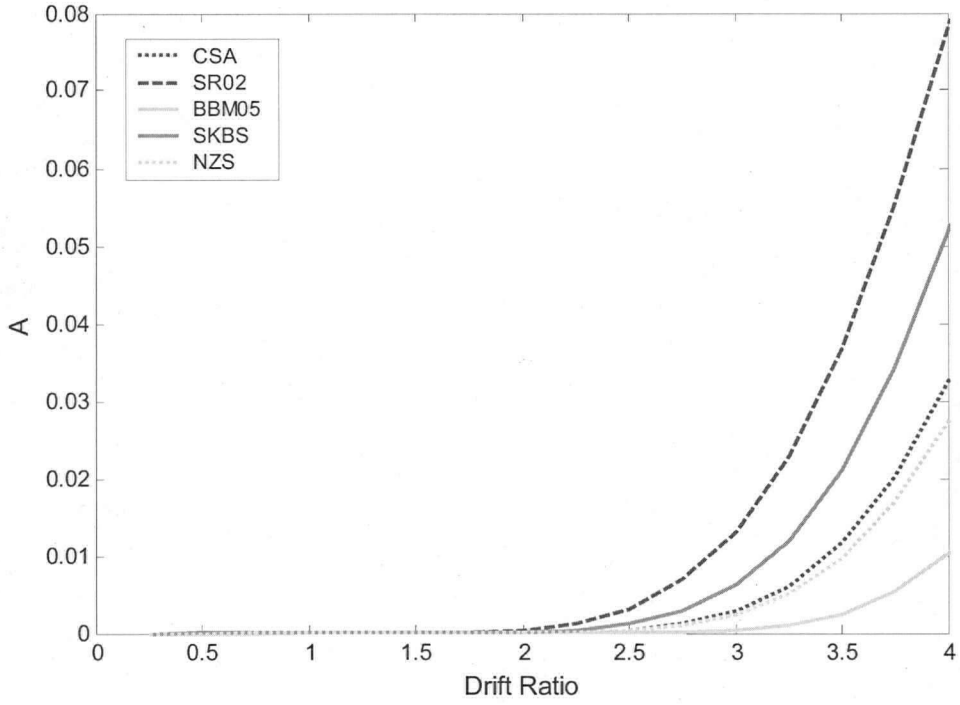

Figure 5.8 A fragility curves

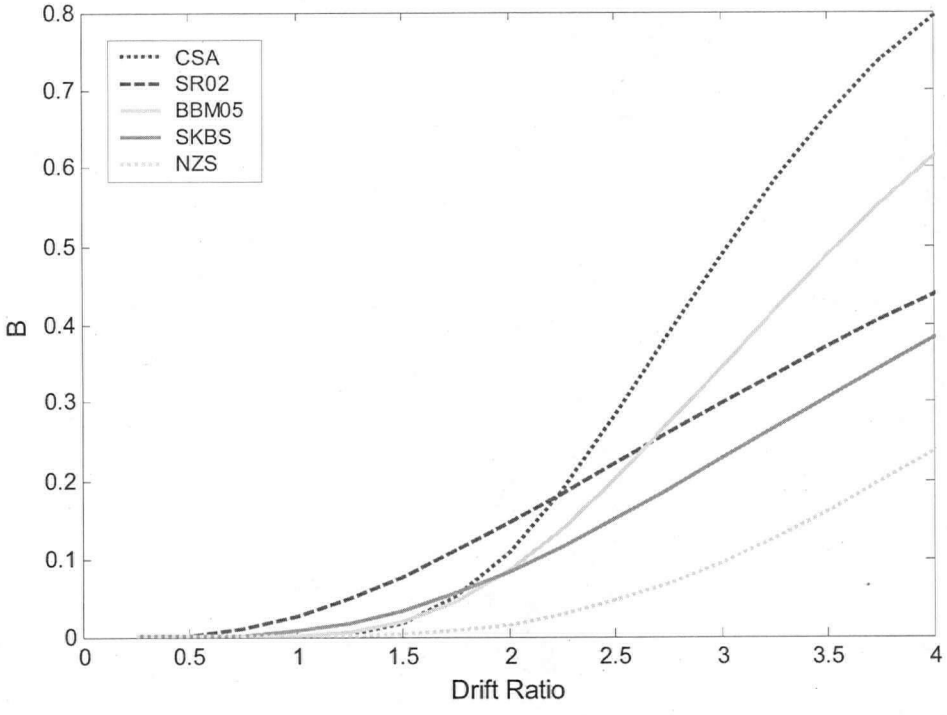

Figure 5.9 B fragility curve

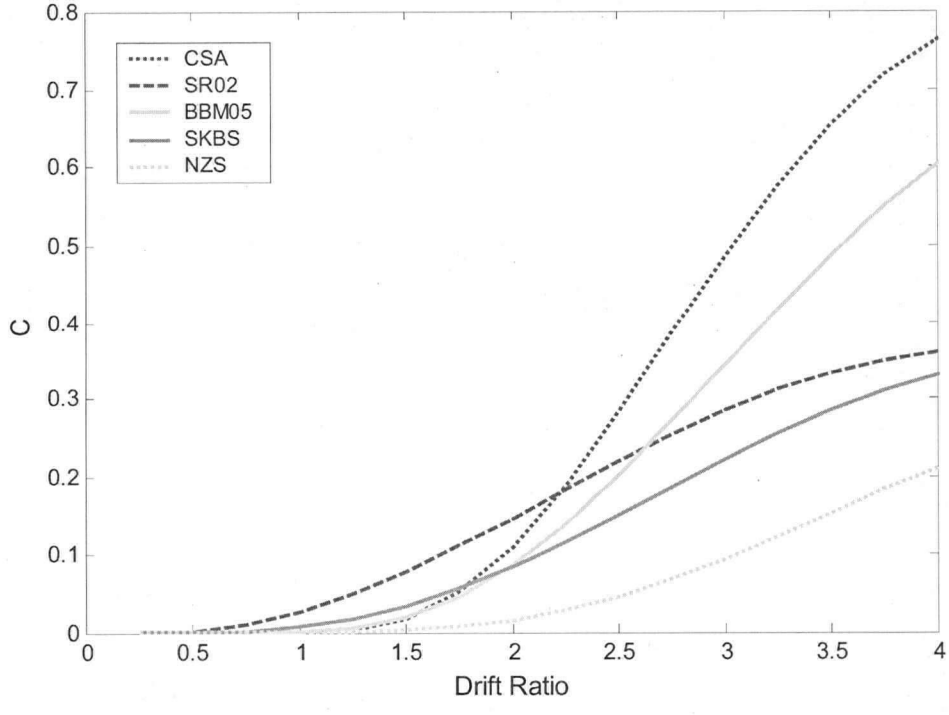

Figure 5.10 C fragility curve

5.3.4 Requirements of Models

A typical circular column was used to examine the volume density requirements of the remaining models. Figure 5.12 shows the confining steel volumetric density required for the example column for the CSA, SR02, and SKBS models. For reference, the ACI model requirements are included in the figure. The density requirement is normalized to represent the trend that can be expected for columns with various material and geometric properties. The figure shows that the density requirement increases linearly for the CSA and SR02 models, and exponentially for the SKBS model. The figure shows that the SKBS model requires only slightly less confinement steel than ACI at low axial load ratios, and has an almost constant value, at axial load ratios below 0.3. However, the SKBS curve requires significantly more confining steel than the other models at higher axial load ratios. At axial load ratios above 0.6 the model requires an amount of confinement that is several times that required by the other models, suggesting that the model becomes unrealistic at these high axial load ratios.

Figure 5.6 further indicates that the SR02 requirement falls below the other two models throughout the range of axial load ratios. The only exception is for axial load ratios below 0.1 where the CSA model becomes the lowest (although minimum limits for the CSA requirements are not included in this figure). This demonstrates that the SR02 requirement is less demanding than the other two which explains why the SR02 model had the largest number of data points move from quadrant 3 to quadrant 1. This less demanding requirement proved to be statistically detrimental for the SR02 model in the rectangular column analysis as it also resulted in a number of columns moving from quadrant 4 into quadrant 2, the opposite of the desired movement. Given that the circular column database had so few columns with low drifts, the effect was not seen here. More tests of circular columns with high axial load are needed to ensure that data movement seen in the rectangular column evaluation does not repeat itself for circular columns. In Chapter 3 it was noted that the drifts achieved by columns with lower axial loads was typically higher for circular columns than for rectangular columns. This could possibly suggest that circular columns in general display better ductility that rectangular columns, or it could simply suggest that more testing is needed to observe the behaviour of circular

columns at higher levels of axial load. Taking this conclusion into consideration and based on the available database, the SR02 model remains a potential replacement model for ACI.

Figure 5.10 showed that for higher drift ratios, where more data are available, the performance of the SR02 model drops below the CSA model. However, in section 4.2.2.4 it was noted that the performance of the SR02 model was underestimated at these higher drift ratios using a constant input variable drift ratio of 2.5%. For the purposes of a design equation, the performance input variable would not appear as a value for the engineer to select, rather it would be provided in the code expression. Therefore, it is recommended that the drift ratio input variable for SR02 should be 3.0% to increase the level of safety provided by the model. Figure 5.11 shows a scatter plot for SR02 using an input drift ratio of both 2.5% and 3%. The performance of the SR02 model is very similar for the two levels input of drift ratios. With an input drift ratio of 3%, the number of data points in quadrant 3 increases from four to seven. The two data points with measured drift ratios also moved further left on the figure. The

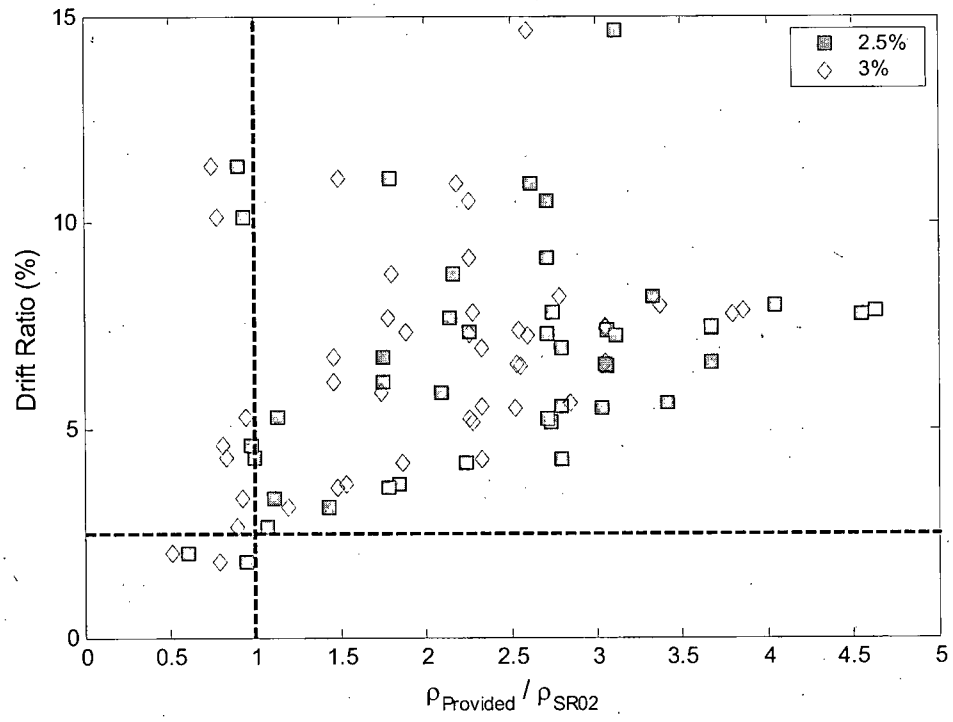

Figure 5.11 SR02 scatter plot drift ratio comparison

figure indicates that implementing an input drift ratio of 3% improves the models conservatism without substantially increasing its overconservatism.

Figure 5.13 shows the confinement spacing requirements for the circular example column. Again the spacing requirement is normalized to represent the trend that can be expected for columns with various material and geometric properties. The figure shows that the spacing requirement increases dramatically as the axial load ratio approaches zero for the CSA and SR02 models. The limiting value for P/P_0 of 0.2 for the SR02 model shows how the limit provides a minimum level of confinement. This confirms the previous suggestion that a minimum level of confinement will have to be applied in connection with the area requirement imposed by a model such as CSA or SR02 which varies linearly with axial load. As expected, the SKBS curve shows a much different spacing requirement than the other two models. The curve shows very little change in the spacing requirement at lower axial load ratios suggesting that this model may be more

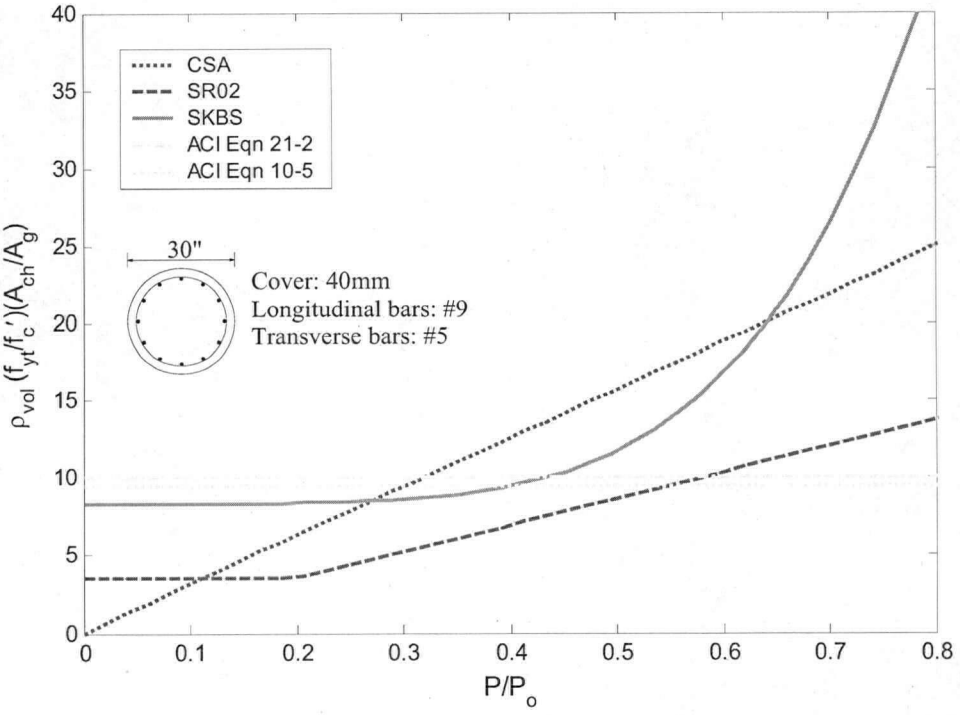

Figure 5.12 Confinement density requirements for range of axial load ratios

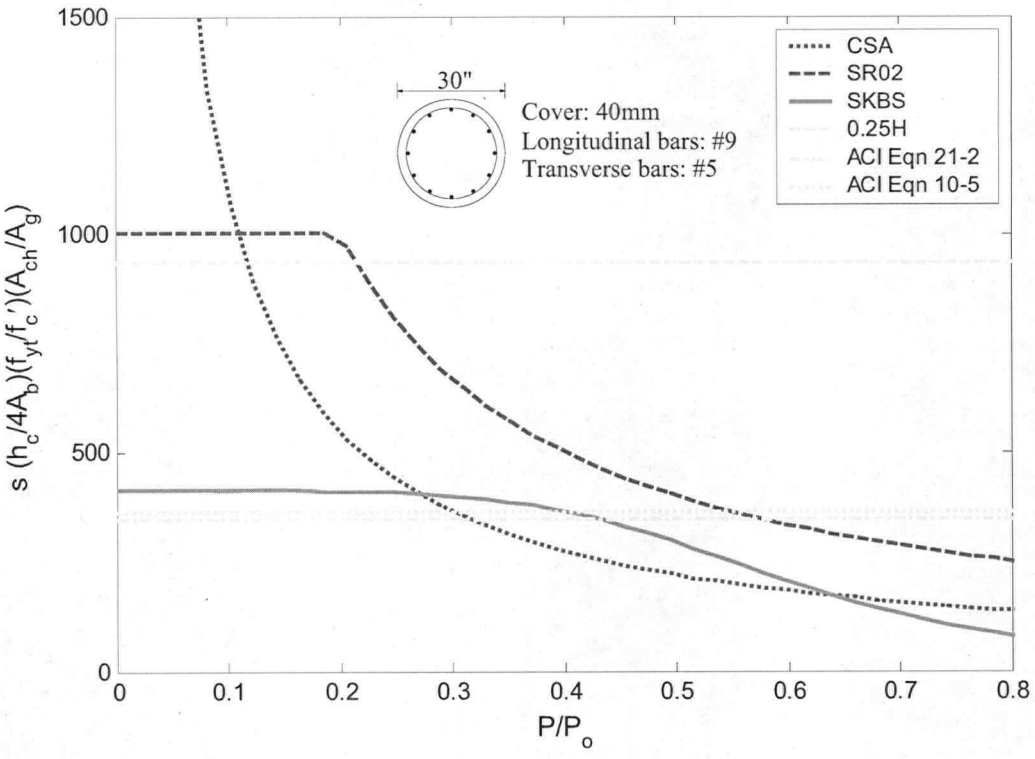

Figure 5.13 Confinement spacing requirements for range of axial load ratios

conservative that the others in this range. This is confirmed by observing that statistics presented in Figure 4.39.

The requirements for the SKBS model shown in Figure 5.12 and Figure 5.13 are less desirable than the CSA and SR02 models. Given that the statistical performance of the SKBS model is not better than the other two models it is removed from the list of potential replacement models.

5.3.5 Conclusion and Recommendation

Comparing the form of the CSA and SR02 models and presented in Chapter 2 shows that significant differences are apparent between the two expressions. The ratio of A_g/A_{ch} is not considered by CSA in the expression for the volumetric density, instead it is included in the expression for the minimum confinement level (Equation 2.14). The SR02 and CSA models do however become identical for an A_g/A_{ch} ratio equal to approximately 1.6. The SR02 model also imposes a minimum value for A_g/A_{ch} of 1.3. The ratio of gross

column area to confined core area has been shown to influence the drift capacity of reinforced concrete columns. For this reason, including the area ratio in the primary expression for confinement is more logical than having it only in the expression for the minimum level. The conclusion therefore is to select the SR02 model with an input drift ratio of 3.0%.

For circular reinforced concrete columns the minimum confinement level is currently expressed in the ACI code by Equation 21-2, and by the spacing limits of ACI 318-05 section 21.4.4.2. To be consistent with the recommendations for the rectangular columns, imposing a minimum level of axial load provides a meaningful minimum level of confinement. A limit of P/P_0 of 0.2 was suggested in the rectangular column recommendation as this limit resulted in a similar minimum level of confinement to the current ACI code. Figure 5.12 shows that the curve for SR02 and the curve for the ACI minimum confinement intersect at a P/P_0 ratio near 0.6. Solving for the P/P_0 ratio which requires a transverse steel ratio equal to the ACI minimum level for the columns in the circular column database confirms this relationship as the mean value for the axial load ratio was 0.66. Imposing a limit of this magnitude would be inappropriate. Until further test results can be used to suggest a more suitable limit, it is recommended that the minimum confinement level be achieved through limiting the P/P_0 ratio to a minimum level of 0.2 as suggested by Saatcioglu and Razvi (2002).

Section 4.2.3 showed that for circular columns, the density requirement was the governing requirement for all but two columns, and that all the columns in the circular column database satisfied the one quarter dimension limit. These results could suggest that the spacing limit is inconsequential. However, the lack of test specimens with low levels of drift and the limited number of full-scale tests makes it difficult to make this conclusion with confidence. Therefore, is it recommended that this spacing limit remain in the code until further evidence can support its removal.

Again it is suggested that the commentary to the code should state that axial loads should be kept below a value that would result in unrealistically small transverse steel spacing.

Therefore, the final recommendation for the design requirements for confinement steel in circular reinforced concrete columns is expressed as follows:

The volumetric ratio of spiral or circular hoop reinforcement shall not be less than:

$$\rho_s = 0.84 k_p \frac{f'_c}{f_{yh}} \left[\frac{A_g}{A_{ch}} - 1 \right]$$

where (a) $\rho_s = \frac{4Ab}{s_c h_c}$

(b) $k_p = P/P_0$

(c) k_p shall not be taken as less that 0.2

(d) A_g/A_{ch} shall not be taken as less than 1.3

(e) s_c shall not exceed $6d_b$ or one quarter of the minimum member dimension

5.4 Final Recommendations vs. ACI

5.4.1 Comparison figure

The figure below gives a comparison of the final area requirements of the recommendations with the current area requirements in ACI 318-05. No suggested changes to the spacing requirements were proposed. The figure shows a comparison for both the rectangular and circular typical columns used for Figure 5.6 and Figure 5.12. The figure demonstrates how the confinement steel requirement of the recommended model compares with the current ACI requirement over a range of axial load level.

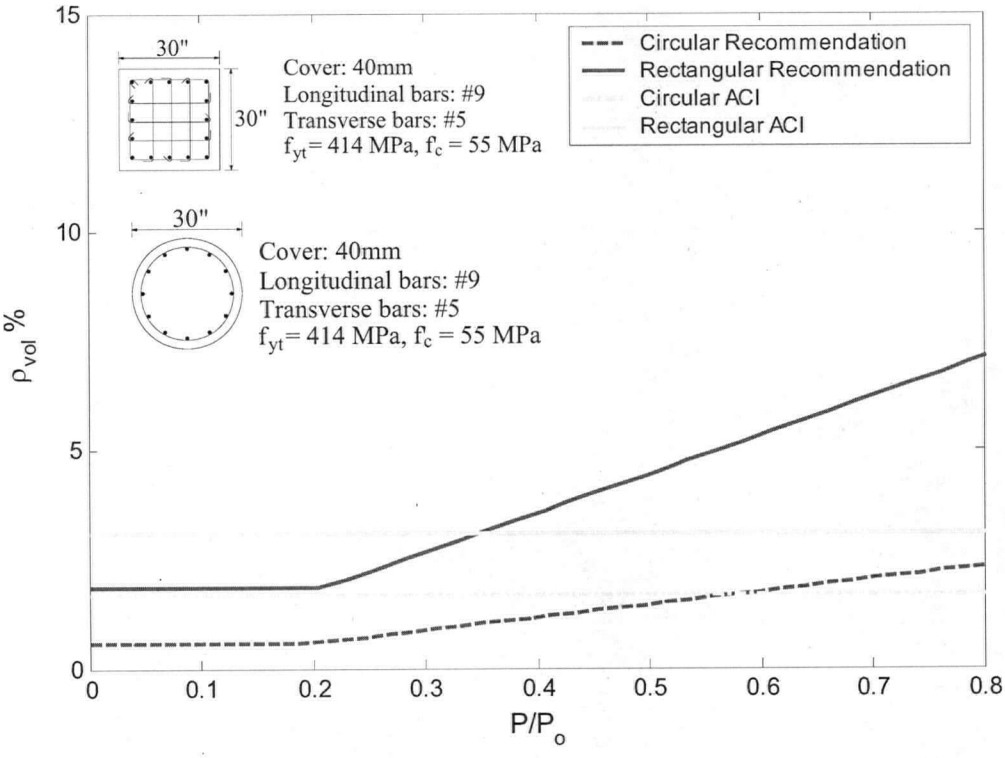

Figure 5.14 Comparison of recommendations and ACI 318-05 requirements

6 SUMMARY AND CONCLUSIONS

6.1 Summary

This study investigated the ACI 318-05 confining steel requirements for reinforced concrete columns. These requirements were compared to the current Canadian and New Zealand codes and proposed models found in the literature to determine their suitability as a performance based design equation for implementation in Chapter 21 of ACI 318. A total of 13 model for rectangular columns and 12 for circular columns were evaluated. This was done by addressing both the area requirements of section 21.4.4.1 and the spacing requirements of section 21.4.4.2. Research has shown that factors such as axial load level and amount and configuration of confinement steel impact the performance of columns when subjected to seismic loading. The aim of this investigation was to determine if and how these factors should be incorporated into the requirements of ACI 318 and to propose a model which would ensure that a column will not experience lateral strength degradation before reaching the prescribed lateral drift limit.

The investigation was performed through evaluation of columns found in the UW/PEER Structural Performance Database. The condensed database used in this investigation consisted solely of columns which exhibited flexural failure and contained 145 rectangular and 50 circular columns.

Two evaluation techniques were used to evaluate each confinement model. First, a scatter plot was used to compare the confining requirements of each model with the lateral drift observed for each column within the database. A drift ratio of 2.5% was selected as the performance target for the evaluation. The scatter plot evaluation distinguished columns in the database into those which met/failed the requirements of a given model, and those which met/failed the performance target. From this, two key column classifications were identified, those which satisfied the requirements of the model but failed the performance target ('unconservative') and those which failed the requirements of the model but

satisfied the performance target ('conservative'). For each model, the percentage of columns falling into these classifications was calculated and compared, and the results were used to determine which models should be investigated further.

Three fragility curves were generated for each model to evaluate their performance across a range of drift ratios as apposed to just 2.5%. The first curve provided the probability of a column being classified as 'unconservative' as a function of the drift ratio, the second curve provided the probability of a column being classified as 'conservative' as a function of drift ratio. The third curve was a combination of the first two and provided insight as to the overall performance of the model. These fragility curves were used to determine which models were most suitable for a performance based design equation in chapter 21 of ACI 318.

Also taken into consideration in the evaluation of the models was the form of each expression and the confinement requirements of each relative to the current ACI 318. Models with confinement expressions which were drastically different than the current form in chapter 21 of ACI were not considered potential alternatives unless their performance in the above evaluation techniques was significant enough to do so. Also, the requirements of each model for columns with various axial load levels were compared to the current requirements of ACI. Models which required drastically more or less steel than the 2005 version of ACI 318 were less favourable than those which required smaller changes in confining steel, but displayed similar statistical behaviour.

For both the rectangular and circular column evaluations, the ACI model was determined to be the least desirable of all models investigated. Based on the evaluation techniques discussed above, specific models were selected as recommended alternatives to the current ACI requirements. For rectangular columns, the current area requirement of the Canadian code (CSA A23.3-2004) was selected as the recommended model. For circular columns, the model proposed by Saatciolgu and Razvi (2002) was selected as the recommended model.

The spacing limit of one quarter cross sectional dimension was also evaluated. The performance of the limit alone demonstrated no improvement over the ACI area requirements, but suggested that together, the two requirements may slightly reduce the instances of 'unconservative' columns. While the spacing limits do not often govern the design of confining steel, it is recommended that the spacing limits of the current ACI code remain in place.

6.2 Recommendations

The following is the recommendations of this study:

ACI 318 clauses 21.4.4.1 (a),(b) and (d) as well as clauses 21.4.4.2 (a) and (c) should be replaced with:

21.4.4.1 Transverse steel for confinement of reinforced concrete columns

The total cross-sectional area of rectangular hoop reinforcement shall not be less than:

$$\frac{A_{sh}}{s_c h_c} = 0.2 k_n k_p \frac{A_g}{A_{ch}} \frac{f_c'}{f_{yh}}$$

where

$k_p = P / P_0$
$k_n = n_l / (n_l - 2)$
k_p shall not be taken as less than 0.2
s_c shall not exceed $6d_b$,one quarter of the minimum member dimension or s_x defined as:

$$s_x \leq 4 + \left(\frac{14 - h_x}{3} \right)$$

where s_x shall not exceed 6 inches and need not be taken less than 4 inches and h_x is the maximum horizontal spacing of hoop or crosstie legs on all faces of the column.

21.4.4.2 Columns confined with circular or spiral hoops

The volumetric ratio of spiral or circular hoop reinforcement shall not be less than:

$$\rho_s = 0.84 k_p \frac{f'_c}{f_{yh}} \left[\frac{A_g}{A_{ch}} - 1 \right]$$

where

$$\rho_s = \frac{4Ab}{s_c h_c}$$

$k_p = P/P_0$

k_p shall not be taken as less that 0.2

A_g/A_{ch} shall not be taken as less than 1.3

s_c shall not exceed $6d_b$ or one quarter of the minimum member dimension

6.3 Recommendations for future research

The UW/PEER Structural Performance Database gives researchers access to significantly more test data than would be possible in a specific testing experiment. This allows researchers to undertake projects such as this one where the results from a small number of individual tests may not provide sufficient data to make recommendations with the same level of confidence. However, to supplement the existing database, further testing is required. This was apparent for the circular column database used in this study where few columns were tested with high axial load ratios, and consequentially few columns exhibited flexural failure at low levels of drift. It is recommended that future investigations of flexural failure in circular columns for building structures be undertaken with appropriate levels of axial load.

It is stated in the commentary of the 2005 ACI 318 code that the axial load and deformation demands required during earthquake loading are not known with sufficient accuracy to justify calculation of required transverse reinforcement as a function of

design earthquake demands. It is the position of this document that the level of axial load on a column during a seismic event need not be known with extreme accuracy for its inclusion in the calculation for required transverse reinforcement. However, further research into the analytical methods which can be used to predict the earthquake axial load demands placed on columns will improve the accuracy of those predictions and the effectiveness of the equations recommended here for implementation into the ACI code.

REFERENCES

American Concrete Institute, 2005, "Building Code Requirements for Structural Concrete", *ACI 318-05*, Farmington Hills, USA.

American Concrete Institute, 2006, "ACI Building Code Requirement of the 20th Century" CD-ROM, ACI Farmington Hill, USA

Applied Technology Council, 1996, "Improved Seismic Design Criteria for California Bridges: Provisional Recommendations", *ATC-32*, Redwood City, USA.

American Association of State Highway and Transportation Officials, 1992, "Standard Specifications for Highway Bridges", 15th Edition, Washington, USA.

Ang B.G., Priestley, M.J.N., and Park, R., 1981, "Ductility of Reinforced Concrete Bridge Piers Under Seismic Loading", *Report 81-3*, Department of Civil Engineering, University of Canterbury, Christchurch, New Zealand.

Atalay, M.B., and Penzien, J., 1975 "The Seismic Behavior of Critical Regions of Reinforced Concrete Components as Influenced by Moment, Shear and Axial Force", *Report* No. *EERC 75-19*, University of California, Berkeley, USA.

Azizinamini, A., Johal, L.S., Hanson, N.W., Musser, D.W., and Corley, W.G., 1988, "Effects of Transverse Reinforcement on Seismic Performance of Columns – A Partial Parametric Investigation", *Project No. CR-9617*, Construction Technology Laboratories, Skokie, USA.

Bayrak O., Sheikh, S., 1998, "Confinement Reinforcement Design Considerations for Ductile HSC Columns", *Journal of Structural Engineering*, Vol.124, No.9, pp. 999-1010

Bayrak, O., Sheikh, S., 1996, "Confinement Steel Requirements for High Strength Concrete Columns", *Paper No. 463, 11th World Conference on Earthquake Engineering*, Mexico.

Bayrak, O., Sheikh, S., 2002, "Design of Rectangular HSC Columns for Ductility", University of Toronto, Canada.

Berry, M., Parrish, M., and Eberhard, M., 2004, "PEER Structural Performance Database User's Manual (Version 1.0)", http://maximus.ce.washington.edu/~peera1/

Brachmann, I., Browning, J., and Matamoros, A., 2004(a), "Relationships Between Drift and Confinement in Reinforced Concrete Columns under Cyclic Loading", *Paper No.2531, 13th World Conference on Earthquake Engineering*, Vancouver, Canada.

Brachmann, I., Browning, J., and Matamoros, A., 2004(b), "Drift-Dependent Confinement Requirements for Reinforced Concrete Columns Under Cyclic Loading", *ACI Structural Journal*, Vol. 101, No.5, pp. 669-677.

Calderone, A.J., Lehman, D.E., Moehle, J.P., 2000, "Behavior of Reinforced Concrete Bridge Columns Having Varying Aspect Ratios and Varying Lengths of Confinement", *Report 2000/08*, Pacific Earthquake Engineering Research Center.

Canadian Standards Association, 2004, "Design of Concrete Structures", *CSA A23.3-04*, Mississauga, Canada.

California Department of Transportation, 1983, "Bridge Design Specifications", Sacramento, USA.

Camarillo, H., 2003, "Evaluation of Shear Strength Methodologies for Reinforced Concrete Columns", *M.Sc Thesis,* University of Washington, USA.

Cheok, G.S., and Stone, W.C., 1986, "Behavior of 1/6-Scale Model Bridge Columns Subjected to Cycle Inelastic Loading", *NBSIR 86-3494*, Center for Building Technology, National Engineering Laboratory, National Institute of Standards and Technology, Gaithersburg, USA..

Cusson, D. and Paultre P., 1995, "Stress-Strain Model for confined high-strength concrete", *Journal of Structural Engineering*, Vol. 121, No. 3, pp. 783-804

Davey, B.E., 1975, "Reinforced Concrete Bridge Piers Under Seismic Loading", *Master of Engineering Report*, Civil Engineering Department, University of Canterbury, Christchurch, New Zealand.

Dodd, L.L., and Cooke, N., 1992, "The Dynamic Behavior of Reinforced Concrete Bridge Piers Subjected to New Zealand Seismicity", *Res. Rep. 92-04*, Dept. of Civ. Engrg., Univ. of Canerbury, Christchurch, New Zealand.

Dodd, L.L., and Restrepo-Posada, J.I., "Model of Predicting Cyclic Behavior of Reinforcing Steel", *Journal of Structural Engineering*, Vol. 121, No.3, pp. 433-445

Elwood, K.J., and Eberhard, M.O., 2006, "Effective Stiffness of Reinforced Concrete Columns", *Research Digest 2006-1*, Pacific Earthquake Engineering Research Center.

Esaki, F., 1996, "Reinforcing Effect of Steel Plate Hoops on Ductility of R/C Square Column", *Paper No. 199, 11th World Conference on Earthquake Engineering,* Mexico.

Galeota, D., Giammatteo, M.M., and Marino, R., 1996, "Seismic Resistance of High Strength Concrete Columns", *Paper No. 1390, 11th World Conference on Earthquake Engineering,* Mexico.

Hamilton, C.H., Pardoen, G.C., and Kazanjy, R.P., 2002, "Experimental Testing of Bridge Columns Subjected to Reversed-Cyclic and Pulse-type Loading Histories", *Report 2001-03*, Civil Engineering Technical Report Series, University of California, Irvine, USA.

Henry, L. and Mahin, S.A., 1999, "Study of Buckling of Longitudinal Bars in Reinforced Concrete Bridge Columns", *Report to the California Department of Transportation.*

Hose, Y.D., Seible, F. and Priestley, M.J.N., 1997, "Strategic Relocation of Plastic Hinges in Bridge Columns", *Structural Systems Research Project, 97/05*, University of California, San Diego, La Jolla, USA.

Kanda, M., Shirai, N., Adachi, H., and Sato, T., 1988, "Analytical Study on Elasto-Plastic Hysteretic Behaviors of Reinforced Concrete Members," *Transactions of the Japan Concrete Institute*, Vol.10, pp. 257-264.

Kono, S., and Watanabe, F., 2000, "Damage Evaluation of Reinforced Concrete Columns Under Multiaxial Cyclic Loadings", *The Second U.S.-Japan Workshop on Performance-Based Earthquake Engineering Methodology for Reinforced Concrete Building Structures*, Sapporo, Japan.

Kowalsky, M.J., Priestley, M.J.N., and Seible, F., 1999, "Shear and Flexural Behavior of Lightweight Concrete Bridge Columns in Seismic Regions", *ACI Structural Journal*, Vol. 96, No. 1, pp. 136-148.

Kunnath, S.K., El-Bahy, A., Taylor, A., and Stone, W., 1997, "Cumulative Seismic Damage of Reinforced Concrete Bridge Piers", *Technical Report NCEER-97-0006*, National Center for Earthquake Engineering Research.

Legeron, F., and Paultre, P., 2000, "Behavior of High-Strength Concrete Columns under Cyclic Flexure and Constant Axial Load", *ACI Structural Journal*, Vol. 97, No. 4, pp. 591-601.

Légeron, F. and Paultre P., 2003, "Uniaxial Confinement Model of Normal and High-Strength Concrete Columns", *Journal of Structural Engineering*, Vol. 129, No. 2, pp. 241-252.

Lehman, D.E., Moehle, J.P., 2000"Seismic Performance of Well-Confined Concrete Bridge Columns", *PEER 1998/01*, Pacific Earthquake Engineering Research Center.

Li, B., and Park, R., 2004, "Confining Reinforcement for High-Strength Concrete Columns", *ACI Structural Journal*, V. 101, No.3, pp. 314-324.

Lim, K.Y., and McLean, D.I., 1991, "Scale Model Studies of Moment-Reducing Hinge Details in Bridge Columns", *ACI Structural Journal*, Vol. 88, No. 4, pp. 465-474.

Mander, J.B., Priestley, M.J.N., and Park, R., 1988, "Theoretical Stress-Strain Model for Confined Concrete", *Journal of Structural Engineering*, Vol. 114, No. 8, pp.1804-1826.

Matamoros, A.B., 1999, "Study of Drift Limits for High-Strength Concrete Columns", Department of Civil Engineering, University of Illinois at Urbana-Champaign, Urbana, USA.

Mo, Y.L., and Wang, S.J., 2000, "Seismic Behavior of RC Columns with Various Tie Configurations", *Journal of Structural Engineering*, Vol. 126, No.10, pp. 1122-1130.

Moyer, M.J. and Kowalsky, M.J., 2003, "Influence of tension strain on buckling of reinforcement in RC bridge columns", *ACI Structural Journal*, Vol. 100, No. 1, pp. 75-85.

Muguruma, H., Watanabe, F., and Komuro, T., 1989, "Applicability of High Strength Concrete to Reinforced Concrete Ductile Column," *Transactions of the Japan Concrete Institute*, Vol. 11, pp. 309-316.

Ohno, T., and Nishioka, T., 1984, "An Experimental Study on Energy Absorption Capacity of Columns in Reinforced Concrete Structures", *Proceedings of the JSCE, Structural Engineering/Earthquake Engineering*, Vol. 1, No 2, pp. 137-147.

Paulay, T., and Priestly, M.J.N., 1992, "Seismic Design of Reinforced Concrete and Masonry Buildings", John Wiley & Sons Inc. New York, USA.

Paultre, P., Legeron, F., and Mongeau, D., 2001, "Influence of Concrete Strength and Transverse Reinforcement Yield Strength on Behavior of High-Strength Concrete Columns", *ACI Structural Journal*, Vol. 98, No. 4, pp. 490-501.

Paultre, P., Legeron, F., 2005, "Confinement Reinforcement Design for Reinforced Concrete Columns", Paper accepted for publication in ASCE Structural Journal 2007.

Pujol, S., 2002, "Drift Capacity of Reinforced Concrete Columns Subjected to Displacement Reversals", *Thesis*, Purdue University, USA.

Razvi, S.R., and Saatcioglu, M., 1999, "Analysis and Design of Concrete Columns for Confinement", *Earthquake Spectra*, Vol. 15, No. 4, pp. 791-811.

Richart, F.E., Brandtzaeg, A., and Brown R.L., 1928, "A Study of the failure of concrete under combined compressive stresses" *Bulletin 185, Univ. of Illinois Engineering Experimental Station*, Champaign, USA.

Saatciolgu, M., 1991, "Deformability of Reinforced Concrete Columns", *ACI SP-127, Earthquake-Resistant Concrete Structures Inelastic Response and Design*, American Concrete Institute, pp. 421-452.

Saatcioglu, M., and Baingo, D., 1999, "Circular High-Strength Concrete Columns Under Simulated Seismic Loading", *Journal of Structural Engineering*, Vol. 125, No. 3, pp. 272-280.

Saatcioglu, M., and Grira, M., 1999, "Confinement of Reinforced Concrete Columns with Welded Reinforcement Grids", *ACI Structural Journal*, Vol. 96, No. 1, pp. 29-39.

Saatcioglu, M., and Ozcebe, G., 1989, "Response of Reinforced Concrete Columns to Simulated Seismic Loading", *ACI Structural Journal*, Vol. 86, No. 1, pp. 3-12.

Saatcioglu, M., Razvi, S.R., 2002, "Displacement-Based Design of Reinforced Concrete Columns for Confinement", *ACI Structural Journal*, Vol. 99, No.1, pp. 3-11.

Sakai, Y., Hibi, J., Otani, S., and Aoyama, H., 1990, "Experimental Study on Flexural Behavior of Reinforced Concrete Columns Using High-Strength Concrete", *Transactions of the Japan Concrete Institute*, Vol. 12, pp. 323-330.

Sheikh, S.A., and Khoury S.S., 1997, "A Performance-Based Approach for the Design of Confining Steel in Tied Columns", *ACI Structural Journal*, Vol.94, No.4, pp. 421-432.

Sheikh, S.A., and Uzumeri, S.M., 1980, "Strength and Ductility of Tied Concrete Columns", *Journal of the Structural Division, ASCE*, Vol. 106, No. 5, pp. 1079-1102.

Sheikh, S.A., and Uzumeri, S.M., 1982, "Analytical Model for Concrete Confinement in Tied Columns", *Journal of the Structural Division, ASCE*, Vol. 108, No. ST12, pp. 2703-2722

Soesianawati, M.T., Park, R., and Priestley, M.J.N., 1986, "Limited Ductility Design of Reinforced Concrete Columns", *Report 86-10*, Department of Civil Engineering, University of Canterbury, Christchurch, New Zealand.

Standards Association of New Zealand, 2006, "Concrete Design Standard, NZS3101:2006, Part 1" and "Commentary on the Concrete Design Standard, NZS 3101:2006, Part 2," Wellington, New Zealand.

Stone, W.C., and Cheok, G.S., 1989, "Inelastic Behavior of Full-Scale Bridge Columns Subjected to Cyclic Loading", *NIST BSS 166*, Building Science Series, Center for Building Technology, National Engineering Laboratory, National Institute of Standards and Technology, Gaithersburg, USA.

Sugano, S., 1996, "Seismic Behavior of Reinforced Concrete Columns Which used Ultra-High-Strength Concrete", *Paper No. 1383, 11th World Conference on Earthquake Engineering*, Mexico.

Takemura, H., and Kawashima, K., 1997, "Effect of loading hysteresis on ductility capacity of bridge piers", *Journal of Structural Engineering*, Vol. 43A, pp. 849-858.

Tanaka, H., and Park, R., 1990, "Effect of Lateral Confining Reinforcement on the Ductile Behavior of Reinforced Concrete Columns", *Report 90-2*, Department of Civil Engineering, University of Canterbury, Christchurch, New Zealand.

Thomsen, J., and Wallace, J., 1994, "Lateral Load Behavior of Reinforced Concrete Columns Constructed Using High-Strength Materials", *ACI Structural Journal*, Vol. 91, No. 5, pp. 605-615.

Vu, N.D., Priestley, M.J.N., Seible, F., and Benzoni, G., 1998, "Seismic Response of Well Confined Circular Reinforced Concrete Columns with Low Aspect Ratios", *5th Caltrans Seismic Research Workshop*.

Watson, S., and Park, R., 1989, "Design of reinforced concrete framces of limited ductility", *Res. Rep. 89-4*, Dept. of Civ. Engrg., Univ. of Canerbury, Christchurch, New Zealand.

Watson, S., Zahn, F.A., and Park, R., 1994, "Confining Reinforcement for Concrete Columns", *Journal of Structural Engineering*, Vol. 120, No.6, pp. 1798-1824

Wehbe, N., Saiidi, M.S., and Sanders, D., 1998, "Confinement of Rectangular Bridge Columns for Moderate Seismic Areas", *National Center for Earthquake Engineering Research (NCEER) Bulletin*, Vol. 12, No. 1.

Wehbe, N., Saiidi, M.S., and Sanders, D., 1999, "Seismic Performance of Rectangular Bridge Columns with Moderate Confinement", *ACI Structural Journal*, Vol. 96, No. 2, pp. 248-258.

William, K.J., and Warnke, E.P., 1975, "Constitutive Model of the triaxial behavior of concrete", *Proc. International Association for Bridge and Structural Engineering*, Vol. 19, pp. 1-30.

Wong, Y.L., Paulay, T., and Priestley, M.J.N., 1990, "Squat Circular Bridge Piers Under Multi-Directional Seismic Attack", *Report 90-4*, Department of Civil Engineering, University of Canterbury, Christchurch, New Zealand.

Xiao, Y., and Martirossyan, A., 1998, "Seismic Performance of High-Strength Concrete Columns", *Journal of Structural Engineering*, Vol. 124, No. 3, pp. 241-251.

Zahn, F.A., Park, R., and Priestley, M.J.N., 1986, "Design of reinforced concrete bridge columns for strength and ductility" *Res. Rep. 86-7*, Dept. of Civ. Engrg., Univ. of Canerbury, Christchurch, New Zealand.

Zhou, X., Satoh, T., Jiang, W., Ono, A., and Shimizu, Y., 1987, "Behavior of Reinforced Concrete Short Column Under High Axial Load," *Transactions of the Japan Concrete Institute*, Vol. 9, pp. 541-548.

APPENDIX A

A1. Rectangular Column Database

Database No.	Specimen Name	f'c (MPa)	P (kN)	P/Agf'c	P/P_o	Geometry				
						B(mm)	H(mm)	L(mm)	A_g (mm^2)	Cover (mm)
7	Soesianawati et al. 1986, No. 1	46.5	744	0.10	0.10	400	400	1600	160000	13.0
8	Soesianawati et al. 1986, No. 2	44	2112	0.30	0.30	400	400	1600	160000	13.0
9	Soesianawati et al. 1986, No. 3	44	2112	0.30	0.30	400	400	1600	160000	13.0
10	Soesianawati et al. 1986, No. 4	40	1920	0.30	0.30	400	400	1600	160000	13.0
13	Watson and Park 1989, No. 5	41	3280	0.50	0.49	400	400	1600	160000	13.0
14	Watson and Park 1989, No. 6	40	3200	0.50	0.49	400	400	1600	160000	13.0
15	Watson and Park 1989, No. 7	42	4704	0.70	0.69	400	400	1600	160000	13.0
16	Watson and Park 1989, No. 8	39	4368	0.70	0.69	400	400	1600	160000	13.0
17	Watson and Park 1989, No. 9	40	4480	0.70	0.69	400	400	1600	160000	40.0
20	Tanaka and Park 1990, No. 3	25.6	819	0.20	0.18	400	400	1600	160000	31.5
32	Ohno and Nishioka 1984, L3	24.8	127	0.03	0.03	400	400	1600	160000	12.5
43	Zhou et al. 1987, No. 214-08	21.1	432	0.80	0.67	160	160	320	25600	35.0
48	Kanda et al. 1988, 85STC-1	27.9	183.9	0.11	0.10	250	250	750	62500	35.0
49	Kanda et al. 1988, 85STC-2	27.9	183.9	0.11	0.10	250	250	750	62500	35.0
50	Kanda et al. 1988, 85STC-3	27.9	183.9	0.11	0.10	250	250	750	62500	9.0
56	Muguruma et al. 1989, AL-1	85.7	1371	0.40	0.40	200	200	500	40000	9.0
58	Muguruma et al. 1989, AL-2	85.7	2156	0.63	0.63	200	200	500	40000	23.5
66	Sakai et al. 1990, B1	99.5	2176	0.35	0.38	250	250	500	62500	23.5
67	Sakai et al. 1990, B2	99.5	2176	0.35	0.38	250	250	500	62500	23.5
68	Sakai et al. 1990, B3	99.5	2176	0.35	0.38	250	250	500	62500	23.5
69	Sakai et al. 1990, B4	99.5	2176	0.35	0.38	250	250	500	62500	23.5
70	Sakai et al. 1990, B5	99.5	2176	0.35	0.38	250	250	500	62500	23.5
71	Sakai et al. 1990, B6	99.5	2176	0.35	0.38	250	250	500	62500	30.5
72	Sakai et al. 1990, B7	99.5	2176	0.35	0.39	250	250	500	62500	32.0
94	Atalay and Penzien 1975, No. 9	33.3	801	0.26	0.26	305	305	1676	93025	32.0
95	Atalay and Penzien 1975, No. 10	32.4	801	0.27	0.26	305	305	1676	93025	32.0
96	Atalay and Penzien 1975, No. 11	31	801	0.28	0.27	305	305	1676	93025	32.0
97	Atalay and Penzien 1975, No. 12	31.8	801	0.27	0.26	305	305	1676	93025	38.1
102	Azizinamini et al. 1988, NC-2	39.3	1690	0.21	0.20	457	457	1372	208850	41.3
103	Azizinamini et al. 1988, NC-4	39.8	2580	0.31	0.30	457	457	1372	208850	22.5
104	Saatcioglu and Ozcebe 1989, U1	43.6	0	0.00	0.00	350	350	1000	122500	22.5
105	Saatcioglu and Ozcebe 1989, U3	34.8	600	0.14	0.12	350	350	1000	122500	22.5
106	Saatcioglu and Ozcebe 1989, U4	32	600	0.15	0.12	350	350	1000	122500	26.0
107	Saatcioglu and Ozcebe 1989, U6	37.3	600	0.13	0.11	350	350	1000	122500	26.0
108	Saatcioglu and Ozcebe 1989, U7	39	600	0.13	0.11	350	350	1000	122500	30.0
117	Galeota et al. 1996, CA1	80	1000	0.20	0.22	250	250	1140	62500	30.0
118	Galeota et al. 1996, CA2	80	1500	0.30	0.33	250	250	1140	62500	30.0
119	Galeota et al. 1996, CA3	80	1000	0.20	0.22	250	250	1140	62500	30.0
120	Galeota et al. 1996, CA4	80	1500	0.30	0.33	250	250	1140	62500	30.0

Database No.	Specimen Name	f'c (MPa)	P (kN)	P/Agf'c	P/P_o	Geometry				
						B(mm)	H(mm)	L(mm)	A_g (mm^2)	Cover (mm)
126	Galeota et al. 1996, BB1	80	1000	0.20	0.18	250	250	1140	62500	30.0
127	Galeota et al. 1996, BB4	80	1500	0.30	0.27	250	250	1140	62500	30.0
128	Galeota et al. 1996, BB4B	80	1500	0.30	0.27	250	250	1140	62500	28.0
133	Wehbe et al. 1998, A1	27.2	615	0.10	0.08	380	610	2335	231800	28.0
134	Wehbe et al. 1998, A2	27.2	1505	0.24	0.20	380	610	2335	231800	25.0
135	Wehbe et al. 1998, B1	28.1	601	0.09	0.08	380	610	2335	231800	25.0
136	Wehbe et al. 1998, B2	28.1	1514	0.23	0.20	380	610	2335	231800	13.0
145	Xiao 1998, HC4-8L19-T10-0.1P	76	489	0.10	0.09	254	254	508	64516	13.0
146	Xiao 1998, HC4-8L19-T10-0.2P	76	979	0.20	0.19	254	254	508	64516	13.0
147	Xiao 1998, HC4-8L16-T10-0.1P	86	534	0.10	0.10	254	254	508	64516	13.0
148	Xiao 1998, HC4-8L16-T10-0.2P	86	1068	0.19	0.20	254	254	508	64516	11.3
151	Sugano 1996, UC10H	118	3579	0.60	0.67	225	225	450	50625	11.3
152	Sugano 1996, UC15H	118	3579	0.60	0.67	225	225	450	50625	11.3
153	Sugano 1996, UC20H	118	3579	0.60	0.67	225	225	450	50625	11.3
154	Sugano 1996, UC15L	118	2089	0.35	0.39	225	225	450	50625	11.3
155	Sugano 1996, UC20L	118	2089	0.35	0.39	225	225	450	50625	25.4
157	Bayrak and Sheikh 1996, ES-1HT	72.1	3353.6	0.50	0.50	305	305	1842	93025	13.4
158	Bayrak and Sheikh 1996, AS-2HT	71.7	2401.2	0.36	0.36	305	305	1842	93025	13.4
159	Bayrak and Sheikh 1996, AS-3HT	71.8	3339.6	0.50	0.50	305	305	1842	93025	11.0
160	Bayrak and Sheikh 1996, AS-4HT	71.9	3344.2	0.50	0.50	305	305	1842	93025	11.0
162	Bayrak and Sheikh 1996, AS-6HT	101.9	4360.5	0.46	0.49	305	305	1842	93025	13.4
163	Bayrak and Sheikh 1996, AS-7HT	102	4269.8	0.45	0.48	305	305	1842	93025	11.0
164	Bayrak and Sheikh 1996, ES-8HT	102.2	4468.4	0.47	0.50	305	305	1842	93025	29.0
166	Saatcioglu and Grira 1999, BG-2	34	1782	0.43	0.39	350	350	1645	122500	29.0
167	Saatcioglu and Grira 1999, BG-3	34	831	0.20	0.18	350	350	1645	122500	29.0
169	Saatcioglu and Grira 1999, BG-5	34	1923	0.46	0.38	350	350	1645	122500	29.0
170	Saatcioglu and Grira 1999, BG-6	34	1900	0.46	0.40	350	350	1645	122500	29.0
171	Saatcioglu and Grira 1999, BG-7	34	1923	0.46	0.38	350	350	1645	122500	29.0
172	Saatcioglu and Grira 1999, BG-8	34	961	0.23	0.19	350	350	1645	122500	29.0
173	Saatcioglu and Grira 1999, BG-9	34	1923	0.46	0.37	350	350	1645	122500	29.0
174	Saatcioglu and Grira 1999, BG-10	34	1923	0.46	0.37	350	350	1645	122500	40.0
175	Matamoros et al. 1999,C10-05N	69.637	142	0.05	0.05	203	203	610	41209	39.8
176	Matamoros et al. 1999,C10-05S	69.637	142	0.05	0.05	203	203	610	41209	25.8
177	Matamoros et al. 1999,C10-10N	67.775	285	0.10	0.10	203	203	610	41209	23.8
178	Matamoros et al. 1999,C10-10S	67.775	285	0.10	0.10	203	203	610	41209	22.0
179	Matamoros et al. 1999,C10-20N	65.5	569	0.21	0.21	203	203	610	41209	14.6
180	Matamoros et al. 1999,C10-20S	65.5	569	0.21	0.21	203	203	610	41209	24.0
181	Matamoros et al. 1999,C5-00N	37.921	0	0.00	0.00	203	203	610	41209	27.8
182	Matamoros et al. 1999,C5-00S	37.921	0	0.00	0.00	203	203	610	41209	38.3

						Geometry				
Database No.	Specimen Name	f'c (MPa)	P (kN)	P/Agf'c	P/P_o	B(mm)	H(mm)	L(mm)	A_g (mm^2)	Cover (mm)
183	Matamoros et al. 1999,C5-20N	48.263	285	0.14	0.13	203	203	610	41209	39.0
184	Matamoros et al. 1999,C5-20S	48.263	285	0.14	0.13	203	203	610	41209	20.7
185	Matamoros et al. 1999,C5-40N	38.059	569	0.36	0.32	203	203	610	41209	20.7
186	Matamoros et al. 1999,C5-40S	38.059	569	0.36	0.32	203	203	610	41209	34.0
187	Mo and Wang 2000,C1-1	24.94	450	0.11	0.09	400	400	1400	160000	34.0
188	Mo and Wang 2000,C1-2	26.67	675	0.16	0.13	400	400	1400	160000	34.0
189	Mo and Wang 2000,C1-3	26.13	900	0.22	0.17	400	400	1400	160000	34.0
190	Mo and Wang 2000,C2-1	25.33	450	0.11	0.09	400	400	1400	160000	34.0
191	Mo and Wang 2000,C2-2	27.12	675	0.16	0.13	400	400	1400	160000	34.0
192	Mo and Wang 2000,C2-3	26.77	900	0.21	0.17	400	400	1400	160000	11.1
202	Thomsen and Wallace 1994, A3	86.3	400.88	0.20	0.20	152.4	152.4	596.9	23226	11.1
204	Thomsen and Wallace 1994, B2	83.4	193.7	0.10	0.10	152.4	152.4	596.9	23226	11.1
205	Thomsen and Wallace 1994, B3	90	418.06	0.20	0.21	152.4	152.4	596.9	23226	11.1
207	Thomsen and Wallace 1994, C2	74.6	173.26	0.10	0.10	152.4	152.4	596.9	23226	11.1
208	Thomsen and Wallace 1994, C3	81.8	379.97	0.20	0.21	152.4	152.4	596.9	23226	11.1
209	Thomsen and Wallace 1994, D1	75.8	352.1	0.20	0.20	152.4	152.4	596.9	23226	11.1
210	Thomsen and Wallace 1994, D2	87	404.13	0.20	0.21	152.4	152.4	596.9	23226	11.1
211	Thomsen and Wallace 1994, D3	71.2	330.73	0.20	0.20	152.4	152.4	596.9	23226	19.0
215	Paultre & Legeron, 2000, No. 1006015	92.4	1200	0.14	0.15	305	305	2000	93025	19.0
216	Paultre & Legeron, 2000, No. 1006025	93.3	2400	0.28	0.29	305	305	2000	93025	19.0
217	Paultre & Legeron, 2000, No. 1006040	98.2	3600	0.39	0.42	305	305	2000	93025	19.0
221	Paultre et al., 2001, No. 806040	78.7	2900	0.40	0.41	305	305	2000	93025	19.0
222	Paultre et al., 2001, No. 1206040	109.2	4200	0.41	0.44	305	305	2000	93025	19.0
223	Paultre et al., 2001, No. 1005540	109.5	3600	0.35	0.44	305	305	2000	93025	19.0
224	Paultre et al., 2001, No. 1008040	104.2	3600	0.37	0.40	305	305	2000	93025	19.0
225	Paultre et al., 2001, No. 1005552	104.5	5150	0.53	0.56	305	305	2000	93025	19.0
226	Paultre et al., 2001, No. 1006052	109.4	5150	0.51	0.54	305	305	2000	93025	25.4
227	Pujol 2002, No. 10-2-3N	33.715	133.45	0.09	0.07	152.4	304.8	685.8	46452	25.4
228	Pujol 2002, No. 10-2-3S	33.715	133.45	0.09	0.07	152.4	304.8	685.8	46452	25.4
229	Pujol 2002, No. 10-3-1.5N	32.13	133.45	0.09	0.08	152.4	304.8	685.8	46452	25.4
230	Pujol 2002, No. 10-3-1.5S	32.13	133.45	0.09	0.08	152.4	304.8	685.8	46452	25.4
231	Pujol 2002, No. 10-3-3N	29.923	133.45	0.10	0.08	152.4	304.8	685.8	46452	25.4
232	Pujol 2002, No. 10-3-3S	29.923	133.45	0.10	0.08	152.4	304.8	685.8	46452	25.4
233	Pujol 2002, No. 10-3-2.25N	27.372	133.45	0.10	0.08	152.4	304.8	685.8	46452	25.4
234	Pujol 2002, No. 10-3-2.25S	27.372	133.45	0.10	0.08	152.4	304.8	685.8	46452	25.4
237	Pujol 2002, No. 20-3-3N	36.404	266.89	0.16	0.14	152.4	304.8	685.8	46452	25.4
238	Pujol 2002, No. 20-3-3S	36.404	266.89	0.16	0.14	152.4	304.8	685.8	46452	25.4
239	Pujol 2002, No. 10-2-2.25N	34.887	133.45	0.08	0.07	152.4	304.8	685.8	46452	25.4
240	Pujol 2002, No. 10-2-2.25S	34.887	133.45	0.08	0.07	152.4	304.8	685.8	46452	25.4

						Geometry				
Database No.	Specimen Name	f'c (MPa)	P (kN)	P/Agf'c	P/P_o	B(mm)	H(mm)	L(mm)	A_g (mm^2)	Cover (mm)
241	Pujol 2002, No. 10-1-2.25N	36.473	133.45	0.08	0.07	152.4	304.8	685.8	46452	25.4
242	Pujol 2002, No. 10-1-2.25S	36.473	133.45	0.08	0.07	152.4	304.8	685.8	46452	18.5
243	Bechtoula et al., 2002, D1N30	37.6	705	0.30	0.27	250	250	625	62500	18.5
244	Bechtoula et. al. 2002, D1N60	37.6	1410	0.60	0.53	250	250	625	62500	44.5
246	Bechtoula et. al. 2002, L1N60	39.2	8000	0.57	0.57	600	600	1200	360000	27.5
248	Takemura 1997, Test 1 (JSCE-4)	35.9	157	0.03	0.03	400	400	1245	160000	27.5
249	Takemura 1997, Test 2 (JSCE-5)	35.7	157	0.03	0.03	400	400	1245	160000	27.5
250	Takemura 1997, Test 3 (JSCE-6)	34.3	157	0.03	0.03	400	400	1245	160000	27.5
251	Takemura 1997, Test 4 (JSCE-7)	33.2	157	0.03	0.03	400	400	1245	160000	27.5
252	Takemura 1997, Test 5 (JSCE-8)	36.8	157	0.03	0.03	400	400	1245	160000	40.0
258	Xaio & Yun 2002, No. FHC5-0.2	64.1	3334	0.20	0.20	510	510	1778	260100	20.0
260	Bayrak & Sheikh, 2002, No. RS-9HT	71.2	2118.2	0.34	0.34	250	350	1842	87500	20.0
261	Bayrak & Sheikh, 2002, No. RS-10HT	71.1	3110.6	0.50	0.50	250	350	1842	87500	20.0
264	Bayrak & Sheikh, 2002, No. RS-13HT	112.1	3433.1	0.35	0.37	250	350	1842	87500	20.0
265	Bayrak & Sheikh, 2002, No. RS-14HT	112.1	4512	0.46	0.49	250	350	1842	87500	20.0
266	Bayrak & Sheikh, 2002, No. RS-15HT	56.2	1770.3	0.36	0.34	250	350	1842	87500	20.0
268	Bayrak & Sheikh, 2002, No. RS-17HT	74.1	2204.5	0.34	0.33	250	350	1842	87500	20.0
269	Bayrak & Sheikh, 2002, No. RS-18HT	74.1	3241.9	0.50	0.49	250	350	1842	87500	20.0
270	Bayrak & Sheikh, 2002, No. RS-19HT	74.2	3441	0.53	0.52	250	350	1842	87500	20.0
272	Bayrak & Sheikh, 2002, No. WRS-21HT	91.3	3754.7	0.47	0.48	350	250	1842	87500	20.0
273	Bayrak & Sheikh, 2002, No. WRS-22HT	91.3	2476.5	0.31	0.32	350	250	1842	87500	20.0
274	Bayrak & Sheikh, 2002, No. WRS-23HT	72.2	2084.8	0.33	0.32	350	250	1842	87500	20.0
275	Bayrak & Sheikh, 2002, No. WRS-24HT	72.2	3158.8	0.50	0.49	350	250	1842	87500	22.5
285	Saatcioglu and Ozcebe 1989, U2	30.2	600	0.16	0.12	350	350	1000	122500	13.0
286	Esaki, 1996 H-2-1/5	23	184	0.20	0.16	200	200	400	40000	13.0
287	Esaki, 1996 HT-2-1/5	20.2	162	0.20	0.16	200	200	400	40000	13.0
288	Esaki, 1996 H-2-1/3	23	307	0.33	0.27	200	200	400	40000	13.0
289	Esaki, 1996 HT-2-1/3	20.2	269	0.33	0.26	200	200	400	40000	13.0

	Longitudinal Reinforcement				Transverse Reinforcement											
Database No.	**D_{bar} (mm)**	**Total # Bars**	**ρ_{long} (%)**	**f_y (MPa)**	**Confin. Type**	**N**	**D_{bar} (mm)**	**s (mm)**	**f_{yh} (MPa)**	**ρ_{area} (%)**	**Δ_{80} (mm)**	**Δ_{max} (mm)**	**Drift Ratio (%)**	**$A_{sh\ Provided}$ (mm^2)**	**$A_{sh\ (ACI)}$ (mm^2)**	**$A_{sh}/A_{sh(ACI)}$**
7	16	12	1.51	446	RO	4	7	85	364	0.493	98.06	98.06	6.13	153.94	358.66	0.366
8	16	12	1.51	446	RO	4	8	78	360	0.704	68.73	98.72	4.30	201.06	314.03	0.546
9	16	12	1.51	446	RO	4	7	91	364	0.461	46.24	53.58	2.89	153.94	363.33	0.361
10	16	12	1.51	446	RO	4	6	94	255	0.327	43.91	57.17	2.74	113.10	488.36	0.197
13	16	12	1.51	474	RO	4	8	81	372	0.678	38.91	38.91	2.43	201.06	294.07	0.583
14	16	12	1.51	474	RO	4	6	96	388	0.320	26.83	32.19	1.68	113.10	327.79	0.294
15	16	12	1.51	474	RO	4	12	96	308	1.302	18.72	25.82	1.17	452.39	426.50	0.904
16	16	12	1.51	474	RO	4	8	77	372	0.713	17.17	18.86	1.07	201.06	265.91	0.645
17	16	12	1.51	474	RO	4	12	52	308	2.825	43.86	44.59	2.74	452.39	220.02	1.753
20	20	8	1.57	474	UJ	3	12	80	333	1.305	57.20	76.70	3.58	339.29	390.19	0.870
32	19	8	1.42	362	R	2	9	100	325	0.348	73.04	74.66	4.57	127.23	365.83	0.348
43	10	8	2.22	341	R	2	5	40	559	1.155	6.54	11.60	2.04	39.27	30.31	1.296
48	12.7	8	1.62	374	R	2	5.5	50	506	0.545	34.60	52.50	4.61	47.52	151.91	0.313
49	12.7	8	1.62	374	R	2	5.5	50	506	0.545	34.60	52.50	4.61	47.52	151.91	0.313
50	12.7	8	1.62	374	R	2	5.5	50	506	0.420	34.60	52.50	4.61	47.52	151.91	0.313
56	12.7	12	3.80	399.6	RI	4	6	35	328.4	1.836	21.44	31.03	4.29	113.10	144.68	0.782
58	12.7	12	3.80	399.6	RI	4	6	35	328.4	2.198	10.89	14.42	2.18	113.10	144.68	0.782
66	12.7	12	2.43	379	RI	4	5	60	774	0.661	10.17	10.26	2.03	78.54	272.25	0.288
67	12.7	12	2.43	379	RI	4	5	40	774	0.992	20.09	20.32	4.02	78.54	181.50	0.433
68	12.7	12	2.43	379	RI	4	5.5	60	344	0.802	10.07	10.62	2.01	95.03	619.33	0.153
69	12.7	12	2.43	379	RI	4	5	60	1126	0.661	10.07	20.58	2.01	78.54	187.14	0.420
70	12.7	12	2.43	379	R	2	5	30	774	0.661	9.46	12.60	1.89	39.27	136.13	0.288
71	12.7	12	2.43	379	R	2	7	60	857	0.705	10.07	13.19	2.01	76.97	256.80	0.300
72	19	4	1.81	339	R	2	5	30	774	0.723	5.06	14.86	1.01	39.27	180.11	0.218
94	22	4	1.63	363	R	2	9.5	76	392	0.806	42.16	53.46	2.52	141.76	329.91	0.430
95	22	4	1.63	363	R	2	9.5	127	392	0.482	40.08	50.51	2.39	141.76	536.40	0.264
96	22	4	1.63	363	R	2	9.5	76	373	0.806	37.65	49.97	2.25	141.76	322.77	0.439
97	22	4	1.63	363	R	2	9.5	127	373	0.509	42.70	50.95	2.55	141.76	553.29	0.256
102	25.4	8	1.94	439	RD	3.41	12.7	102	454	1.171	66.64	69.78	4.86	431.97	527.84	0.818
103	25.4	8	1.94	439	RD	3.41	9.5	102	616	0.589	38.62	39.32	2.81	241.71	410.14	0.589
104	25	8	3.21	430	R	2	10	150	470	0.355	48.70	84.00	4.87	157.08	502.00	0.313
105	25	8	3.21	430	R	2	10	75	470	0.710	51.10	72.00	5.11	157.08	200.34	0.784
106	25	8	3.21	438	R	2	10	50	470	1.091	89.90	102.00	8.99	157.08	122.81	1.279
107	25	8	3.21	437	RJ	6	6.4	65	425	1.018	89.80	89.80	8.98	193.02	219.91	0.585
108	25	8	3.21	437	RJ	6	6.4	65	425	1.047	88.00	88.00	8.80	193.02	229.93	0.560
117	10	12	1.51	531	RI	4	8	50	531	2.209	67.02	69.81	5.88	201.06	450.44	0.446
118	10	12	1.51	531	RI	4	8	50	531	2.209	53.54	54.92	4.70	201.06	450.44	0.446
119	10	12	1.51	531	RI	4	8	50	531	2.209	37.06	62.31	3.25	201.06	450.44	0.446
120	10	12	1.51	531	RI	4	8	50	531	2.209	40.52	62.05	3.55	201.06	450.44	0.446

	Longitudinal Reinforcement				Transverse Reinforcement											
Database No.	**D_{bar} (mm)**	**Total # Bars**	**ρ_{long} (%)**	**f_y (MPa)**	**Confin. Type**	**N**	**D_{bar} (mm)**	**s (mm)**	**f_{yh} (MPa)**	**ρ_{area} (%)**	**Δ_{80} (mm)**	**Δ_{max} (mm)**	**Drift Ratio (%)**	**$A_{sh\ Provided}$ (mm^2)**	**$A_{sh\ (ACI)}$ (mm^2)**	**$A_{sh}/A_{sh(ACI)}$**
126	20	12	6.03	579	RI	4	8	100	579	1.105	58.03	58.03	5.09	201.06	900.87	0.223
127	20	12	6.03	579	RI	4	8	100	579	1.105	71.81	71.81	6.30	201.06	900.87	0.223
128	20	12	6.03	579	RI	4	8	100	579	1.081	75.33	75.33	6.61	201.06	900.87	0.223
133	19.1	18	2.22	448	RJ	4	6	110	428	0.323	122.10	162.89	5.23	113.10	220.19	0.514
134	19.1	18	2.22	448	RJ	4	6	110	428	0.317	102.26	122.24	4.38	113.10	220.19	0.514
135	19.1	18	2.22	448	RJ	4	6	83	428	0.421	160.79	183.71	6.89	113.10	158.90	0.712
136	19.1	18	2.22	448	RJ	4	6	83	428	0.392	129.78	151.16	5.56	113.10	158.90	0.712
145	19.1	8	3.55	510	RJ	3	9.5	51	510	1.908	47.76	48.20	9.40	212.65	173.96	1.562
146	19.1	8	3.55	510	RJ	3	9.5	51	510	1.908	40.94	45.85	8.06	212.65	173.96	1.562
147	15.9	8	2.46	510	RJ	3	9.5	51	510	1.908	37.59	38.79	7.40	212.65	196.85	1.380
148	15.9	8	2.46	510	RJ	3	9.5	51	510	1.878	35.01	44.31	6.89	212.65	196.85	1.380
151	10	12	1.86	393	RI	4	5.1	45	1415	0.920	4.09	4.10	0.91	81.71	66.67	1.226
152	10	12	1.86	393	RI	4	6.4	45	1424	1.458	8.24	13.79	1.83	128.68	69.42	1.854
153	10	12	1.86	393	RI	4	6.4	35	1424	1.875	16.30	20.66	3.62	128.68	54.00	2.383
154	10	12	1.86	393	RI	4	6.4	45	1424	1.458	20.40	32.37	4.53	128.68	69.42	1.854
155	10	12	1.86	393	RI	4	6.4	35	1424	2.191	28.30	32.43	6.29	128.68	54.00	2.383
157	19.54	8	2.58	454	R	2	15.98	95	463	1.610	32.17	36.96	1.75	401.12	371.12	1.078
158	19.54	8	2.58	454	RD	3.41	11.28	90	542	1.418	63.42	99.68	3.44	340.77	301.37	1.132
159	19.54	8	2.58	454	RD	3.41	11.28	90	542	1.393	34.12	51.53	1.85	340.77	301.79	1.130
160	19.54	8	2.58	454	RD	3.41	15.98	100	463	2.561	51.62	72.54	2.80	683.91	389.57	1.751
162	19.54	8	2.58	454	RD	3.41	15.98	76	463	3.430	55.69	70.68	3.02	683.91	419.60	1.625
163	19.54	8	2.58	454	RD	3.41	11.28	94	542	1.334	23.06	43.32	1.25	340.77	447.78	0.762
164	19.54	8	2.58	454	R	2	15.98	70	463	2.480	25.01	29.72	1.36	401.12	387.61	1.032
166	19.5	8	1.95	455.56	RI	3	9.53	76	570	0.997	66.52	87.02	4.04	213.99	205.64	1.388
167	19.5	8	1.95	455.56	RI	3	9.53	76	570	0.997	116.02	116.52	7.05	213.99	205.64	1.388
169	19.5	12	2.93	455.56	RI	4	9.53	76	570	1.329	100.03	117.01	6.08	285.32	205.64	1.388
170	29.9	4	2.29	477.78	RI	4	9.53	76	570	1.329	100.03	117.01	6.08	285.32	205.64	1.388
171	19.5	12	2.93	455.56	RI	4	6.6	76	580	0.631	100.03	117.01	6.08	136.85	192.23	0.712
172	19.5	12	2.93	455.56	RI	4	6.6	76	580	0.631	118.00	118.00	7.17	136.85	192.23	0.712
173	16	20	3.28	427.78	RI	4	6.6	76	580	0.631	116.00	118.00	7.05	136.85	192.23	0.712
174	16	20	3.28	427.78	RI	4	9.53	76	570	1.442	99.51	118.00	6.05	285.32	205.64	1.388
175	15.9	4	1.93	586.05	R	2	9.5	76.2	406.79	1.633	38.61	52.32	6.33	141.76	977.11	0.145
176	15.9	4	1.93	586.05	R	2	9.5	76.2	406.79	1.311	38.10	44.70	6.25	141.76	968.92	0.146
177	15.9	4	1.93	572.26	R	2	9.5	76.2	513.66	1.275	44.45	44.45	7.29	141.76	448.26	0.316
178	15.9	4	1.93	573.26	R	2	9.5	77.2	514.66	1.228	44.70	44.70	7.33	141.76	416.04	0.341
179	15.9	4	1.93	572.26	R	2	9.5	76.2	513.66	1.133	38.35	38.61	6.29	141.76	367.69	0.386
180	15.9	4	1.93	573.26	R	2	9.5	77.2	514.66	1.263	38.10	38.35	6.25	141.76	255.44	0.555
181	15.9	4	1.93	572.26	R	2	9.5	76.2	513.66	1.350	38.86	50.80	6.37	141.76	232.58	0.610
182	15.9	4	1.93	573.26	R	2	9.5	77.2	514.66	1.570	38.90	50.80	6.38	141.76	274.88	0.516

	Longitudinal Reinforcement				Transverse Reinforcement											
Database No.	D_{bar} (mm)	Total # Bars	ρ_{long} (%)	f_y (MPa)	Confin. Type	N	D_{bar} (mm)	s (mm)	f_{yh} (MPa)	ρ_{area} (%)	Δ_{80} (mm)	Δ_{max} (mm)	Drift Ratio (%)	$A_{sh\ Provided}$ (mm^2)	$A_{sh\ (ACI)}$ (mm^2)	$A_{sh}/A_{sh(ACI)}$
183	15.9	4	1.93	586.05	R	2	9.5	76.2	406.79	1.611	32.30	44.20	5.30	141.76	638.42	0.222
184	15.9	4	1.93	587.05	R	2	9.5	77.2	407.79	1.208	32.00	43.90	5.25	141.76	662.10	0.214
185	15.9	4	1.93	572.26	R	2	9.5	76.2	513.66	1.224	26.40	26.40	4.33	141.76	201.76	0.703
186	15.9	4	1.93	573.26	R	2	9.5	77.2	514.66	1.463	25.40	25.40	4.16	141.76	204.01	0.695
187	19.05	12	2.14	497	RJ	4	6.35	50	459.5	0.778	88.39	102.26	6.31	126.68	134.67	0.941
188	19.05	12	2.14	497	RJ	4	6.35	50	459.5	0.778	96.57	105.05	6.90	126.68	144.40	0.877
189	19.05	12	2.14	497	RJ	4	6.35	50	459.5	0.778	88.10	110.51	6.29	126.68	141.16	0.897
190	19.05	12	2.14	497	RI	4	6.35	52	459.5	0.748	98.02	112.97	7.00	126.68	142.30	0.890
191	19.05	12	2.14	497	RI	4	6.35	52	459.5	0.748	94.86	119.47	6.78	126.68	152.43	0.831
192	19.05	12	2.14	497	RI	4	6.35	52	459.5	0.656	77.02	114.71	5.50	126.68	150.74	0.840
202	9.525	8	2.45	517.13	RJ	3	3.175	25.4	793	0.736	20.24	36.53	3.39	23.75	46.33	0.684
204	9.525	8	2.45	455.07	RD	3.41	3.175	25.4	793	0.837	14.63	37.56	2.45	27.00	44.77	0.603
205	9.525	8	2.45	455.07	RD	3.41	3.175	25.4	793	0.837	13.78	39.73	2.31	27.00	48.32	0.559
207	9.525	8	2.45	475.76	RD	3.41	3.175	25.4	1262	0.837	29.83	40.18	5.00	27.00	25.17	1.073
208	9.525	8	2.45	475.76	RD	3.41	3.175	25.4	1262	0.837	19.05	40.89	3.19	27.00	27.60	0.978
209	9.525	8	2.45	475.76	RD	3.41	3.175	31.75	1262	0.670	18.89	39.05	3.16	27.00	31.96	0.845
210	9.525	8	2.45	475.76	RD	3.41	3.175	38.1	1262	0.558	11.86	40.29	1.99	27.00	44.02	0.613
211	9.525	8	2.45	475.76	RD	3.41	3.175	44.45	1262	0.546	12.06	40.07	2.02	27.00	42.03	0.642
215	19.54	8	2.15	451	RD	3.41	11.3	60	391	2.229	182.76	212.57	9.14	341.98	459.85	0.744
216	19.54	8	2.15	430	RD	3.41	11.3	60	391	2.229	144.46	201.03	7.22	341.98	464.33	0.737
217	19.54	8	2.15	451	RD	3.41	11.3	60	418	2.229	63.20	141.00	3.16	341.98	457.15	0.748
221	19.54	8	2.15	446	RD	3.41	11.3	60	438	2.229	174.41	208.33	8.72	341.98	349.64	0.978
222	19.54	8	2.15	446	RD	3.41	11.3	60	438	2.229	122.09	162.35	6.10	341.98	485.14	0.705
223	19.54	8	2.15	446	RD	3.41	9.5	55	825	1.707	97.98	168.94	4.90	241.71	236.75	1.445
224	19.54	8	2.15	446	RD	3.41	9.5	80	825	1.173	52.55	108.01	2.63	241.71	327.70	1.044
225	19.54	8	2.15	446	RD	3.41	9.5	55	744	1.707	66.37	91.84	3.32	241.71	250.54	1.365
226	19.54	8	2.15	446	RD	3.41	11.3	60	492	2.346	66.06	90.86	3.30	341.98	432.68	0.790
227	19.05	4	2.45	452.99	R	2	6.35	76.2	410.9	0.873	21.85	21.85	3.19	63.34	173.09	0.366
228	19.05	4	2.45	452.99	R	2	6.35	76.2	410.9	0.873	20.94	20.94	3.05	63.34	173.09	0.366
229	19.05	4	2.45	452.99	R	2	6.35	38.1	410.9	1.745	27.91	28.91	4.07	63.34	82.44	0.768
230	19.05	4	2.45	452.99	R	2	6.35	38.1	410.9	1.745	28.76	29.88	4.19	63.34	82.44	0.768
231	19.05	4	2.45	452.99	R	2	6.35	76.2	410.9	0.873	21.49	22.71	3.13	63.34	153.57	0.412
232	19.05	4	2.45	452.99	R	2	6.35	76.2	410.9	0.873	21.59	21.59	3.15	63.34	153.57	0.412
233	19.05	4	2.45	452.99	R	2	6.35	57.15	410.9	1.164	20.95	21.97	3.05	63.34	105.55	0.600
234	19.05	4	2.45	452.99	R	2	6.35	57.15	410.9	1.164	22.07	22.07	3.22	63.34	105.55	0.600
237	19.05	4	2.45	452.99	R	2	6.35	76.2	410.9	0.873	22.85	23.55	3.33	63.34	186.96	0.339
238	19.05	4	2.45	452.99	R	2	6.35	76.2	410.9	0.873	23.01	23.58	3.36	63.34	186.96	0.339
239	19.05	4	2.45	452.99	R	2	6.35	57.15	410.9	1.164	22.01	22.01	3.21	63.34	134.44	0.471
240	19.05	4	2.45	452.99	R	2	6.35	57.15	410.9	1.164	21.73	21.73	3.17	63.34	134.44	0.471

	Longitudinal Reinforcement				Transverse Reinforcement											
Database No.	D_{bar} (mm)	Total # Bars	ρ_{long} (%)	f_y (MPa)	Confin. Type	N	D_{bar} (mm)	s (mm)	f_{yh} (MPa)	ρ_{area} (%)	Δ_{80} (mm)	Δ_{max} (mm)	Drift Ratio (%)	$A_{sh\ Provided}$ (mm^2)	$A_{sh\ (ACI)}$ (mm^2)	$A_{sh}/A_{sh(ACI)}$
241	19.05	4	2.45	452.99	R	2	6.35	57.15	410.9	1.164	22.05	22.05	3.22	63.34	140.60	0.450
242	19.05	4	2.45	452.99	R	2	6.35	57.15	410.9	1.016	21.53	21.58	3.14	63.34	140.60	0.450
243	12.7	12	2.43	461	RU	4	4	40	485	0.601	24.75	24.75	3.96	50.27	83.77	0.600
244	12.7	12	2.43	461	RU	4	4	40	485	0.800	18.73	18.73	3.00	50.27	83.77	0.600
246	25.4	12	1.69	388	RU	4	12.7	100	524	0.952	31.27	31.27	2.61	506.71	503.07	1.007
248	12.7	20	1.58	363	R	2	6	70	368	0.238	43.71	76.39	3.51	56.55	272.42	0.208
249	12.7	20	1.58	363	R	2	6	70	368	0.238	48.50	79.78	3.90	56.55	270.90	0.209
250	12.7	20	1.58	363	R	2	6	70	368	0.238	74.18	94.85	5.96	56.55	260.28	0.217
251	12.7	20	1.58	363	R	2	6	70	368	0.238	101.44	112.17	8.15	56.55	251.93	0.224
252	12.7	20	1.58	363	R	2	6	70	368	0.257	84.52	95.60	6.79	56.55	279.25	0.203
258	35.8	8	2.60	473	RJ	3	15.9	150	445	0.874	105.28	105.28	5.92	595.67	1387.20	0.573
260	19.54	8	2.74	454	RD	3.41	11.3	80	542	2.151	84.97	100.00	4.61	341.98	297.10	1.151
261	19.54	8	2.74	454	RD	3.41	11.3	80	542	2.151	42.23	65.88	2.29	341.98	296.69	1.153
264	19.54	8	2.74	454	RD	3.41	11.3	70	465	2.459	56.23	80.11	3.05	341.98	477.08	0.717
265	19.54	8	2.74	454	RD	3.41	11.3	70	465	2.459	41.15	46.11	2.23	341.98	477.08	0.717
266	19.54	8	2.74	454	RD	3.41	11.284	100	465	1.716	69.33	85.30	3.76	341.01	341.57	0.998
268	19.54	8	2.74	521	RD	3.41	8	75	850	1.131	62.13	62.78	3.37	171.41	172.09	0.996
269	19.54	8	2.74	521	RD	3.41	8	75	850	1.131	26.87	48.63	1.46	171.41	172.09	0.996
270	19.54	8	2.74	521	RD	3.41	11.1	75	850	2.212	50.94	81.94	2.77	329.98	184.31	1.790
272	19.54	8	2.74	521	RD	3.41	11.284	70	465	1.631	46.27	48.48	2.51	341.01	583.89	0.584
273	19.54	8	2.74	521	RD	3.41	11.284	70	465	1.631	86.37	102.75	4.69	341.01	583.89	0.584
274	19.54	8	2.74	521	RD	3.41	11.3	80	542	1.431	88.74	88.74	4.82	341.98	452.90	0.755
275	19.54	8	2.74	521	RD	3.41	11.3	80	542	1.455	33.43	56.16	1.81	341.98	452.90	0.755
285	25	8	3.21	453	R	2	10	150	470	0.333	42.00	58.60	4.20	157.08	347.71	0.452
286	12.7	8	2.53	363	R	2	5.75	50	364	0.617	10.10	11.77	2.53	51.93	65.86	0.789
287	12.7	8	2.53	363	RJ	3	5.75	75	364	0.617	11.75	14.37	2.94	77.90	86.77	1.197
288	12.7	8	2.53	363	R	2	5.75	40	364	0.772	7.97	11.40	1.99	51.93	52.69	0.986
289	12.7	8	2.53	363	RJ	3	5.75	60	364	0.772	9.95	12.06	2.49	77.90	69.42	1.496

f'c	Characteristic compressive strength of concrete
P	Axial compressive load
A_g	Gross sectional area of column
f_y	Yield stress of longitudinal reinforcement
f_{yh}	Yield stress of transverse reinforcement
B	Column Width
H	Column Depth
L	Length of equivalent cantilever
D_{bar}	Diameter of transverse / longitudinal reinforcement
s	Spacing of transverse reinforcement
Cover	ce
ρ_{long}	Longitudinal reinforcement ratio (A_{st} / A_g)
ρ_{area}	Transverse reinforcement ratio (A_{sh} / s*h_c)
N	Effective number of transverse bars in cross section
Δ_{max}	Maximum recorded deflection
Δ_{80}	Deflection at 80% effective force (20% loss of strength)
Drift Ratio	Drift Ratio (Δ_{80} / L)
$A_{sh\ Provided}$	Area of transverse reinforcement provided in specimen
$A_{sh\ (ACI)}$	Area of transverse reinforcement required by ACI 318-05 21.4.4.1

A2. Circular Column Database

Database No.	Specimen Name	f'c (Mpa)	P (kN)	P/Agf'c	P/P_o	Geometry				
						Diameter (mm)	Length (mm)	A_g (mm^2)	Cover (mm)	Section Code
1	Davey 1975, No. 1	33.2	380	0.06	0.05	500	2750	207110	20.3	2
3	Davey 1975, No. 3	33.8	380	0.06	0.05	500	3250	207110	20.3	2
8	Ang et al 1981, No. 2	28.5	2111	0.56	0.51	400	1600	132550	18.0	2
22	Ang et al. 1985, No. 9	29.9	751	0.20	0.15	400	1000	125660	18.0	0
40	Zahn et al. 1986, No. 6	27	2080	0.58	0.51	400	1600	132550	18.0	2
41	Watson & Park 1989, No 10	40	2652	0.50	0.48	400	1600	132550	17.0	2
42	Watson & Park 1989, No 11	39	3620	0.70	0.66	400	1600	132550	18.0	2
43	Wong et al. 1990, No. 1	38	907	0.19	0.16	400	800	125660	20.0	0
45	Wong et al. 1990, No. 3	37	1813	0.39	0.32	400	800	125660	20.0	0
50	Lim et al. 1990, Con1	34.5	151	0.24	0.16	152	1140	18146	10.2	0
52	Lim et al. 1990, Con1	34.5	220	0.35	0.23	152	570	18146	10.2	0
53	NIST, Full Scale Flexure	35.8	4450	0.07	0.06	1520	9140	1814600	58.7	0
54	NIST, Full Scale Shear	34.3	4450	0.07	0.06	1520	4570	1814600	60.3	0
55	NIST, Model N1	24.1	120	0.10	0.09	250	750	49087	9.9	0
56	NIST, Model N2	23.1	239	0.21	0.18	250	750	49087	9.9	0
57	NIST, Model N3	25.4	120	0.10	0.08	250	1500	49087	9.7	0
58	NIST, Model N4	24.4	120	0.10	0.08	250	750	49087	9.9	0
59	NIST, Model N5	24.3	239	0.20	0.17	250	750	49087	9.9	0
60	NIST, Model N6	23.3	120	0.11	0.09	250	1500	49087	9.7	0
93	Kunnath et al. 1997, A2	29	200	0.09	0.08	305	1372	73062	14.5	0
95	Kunnath et al. 1997, A4	35.5	222	0.09	0.08	305	1372	73062	14.5	0
96	Kunnath et al. 1997, A5	35.5	222	0.09	0.08	305	1372	73062	14.5	0
97	Kunnath et al. 1997, A6	35.5	222	0.09	0.08	305	1372	73062	14.5	0
100	Kunnath et al. 1997, A9	32.5	222	0.09	0.08	305	1372	73062	14.5	0
101	Kunnath et al. 1997, A10	27	200	0.10	0.09	305	1372	73062	14.5	0
102	Kunnath et al. 1997, A11	27	200	0.10	0.09	305	1372	73062	14.5	0
103	Kunnath et al. 1997, A12	27	200	0.10	0.09	305	1372	73062	14.5	0
106	Hose et al., 1997, SRPH1	41.1	1780	0.15	0.13	610	3660	292250	27.8	0
107	Vu et al. 1998, NH1	38.3	1928	0.31	0.28	457	910	164030	24.8	0
109	Vu et al. 1998, NH3	39.4	970	0.15	0.14	457	910	164030	24.8	0
112	Vu et al. 1998, NH6	35	1914	0.33	0.22	457	910	164030	26.4	0
115	Kowalsky et al. 1996, FL3	38.6	1780	0.28	0.22	457	3656	164030	30.2	0
116	Lehman et al. 1998, 415	31.03	653.86	0.07	0.07	609.6	2438.4	291860	22.2	0
117	Lehman et al. 1998, 815	31.03	653.86	0.07	0.07	609.6	4876.8	291860	22.2	0
118	Lehman et al. 1998, 1015	31.03	653.86	0.07	0.07	609.6	6096	291860	22.2	0
119	Lehman et al.1998, 407	31.03	653.86	0.07	0.08	609.6	2438.4	291860	22.2	0
120	Lehman et al. 1998, 430	31.03	653.86	0.07	0.06	609.6	2438.4	291860	22.2	0
121	Calderone et al. 2000, 328	34.475	911.84	0.09	0.08	609.6	1828.8	291860	28.6	0

						Geometry				
Database No.	**Specimen Name**	**f'c (Mpa)**	**P (kN)**	**P/Agf'c**	**P/P$_o$**	**Diameter (mm)**	**Length (mm)**	**A$_g$ (mm^2)**	**Cover (mm)**	**Section Code**
123	Calderone et al. 2000,1028	34.475	911.84	0.09	0.08	609.6	6096	291860	28.6	0
130	Saatcioglu & Baingo 1999, RC4	90	1850	0.42	0.43	250	1645	49087	14.0	0
133	Saatcioglu & Baingo 1999, RC8	90	1850	0.42	0.43	250	1645	49087	13.8	0
141	Henry 1998, 415p	37.23	1308	0.12	0.12	609.6	2438.4	291860	22.2	0
142	Henry 1998, 415s	37.23	654	0.06	0.06	609.6	2438.4	291860	22.2	0
144	Soderstrom 2001 C1	60.6	0	0.00	0.00	419	1968.5	145440	55.6	2
145	Soderstrom 2001 C2	62.6	0	0.00	0.00	419	1968.5	145440	55.6	2
152	Kowalsky & Moyer 2001 No.1	32.723	231.31	0.04	0.04	457.2	2438.4	173170	12.7	2
153	Kowalsky & Moyer 2001 No.2	34.226	231.31	0.04	0.04	457.2	2438.4	173170	12.7	2
157	Hamilton 2002 UCI1	36.494	0	0.00	0.00	406.4	1854.2	129720	15.0	0
158	Hamilton 2002 UCI2	36.494	0	0.00	0.00	406.4	1854.2	129720	15.0	0
162	Hamilton 2002 UCI6	35.646	0	0.00	0.00	406.4	1854.2	129720	15.0	0

	Longitudinal Reinforcement				Transverse Reinforcement								
Database No.	**D_{bar} (mm)**	**Total # Bars**	**ρ_{long} %**	**f_y (Mpa)**	**D_{bar} (mm)**	**s (mm)**	**f_{yh} (Mpa)**	**ρ_s (%)**	**Δ_{80} (mm)**	**Δ_{max} (mm)**	**Drift Ratio (%)**	**$\rho_{s\,(ACI)}$ (%)**	**$\rho_s / \rho_{s(ACI)}$**
1	18.4	20	2.568	373	6.5	65	312	0.444	119.25	119.25	4.34	1.277	0.348
3	18.4	20	2.568	373	6.5	65	342	0.444	86.83	116.21	2.67	1.186	0.375
8	16	16	2.427	308	10.0	55	280	1.569	50.09	50.09	3.13	1.254	1.251
22	16	20	3.200	448	6.0	30	372	1.036	65.58	65.58	6.56	0.965	1.074
40	16	16	2.427	337	10.0	75	466	1.151	59.04	59.36	3.69	0.714	1.612
41	16	12	1.820	474	8.0	84	372	0.654	32.54	32.94	2.03	1.290	0.507
42	16	12	1.820	474	10.0	57	338	1.514	29.00	36.24	1.81	1.421	1.065
43	16	20	3.200	423	10.0	60	300	1.454	41.43	41.43	5.18	1.520	0.957
45	16	20	3.200	475	10.0	60	300	1.454	28.82	33.90	3.60	1.480	0.983
50	12.7	8	5.585	448	3.7	22.2	620	1.496	89.54	90.75	7.85	0.837	1.788
52	12.7	8	5.585	448	3.7	22.2	620	1.496	45.59	45.59	8.00	0.837	1.788
53	43	25	2.001	475	15.9	88.9	493	0.637	540.99	593.37	5.92	0.871	0.731
54	43	25	2.001	475	19.1	54	435	1.509	355.70	356.08	7.78	0.946	1.594
55	7	25	1.960	446	3.1	8.89	441	1.428	82.50	104.15	11.00	0.656	2.178
56	7	25	1.960	446	3.1	8.89	441	1.428	60.41	73.60	8.06	0.629	2.272
57	7	25	1.960	446	2.7	14.48	476	0.686	110.64	128.85	7.38	0.640	1.071
58	7	25	1.960	446	3.1	8.89	441	1.428	54.69	67.52	7.29	0.664	2.151
59	7	25	1.960	446	3.1	8.89	441	1.428	52.60	64.30	7.01	0.661	2.160
60	7	25	1.960	446	2.7	14.48	476	0.686	123.09	127.72	8.21	0.587	1.168
93	9.5	21	2.037	448	4.0	19	434	0.959	77.20	77.20	5.63	0.802	1.195
95	9.5	21	2.037	448	4.0	19	434	0.959	58.56	58.56	4.27	0.982	0.977
96	9.5	21	2.037	448	4.0	19	434	0.959	76.35	76.35	5.56	0.982	0.977
97	9.5	21	2.037	448	4.0	19	434	0.959	95.49	95.49	6.96	0.982	0.977
100	9.5	21	2.037	448	4.0	19	434	0.959	90.54	90.54	6.60	0.899	1.067
101	9.5	21	2.037	448	4.0	19	434	0.959	90.66	90.66	6.61	0.747	1.284
102	9.5	21	2.037	448	4.0	19	434	0.959	102.16	102.16	7.45	0.747	1.284
103	9.5	21	2.037	448	4.0	19	434	0.959	102.43	102.43	7.47	0.747	1.284
106	22.23	20	2.656	455	9.5	57	414	0.902	319.79	319.79	8.74	1.191	0.757
107	15.875	20	2.413	427.5	9.5	60	430.2	1.166	38.13	46.46	4.19	1.068	1.091
109	15.875	20	2.413	427.5	9.5	60	430.2	1.166	50.33	50.33	5.53	1.099	1.061
112	19.05	30	5.213	486.2	12.7	40	434.4	3.133	87.47	87.47	9.61	1.007	3.112
115	15.875	30	3.620	477	9.5	76	445	0.945	281.60	340.50	7.70	1.278	0.740
116	15.875	22	1.492	461.96	6.4	31.75	606.76	0.706	178.00	179.00	7.30	0.614	1.150
117	15.875	22	1.492	461.96	6.4	31.75	606.76	0.706	446.00	446.00	9.15	0.614	1.150
118	15.875	22	1.492	461.96	6.4	31.75	606.76	0.706	639.83	639.83	10.50	0.614	1.150
119	15.875	11	0.746	461.96	6.4	31.75	606.76	0.706	128.00	128.00	5.25	0.614	1.150
120	15.875	44	2.984	461.96	6.4	31.75	606.76	0.706	178.00	181.00	7.30	0.614	1.150
121	19.05	28	2.734	441.28	6.4	25.4	606.76	0.903	133.00	133.00	7.27	0.682	1.324

	Longitudinal Reinforcement				Transverse Reinforcement								
Database No.	**D_{bar} (mm)**	**Total # Bars**	**ρ_{long} %**	**f_y (Mpa)**	**D_{bar} (mm)**	**s (mm)**	**f_{yh} (Mpa)**	**ρ_s (%)**	**Δ_{80} (mm)**	**Δ_{max} (mm)**	**Drift Ratio (%)**	**$\rho_{s\,(ACI)}$ (%)**	**$\rho_s / \rho_{s(ACI)}$**
123	19.05	28	2.734	441.28	6.4	25.4	606.76	0.903	891.54	894.08	14.63	0.682	1.324
130	16	8	3.277	419	8.0	50	580	1.811	54.75	73.10	3.33	1.872	0.967
133	16	8	3.277	419	7.5	50	1000	1.588	75.78	75.78	4.61	1.080	1.471
141	15.875	22	1.492	462	6.4	31.75	606.76	0.706	137.64	179.07	3.76	0.736	0.959
142	15.875	22	1.492	462	6.4	63.5	606.76	0.353	199.01	180.11	10.11	0.736	0.479
144	22.2	8	0.021	429.5	9.5	50.8	413.7	41370.000	199.01	199.01	7.55	6.292	6574.598
145	22.2	8	0.021	429.5	9.5	50.8	413.7	41370.000	223.70	224.01	10.58	6.500	6364.517
152	19.05	12	0.020	565.37	9.5	76.2	434.37	43437.000	190.46	190.46	10.68	0.904	48049.247
153	19.05	12	0.020	565.37	9.5	76.2	434.37	43437.000	266.69	266.69	13.15	0.946	45939.314
157	12.7	12	0.012	458.5	4.5	31.75	691.54	69154.000	114.30	114.30	6.16	0.633	109203.171
158	12.7	12	0.012	458.5	4.5	31.75	691.54	69154.000	124.92	268.15	6.74	0.633	109203.171
162	12.7	12	0.012	458.5	4.5	31.75	691.54	69154.000	205.00	241.00	11.06	0.619	111800.178

f'c	Characteristic compressive strength of concrete
Diameter	Diameter of column (For square and octagonal sections D refers to the largest circle that can be inscribed in the section)
A_g	Gross sectional area
P	Axial load
Length	Length of equivalent cantilever
f_y	Yield stress of longitudinal reinforcement
f_{yh}	Yield stress of transverse reinforcement
Length	Length of equivalent cantilever
s	Spacing of transverse reinforcement
Cover	Distance between outer surface of column and center of spiral reinforcement If there is no spiral, cover is taken as distance between outer surface and outside of longitudinal reinforcement
D_{bar}	Diameter of transverse / longitudinal reinforcement
ρ_{long}	Longitudinal reinforcement ratio (A_{st} / A_g)
Δ_{max}	Maximum recorded deflection
Δ_{80}	Deflection at 80% effective force (20% loss of strength)
Drift Ratio	Drift Ratio (D_{80} / L)
$\rho_{s\ Provided}$	Area of transverse reinforcement provided in specimen
$\rho_{s\,(ACI)}$	Area of transverse reinforcement required by ACI 318-05 21.4.4.1

APPENDIX B

B1 Rectangular Typical Columns Details

				Geometry				Vert. Reinf			Trans. Reinf			Loading Details	
Bldg	Detail	Nv	f'c (MPa)	B (mm)	H (mm)	h_c (mm)	Ag (mm^2)	No of bars	bar #	ρ_{long} (%)	Bar #	s (mm)	ρ_{area} (%)	P (kN) **	$P/A_g f_c'$
A	A1	4	55.16	609.6	609.6	517.5	371612.16	12	8	1.64	5	102	1.50	8807	0.43
	A2	5	68.95	762	762	669.9	580644	16	8	1.40	5	102	1.45	18966	0.47
	A3	5 *	68.95	762	1016	669.9	774192	20	8	1.31	5	102	1.45	21675	0.41
B	B1	5 *	55.16	762	1219.2	669.9	929030.4	20	9	1.38	5	102	1.45	23032	0.45
	B1	5 *	72.40	762	1219.2	669.9	929030.4	20	9	1.38	5	76	1.94	26323	0.39
	B3	4 *	55.16	762	914.4	669.9	696772.8	14	9	1.29	5	102	1.16	13469	0.35
	B3	4 *	72.40	762	914.4	669.9	696772.8	14	9	1.29	5	76	1.55	16782	0.33
C	C1	3	27.58	457.2	457.2	368.3	209031.84	12	9	3.68	4	114	0.90	4083	0.71
	C2	3 *	41.37	457.2	609.6	368.3	278709.12	12	11	4.12	4	76	1.35	7757	0.67
	C3	3 *	55.16	457.2	914.4	365.1	418063.68	16	11	3.66	5	89	1.83	13068	0.57

* Nv given for shorter dimension only

** P = DL + LL

† All steel yield strength is 414 MPa

B2 Rectangular Typical Column Cross Sections

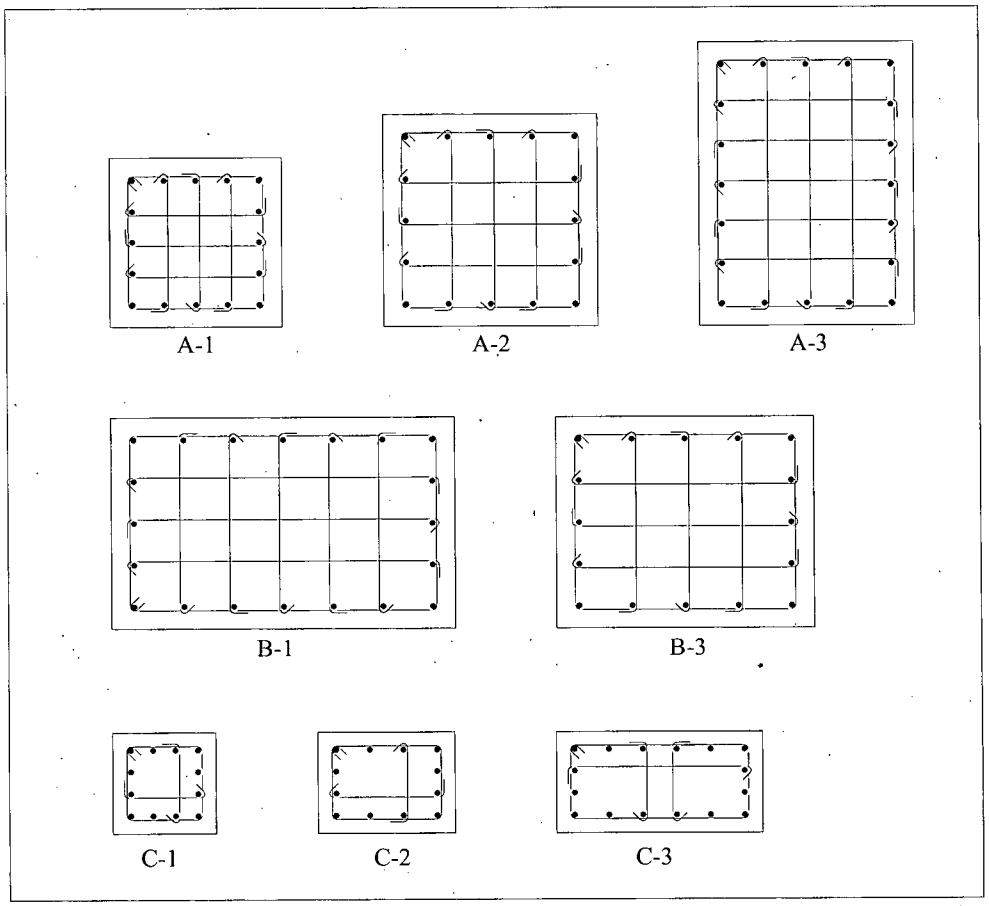

B3 Circular Typical Columns Details

			Geometry			Vert. Reinf.			Trans. Reinf.			Loading Details	
Bldg ID	Detail	f'c (MPa)	D (mm)	bc (mm)	Ag (mm^2)	No. of Bars	bar #	ρlong	bar #	s (mm)	ρvol	P (kN) *	P/Agf'c
A	A	55	457.2	381	164173.1	6	6 / 3	2.02%	5	76.2	2.76%	4061	0.45
	A	41	457.2	381	164173.1	6	11	3.68%	5	76.2	2.76%	3719	0.55
	A	41	457.2	381	164173.1	6	11	3.68%	5	76.2	2.76%	3968	0.58
	A	41	457.2	381	164173.1	6	6 / 3	2.02%	5	76.2	2.76%	2824	0.42
B	10	48	609.6	520.7	291863.3	12	8	2.10%	5	63.5	2.42%	209	0.01
	11	48	762	673.1	456036.3	14	10	2.52%	5	63.5	1.87%	2139	0.10
	12	48	863.6	774.7	585753.4	16	9	1.76%	5	63.5	1.63%	4079	0.14
	11	34	762	673.1	456036.3	14	7	1.19%	5	63.5	1.87%	756	0.05
C	E	69	609.6	533.4	291863.3	8	8	1.40%	5	88.9	1.69%	3892	0.19
	F	69	762	685.8	456036.3	12	8	1.34%	5	101.6	1.15%	11925	0.38
	F	69	762	685.8	456036.3	12	8	1.34%	5	101.6	1.15%	9172	0.29
	F	69	762	685.8	456036.3	12	8	1.34%	5	88.9	1.31%	4479	0.14

* P = DL + LL

† All steel yield strength is 414 MPa

B4 Circular Typical Column Cross Sections

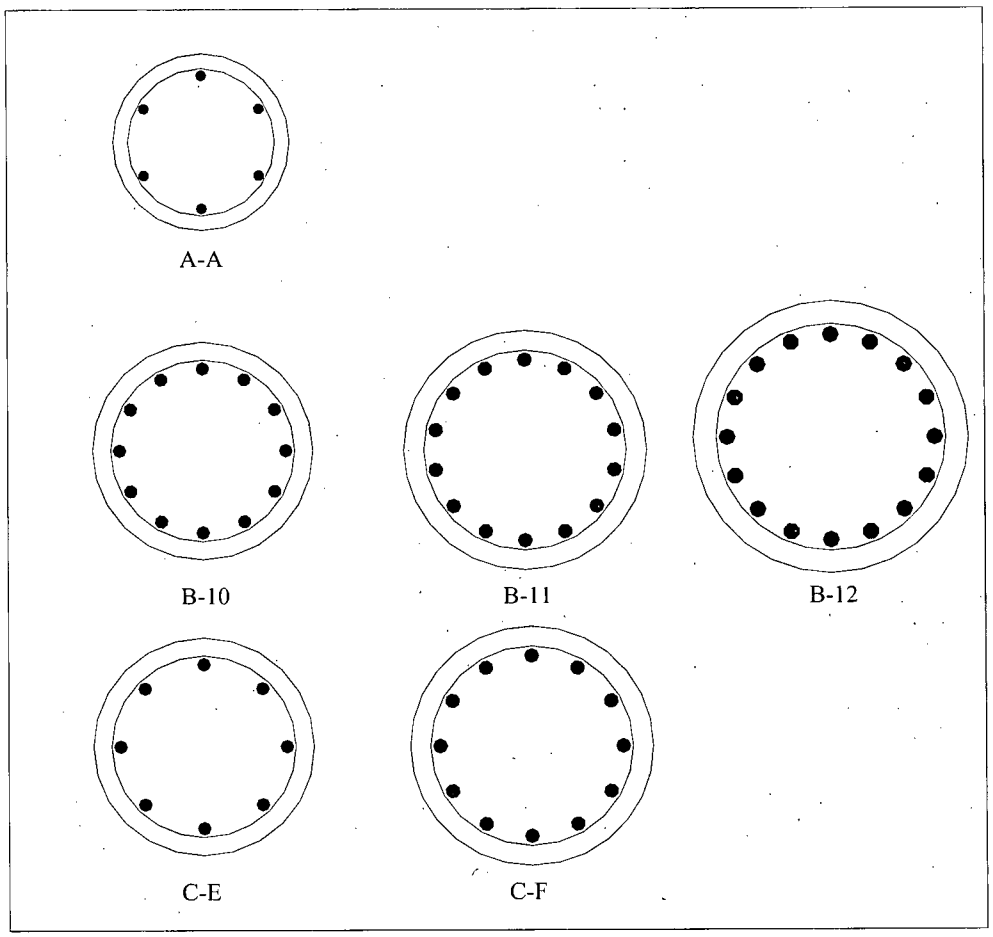

Figure B2.1 Typical Rectangular Column detail drawings

APPENDIX C

C1 Rectangular Confinement Models

Model	Equation
ACI	$0.3\frac{f_c'}{f_{yh}}\left(\frac{A_g}{A_{ch}}-1\right) \geq 0.09\frac{f'_c}{f_{yh}}$
CSA	$0.2k_n k_p \frac{A_g}{A_{ch}}\frac{f_c'}{f_{yh}}$ $k_n = n_l/(n_l-2)$, $k_p = P/P_0$
NSZ	$\left(\frac{A_g}{A_{ch}}\frac{1.0-\rho_t m}{3.3}\frac{f_c'}{f_{yh}}\frac{P}{\phi f_c' A_g}\right)-0.0065$
SK97	(ACI) *(α)$\left(1+13\left(\frac{P}{P_0}\right)^5\right)\left(\frac{(\mu_\phi)^{1.15}}{29}\right)$ α – steel configuration parameter μ_ϕ - target curvature ductility
BS98	(ACI) *$\left(1+13\left(\frac{P}{P_0}\right)^5\right)\left(\frac{(\mu_\phi)^{0.82}}{8.12}\right)$ α – steel configuration parameter μ_ϕ - target curvature ductility
WSS99	$0.1\mu_\Delta\sqrt{\frac{27.6MPa}{f'_c}}\left[0.12\frac{f'_c}{f_{yh}}\left(0.5+1.25\frac{P}{f'_c A_g}\right)+0.13\left(\rho_t\frac{f_{yh}}{414MPa}-0.01\right)\right]$ μ_Δ - target displacement ductility
SR02	$14\frac{f'_c}{f_{yh}}\left[\frac{A_g}{A_{ch}}-1\right]\frac{1}{\sqrt{k_2}}\frac{P}{P_0}\delta$ $k_2 = 0.15\sqrt{\frac{h_c}{s}\cdot\frac{h_c}{s_l}}$, δ - target drift ratio

Model	Equation
BBM05	$\left(\frac{\gamma}{1-0.8f_{pc}}\right)^2 \frac{f'_c}{f_{yh}}$ γ - as per Table 2.1
PP92	$k\frac{f_c'}{f_{yh}}\frac{A_g}{A_{ch}}\left(\frac{P}{A_g f_c'}-0.08\right)$ *$k = 0.35$ for high ductility demand, $= 0.25$ for low ductility demand*
WZP94	$\left(\frac{A_g}{A_{ch}}\frac{(\phi_u/\phi_y)-33\rho_t m+22}{111}\frac{f_c'}{f_{yh}}\frac{P}{\phi f_c' A_g}\right)-0.006$ ϕ_u/ϕ_y - target curvature ductility factor
LP04	$\left(\frac{A_g}{A_{ch}}\frac{(\phi_u/\phi_y)-33\rho_t m+22}{\lambda}\frac{f_c'}{f_{yh}}\frac{P}{\phi f_c' A_g}\right)-0.006$ (f_{yh}<500MPa) *$\lambda = 117$ when $f_c < 70$ MPa, $0.05(f_c')2-9.54f_c'+539.4$ when $f_c \geq 70$ MPa.* $\left(\frac{A_g}{A_{ch}}\frac{(\phi_u/\phi_y)-30\rho_t m+22}{91-0.1f_c'}\frac{f_c'}{f_{yh}}\frac{P}{\phi f_c' A_g}\right)$ (f_{yh} > 500MPa) *ϕ_u/ϕ_y - target curvature ductility factor*

C2 Circular Confinement Models

Model	Equation
ACI	$0.45\left(\frac{A_g}{A_{ch}}-1\right)\frac{f_c'}{f_{yh}} \geq 0.12\frac{f'_c}{f_{yh}}$
CSA	$0.4k_p\frac{f_c'}{f_{yh}}$ $k_p = P/P_0$
NSZ	$\left(\frac{A_g}{A_{ch}}\frac{1.0-\rho_t m}{2.4}\frac{f_c'}{f_{yh}}\frac{P}{\phi f_c' A_g}\right)-0.0084$

Model	Equation
SK97	(ACI) *(α)$\left(1+13\left(\frac{P}{P_0}\right)^5\right)\left(\frac{(\mu_\phi)^{1.15}}{29}\right)$ α – steel configuration parameter μ_ϕ - target curvature ductility
BS98	(ACI) *$\left(1+13\left(\frac{P}{P_0}\right)^5\right)\left(\frac{(\mu_\phi)^{0.82}}{8.12}\right)$ α – steel configuration parameter μ_ϕ - target curvature ductility
SR02	$28\frac{f'_c}{f_{yh}}\left[\frac{A_g}{A_{ch}}-1\right]\frac{P}{P_0}\delta$ δ - target drift ratio
BBM05	$\left(\frac{\gamma}{1-0.8f_{pc}}\right)^2\frac{f'_c}{f_{yh}}$ γ - as per Table 2.1
PP92	$k\frac{f_c'}{f_{yh}}\frac{A_g}{A_{ch}}\left(\frac{P}{A_g f_c'}-0.08\right)$ *k = 0.5 for high ductility demand, = 0.35 for low ductility demand*
WZP94	$1.4\left(\frac{A_g}{A_{ch}}\frac{(\phi_u/\phi_y)-33\rho_t m+22}{111}\frac{f_c'}{f_{yh}}\frac{P}{\phi f_c' A_g}\right)-0.008$ ϕ_u/ϕ_y - target curvature ductility factor
LP04	$\left(\left(\frac{A_g}{A_{ch}}\frac{(\phi_u/\phi_y)-33\rho_t m+22}{111}\frac{f_c'}{f_{yh}}\frac{P}{\phi f_c' A_g}\right)-0.006\right)\alpha$ (f_{yh}<500MPa) α = 1.1 when f_c < 80 MPa and α = 1.0 when $f_c \geq$ 80 MPa $\left(\frac{A_g}{A_c}\frac{(\phi_u/\phi_y)-55\rho_t m+25}{79}\frac{f_c'}{f_{yh}}\frac{P_e}{\phi f_c' A_g}\right)$ (f_{yh} > 500MPa) *ϕ_u/ϕ_y - target curvature ductility factor*

APPENDIX D

D.1 Rectangular Column Scatter Plots (with ACI Minimum)

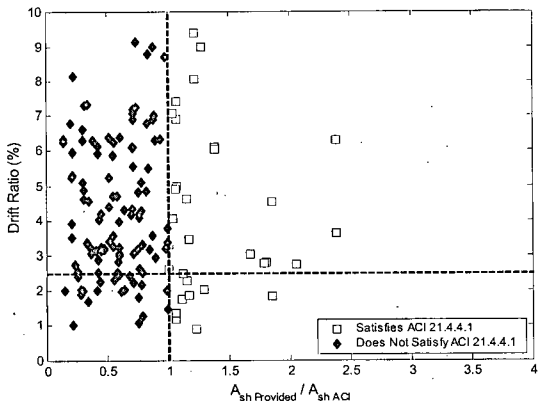

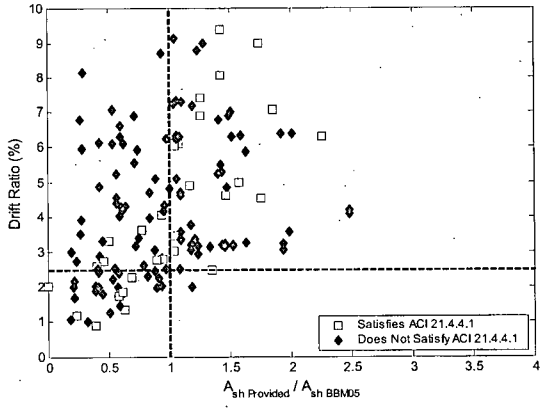

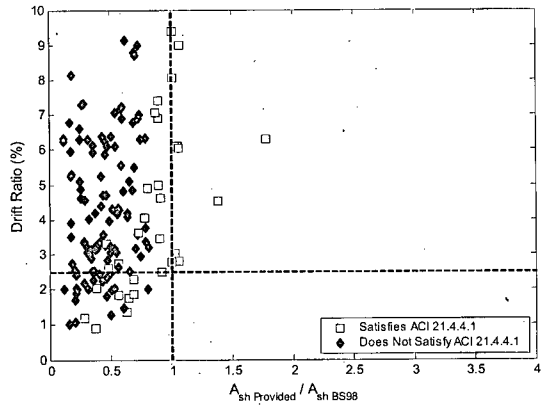

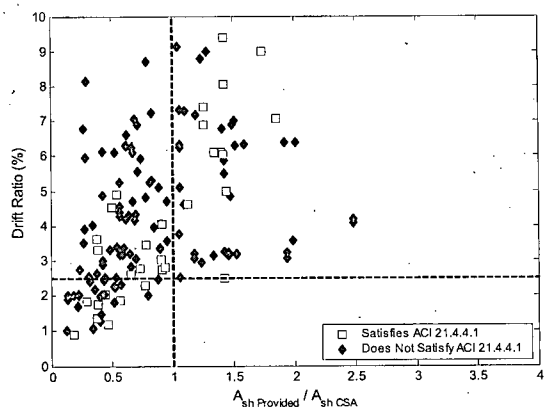

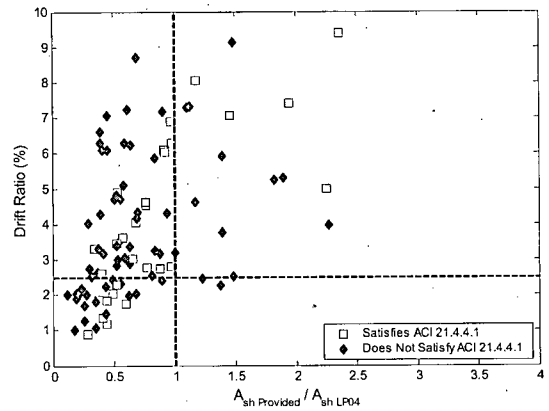

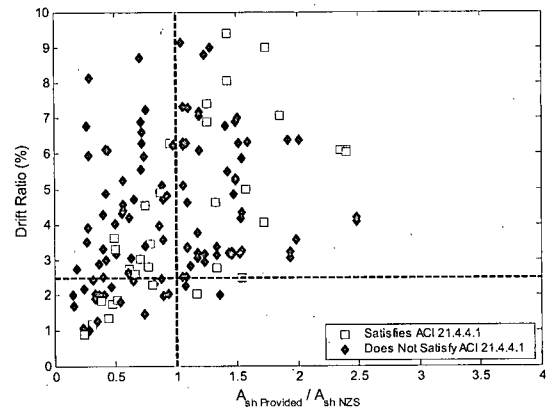

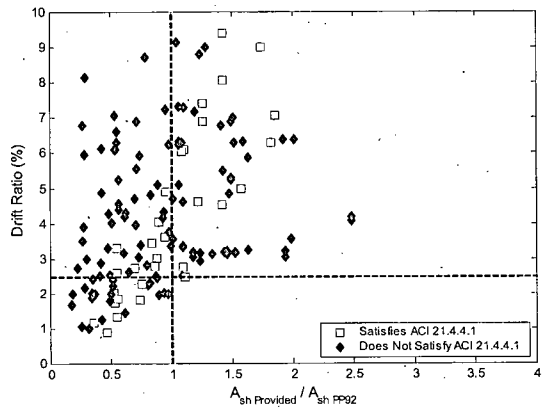
Drift Ratio (%)
$A_{sh\ Provided}$ / $A_{sh\ PP92}$
Satisfies ACI 21.4.4.1
Does Not Satisfy ACI 21.4.4.1

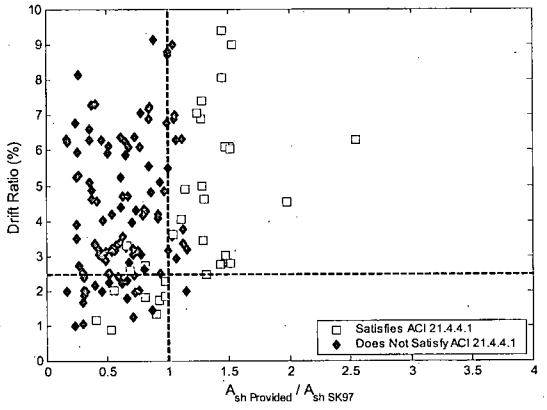
Drift Ratio (%)
$A_{sh\ Provided}$ / $A_{sh\ SK97}$
Satisfies ACI 21.4.4.1
Does Not Satisfy ACI 21.4.4.1

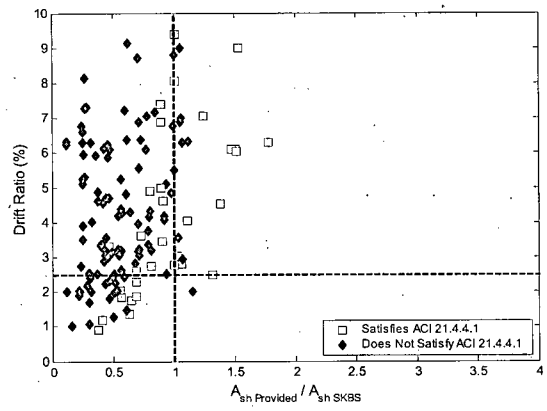
Drift Ratio (%)
$A_{sh\ Provided}$ / $A_{sh\ SKBS}$
Satisfies ACI 21.4.4.1
Does Not Satisfy ACI 21.4.4.1

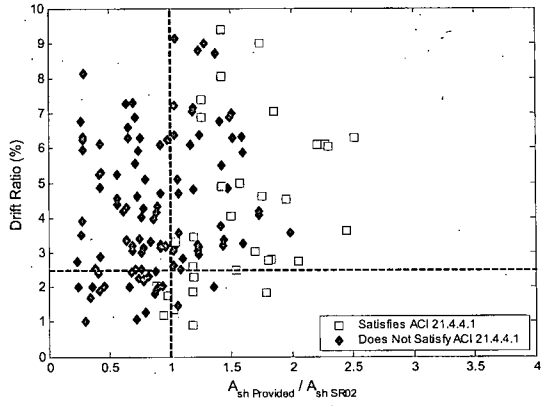
Drift Ratio (%)
$A_{sh\ Provided}$ / $A_{sh\ SR02}$
Satisfies ACI 21.4.4.1
Does Not Satisfy ACI 21.4.4.1

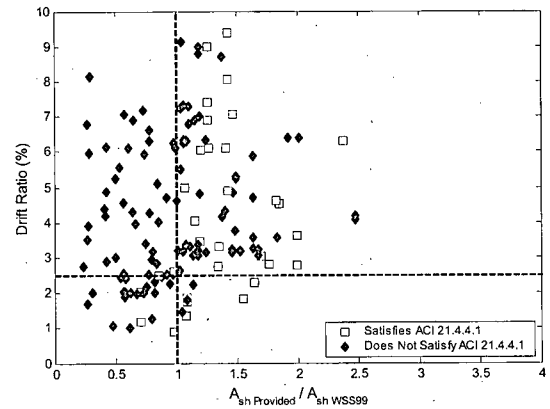
Drift Ratio (%)
$A_{sh\ Provided}$ / $A_{sh\ WSS99}$
Satisfies ACI 21.4.4.1
Does Not Satisfy ACI 21.4.4.1

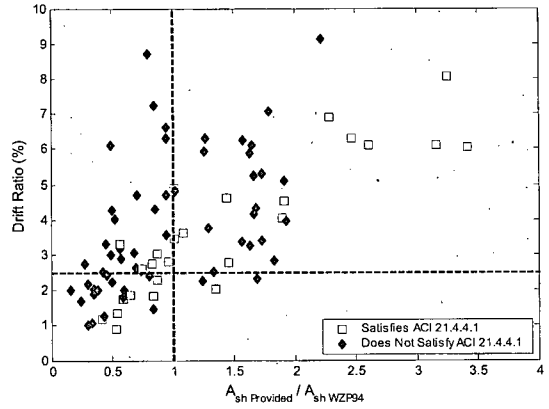
Drift Ratio (%)
$A_{sh\ Provided}$ / $A_{sh\ WZP94}$
Satisfies ACI 21.4.4.1
Does Not Satisfy ACI 21.4.4.1

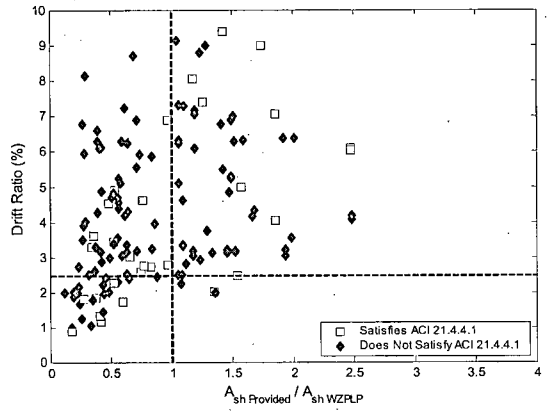

Table D.1 Rectangular scatter plot statistics (with ACI limit)

Model	A	B	C
ACI	28.1	18.6	-9.5
A23	2.0	30.9	28.9
PP92	1.6	34.9	33.3
SR02	11.6	28.9	17.4
WSS99	9.6	35.5	25.8
BBM05	2.9	36.8	33.9
SK97	5.6	25.7	20.1
BS98	0.0	22.4	22.4
SKBS	8.3	23.1	14.8
WZP94	10.4	25.8	15.4
LP04	13.3	22.6	9.3
WZPLP	6.6	31.0	24.4
NZS	5.7	34.7	29.0

D.2 Rectangular Column Scatter Plots (without ACI Minimum)

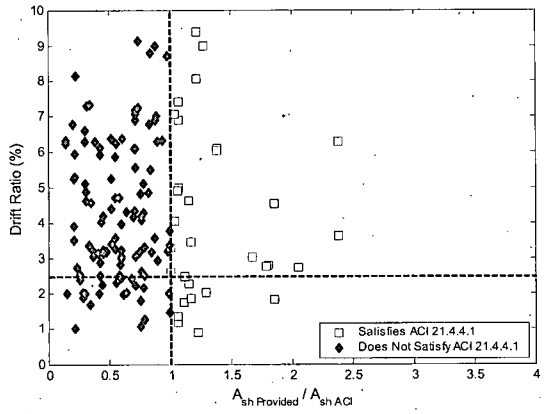

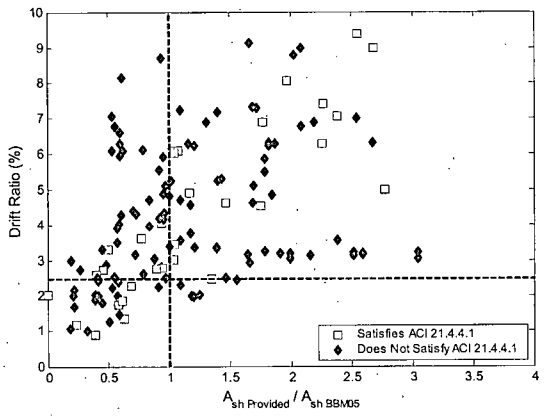

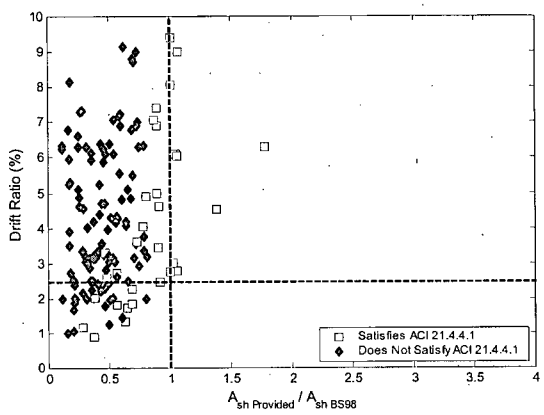
Drift Ratio (%)
Satisfies ACI 21.4.4.1
Does Not Satisfy ACI 21.4.4.1
$A_{sh\ Provided} / A_{sh\ BS98}$

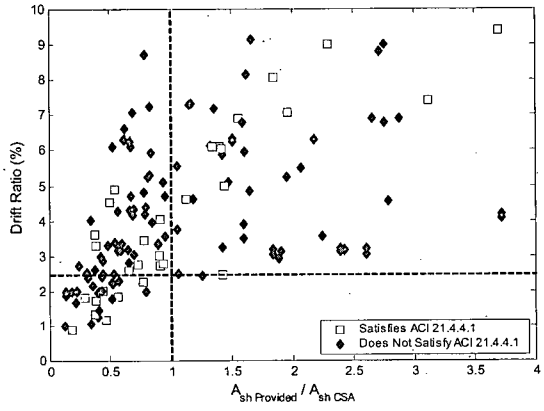
Drift Ratio (%)
Satisfies ACI 21.4.4.1
Does Not Satisfy ACI 21.4.4.1
$A_{sh\ Provided} / A_{sh\ CSA}$

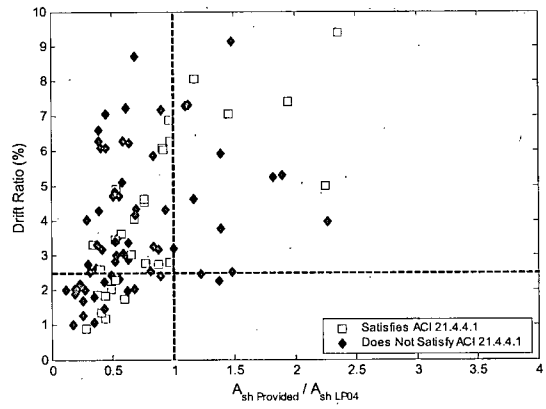
Drift Ratio (%)
Satisfies ACI 21.4.4.1
Does Not Satisfy ACI 21.4.4.1
$A_{sh\ Provided} / A_{sh\ LP04}$

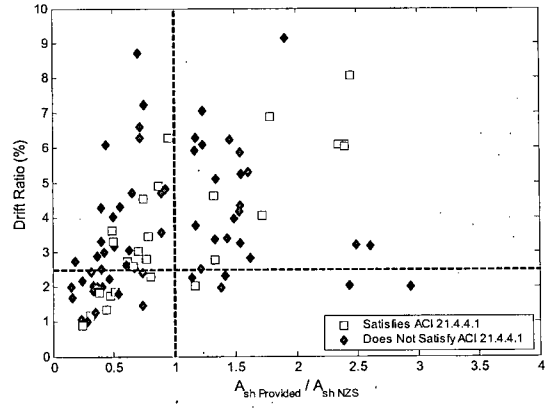
Drift Ratio (%)
Satisfies ACI 21.4.4.1
Does Not Satisfy ACI 21.4.4.1
$A_{sh\ Provided} / A_{sh\ NZS}$

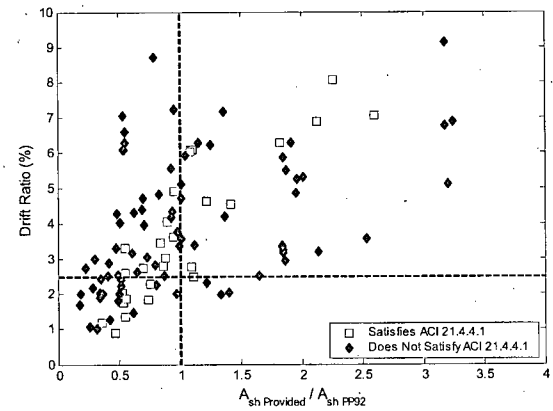
Drift Ratio (%)
Satisfies ACI 21.4.4.1
Does Not Satisfy ACI 21.4.4.1
$A_{sh\ Provided} / A_{sh\ PP92}$

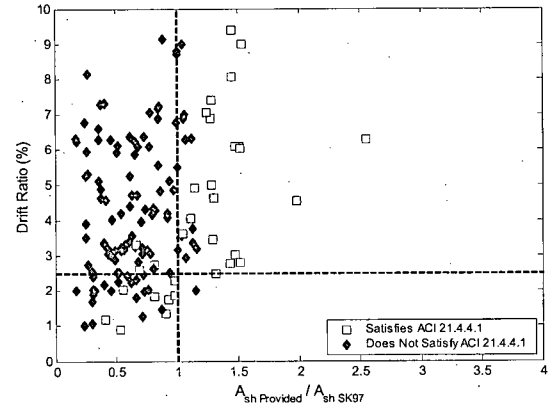
Drift Ratio (%)
Satisfies ACI 21.4.4.1
Does Not Satisfy ACI 21.4.4.1
$A_{sh\ Provided} / A_{sh\ SK97}$

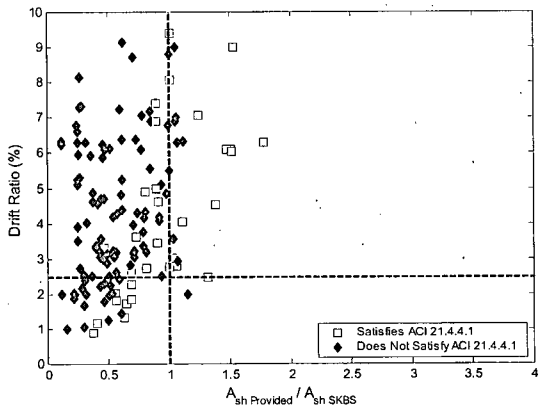
Drift Ratio (%)
Satisfies ACI 21.4.4.1
Does Not Satisfy ACI 21.4.4.1
$A_{sh\ Provided} / A_{sh\ SKBS}$

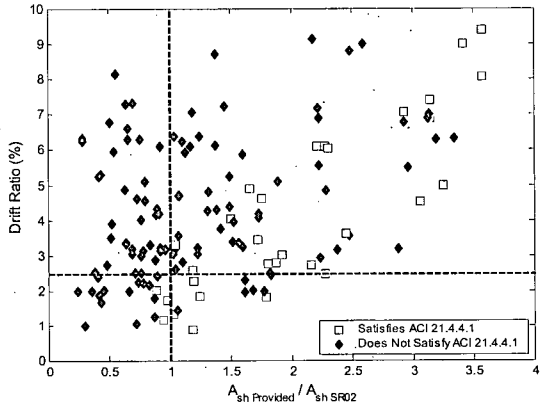
Drift Ratio (%)
Satisfies ACI 21.4.4.1
Does Not Satisfy ACI 21.4.4.1
$A_{sh\ Provided} / A_{sh\ SR02}$

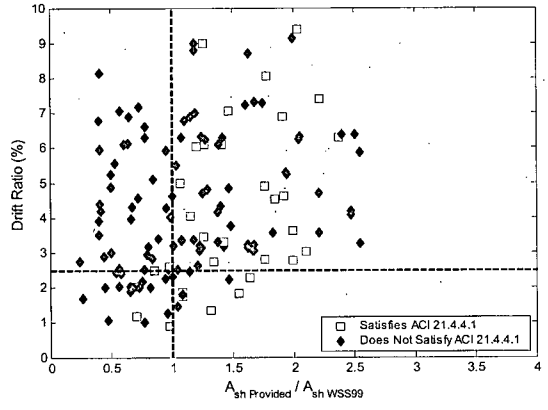
Drift Ratio (%)
Satisfies ACI 21.4.4.1
Does Not Satisfy ACI 21.4.4.1
$A_{sh\ Provided} / A_{sh\ WSS99}$

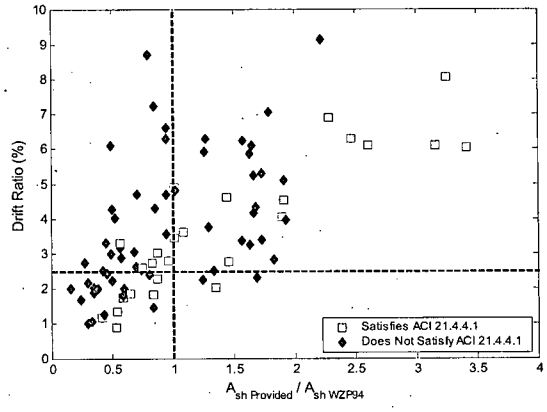
Drift Ratio (%)
Satisfies ACI 21.4.4.1
Does Not Satisfy ACI 21.4.4.1
$A_{sh\ Provided} / A_{sh\ WZP94}$

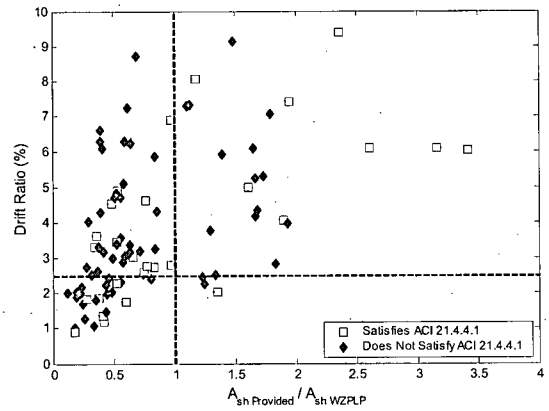
Drift Ratio (%)
Satisfies ACI 21.4.4.1
Does Not Satisfy ACI 21.4.4.1
$A_{sh\ Provided} / A_{sh\ WZPLP}$

Table D.2 Rectangular scatter plot statistics (without ACI limit)

Model	A	B	C
ACI	28.1	18.6	-9.5
A23	3.2	34.1	31.0
PP92	7.4	32.5	25.1
SR02	14.1	30.0	15.9
WSS99	11.2	35.7	24.5
BBM05	7.7	35.8	28.1
SK97	5.6	25.7	20.1
BS98	0.0	22.4	22.4
SKBS	8.3	23.1	14.8
WZP94	10.4	25.8	15.4
LP04	13.3	22.6	9.3
WZPLP	12.5	23.0	10.5
NZS	14.3	24.0	9.7

D.3 Rectangular Column Scatter Plots (Maximum Recorded Drifts)

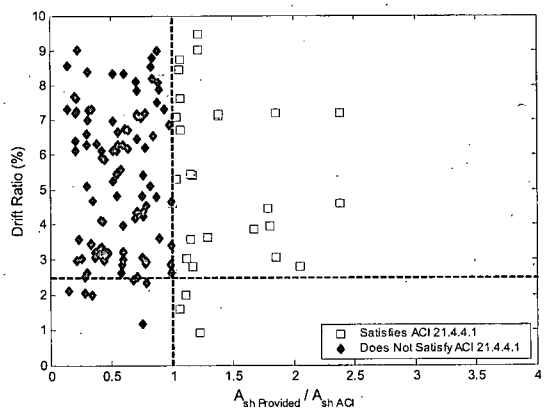

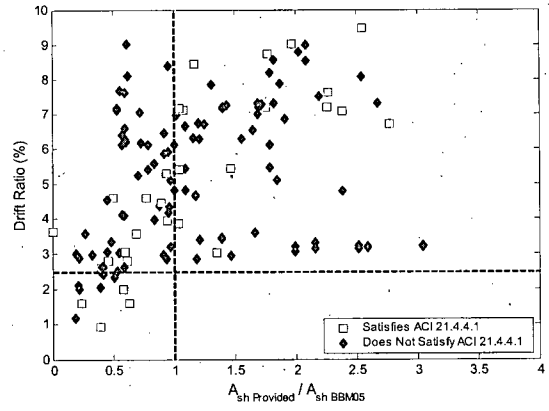

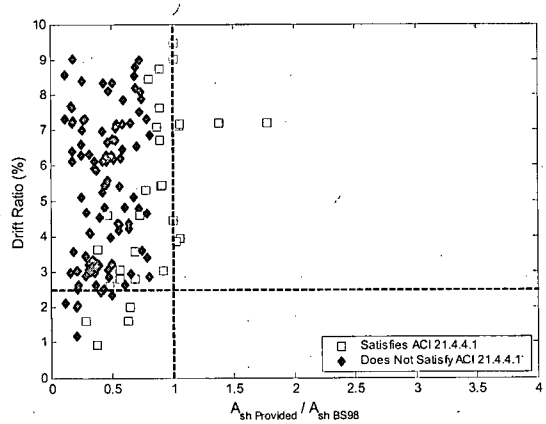

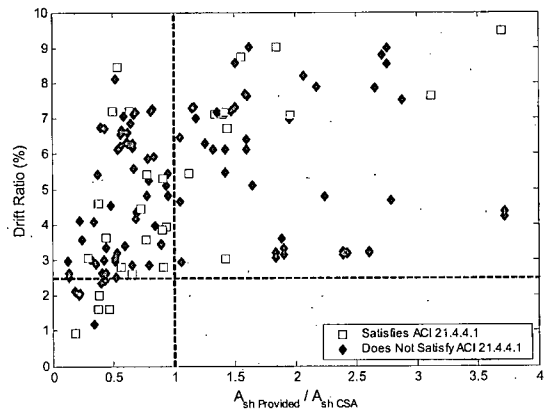

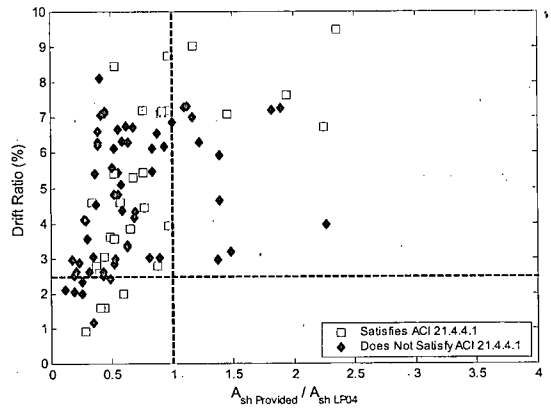
Drift Ratio (%)
Satisfies ACI 21.4.4.1
Does Not Satisfy ACI 21.4.4.1
$A_{sh\ Provided} / A_{sh\ LP04}$

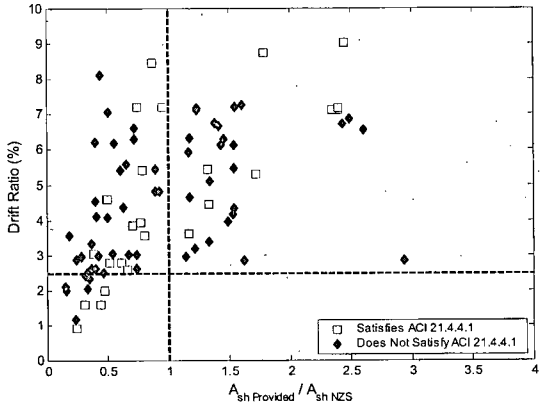
Drift Ratio (%)
Satisfies ACI 21.4.4.1
Does Not Satisfy ACI 21.4.4.1
$A_{sh\ Provided} / A_{sh\ NZS}$

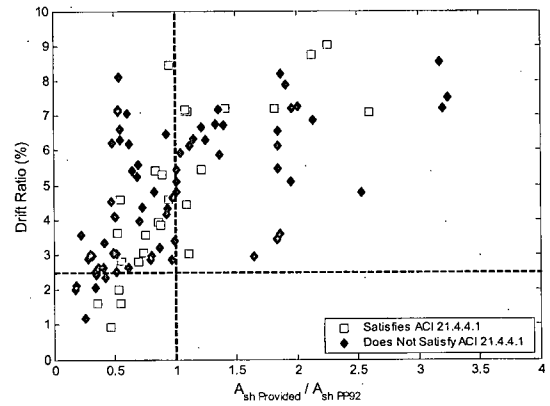
Drift Ratio (%)
Satisfies ACI 21.4.4.1
Does Not Satisfy ACI 21.4.4.1
$A_{sh\ Provided} / A_{sh\ PP92}$

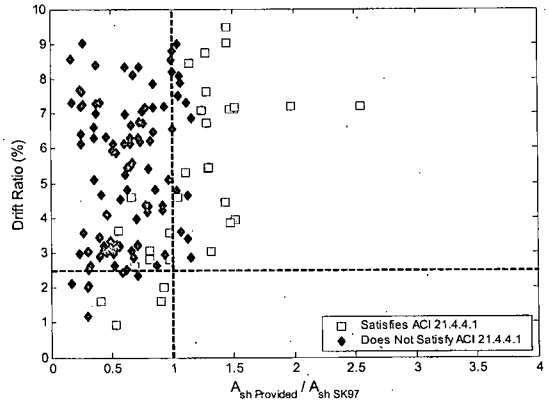
Drift Ratio (%)
Satisfies ACI 21.4.4.1
Does Not Satisfy ACI 21.4.4.1
$A_{sh\ Provided} / A_{sh\ SK97}$

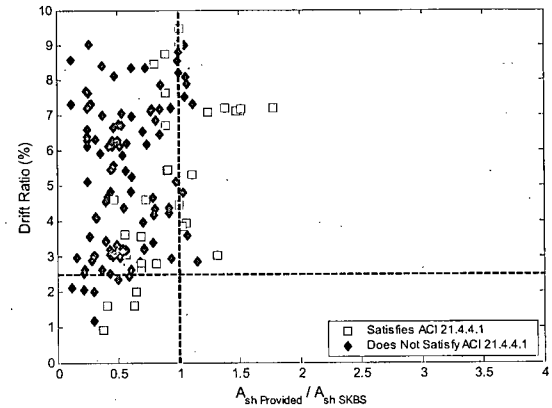
Drift Ratio (%)
Satisfies ACI 21.4.4.1
Does Not Satisfy ACI 21.4.4.1
$A_{sh\ Provided} / A_{sh\ SKBS}$

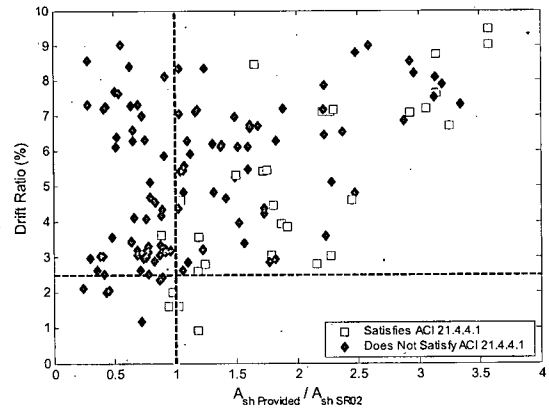
Drift Ratio (%)
Satisfies ACI 21.4.4.1
Does Not Satisfy ACI 21.4.4.1
$A_{sh\ Provided} / A_{sh\ SR02}$

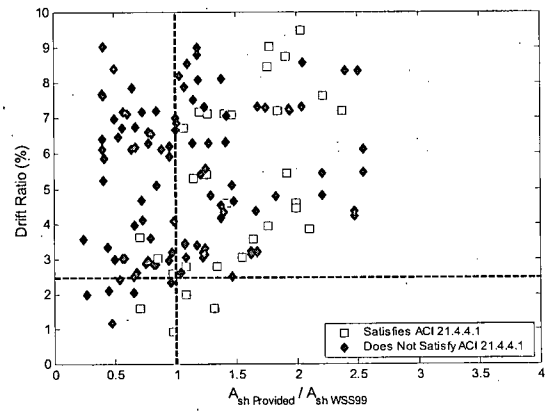

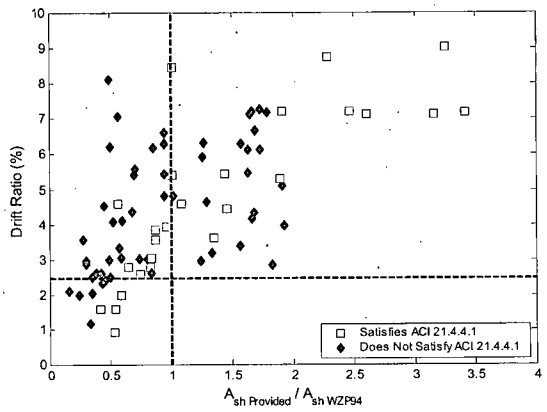

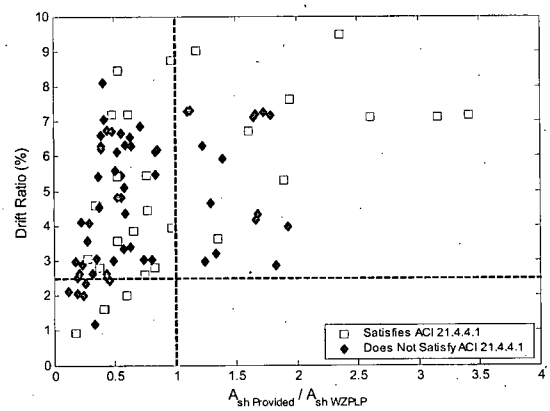

Table D.3 Rectangular scatter plot statistics (Maximum Recorded Drift)

Model	A	B	C
ACI	12.5	5.3	-7.2
A23	0	12.2	12.2
PP92	0	13.0	12.987
SR02	2.4	13.3	10.9
WSS99	2.2	14.3	12.1
BBM05	0	14.9	14.9
SK97	0	9.2	9.2
BS98	0	7.5	7.5
SKBS	0	8.3	8.3
WZP94	0	10.3	10.3
LP04	0	8.7	8.7
WZPLP	0	8.8	8.8
NZS	0	10.5	10.5

D.4 Rectangular Column A Fragility Curves (with ACI Minimum)

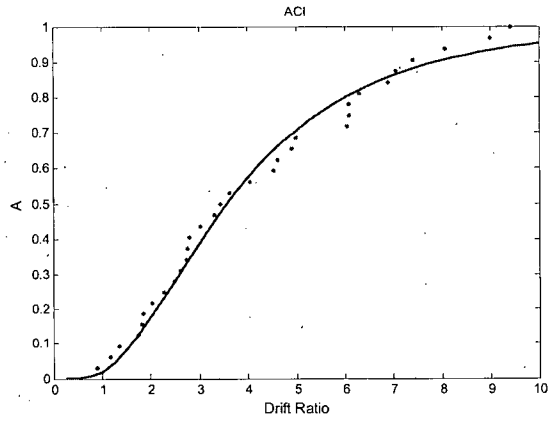

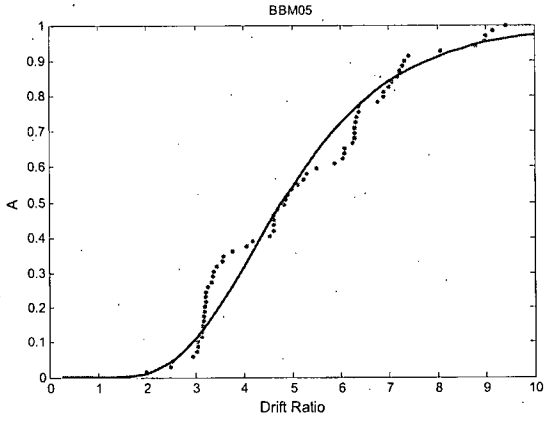

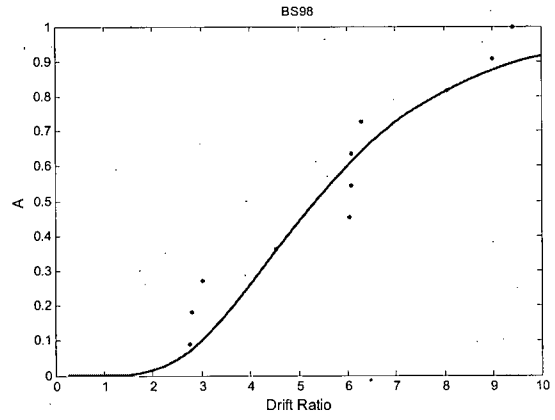

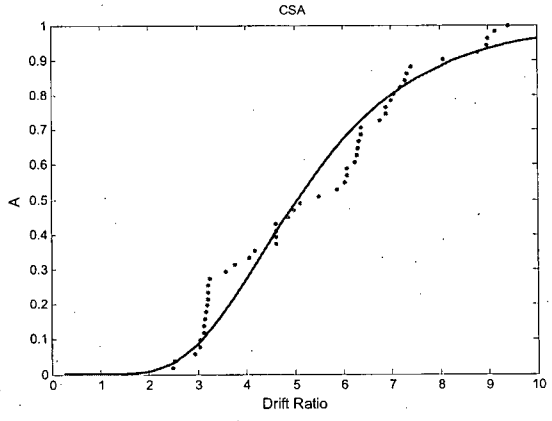

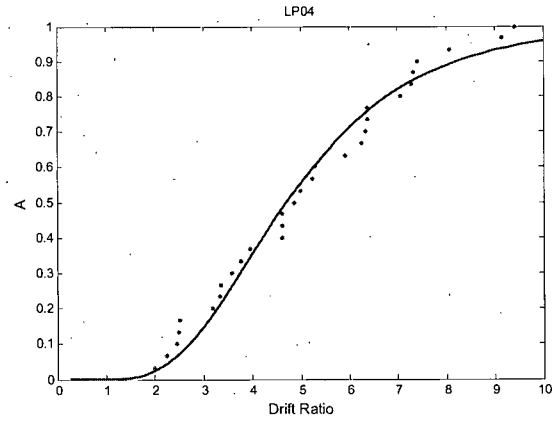

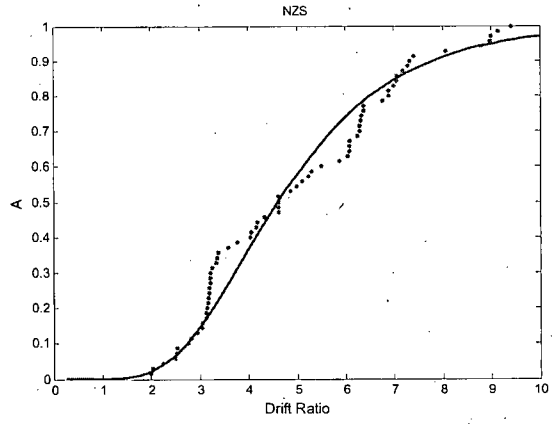

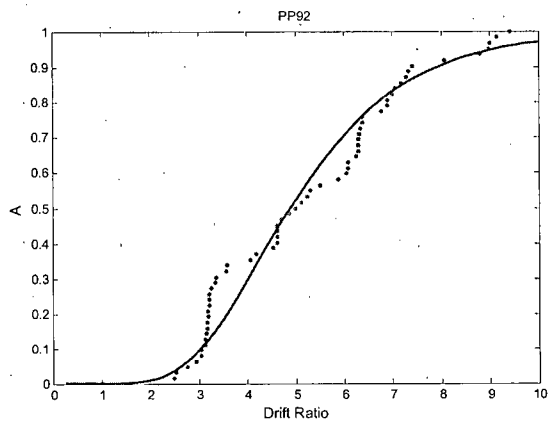
PP92
A
Drift Ratio

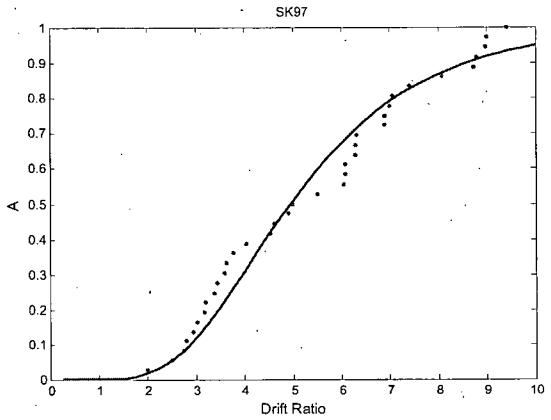
SK97
A
Drift Ratio

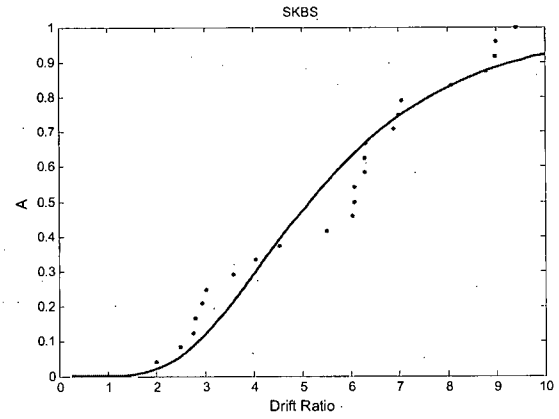
SKBS
A
Drift Ratio

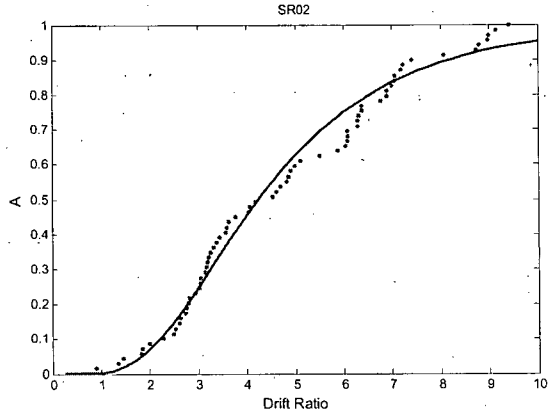
SR02
A
Drift Ratio

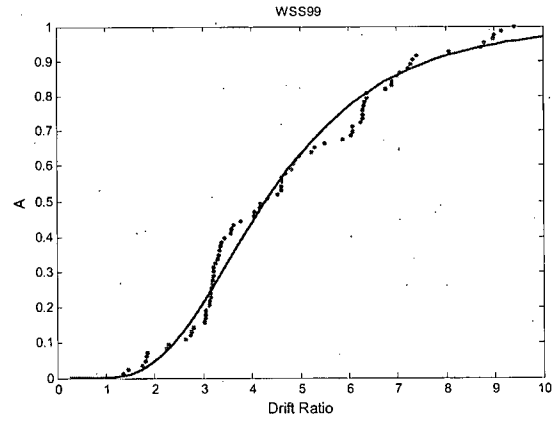
WSS99
A
Drift Ratio

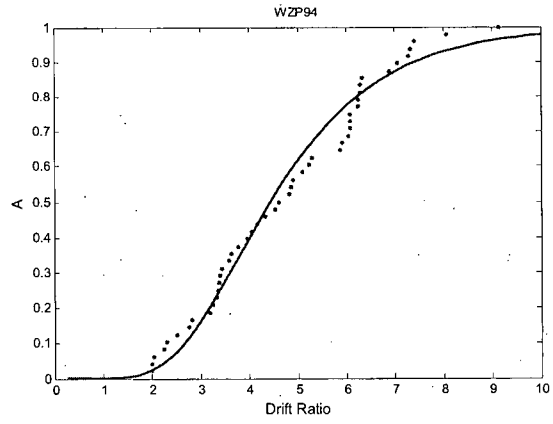
WZP94
A
Drift Ratio

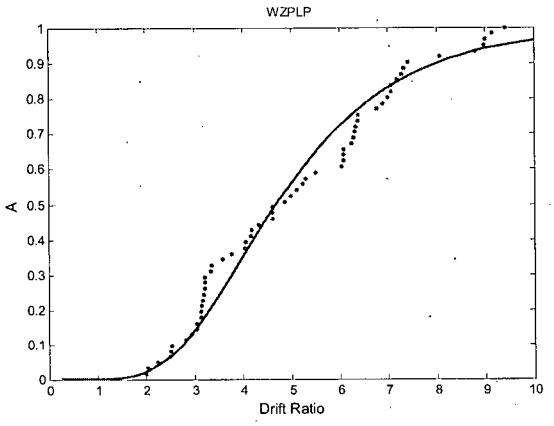

D.5 Rectangular Column B Fragility Curves (with ACI Minimum)

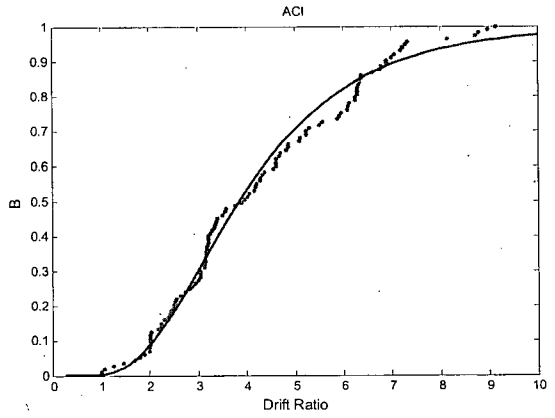

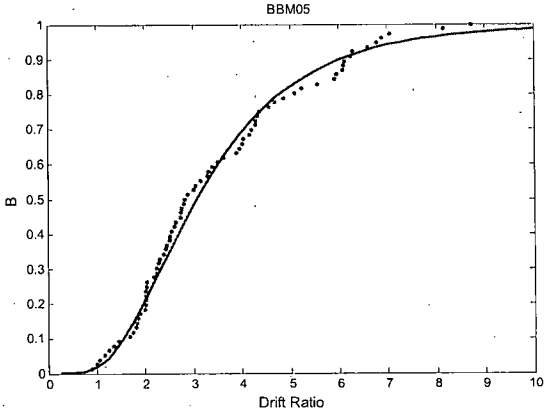

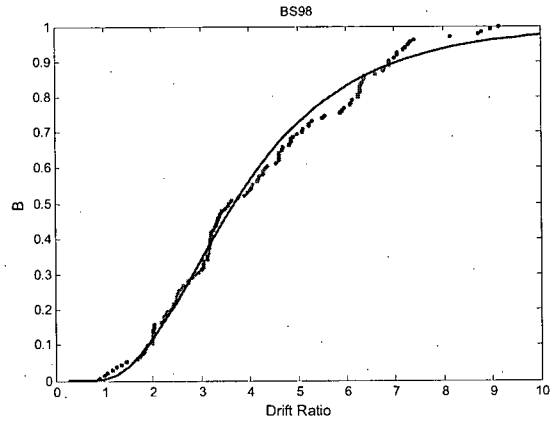

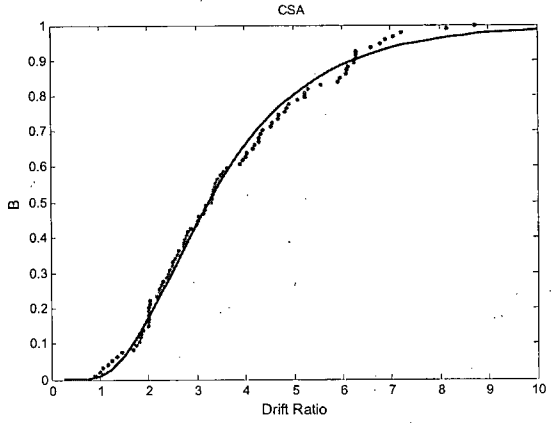

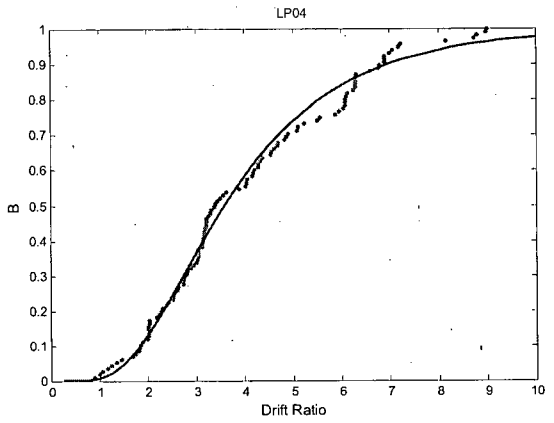
LP04
B
Drift Ratio

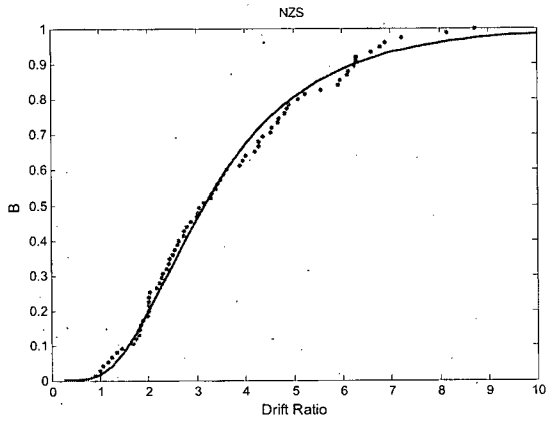
NZS
B
Drift Ratio

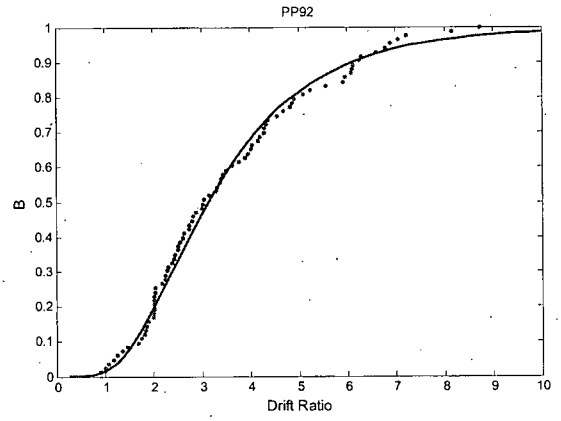
PP92
B
Drift Ratio

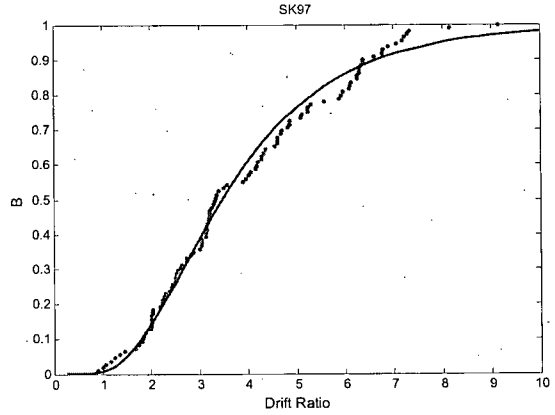
SK97
B
Drift Ratio

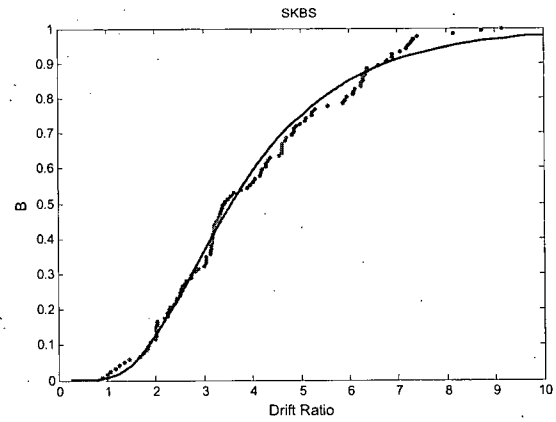
SKBS
B
Drift Ratio

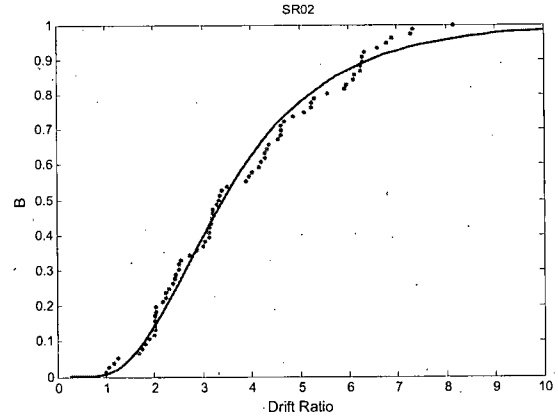
SR02
B
Drift Ratio

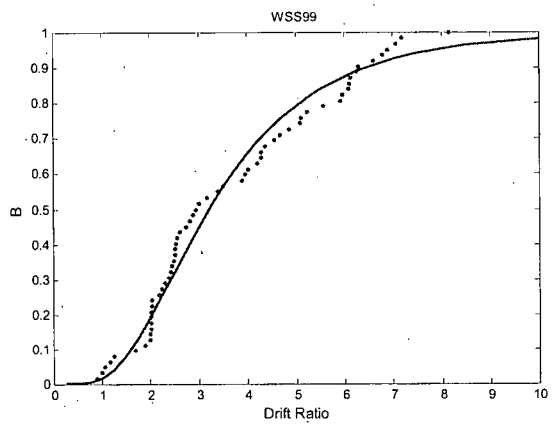

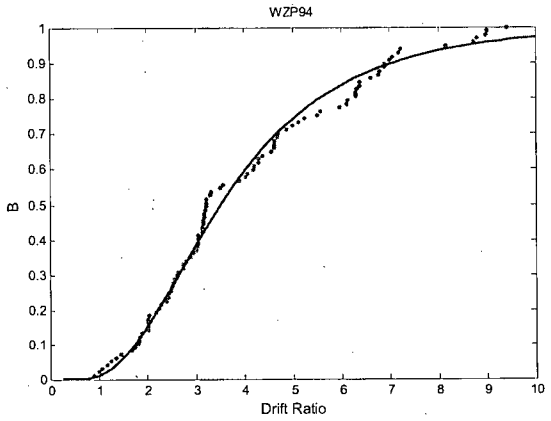

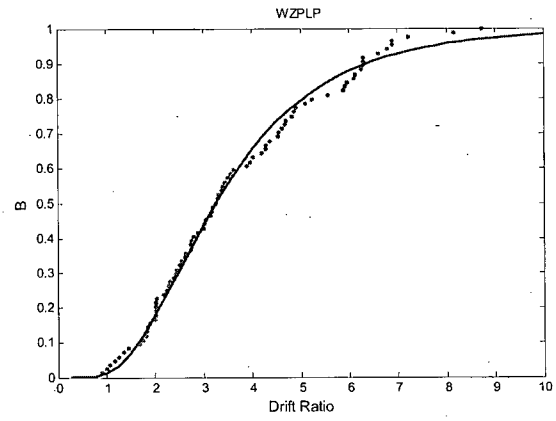

D.6 Rectangular Column C Fragility Curves (with ACI Minimum)

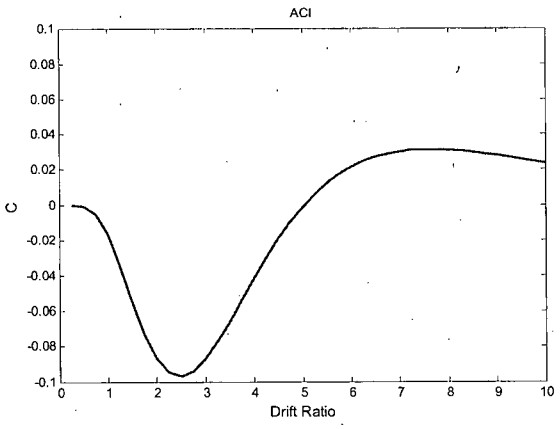

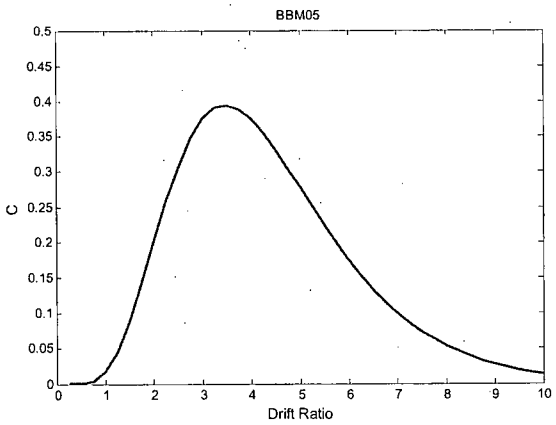

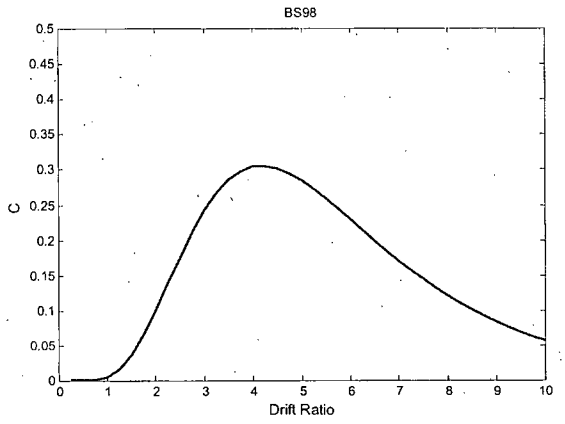
BS98
C
Drift Ratio

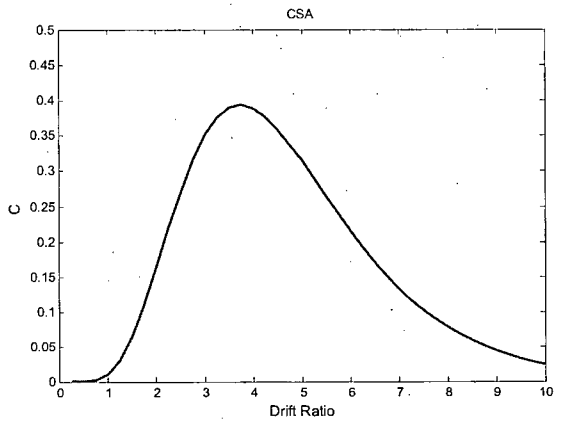
CSA
C
Drift Ratio

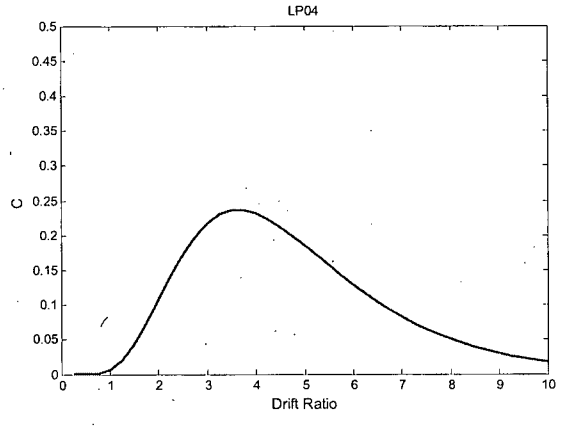
LP04
C
Drift Ratio

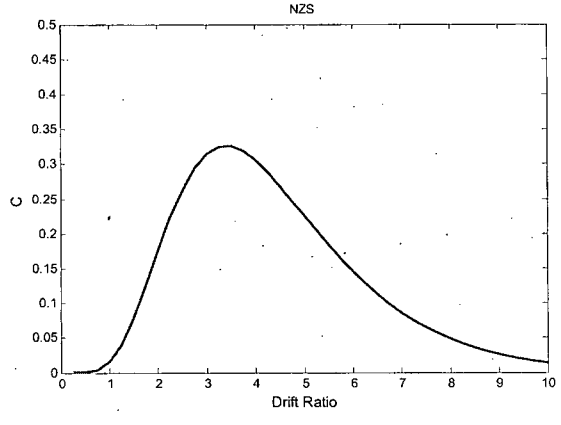
NZS
C
Drift Ratio

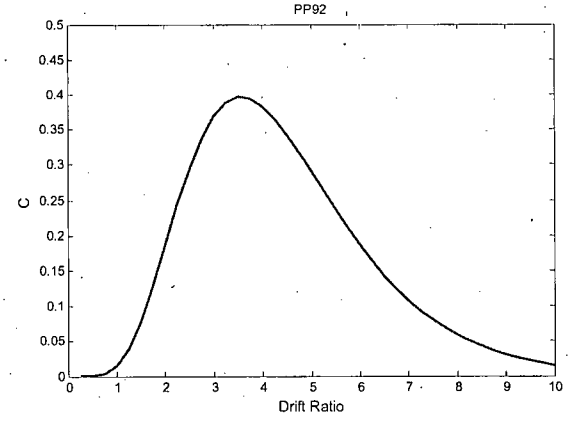
PP92
C
Drift Ratio

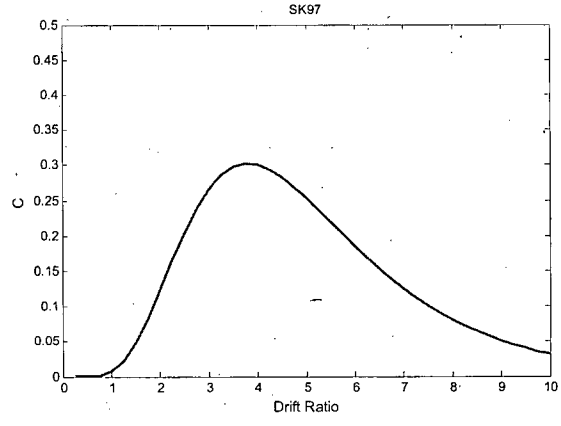
SK97
C
Drift Ratio

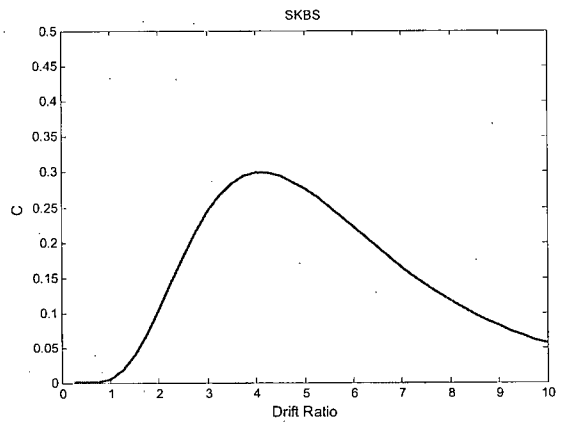
SKBS
C
Drift Ratio

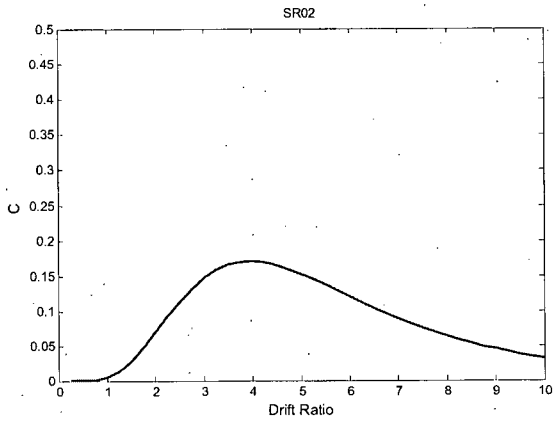
SR02
C
Drift Ratio

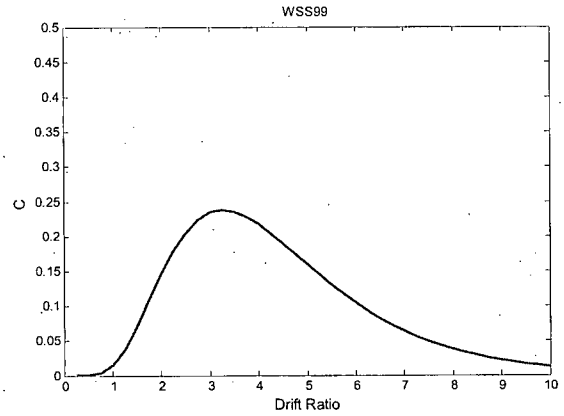
WSS99
C
Drift Ratio

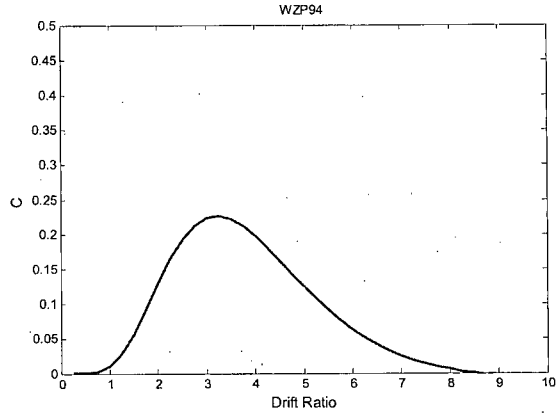
WZP94
C
Drift Ratio

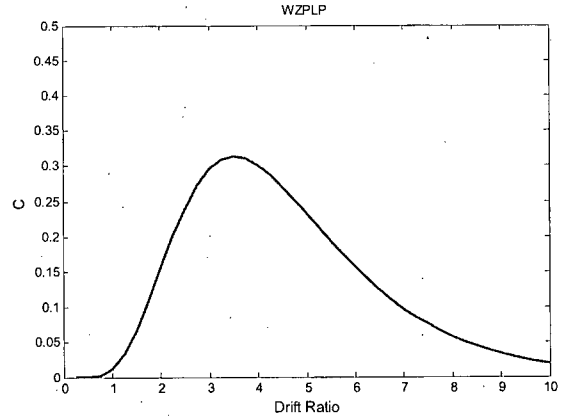
WZPLP
C
Drift Ratio

D.7 Rectangular Column A Fragility curves (without ACI Minimum)

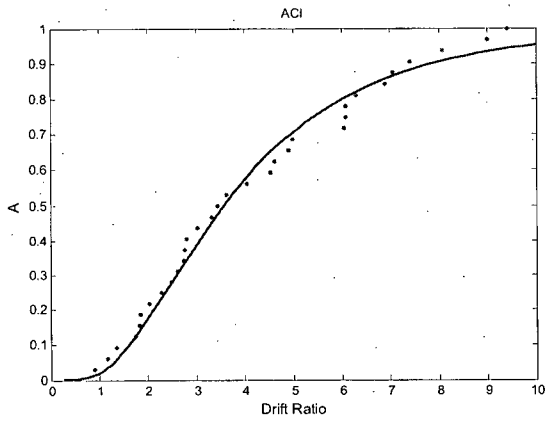

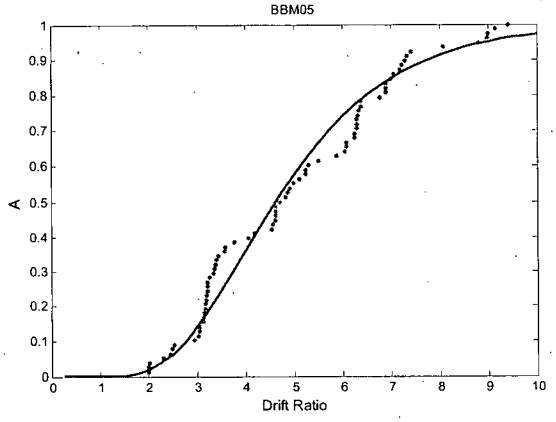

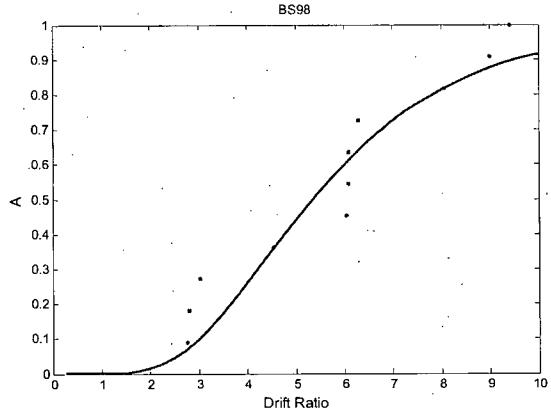

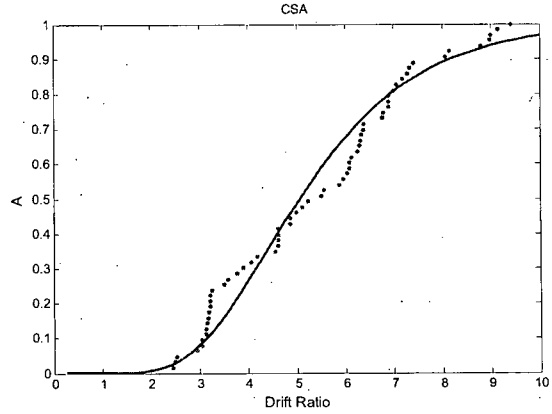

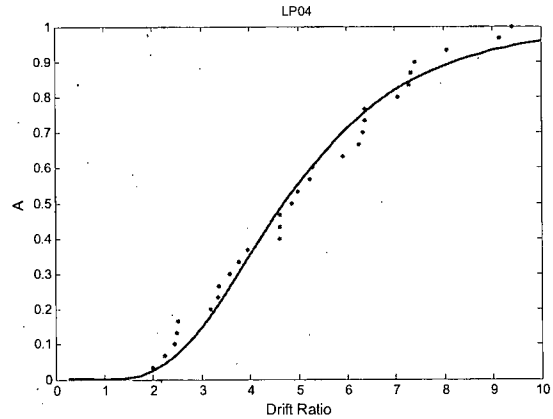

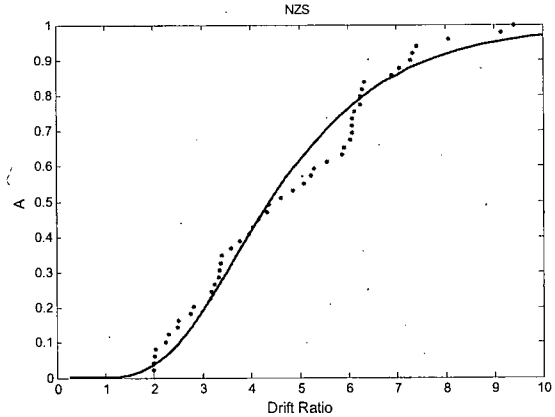

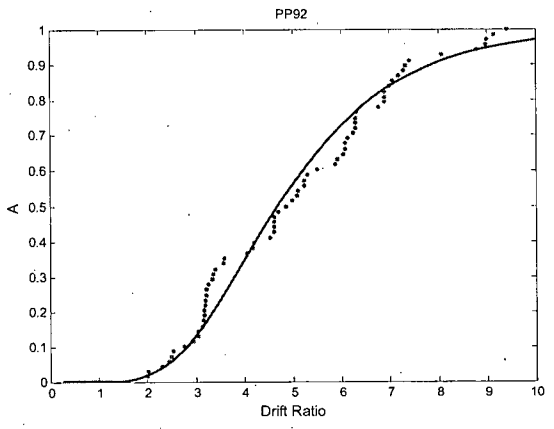
PP92
A
Drift Ratio

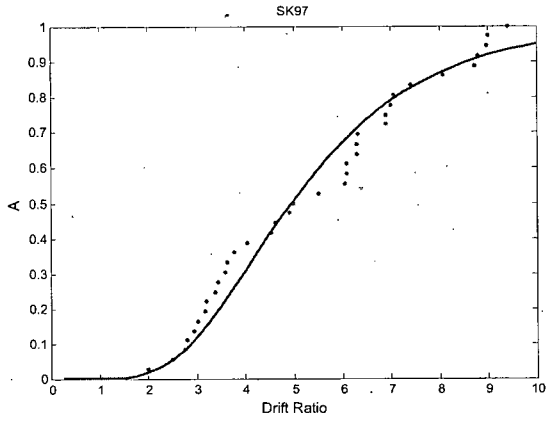
SK97
A
Drift Ratio

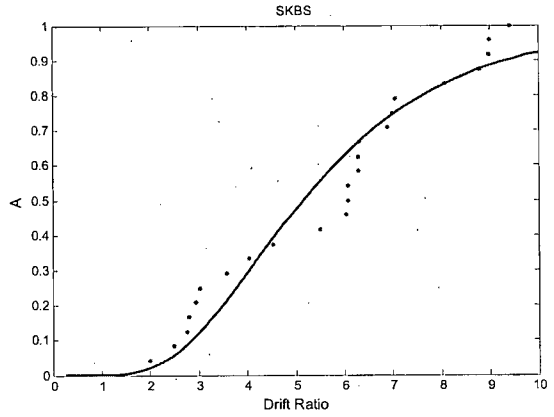
SKBS
A
Drift Ratio

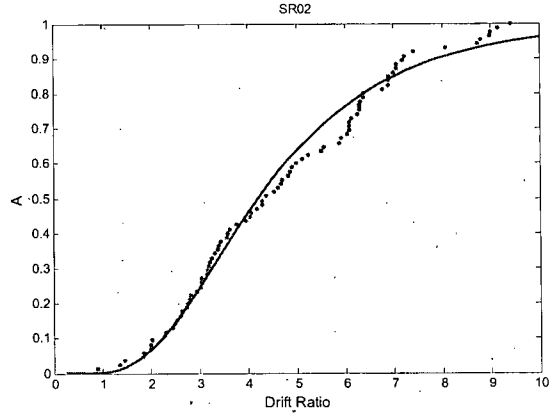
SR02
A
Drift Ratio

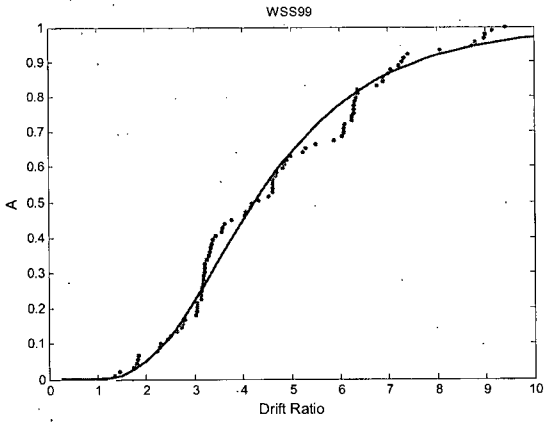
WSS99
A
Drift Ratio

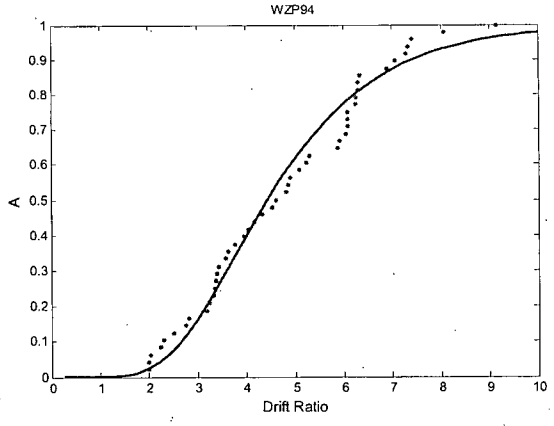
WZP94
A
Drift Ratio

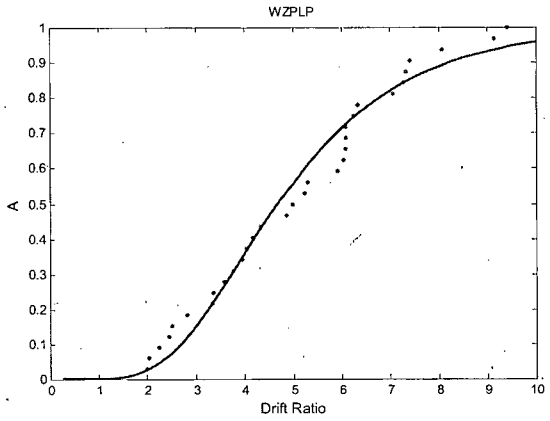

D.8 Rectangular Column B Fragility Curves (without ACI Minimum)

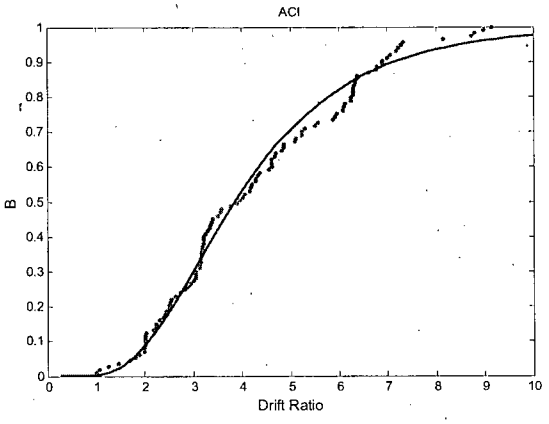

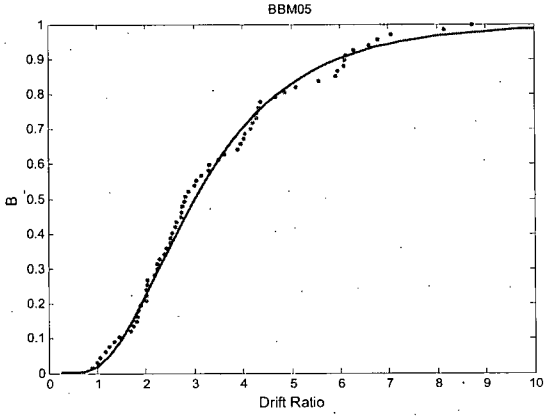

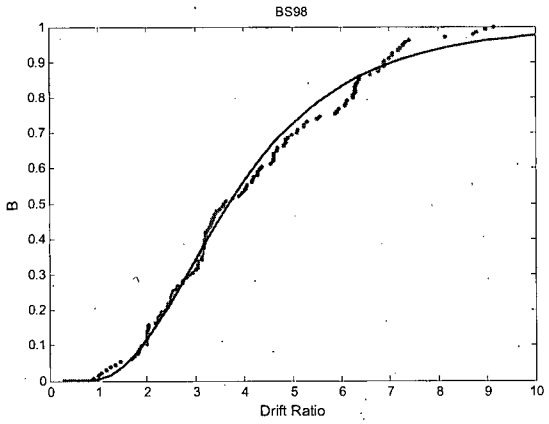

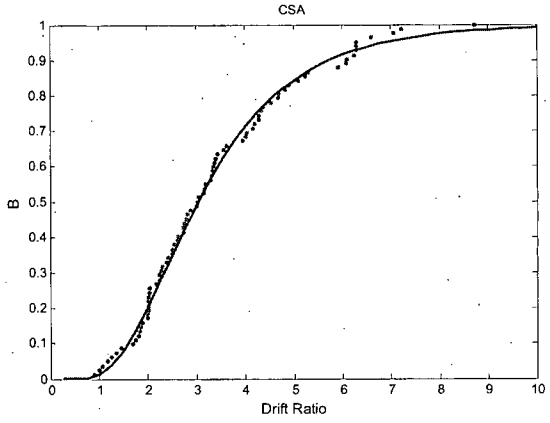

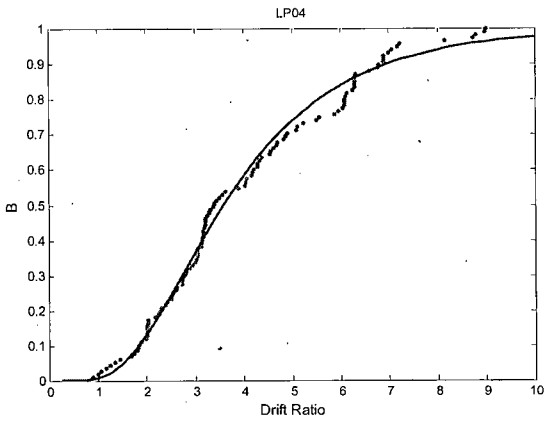
LP04
B
Drift Ratio

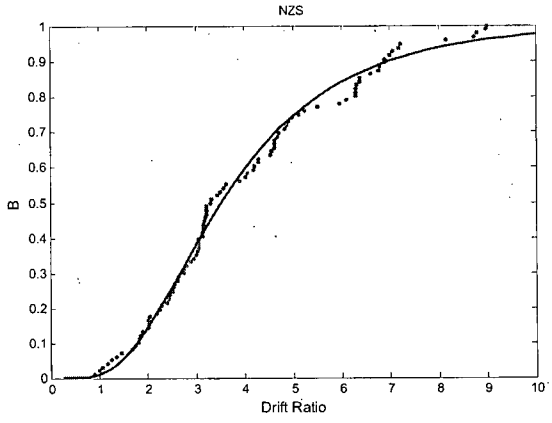
NZS
B
Drift Ratio

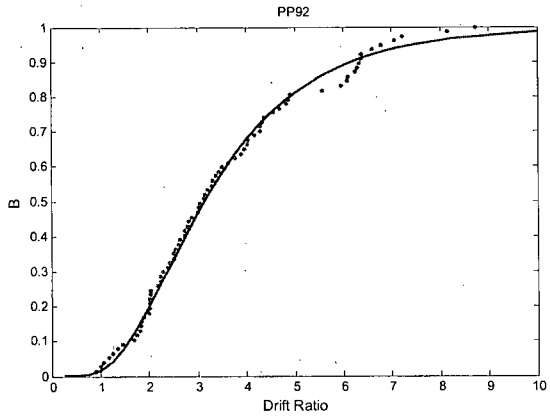
PP92
B
Drift Ratio

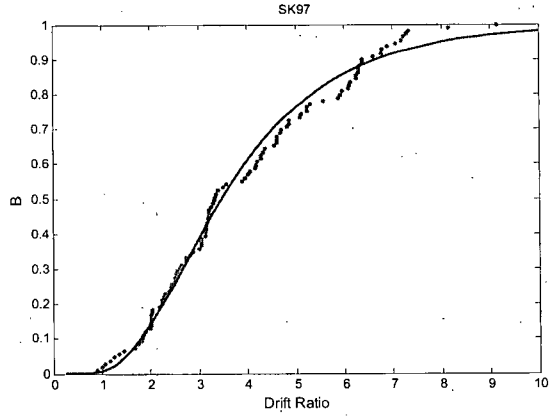
SK97
B
Drift Ratio

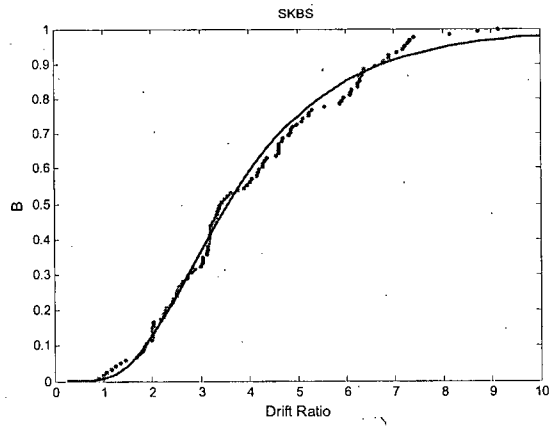
SKBS
B
Drift Ratio

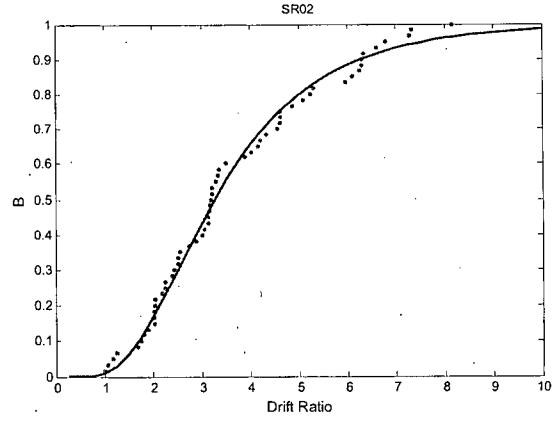
SR02
B
Drift Ratio

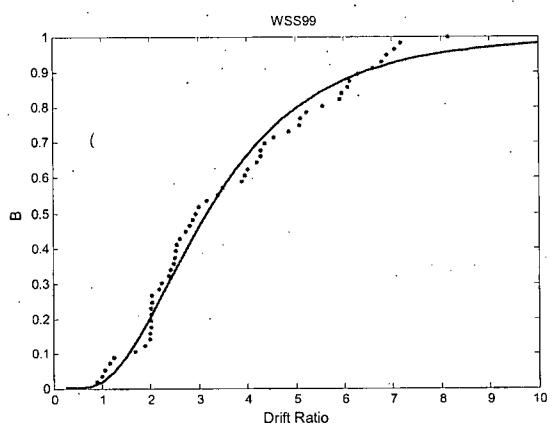

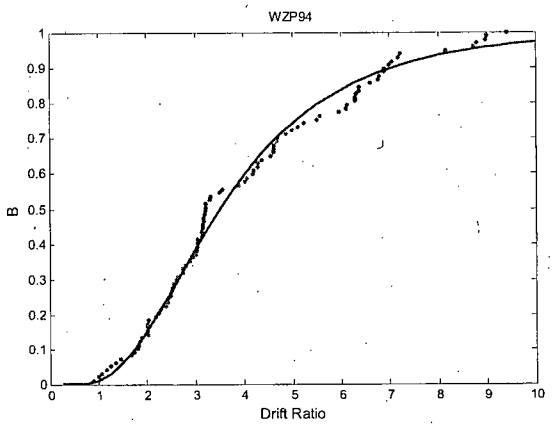

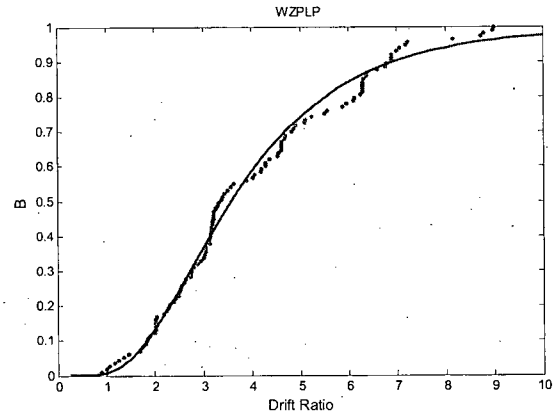

D.9 Rectangular Column C Fragility Curves (without ACI Minimum)

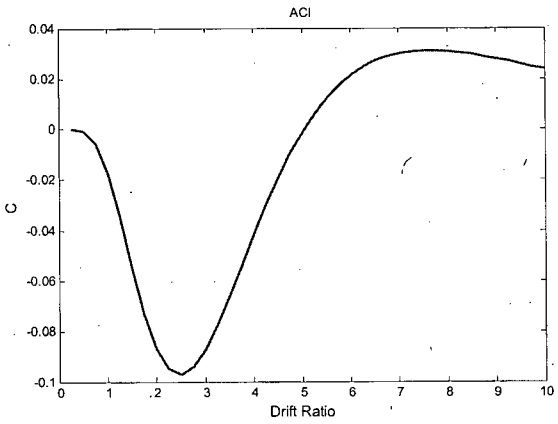

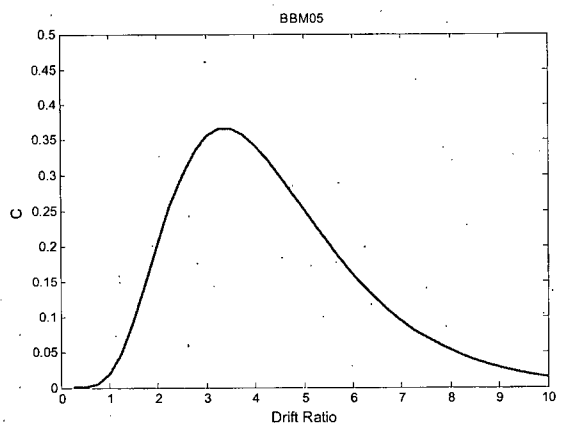

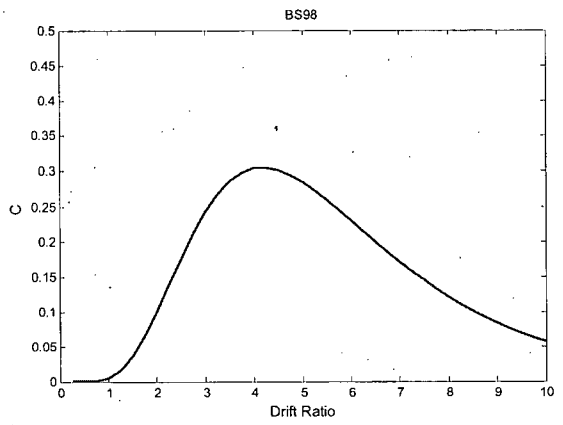
BS98
C
Drift Ratio

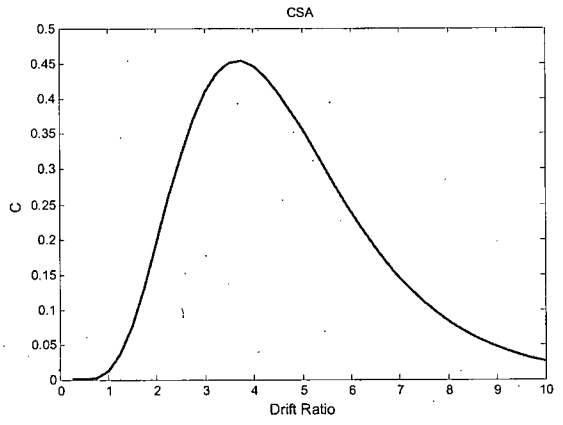
CSA
C
Drift Ratio

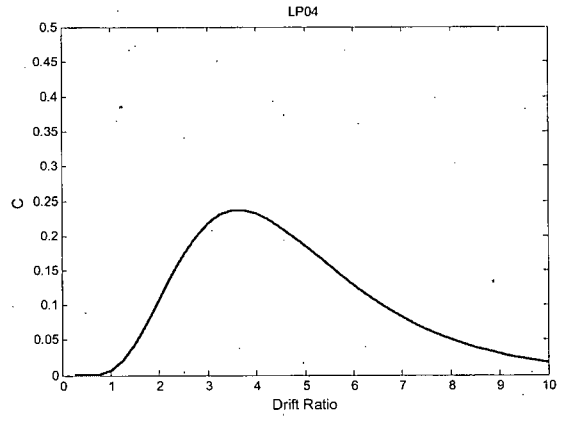
LP04
C
Drift Ratio

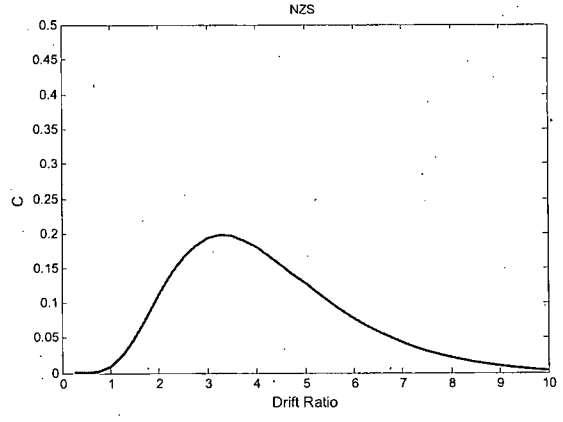
NZS
C
Drift Ratio

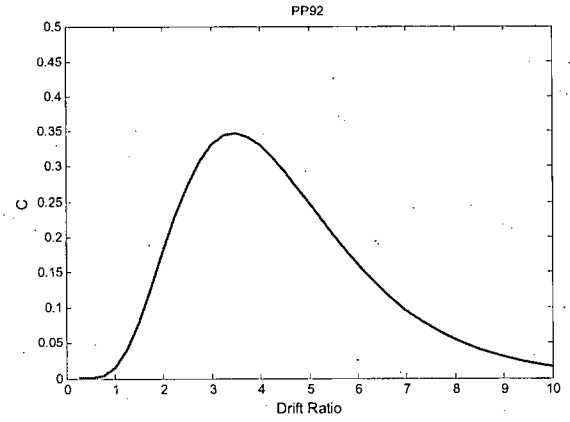
PP92
C
Drift Ratio

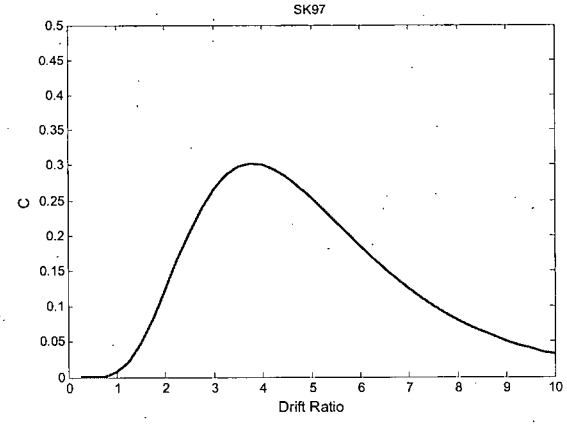
SK97
C
Drift Ratio

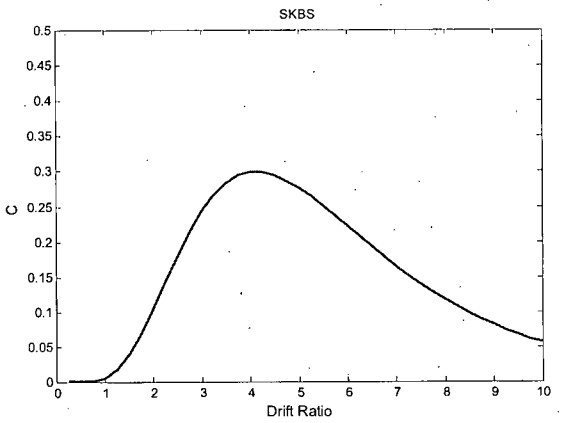
SKBS
C
Drift Ratio

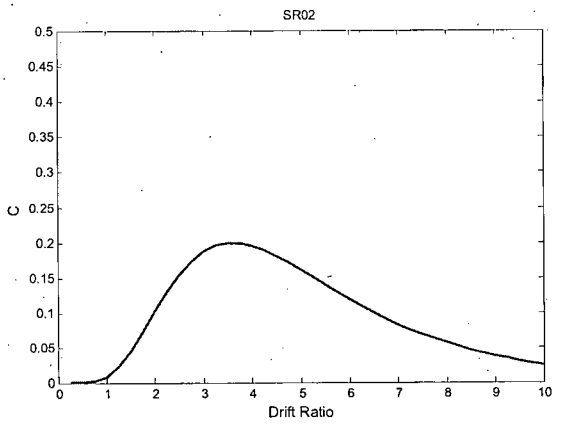
SR02
C
Drift Ratio

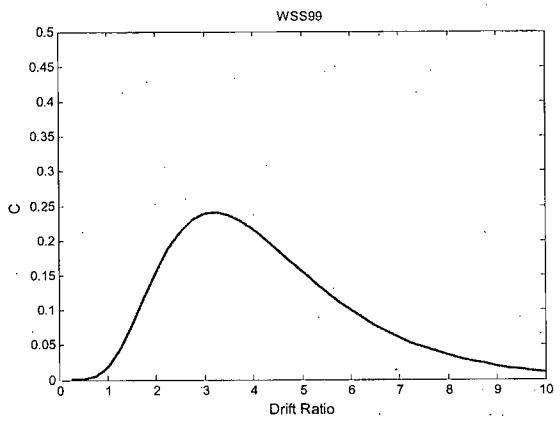
WSS99
C
Drift Ratio

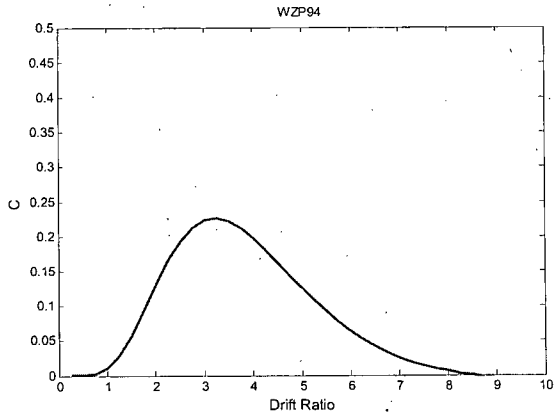
WZP94
C
Drift Ratio

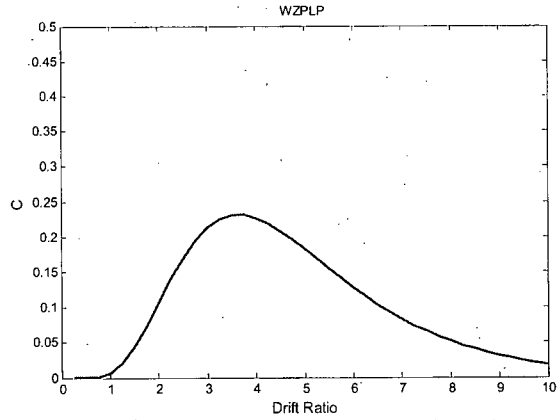
WZPLP
C
Drift Ratio

D.10 Rectangular Column A Fragility Curves (Maximum Recorded Drifts)

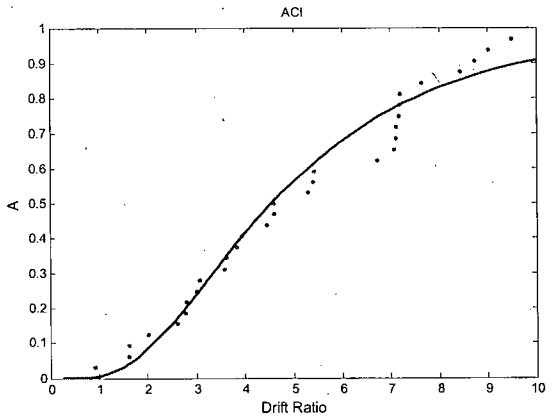

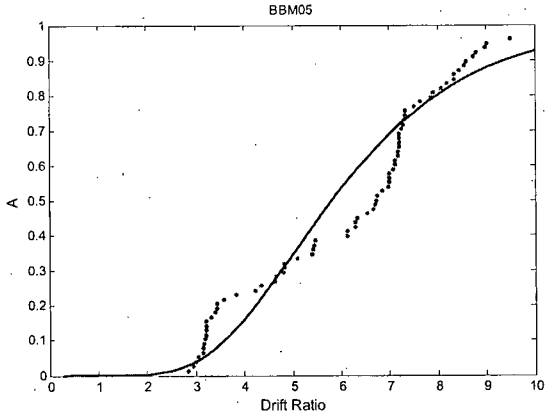

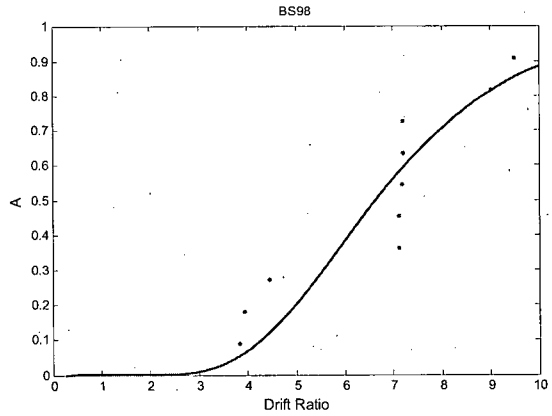

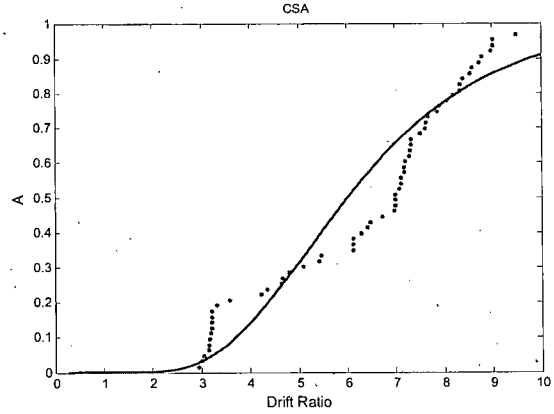

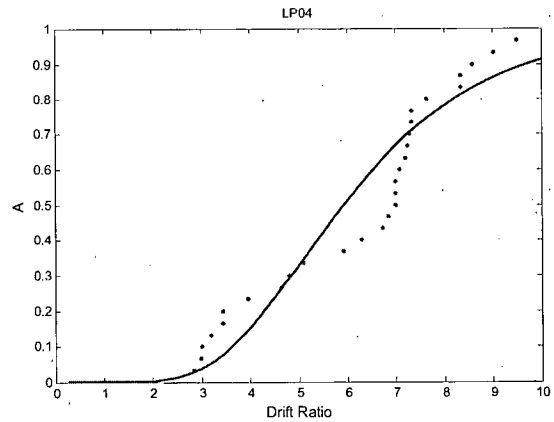

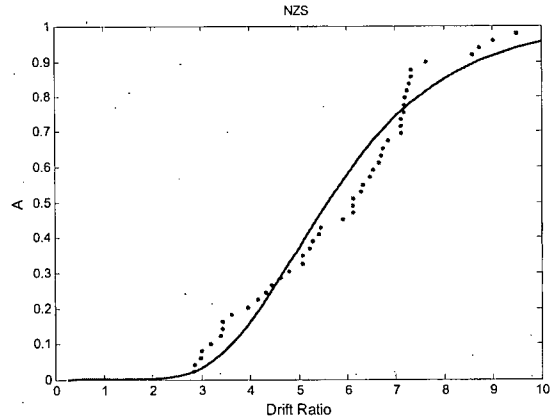

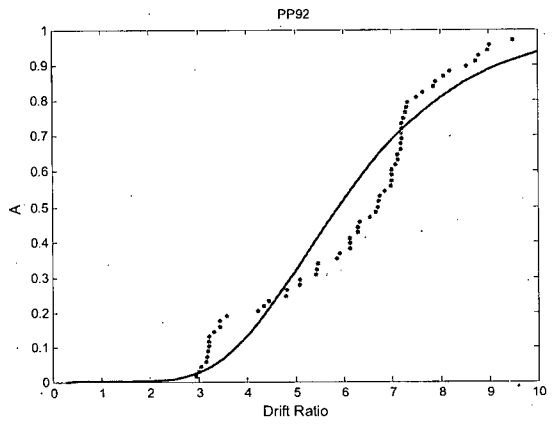
PP92
A
Drift Ratio

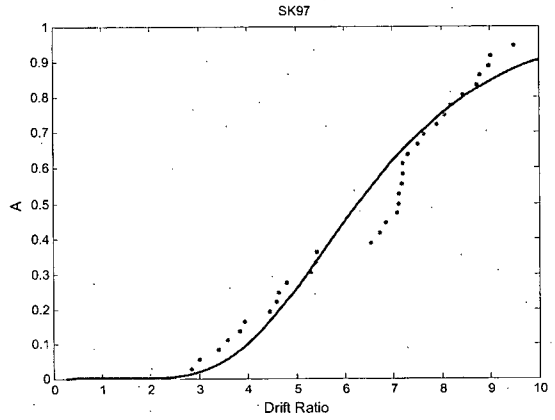
SK97
A
Drift Ratio

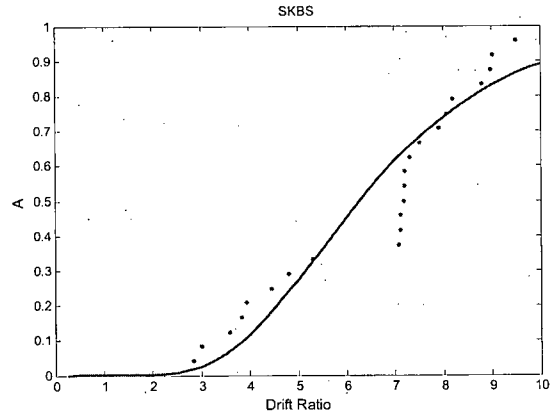
SKBS
A
Drift Ratio

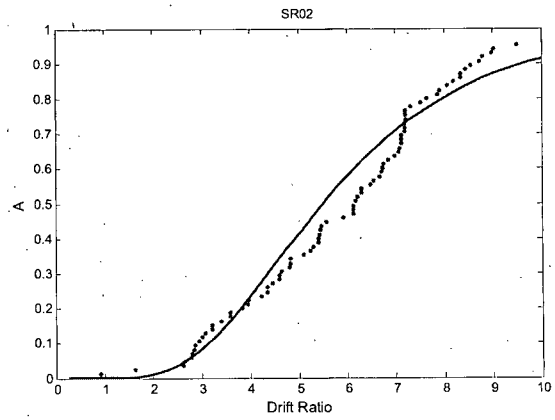
SR02
A
Drift Ratio

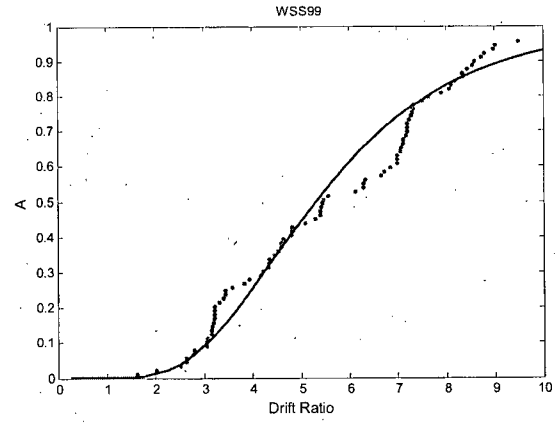
WSS99
A
Drift Ratio

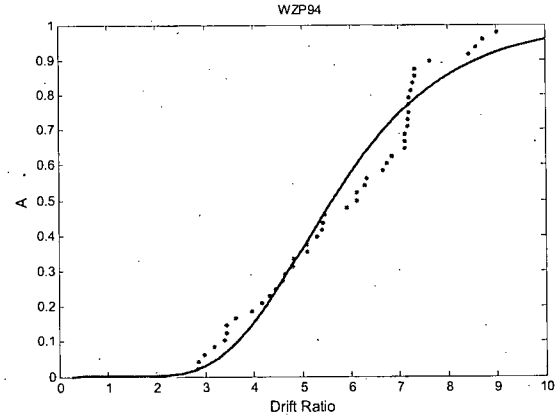
WZP94
A
Drift Ratio

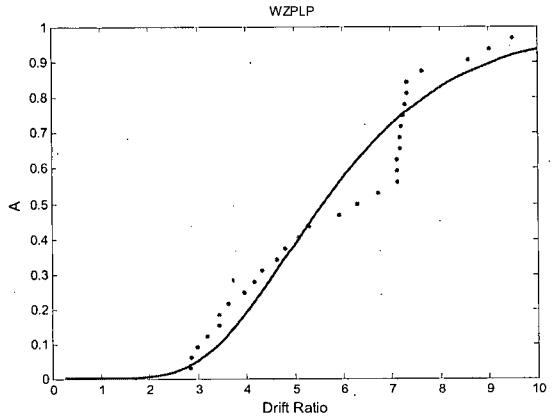

D.11 Rectangular Column B Fragility Curves (Maximum Recorded Drifts)

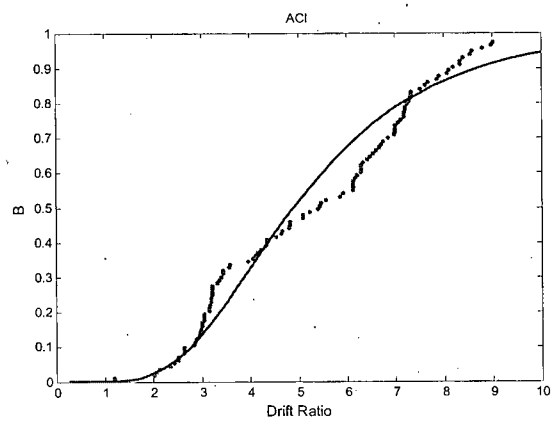

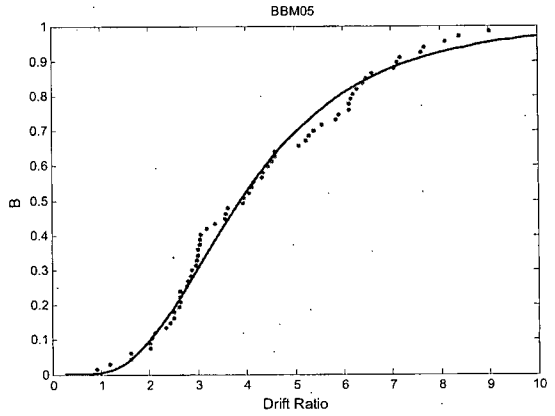

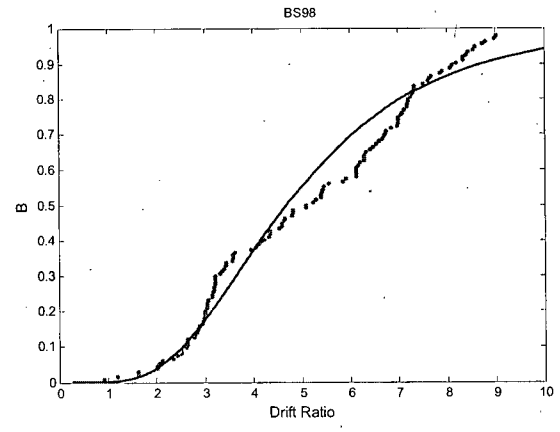

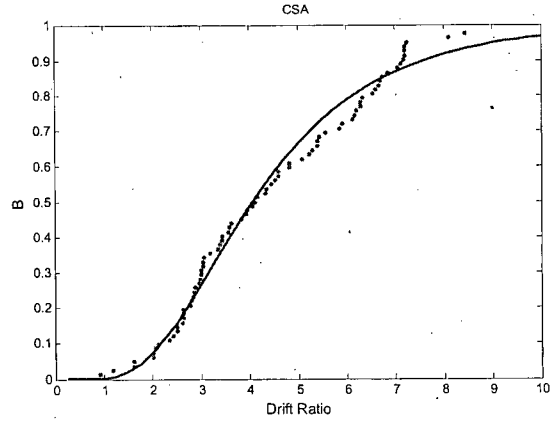

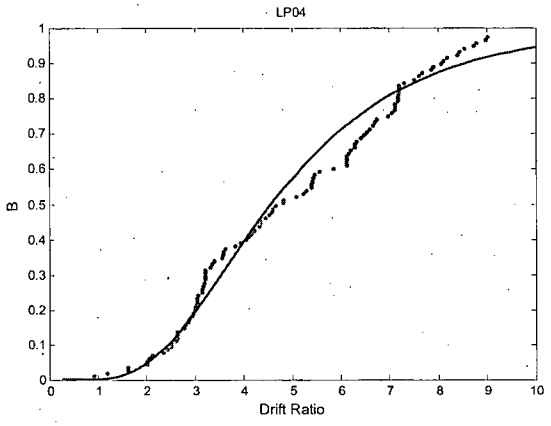
LP04
B
Drift Ratio

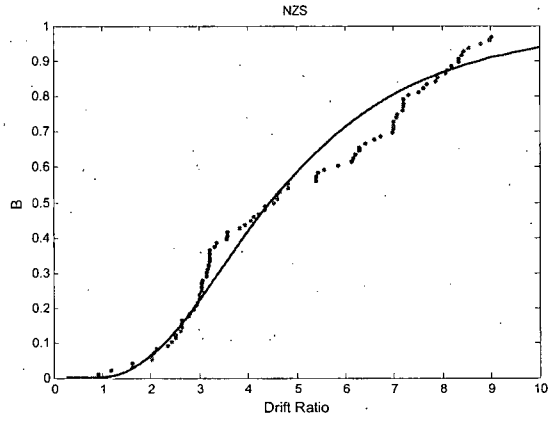
NZS
B
Drift Ratio

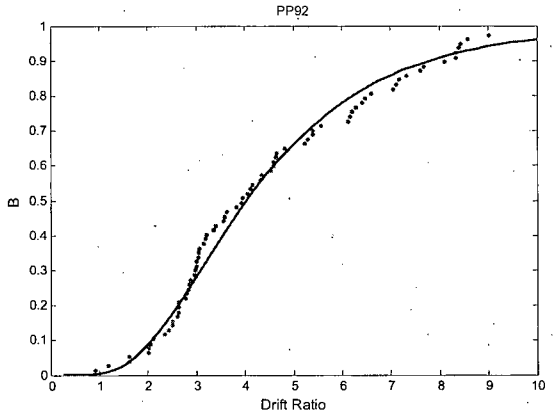
PP92
B
Drift Ratio

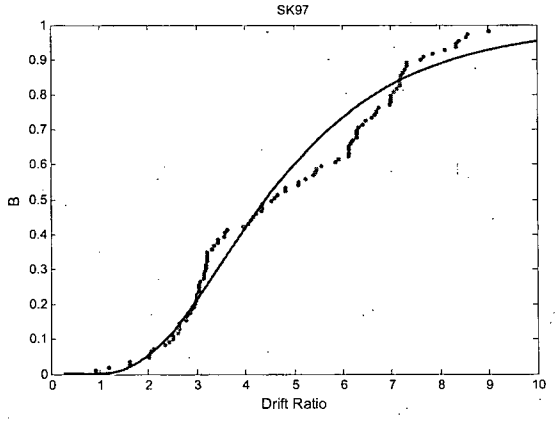
SK97
B
Drift Ratio

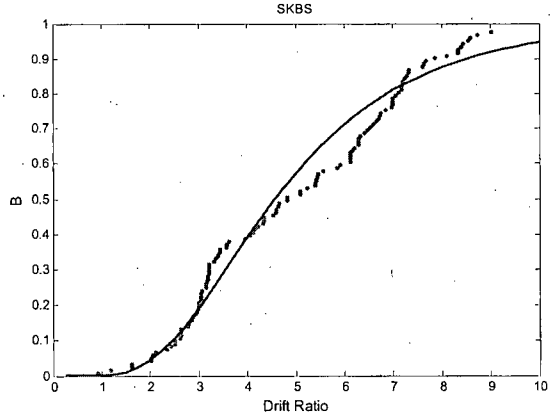
SKBS
B
Drift Ratio

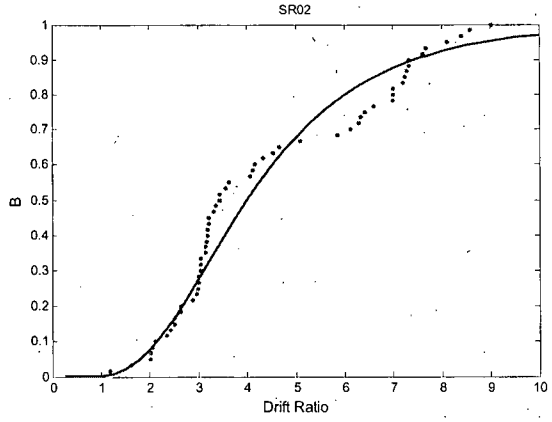
SR02
B
Drift Ratio

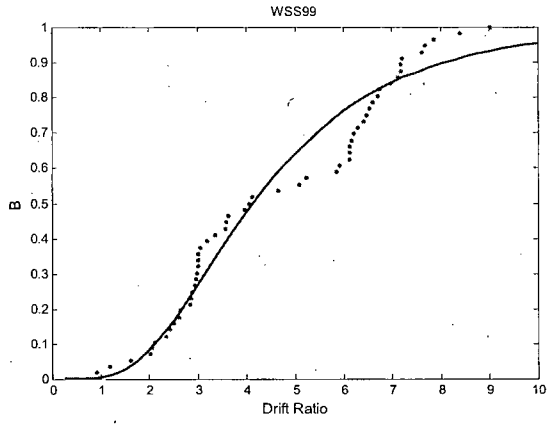

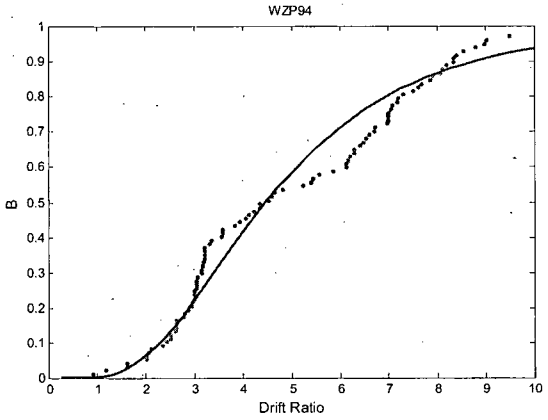

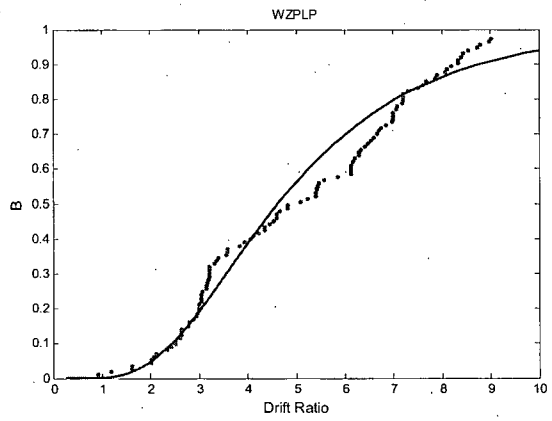

D.12 Rectangular Column C Fragility Curves (Maximum Recorded Drifts)

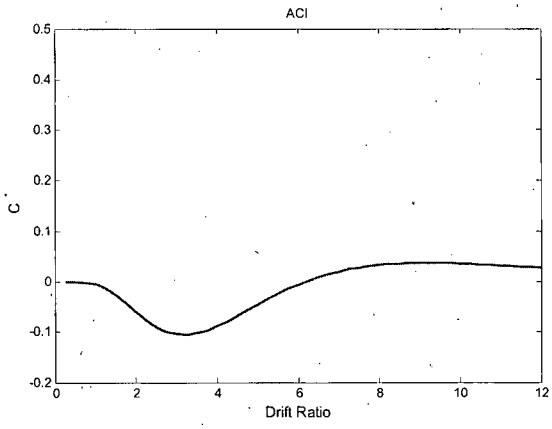

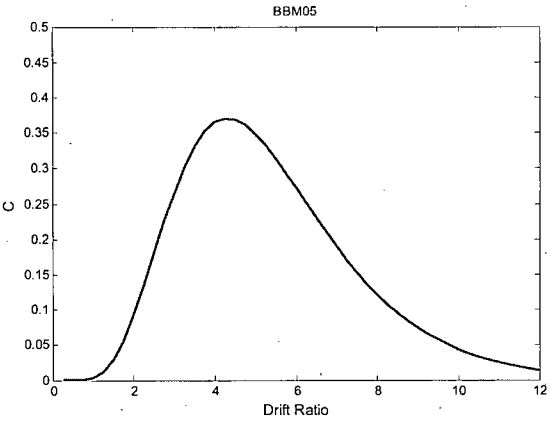

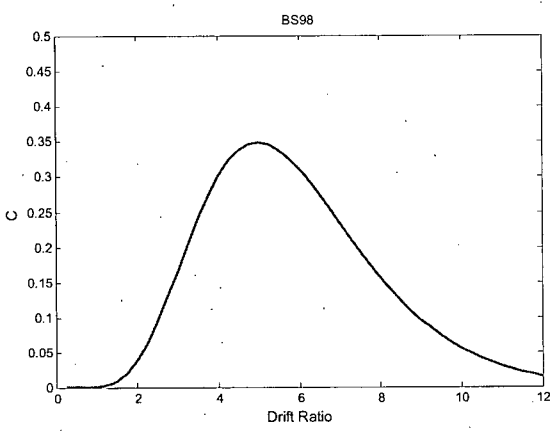
BS98
C
Drift Ratio

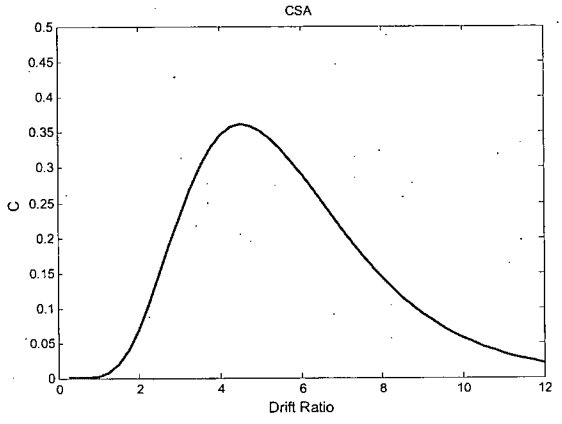
CSA
C
Drift Ratio

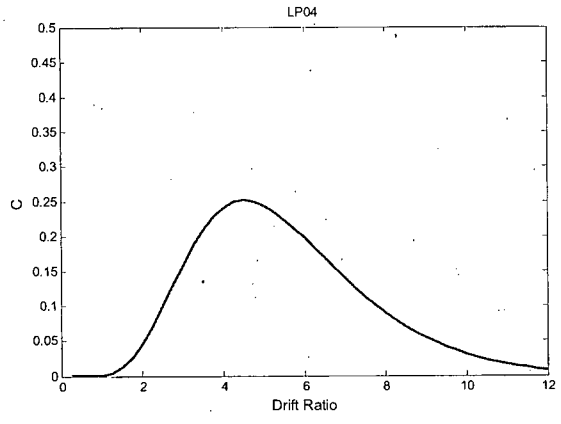
LP04
C
Drift Ratio

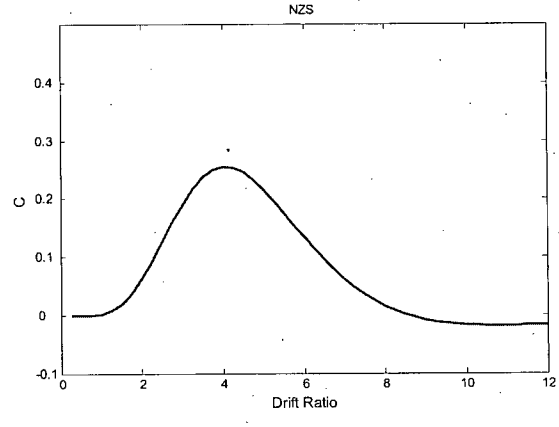
NZS
C
Drift Ratio

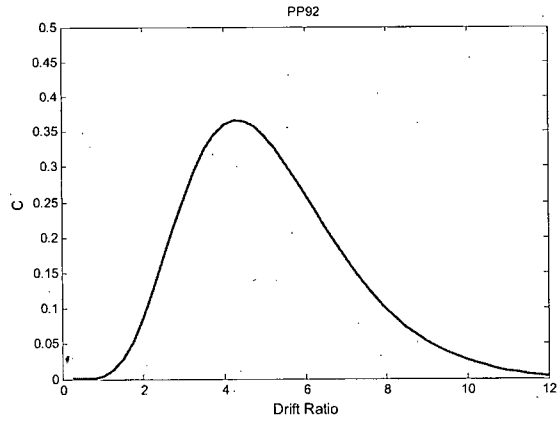
PP92
C
Drift Ratio

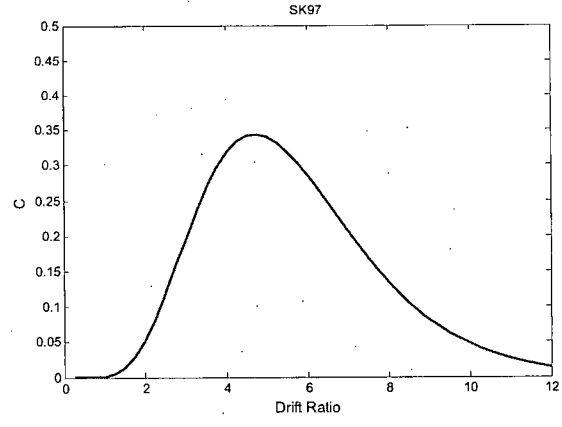
SK97
C
Drift Ratio

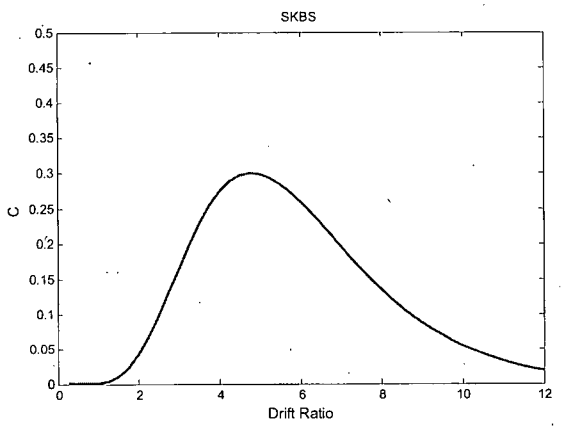
SKBS
C
Drift Ratio

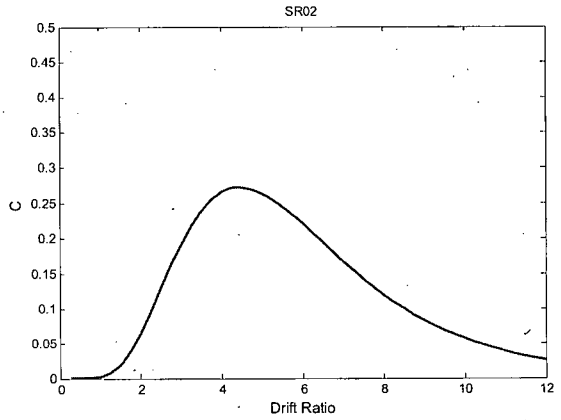
SR02
C
Drift Ratio

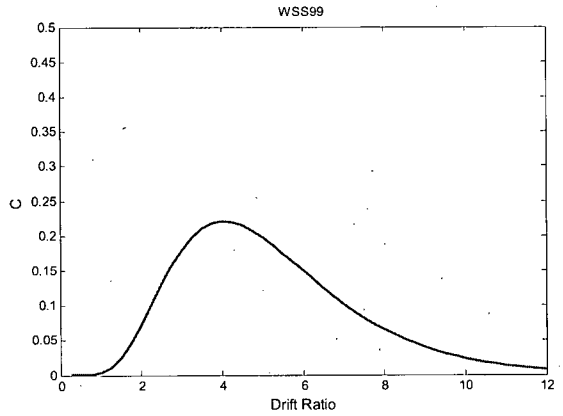
WSS99
C
Drift Ratio

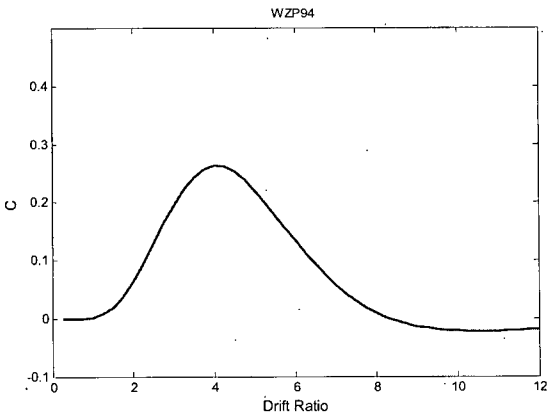
WZP94
C
Drift Ratio

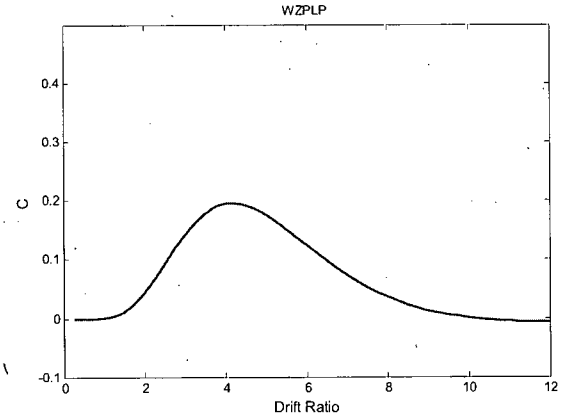
WZPLP
C
Drift Ratio

D.13 Circular Column Scatter Plots (with ACI Minimum)

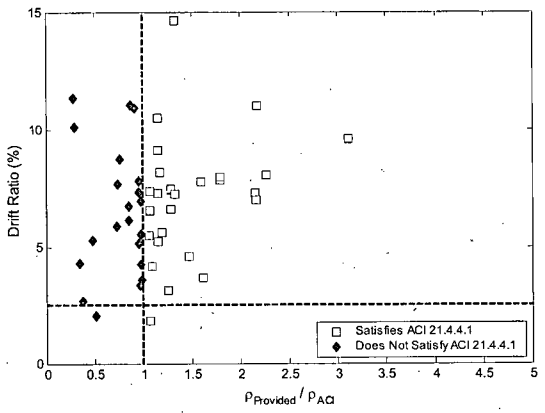

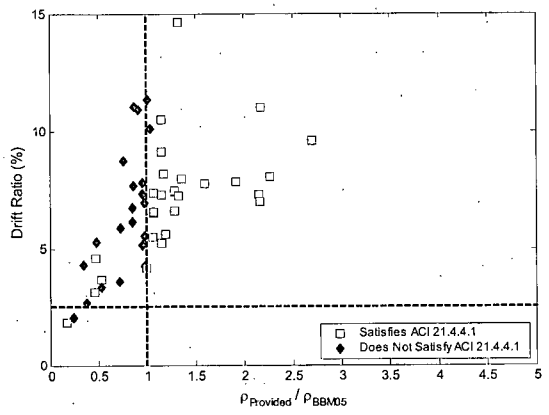

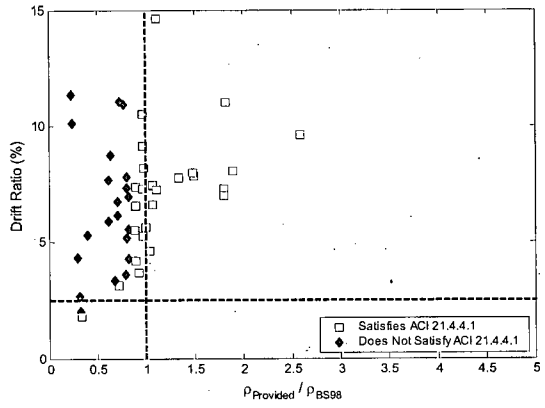

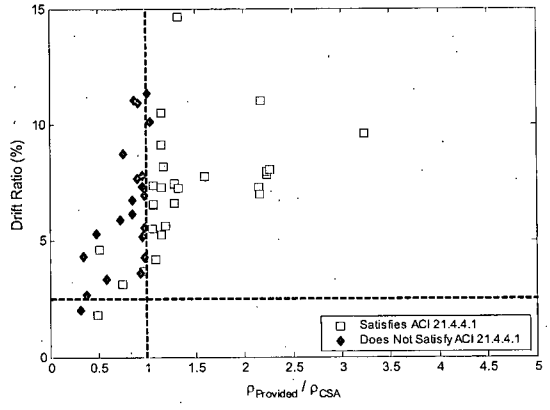

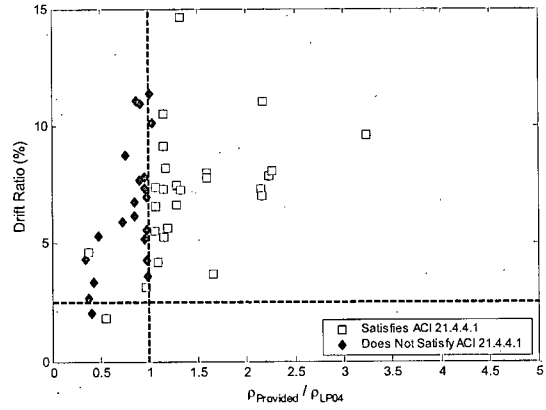

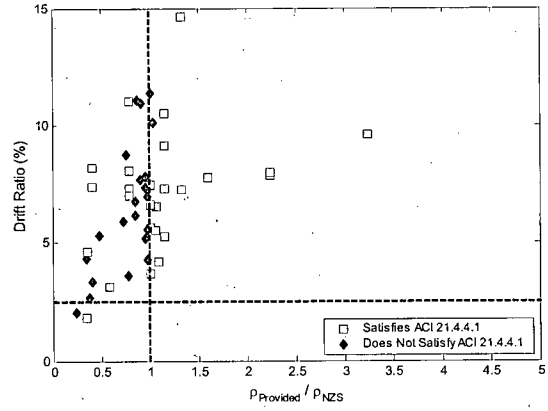

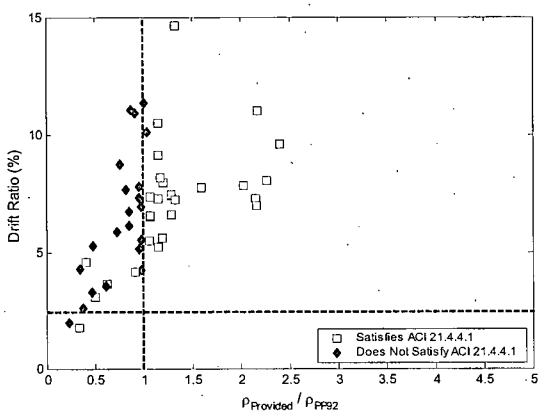
Drift Ratio (%)
Satisfies ACI 21.4.4.1
Does Not Satisfy ACI 21.4.4.1
ρProvided / ρPP92

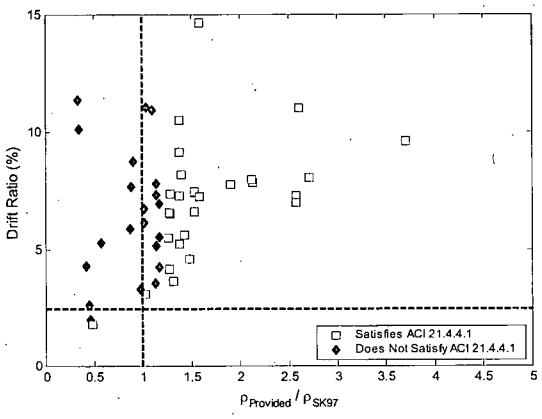
Drift Ratio (%)
Satisfies ACI 21.4.4.1
Does Not Satisfy ACI 21.4.4.1
ρProvided / ρSK97

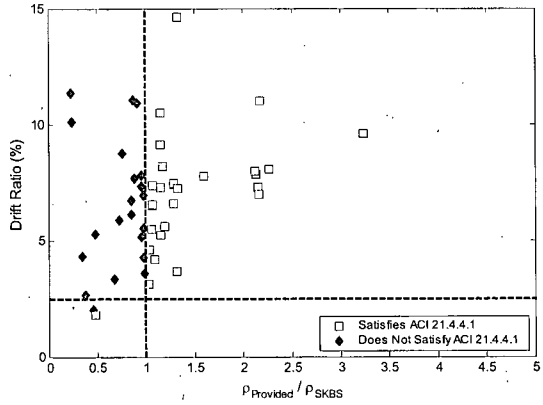
Drift Ratio (%)
Satisfies ACI 21.4.4.1
Does Not Satisfy ACI 21.4.4.1
ρProvided / ρSKBS

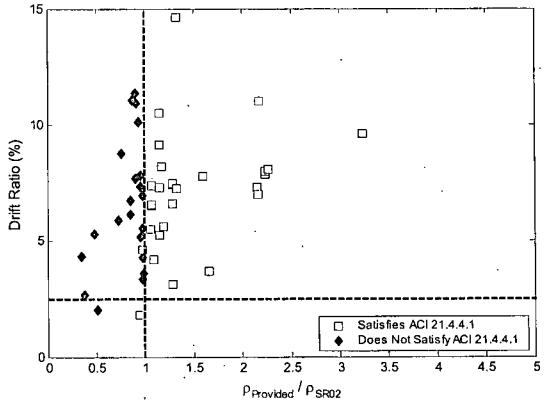
Drift Ratio (%)
Satisfies ACI 21.4.4.1
Does Not Satisfy ACI 21.4.4.1
ρProvided / ρSR02

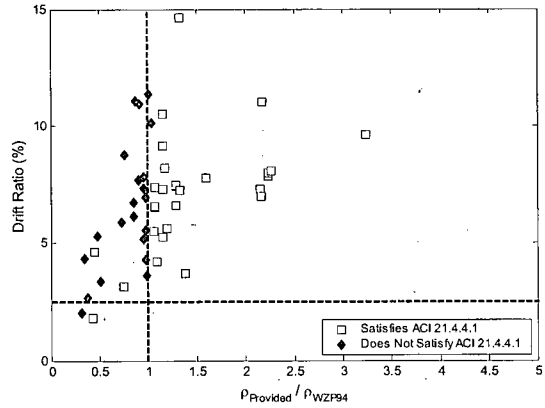
Drift Ratio (%)
Satisfies ACI 21.4.4.1
Does Not Satisfy ACI 21.4.4.1
ρProvided / ρWZP94

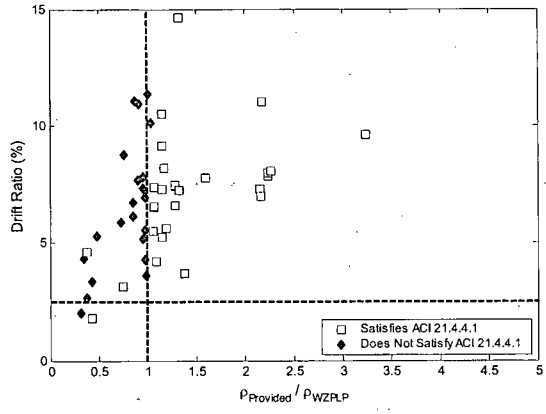
Drift Ratio (%)
Satisfies ACI 21.4.4.1
Does Not Satisfy ACI 21.4.4.1
ρProvided / ρWZPLP

Table D.4 Circular scatter plot statistics (with ACI limit)

Model	A	B	C
ACI	3.4	4.8	1.3
A23	0.0	8.7	8.7
PP92	0.0	8.3	8.3
SR02	0.0	8.7	8.7
BBM05	0.0	8.7	8.7
SK97	0.0	18.2	18.2
BS98	0.0	5.6	5.6
SKBS	0.0	9.1	9.1
WZP94	0.0	9.1	9.1
LP04	0.0	9.1	9.1
WZPLP	0.0	9.1	9.1
NZS	0.0	7.1	7.1

D.14 Circular Column Scatter Plots (without ACI Minimum)

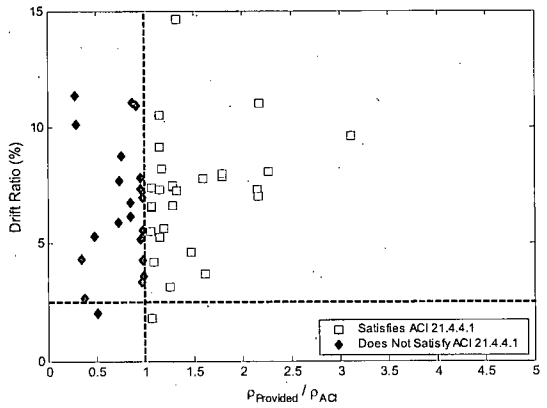

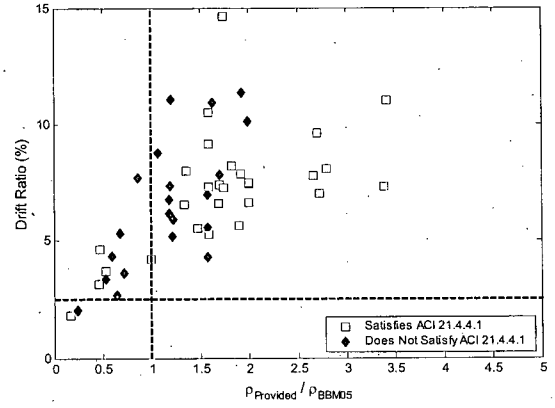

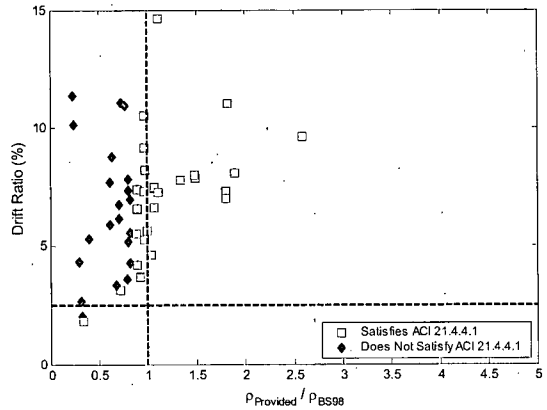

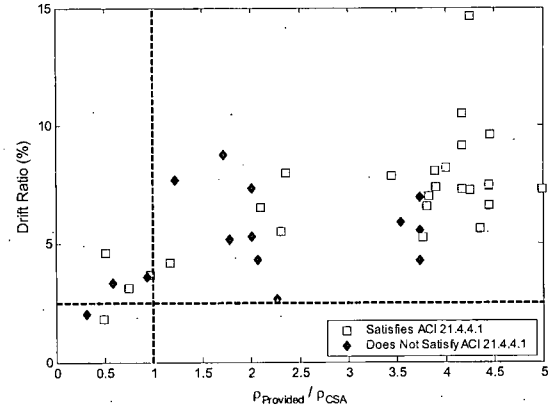

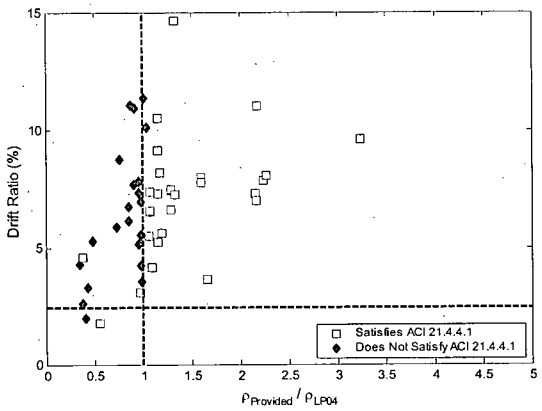
Drift Ratio (%)
Satisfies ACI 21.4.4.1
Does Not Satisfy ACI 21.4.4.1
ρProvided / ρLP04

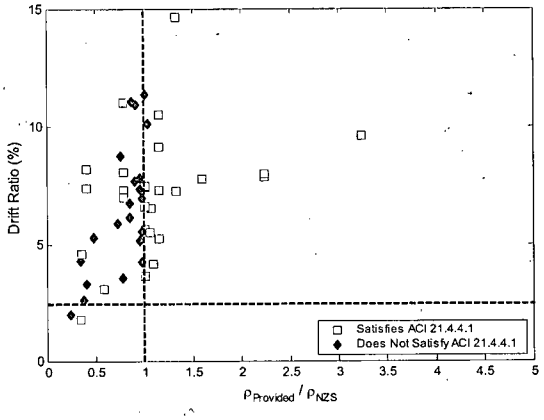
Drift Ratio (%)
Satisfies ACI 21.4.4.1
Does Not Satisfy ACI 21.4.4.1
ρProvided / ρNZS

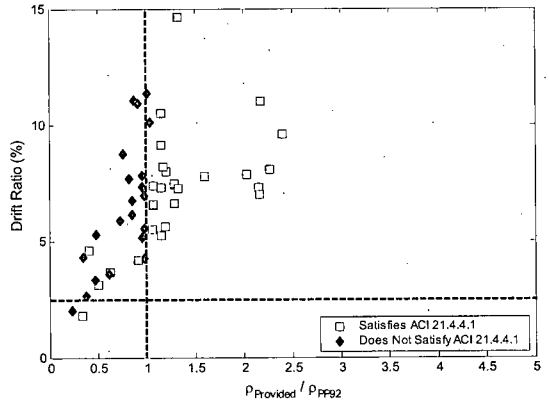
Drift Ratio (%)
Satisfies ACI 21.4.4.1
Does Not Satisfy ACI 21.4.4.1
ρProvided / ρPP92

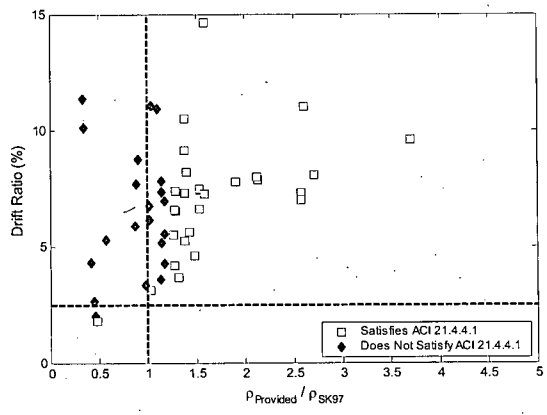
Drift Ratio (%)
Satisfies ACI 21.4.4.1
Does Not Satisfy ACI 21.4.4.1
ρProvided / ρSK97

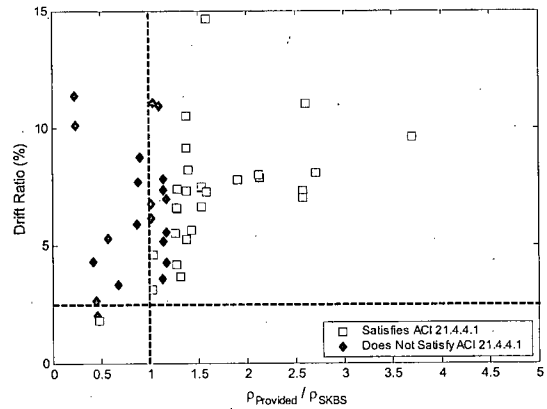
Drift Ratio (%)
Satisfies ACI 21.4.4.1
Does Not Satisfy ACI 21.4.4.1
ρProvided / ρSKBS

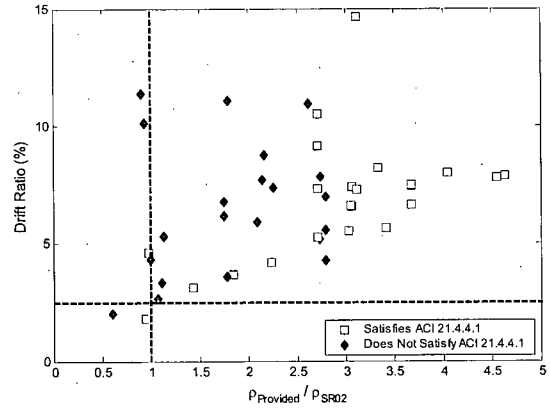
Drift Ratio (%)
Satisfies ACI 21.4.4.1
Does Not Satisfy ACI 21.4.4.1
ρProvided / ρSR02

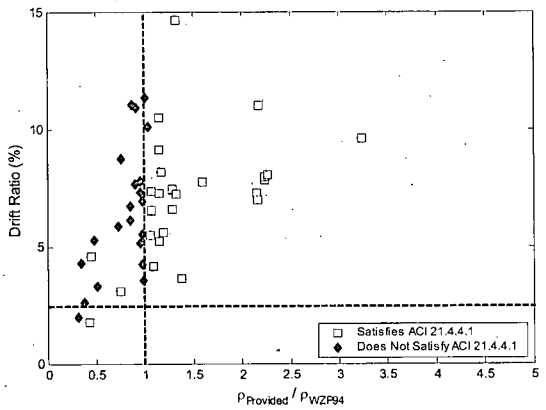

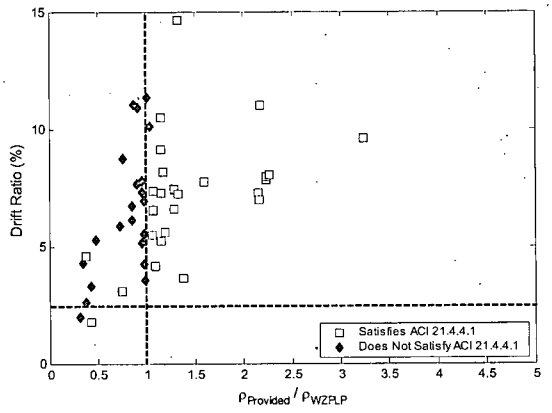

Table D.5 Circular scatter plot statistics (without ACI limit)

Model	A	B	C
ACI	3.4	4.8	1.3
A23	0.0	28.6	28.6
PP92	0.0	8.3	8.3
SR02	0.0	33.3	33.3
BBM05	0.0	18.2	18.2
SK97	0.0	18.2	18.2
BS98	0.0	5.6	5.6
SKBS	0.0	18.2	18.2
WZP94	0.0	9.1	9.1
LP04	0.0	9.1	9.1
WZPLP	0.0	9.1	9.1
NZS	0.0	7.1	7.1

D.15 Circular Column A Fragility Curves (with ACI Minimum)

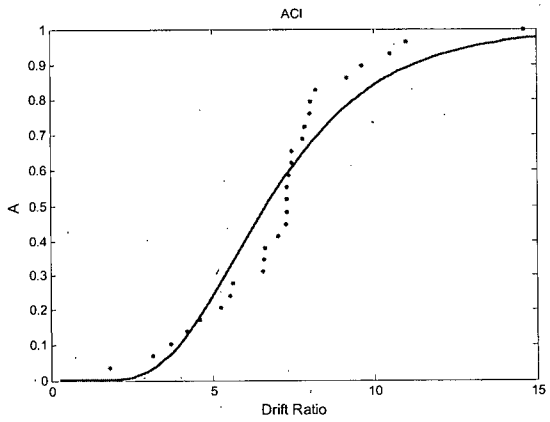

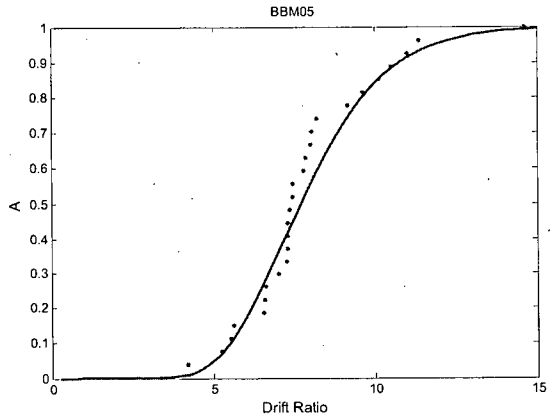

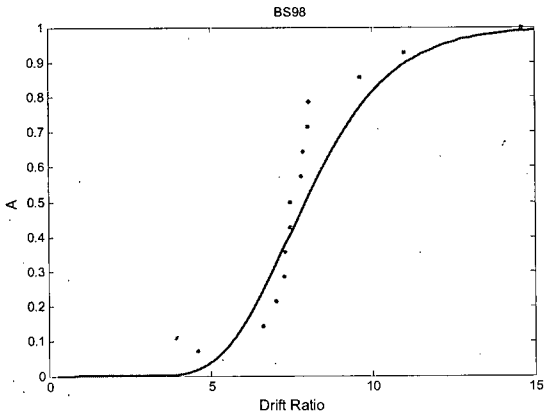

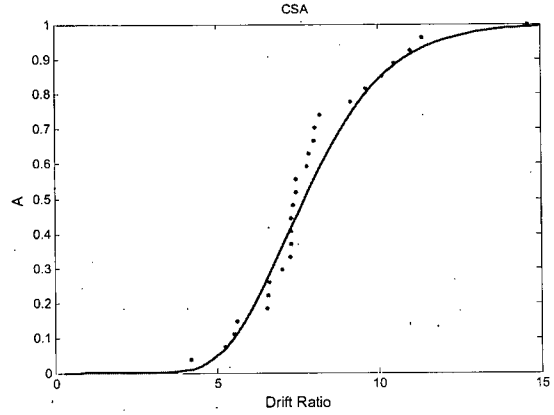

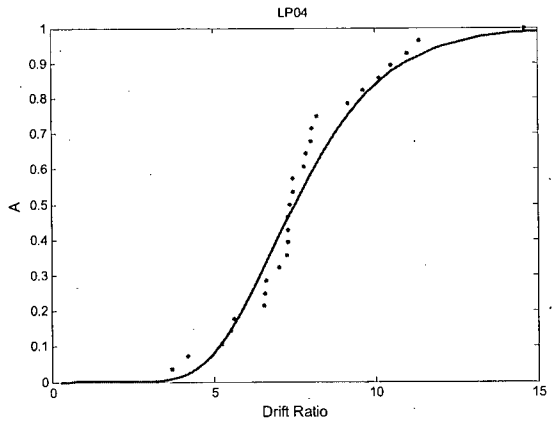

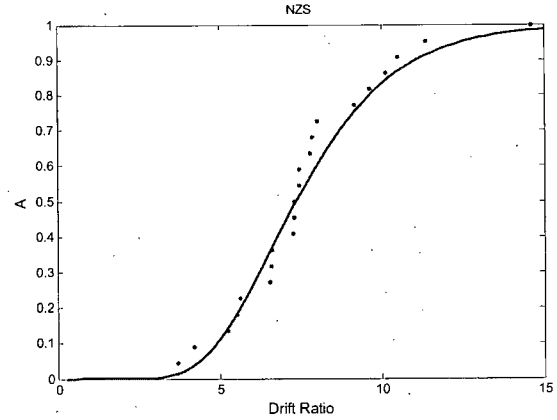

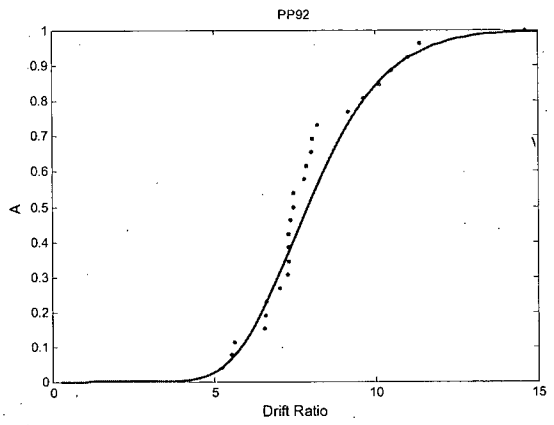
PP92
A
Drift Ratio

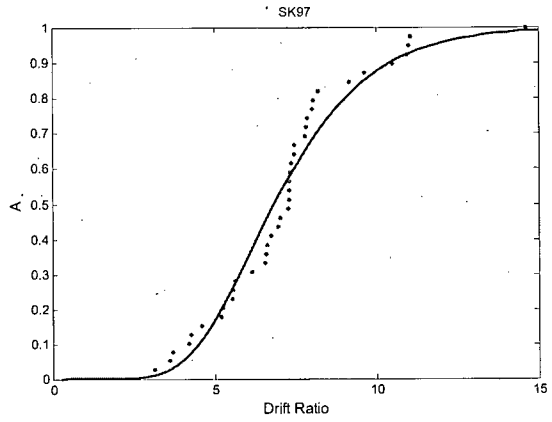
SK97
A
Drift Ratio

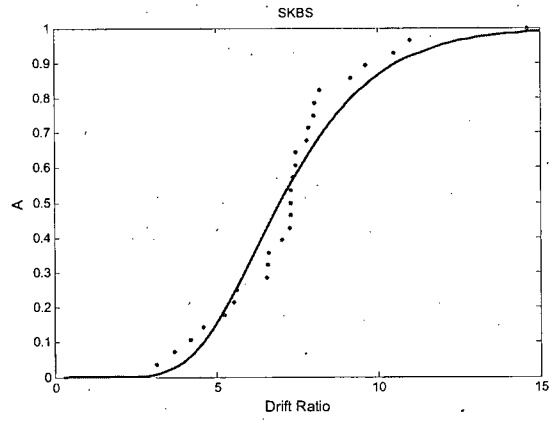
SKBS
A
Drift Ratio

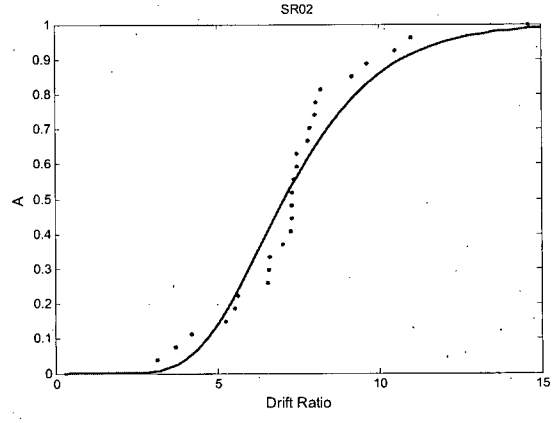
SR02
A
Drift Ratio

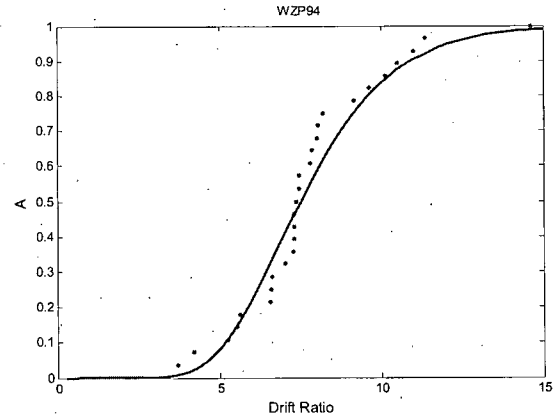
WZP94
A
Drift Ratio

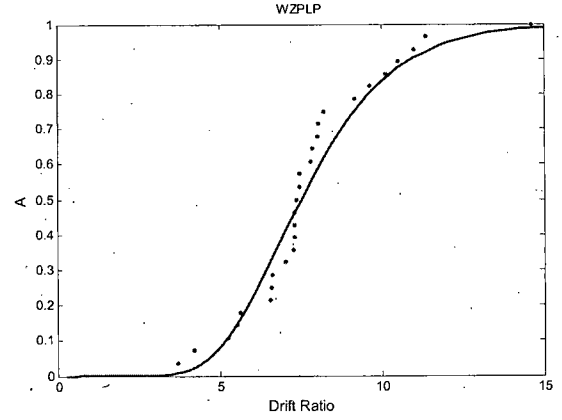
WZPLP
A
Drift Ratio

D.16 Circular Column B Fragility Curves (with ACI Minimum)

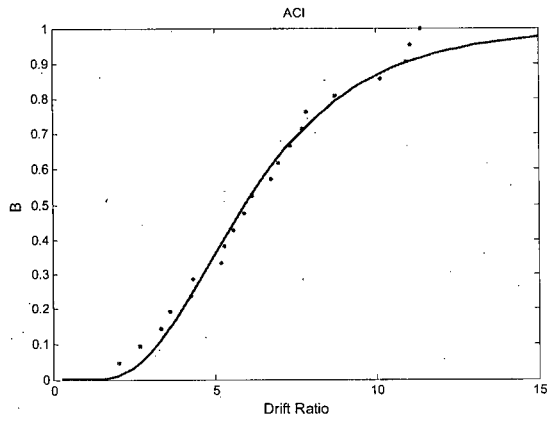

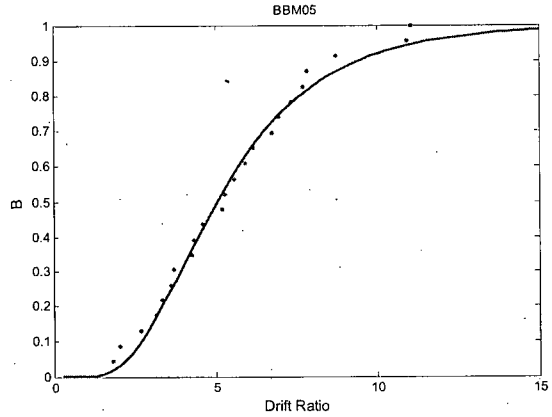

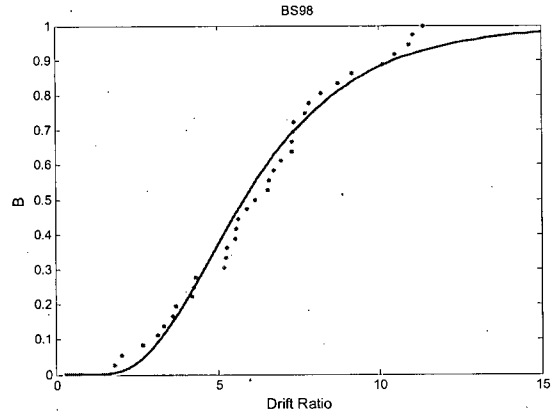

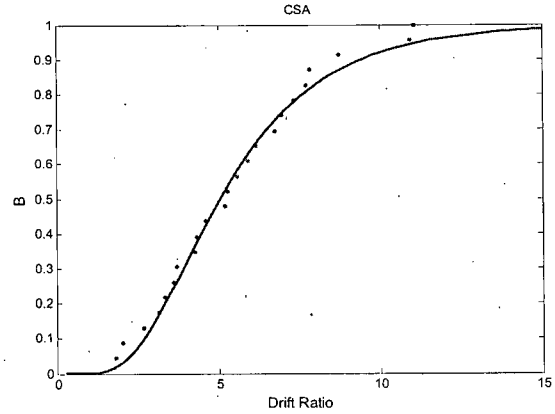

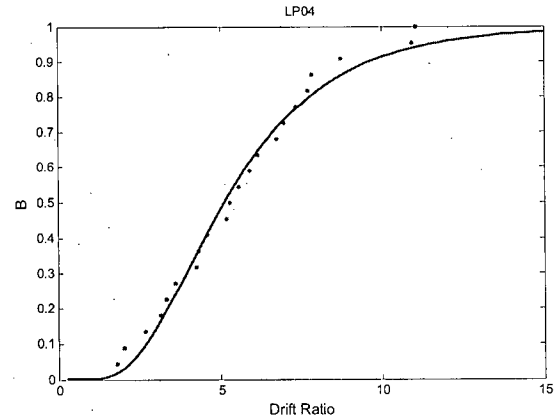

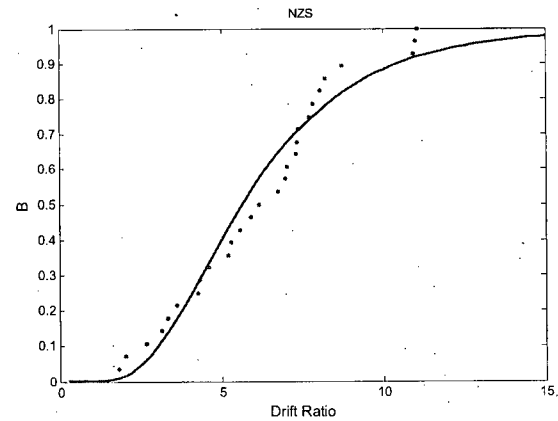

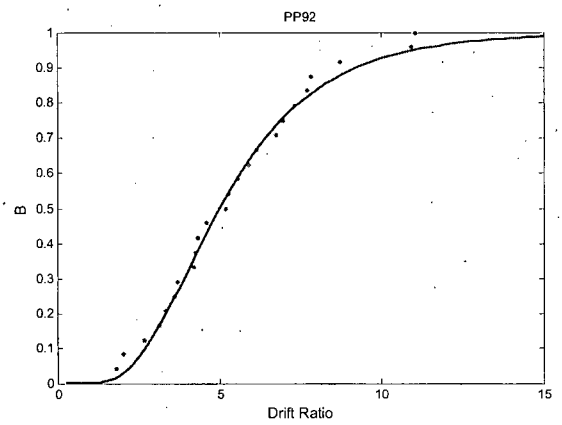
PP92
B
Drift Ratio

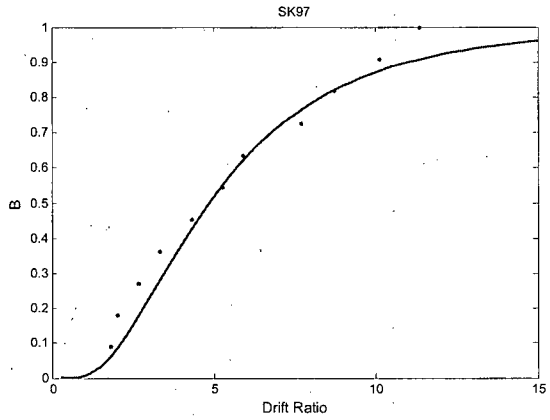
SK97
B
Drift Ratio

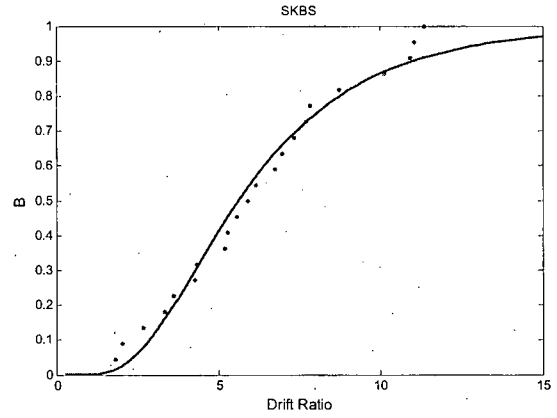
SKBS
B
Drift Ratio

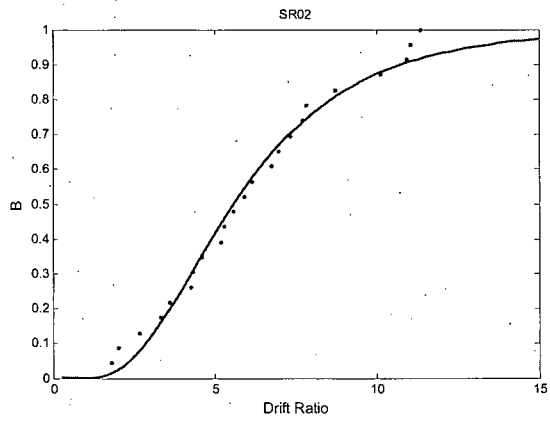
SR02
B
Drift Ratio

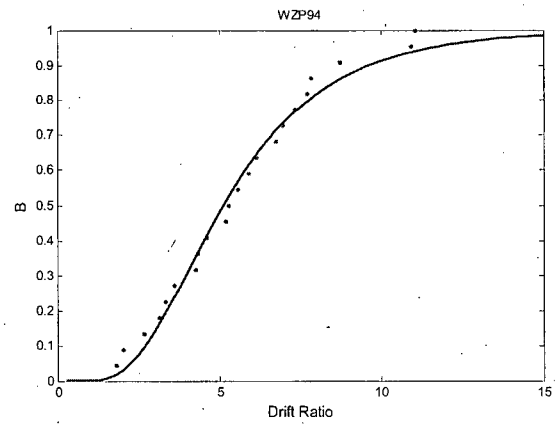
WZP94
B
Drift Ratio

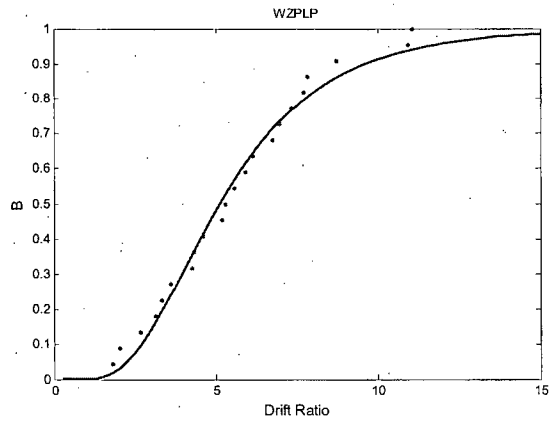
WZPLP
B
Drift Ratio

D.17 Circular Column C Fragility Curves (with ACI Minimum)

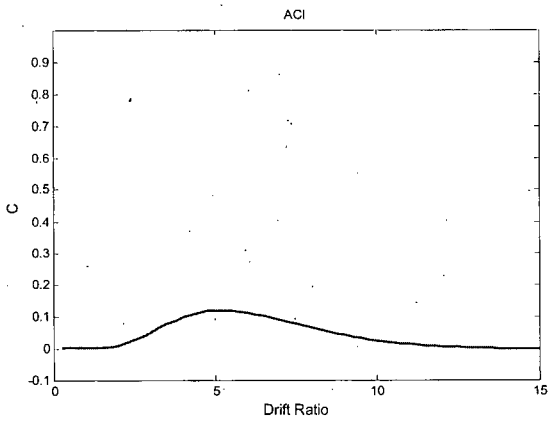

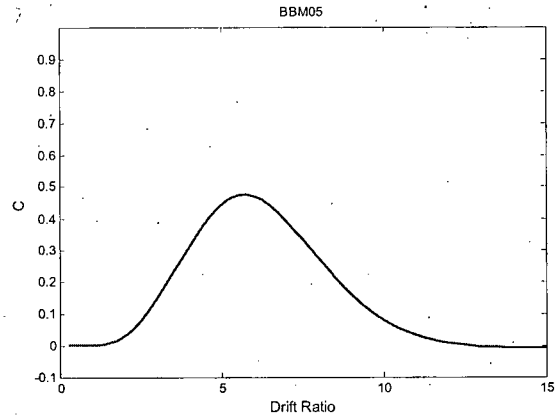

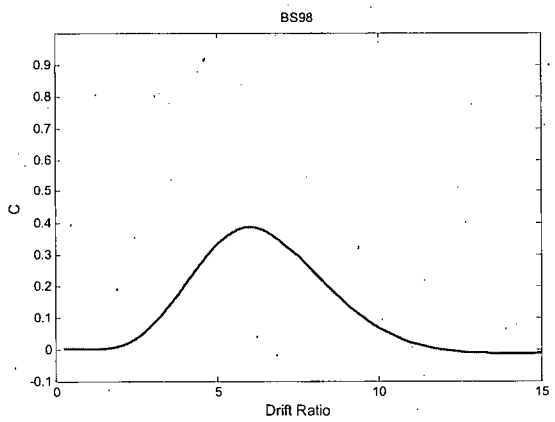

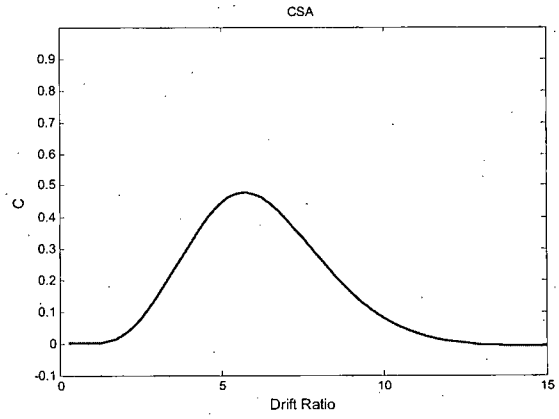

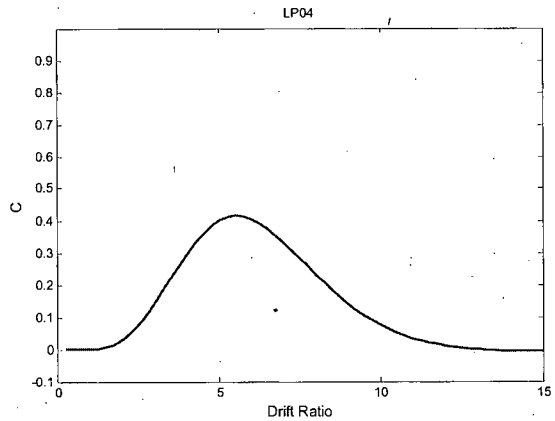

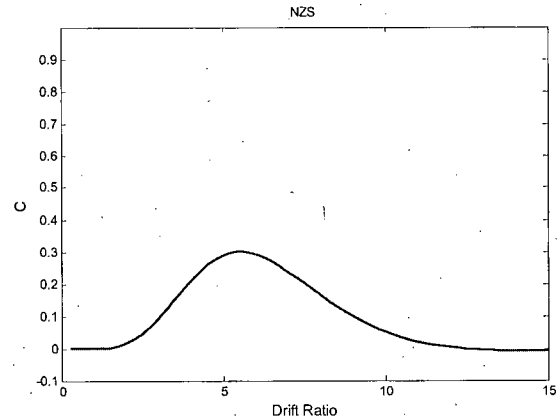

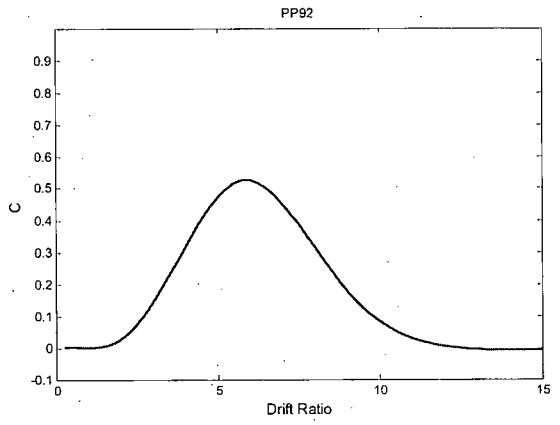
PP92
C
Drift Ratio

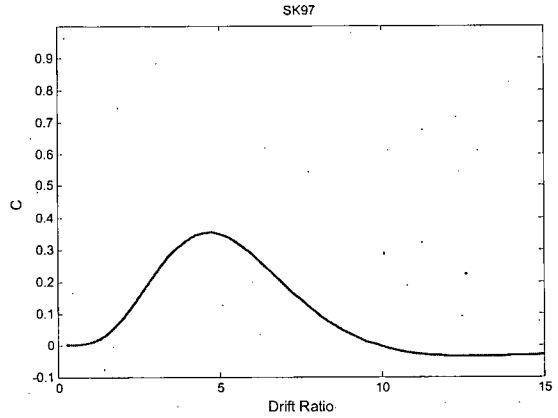
SK97
C
Drift Ratio

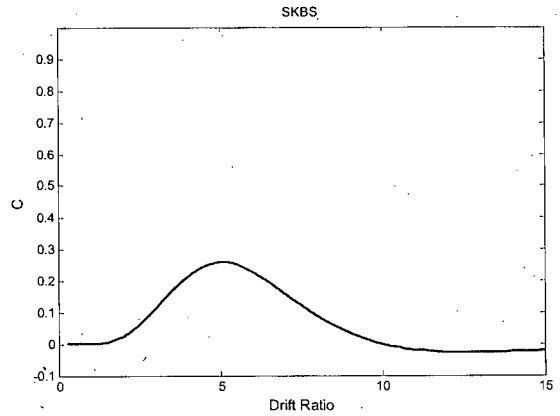
SKBS
C
Drift Ratio

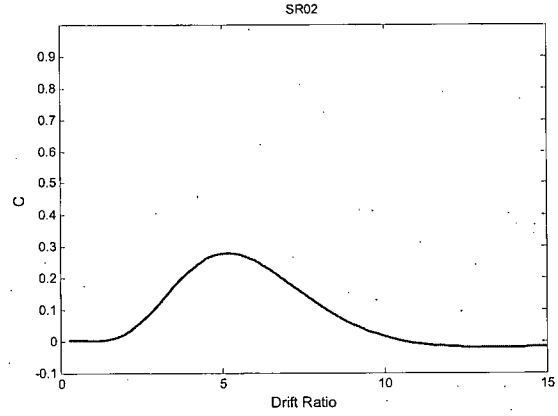
SR02
C
Drift Ratio

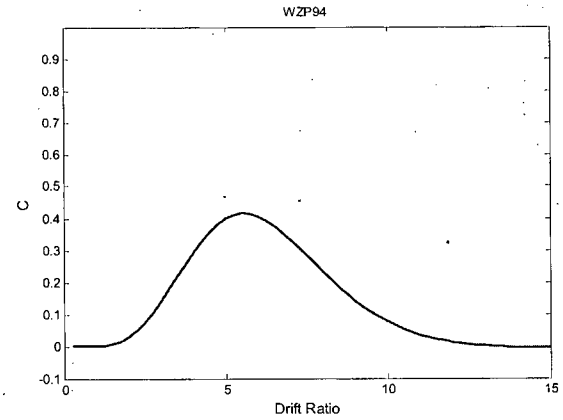
WZP94
C
Drift Ratio

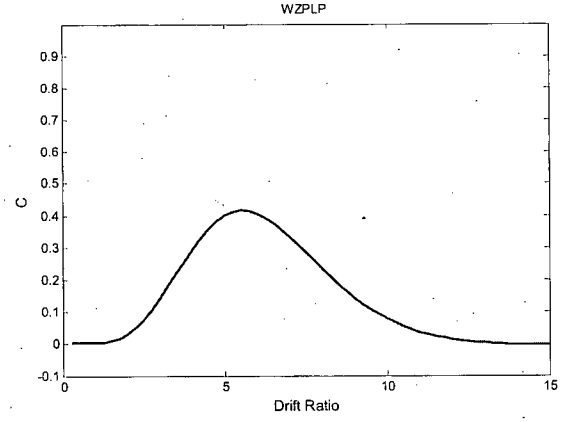
WZPLP
C
Drift Ratio

D.18 Circular Column A Fragility Curves (without ACI Minimum)

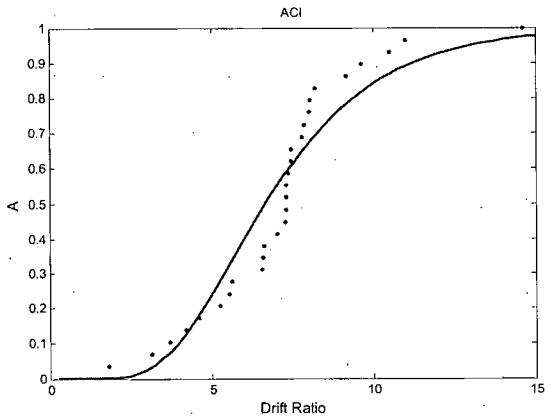

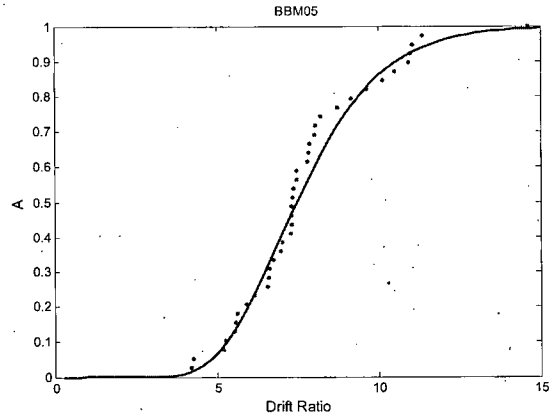

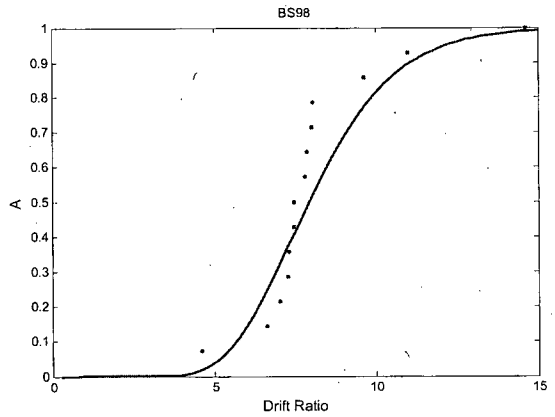

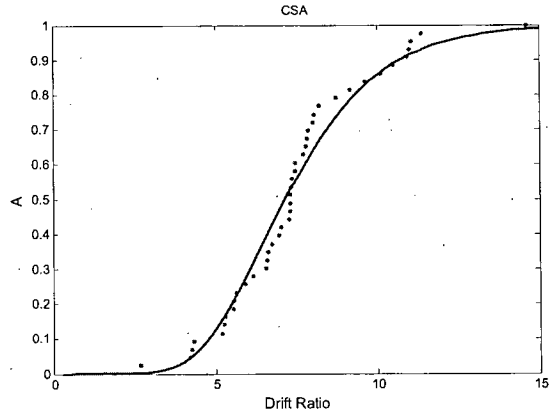

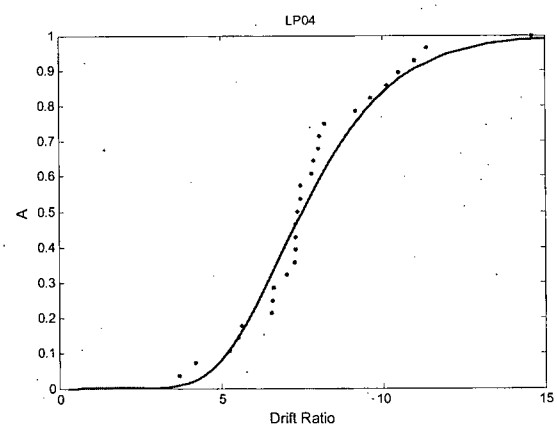

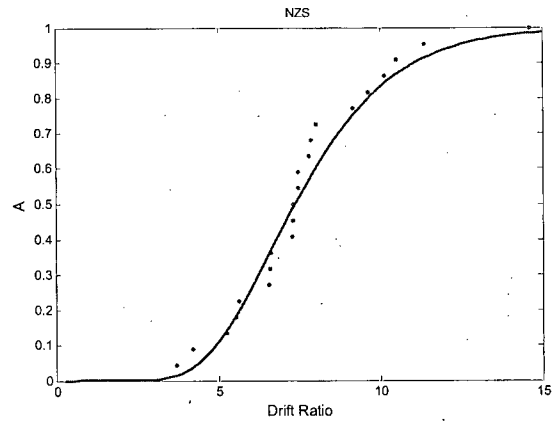

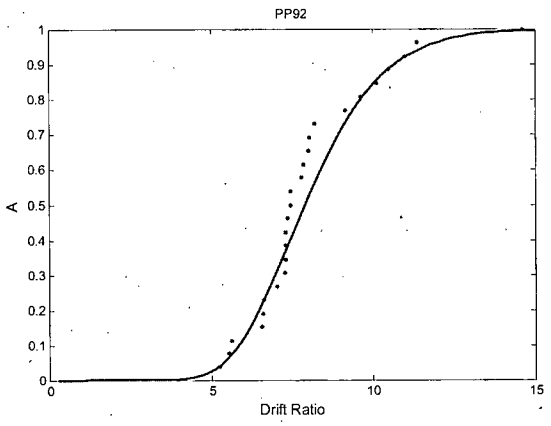
PP92
A
Drift Ratio

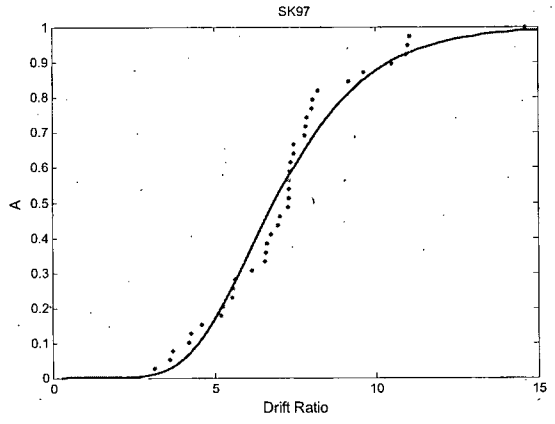
SK97
A
Drift Ratio

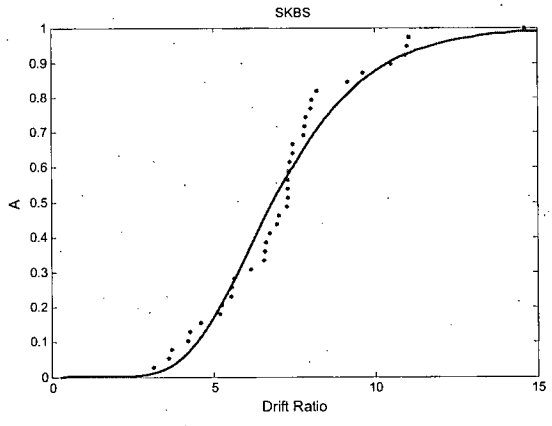
SKBS
A
Drift Ratio

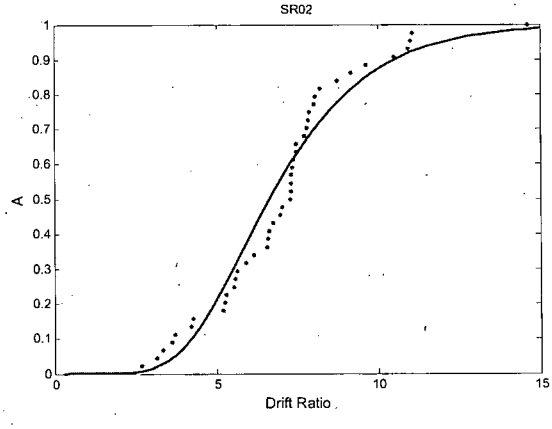
SR02
A
Drift Ratio

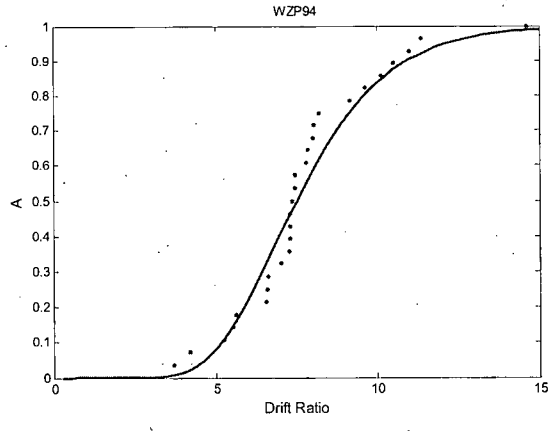
WZP94
A
Drift Ratio

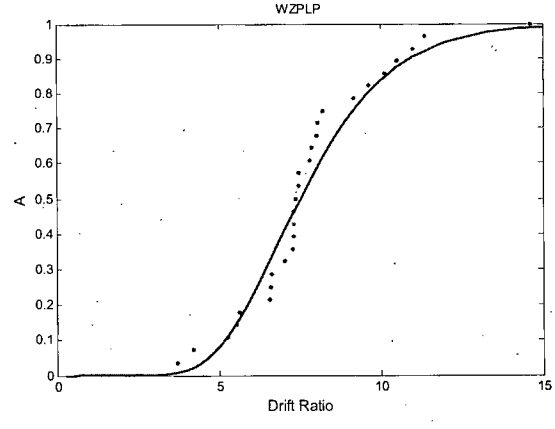
WZPLP
A
Drift Ratio

D.19 Circular Column B Fragility Curves (without ACI Minimum)

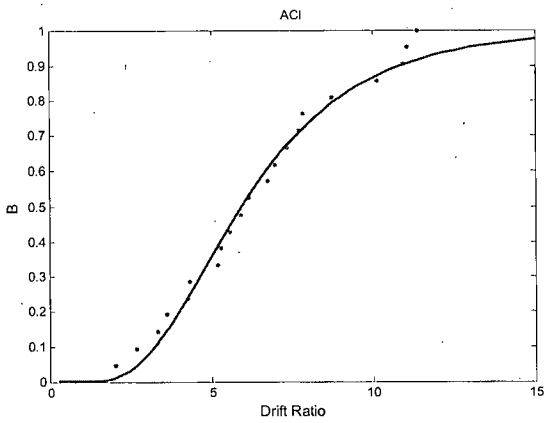

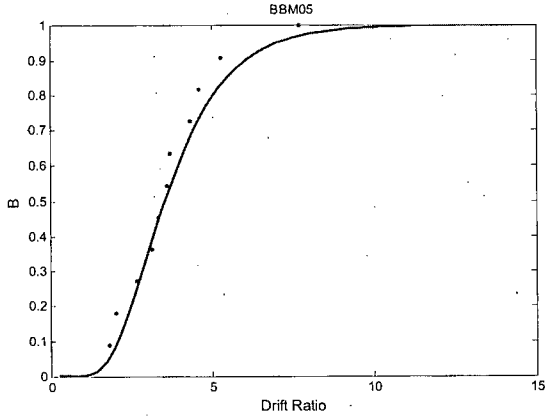

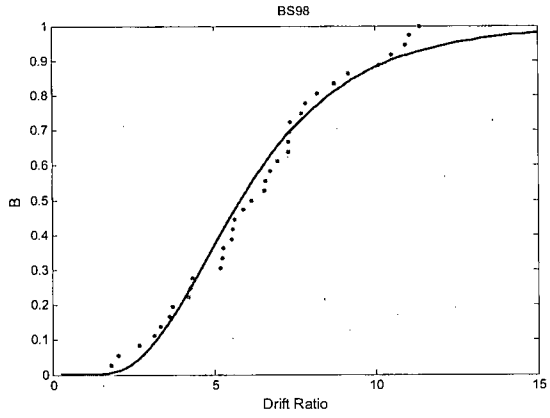

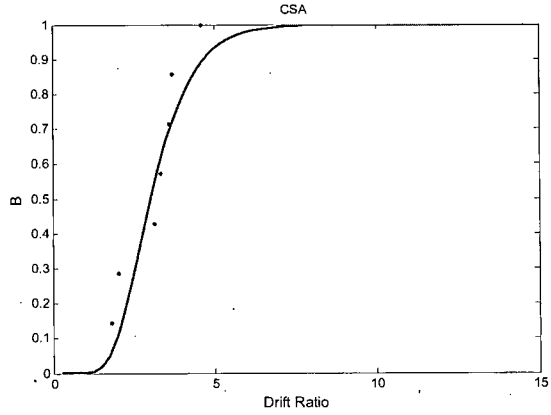

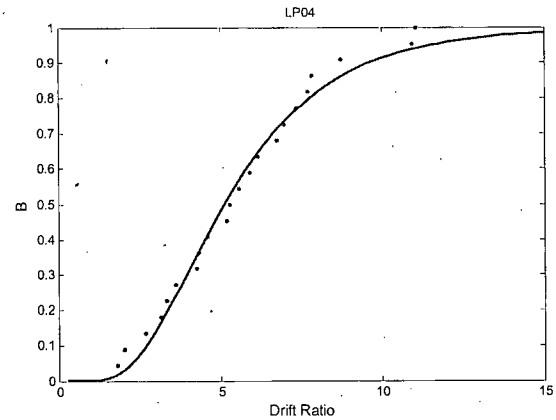

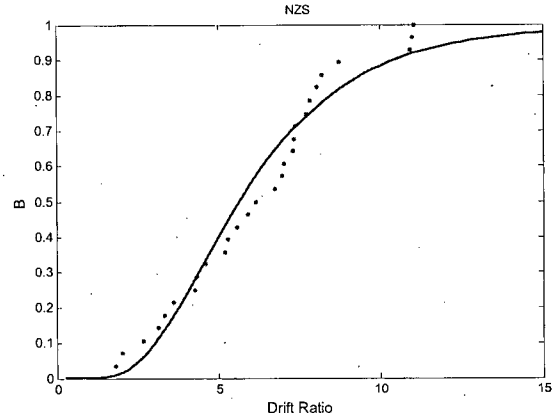

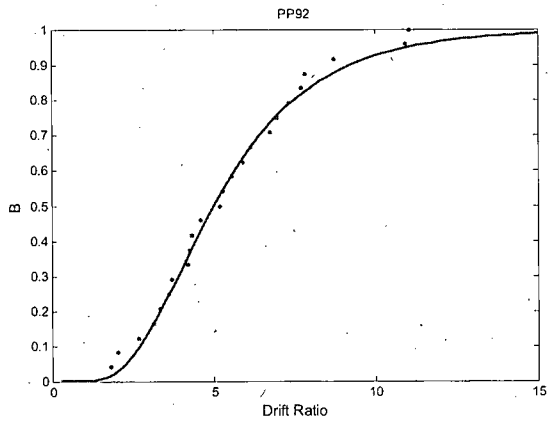
PP92
B
Drift Ratio

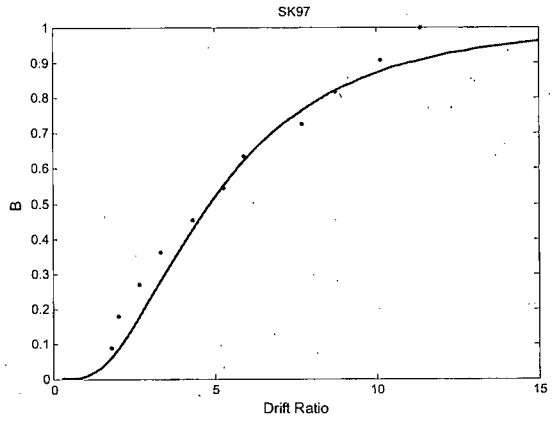
SK97
B
Drift Ratio

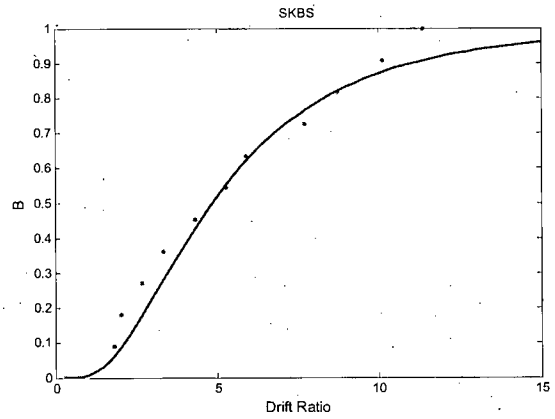
SKBS
B
Drift Ratio

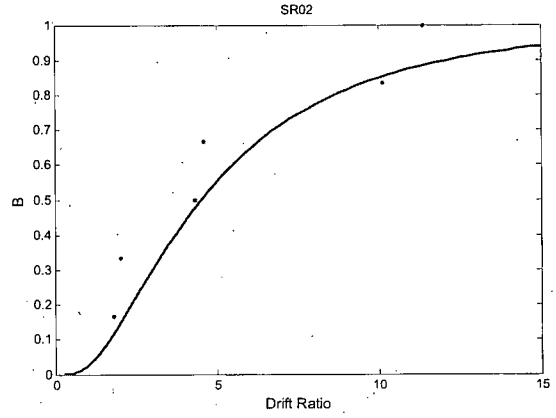
SR02
B
Drift Ratio

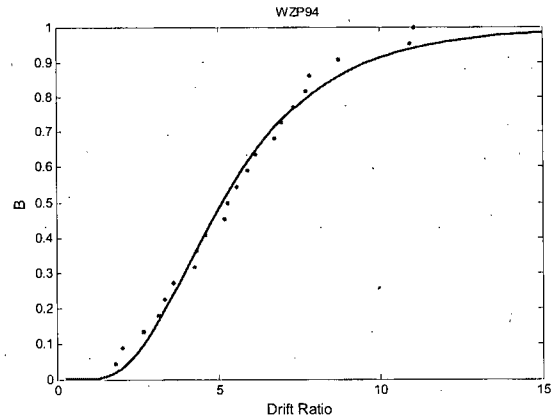
WZP94
B
Drift Ratio

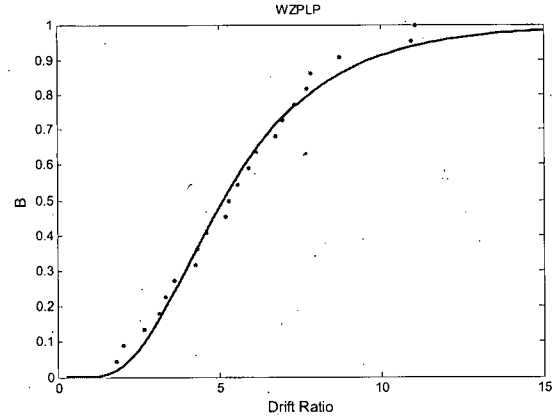
WZPLP
B
Drift Ratio

D.20 Circular Column C Fragility Curves (without ACI Minimum)

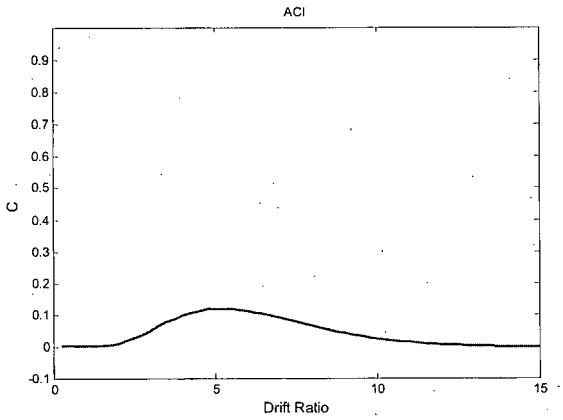

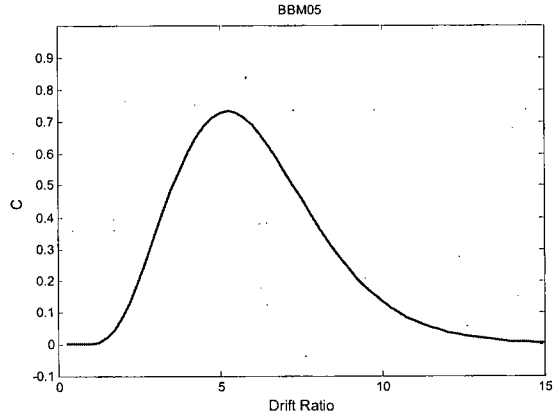

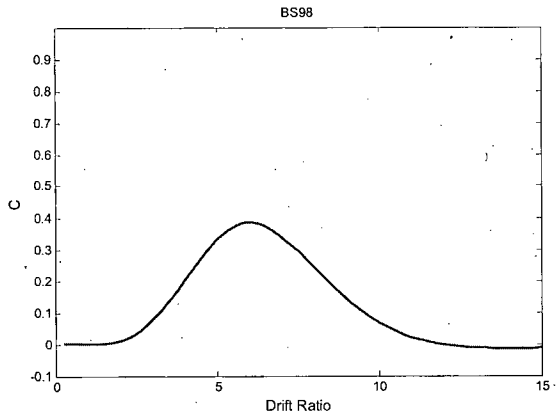

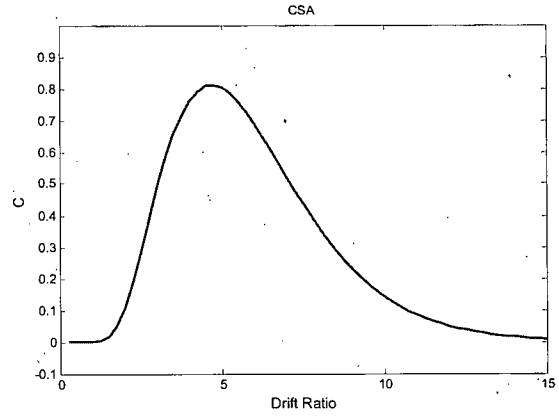

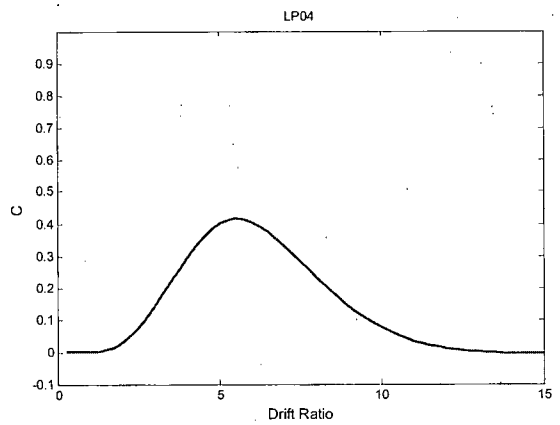

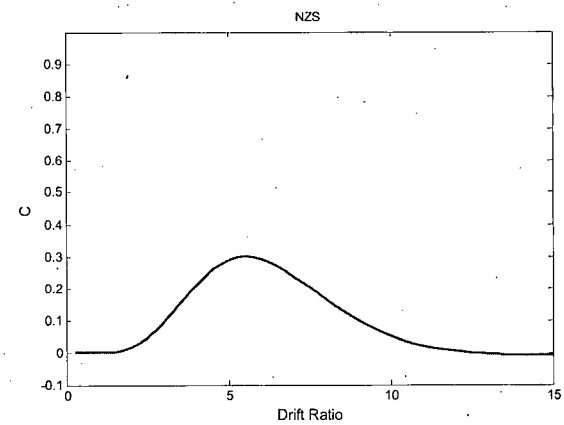

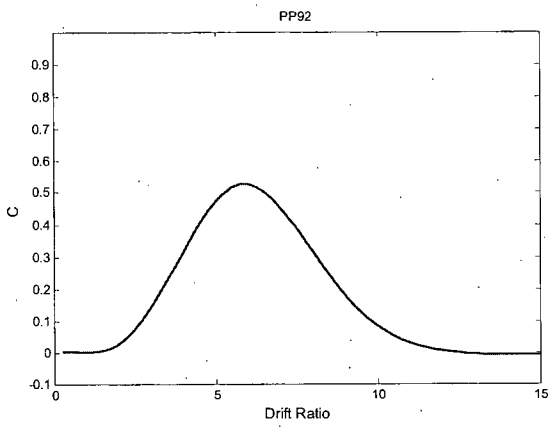
PP92
C
Drift Ratio

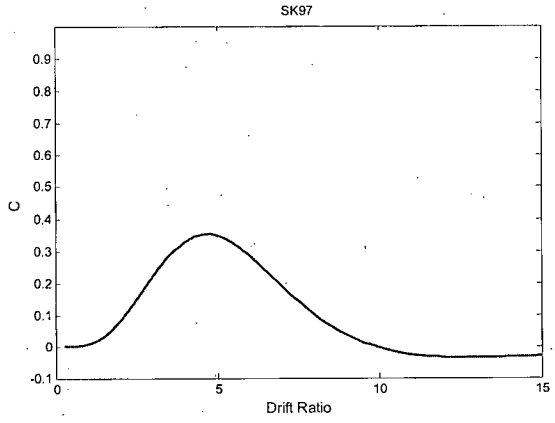
SK97
C
Drift Ratio

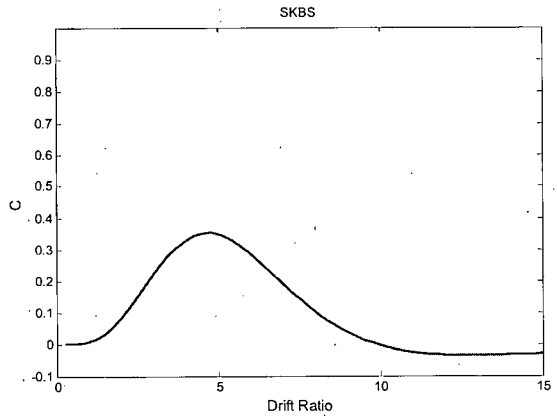
SKBS
C
Drift Ratio

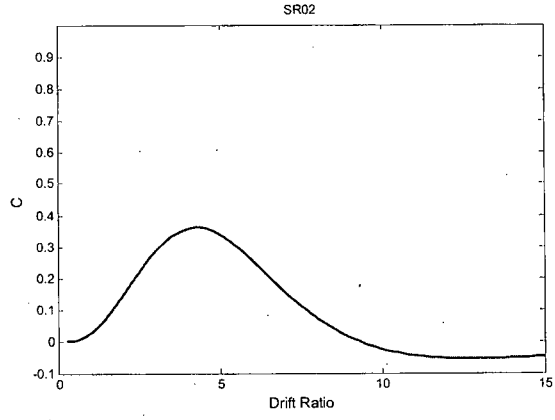
SR02
C
Drift Ratio

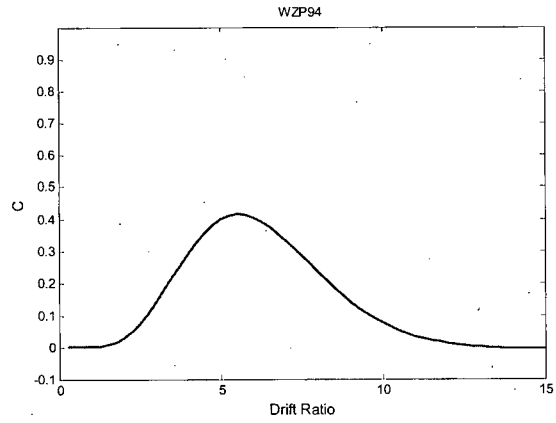
WZP94
C
Drift Ratio

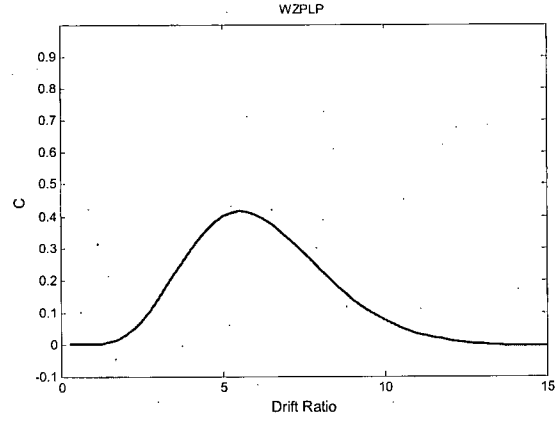
WZPLP
C
Drift Ratio